An Investigation into the Impact of Early Development and Manufacturing Processes on Cell Product Quality

A thesis submitted for the degree of Doctor of Philosophy by

Charlotte Kay

Department of Life and Health Sciences, Brunel University, London

Abstract

Cell and Gene Therapy (CGT) now offers curative treatment for several genetic disorders and haematological malignancies; however, development and manufacturing still hamper broader clinical application. This thesis investigates early development and manufacturing processes to reduce cost, whilst keeping product safety, quality and efficacy in mind.

In Chapter 1, Retrogenix™ was assessed for its suitability as an early development screening platform to reduce the number of candidate constructs progressed by screening for off-target binding, which was observed with CAR-X binding to the Netrin1 receptor. However, a missed off-target binding hit with CAR-A, the unsuitability for engineered TCR-T cells and high costs, all limited the suitability of Retrogenix™ for screening large numbers of candidates.

In Chapters 2 and 3, methods to reduce “vein-to-vein” time for apheresis, treatment, and re-infusion into the patient, were explored. With limitations on cell expansion rate focussed upon within chapter 2, and T cell transduction efficiency enhancement investigated within chapter 3.

As monocyte contamination of peripheral blood mononuclear cell (PBMC) populations is believed to reduce cell product expansion, these were removed, however, this did not significantly impact T cell expansion and bulk PBMCs were transduced by lentiviral vectors (LVV) at higher levels than isolated T cells. To investigate culture vessel impact on T cell expansion, G-REX® vessels, that provide increased oxygen perfusion and nutrient availability to cells, were compared to standard flat-bottom culture plates and found to significantly improve T cell expansion. Additionally, cytokines were investigated on cell expansion using IL-2 alone or a combination of IL-7/IL-15. This resulted in neither being able to increase T cell expansion or transduction efficiency, however, IL-7/IL-15 did impact the CD4:CD8 T cell ratio. Finally, using small molecule compounds, T cell transduction was investigated with two candidate compounds identified that improved LV transduction efficiency.

To conclude, this work identified and enabled implementation of several process improvements that have benefitted GSKs CGT development process. These findings will be discussed with consideration of ways to reduce the cost of gene therapy products thereby making them more attractive to the marketplace.

Contents

Table of Contents

1. Introduction

1.1. The Field of Cell and Gene Therapy

Cell and Gene Therapy (CGT) is a rapidly advancing field worldwide, with the UK involved in an estimated 9% of all advanced therapy medicinal product (ATMP) clinical trials (Catapult, 2022). 168 ATMP trials were identified as ongoing within the UK in 2021, 72.4% of which were identified as gene therapies with an almost equal distribution between *in vivo* and *ex vivo* studies (Catapult, 2022). The remaining UK ATMP trials were identified as either somatic-cell therapies (18.9%) or tissue engineered therapies (8.7%) (Catapult, 2022).

Gene therapy involves the introduction of genetic material to replace or repair faulty genes, augment gene function or introduce a novel function to a cell. This can be performed *in vivo* (directly in the patient) or *ex vivo* (the modification and re-infusion of cells removed from the patient). There are several approaches to introduce deoxyribonucleic acid (DNA) into a host genome, including non-viral transfection methods and use of recombinant viral vectors. The approach that will be discussed within this thesis will be the use of viral vectors, as these are the most used methods for both *in vivo* and *ex vivo* gene therapies (Catapult, 2022).

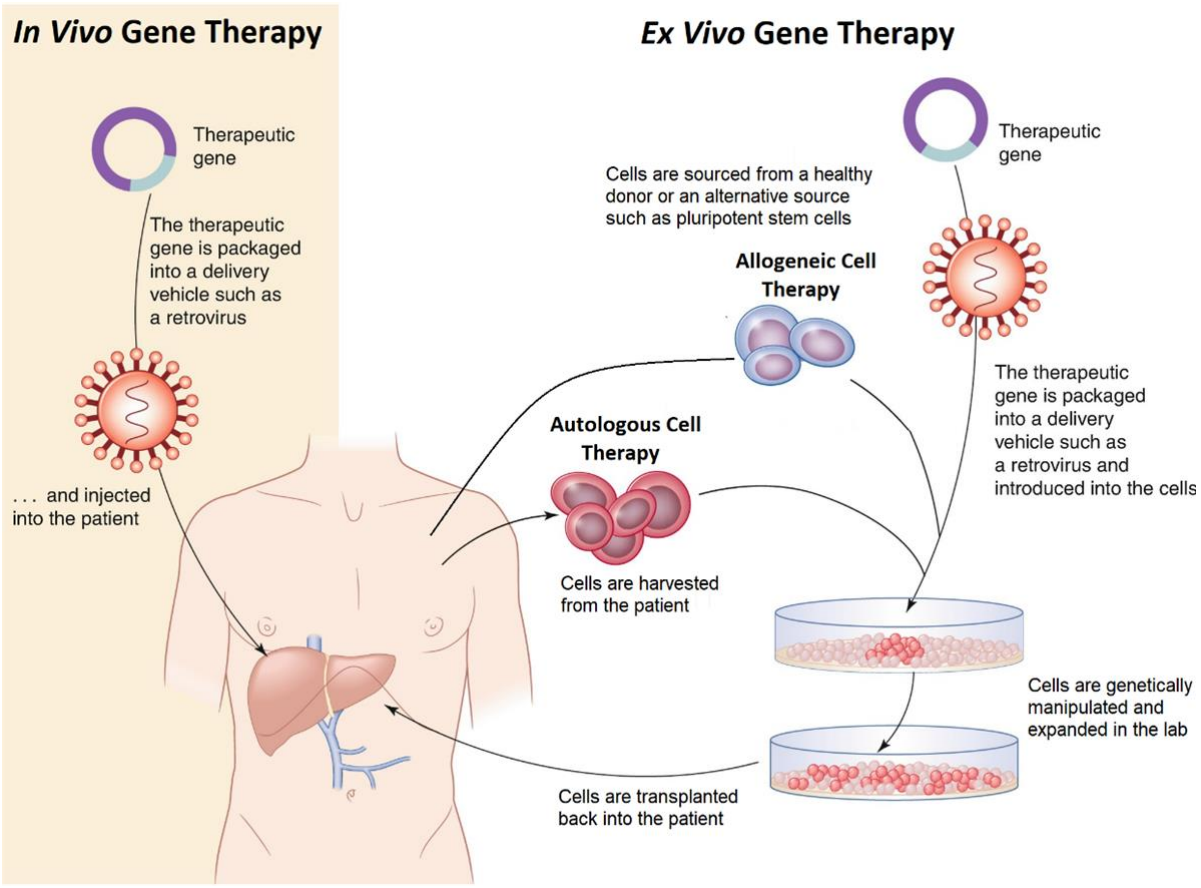

Figure 1: Overview of Gene Therapy Manufacturing Process

In vivo gene therapy involves introduction of therapeutic genetic material directly into the patient through the use of a delivery vehicle such as a viral vector. Ex vivo gene therapy involves the removal of the cells of interest from the patient or a matched donor prior to modification with the therapeutic gene and re-infusion to the patient. Image adapted from (Wu et al., 2019).

Cell therapy involves the introduction of cells, often stem cells, which are either; autologous (taken from the patient) or allogeneic (from a Human Leukocyte Antigen (HLA) matched donor or haploidentical donor), to treat disease. Allogeneic haematopoietic stem cell (HSC) therapy was first performed in 1957 by E. Donnall Thomas (Henig & Zuckerman, 2014), whilst autologous HSC therapy was first reported in 1977 by Gorin *et al.* (Gorin, 1998). The introduction of genetically modified autologous cells then quickly followed – first controversially performed, without prior approval from ethics boards, by Cline *et al.* in 1980, who transfected bone marrow cells from thalassemia patients with the human globulin gene prior to re-infusion

(Friedmann, 1992). Following this, R. Michael Blaese's laboratory began to investigate the use of CGT for the treatment of Adenosine Deaminase Deficiency Severe Combined Immunodeficiency (ADA-SCID), a monogenic disorder caused by a genetic defect within the purine catabolic enzyme adenosine deaminase, which results in a toxic build-up of deoxyadenosine triphosphate within T cells, leading to a compromised immune system. ADA-SCID is curable through allogeneic HSC transplantation, however a suitable HLA matched donor is not always available. For this reason, Blaese *et al.* initially attempted the transduction of primate HSCs but discovered that transduction efficiency was limited to the T cells. This spurred on the move to transduction of human peripheral T cells with a viral vector containing the adenosine deaminase (ADA) gene. With success shown within *in vitro* studies, the first successful human clinical trial to treat two patients suffering from ADA-SCID using gene edited T cells was started in 1990 and demonstrated long term persistence of the corrected T cells with re-stored ADA function (Blaese *et al.*, 1995). In later years, methods to efficiently transduce HSC were developed leading to the use of CGT to treat several monogenenic disorders including X-linked Severe Combined Immunodeficiency (X-SCID) (Cavazzana-Calvo, 2000; Hacein-Bey-Abina *et al.*, 2002) and Wiskott-Aldrich Syndrome (WAS) (Braun *et al.*, 2014). The use of CGT to correct monogenic disorders has now advanced to the point that the first product of this kind has been accepted by the European Medicines Agency (EMA) for market authorisation, with GlaxoSmithKline/Telethon Institute for Gene Therapy (TIGET) (now Orchard/TIGET) CGT product, Strimvelis, for the treatment for ADA-SCID (Ylä-Herttuala, 2016).

1.2. Advancement of the Cell Therapy Field

Blaese *et al.* originally used genetically modified T cells for the treatment of ADA-SCID before advancing to the use of genetically modified HSCs for long term correction of faulty genes for the treatment of monogenic disorders. However, the ability to genetically modify T cells was repurposed for the treatment of acquired diseases, particularly cancer, with major successes seen with *ex vivo* gene therapy for the treatment of haematological malignancies, such as B cell Acute Lymphoblastic Leukaemia (B-ALL) (Brentjens *et al.*, 2013; Locke *et al.*, 2015). Initial clinical success with *ex vivo* gene therapy has used Chimeric Antigen Receptor (CAR) technology for

the treatment of haematological malignancies, in which T cells are isolated from the patient's peripheral blood and transduced with a viral vector encoding a CAR specific for an antigen expressed on the surface of tumour cells (further discussed in section 1.4.1.1). Upon re-infusion to the patient, CAR expressing T cells are re-directed to recognise and kill antigen expressing tumour cells. This strategy was successfully used by Novartis who developed the CD19 CAR T product, Kymriah®, for the treatment of B cell lymphoma. This was the first CAR T product to be licensed by the Food and Drug Agency (FDA) in 2017, and was quickly followed by Yescarta®, a CAR T product developed by KITE therapeutics (Ginn *et al.*, 2018).

The use of CAR T therapy for the treatment of solid tumours has been extensively investigated, with approximately 200 clinical trials initiated worldwide by 2021 (Liu & Rui *et al.*, 2021) and promising results from studies investigating a number of tumour-associated antigens, including HER2 (Ahmed *et al.*, 2015; Budi *et al.*, 2022), prostate specific membrane antigen (PSMA) (Perera *et al.*, 2022), Claudin-6 (Mackensen *et al.*, 2021), Claudin 18.2 (Qi *et al.*, 2022), and guanylate cyclase-C (GCC) (Cui *et al.*, 2022). There are aspects of the tumour microenvironment that make the targeting of solid tumours more challenging than haematological cancers, including; the occlusive tumour extracellular matrix and abnormal vasculature, which can prevent CAR T infiltration; abnormal metabolic environment such as hypoxia and low pH, which impact T cell survival; and immunosuppressive factors including recruitment of regulatory T cells (Tregs), production of immunosuppressive cytokines (i.e. TGF beta) and expression of immunosuppressive molecules (i.e. Programmed Death Ligand 1 (PD-L1)), which suppress cytotoxic functionality of T cells (Beatty & O'Hara, 2016; Liu & Rui *et al.*, 2021). However, several methods to overcome the immunosuppressive tumour microenvironment have been utilised to enable the successful targeting of solid tumours. These include, but are not limited to;

- Use of checkpoint inhibitors (i.e. anti-PD-1 antibody and anti-PD-L1 antibody), which can be given in combination with CAR T therapy to prevent suppression of T cell activity (Liu & Rui *et al.*, 2021)
- Use of CAR T cells targeting fibroblast activation protein (FAP), highly expressed on cancer-associated fibroblasts, which are a major component of the tumour-associated stroma that excludes T cells from the tumour microenvironment (Busek *et al.*, 2018)

- Use of indoleamine 2,3 dioxygenase (IDO) inhibitors. IDO, produced by tumour cells, catalyses the breakdown of tryptophan which contributes to T cell suppression. Inhibition of IDO in combination with CAR T therapy can reduce suppression of CAR T cells (Holmgaard *et al.*, 2013)
- Use of CoupledCARs – as used within the GCC19-CAR trial, whereby the solid tumour associated antigen GCC targeting CAR is coupled with a CD19-CAR to amplify the proliferation of solid tumour targeting CAR T cells. (Cui *et al.*, 2022)

Despite initial focus of clinical trials and licensed products on CAR T therapies, there has also been advancements using engineered T cell receptor (TCR) T cell technology, with the differences between the two technologies described further within section 1.4.1.

1.3. Components of Peripheral Blood

Peripheral blood consists of blood cells, including erythrocytes (Red Blood Cells (RBCs)), thrombocytes (platelets) and leukocytes (white blood cells (WBCs)) contained within plasma, which is made up of mostly water but also contains essential clotting factors, proteins, glucose and hormones. RBCs make up the majority of peripheral blood at 93-96%, whilst platelets and WBCs make up 4-7% and 0.1-0.2% of blood cells respectively. Multipotent HSC, which reside within the bone marrow, differentiate to form progenitor cells of one of three lineages, the megakaryocyte/erythrocyte progenitor, the myeloid progenitor and the lymphoid progenitor. These progenitor cells differentiate into all of the cells of their lineage as shown in Figure 2.

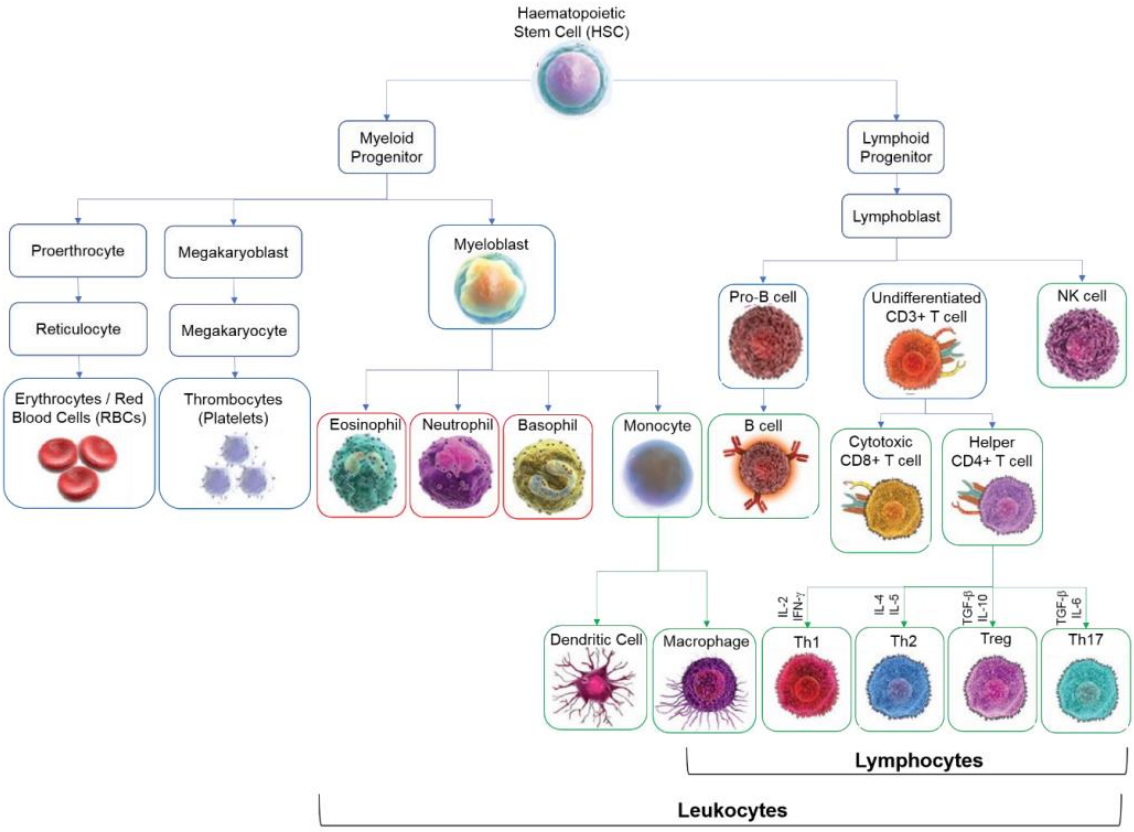

Figure 2: Haematopoiesis

HSC differentiate into all cells of the blood through a process known as haematopoiesis. Polymorphonuclear leukocytes (PMNs) are indicated in red. Peripheral Blood Mononuclear Cells (PBMCs) are indicated in green. Cytokines that drive the differentiation of CD4+ T cells are noted above each subtype. Figure adapted from (PeproTech).

1.3.1. Leukocytes

Leukocytes (also known as WBCs) are involved in the immune response. They arise from both the myeloid and lymphoid lineages and are grouped based on their nuclear morphology and cytoplasmic granularity. Originating from the myeloid lineage, neutrophils, eosinophils and basophils form a group known as the polymorphonuclear leukocytes (PMNs) or granulocytes. Whereas, monocytes and dendritic cells of the myeloid lineage and all the cells of the lymphoid lineage form a group known as Peripheral Blood Mononuclear Cells (PBMCs) or agranulocytes. The frequency of cell types found within the leukocyte population are described within Table 1.

Table 1: Frequency of Leukocyte Lineages

Cell Type	Average Frequency within Leukocyte Population (%)
Granulocytes	45-65
T cells	10-25
B cells	3-10
Monocytes	3-10
NK cells	2-5
Dendritic Cells	0.5-1

Table 1: Average frequency of cells within the leukocyte population (BioRad, 2017)

1.3.2. Peripheral Blood Mononuclear Cells

PBMCs are non-granular cells with a single nucleus, consisting of lymphocytes, monocytes and dendritic cells. The lymphocytes can be further divided into B cells, (maturation in the bone marrow), T cells (maturation in the thymus) and NK cells. The frequency of cell types within the PBMC population are described in Table 2.

It is the PBMC population that is commonly isolated from whole peripheral blood for research purposes using a technique known as gradient density centrifugation. This technique uses Histopaque 1077, which is a solution of high molecular weight sucrose polymers enabling the separation of peripheral blood cells by density. RBCs and PMNs (including neutrophils and eosinophils) have a density greater than 1.077g/ml, resulting in a layer sitting below the histopaque layer after centrifugation. Whereas, PBMCs have a density of less than 1.077g/mL resulting in a layer sitting above the histopaque layer, known as the buffy coat. Basophils can contaminate this buffy coat, as their density can be greater or less than 1.077g/mL. It is this buffy coat layer that is isolated using a Pasteur pipette for the culture of T cells. This method is described in detail within section 3.2.1.

Table 2: Frequency of PBMC cells

Cell Type	Average Frequency within PBMC Population (%)
T cells	45-70
B cells	<15
NK cells	<15
Monocytes	10-30
Dendritic Cells	1-2

Table 2: Average frequency of cell subsets within the PBMC population (Miyahira, 2012)

1.3.3. T cells

T cells, originally known as thymus dependent lymphocytes, originate from HSC in the bone marrow but migrate to the thymus for maturation. There are two lineages of T cells, the majority being alpha:beta T cells with less than 5% gamma:delta T cells (Shah *et al.*, 2021). These lineages are formed through re-arrangements of genes encoding the T cell receptor (TCR), with heterodimers formed between TCR alpha and TCR beta chains or TCR gamma and TCR delta chains. The alpha:beta TCR heterodimers form complexes with CD3 protein dimers, including an epsilon:delta heterodimer, an epsilon:gamma heterodimer and a zeta:zeta homodimer (Figure 3). There are 10 immunoreceptor tyrosine-based activation motifs (ITAMs) present across the three CD3 dimers, one ITAM on each epsilon, gamma and delta chain and three ITAMs on each zeta chain. In absence of peptide binding to the MHC complex, the intracellular domains of the CD3 chains remain in close proximity, preventing the phosphorylation of ITAMs by protein tyrosine kinases, which is required for signal transduction (Shah *et al.*, 2021).

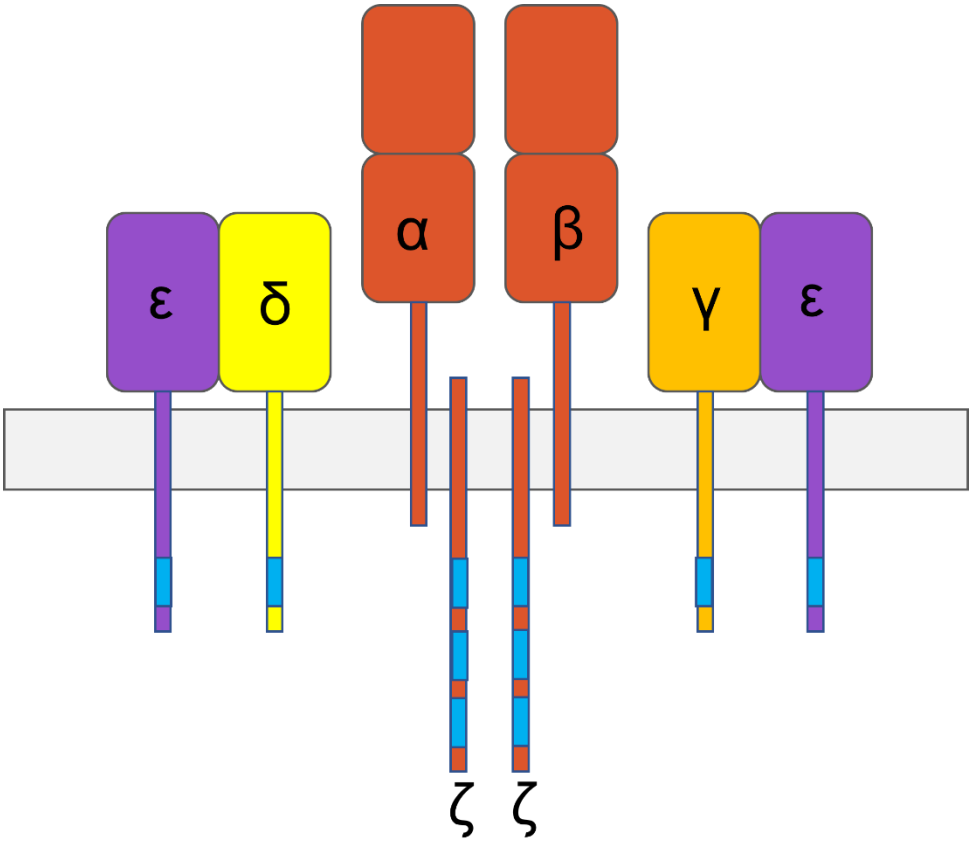

Figure 3: TCR Complex of alpha:beta T cells

The TCR complex of alpha:beta T cells is formed of a heterodimer of alpha and beta TCR chains associated with three CD3 protein dimers via non-covalent hydrophobic interactions. These include an epsilon:delta heterodimer, an epsilon:gamma heterodimer and a zeta:zeta homodimer. The 10 ITAMs present on the CD3 dimers are shown in blue.

Within the thymus, alpha:beta T cells undergo a process of negative selection in which T cells bearing TCRs with high affinity for self-peptide major histocompatibility complex (MHC) undergo apoptosis removing potentially self-reactive T cells, whilst those with low affinity TCRs are allowed to differentiate into mature double positive T cells (CD4+ and CD8+) (Shah *et al.*, 2021). These double positive T cells then undergo positive selection against a self-peptide presented by the two classes of MHC that are expressed on thymic epithelial cells. This process of positive selection differentiates double positive T cells into naïve single positive CD8+ (cytotoxic) T cells or CD4+ (helper) T cells, which leave the thymus and enter peripheral lymphoid organs (Parham, 2009).

The TCR of CD4+ T cells binds to peptides displayed within the context of MHC Class II, which is only expressed on specialised antigen presenting cells (macrophages, dendritic cells and B cells). These antigen presenting cells phagocytose exogenous proteins, process the peptide and display it within MHC Class II (Figure 4). CD4+ T cells with complementary TCRs will recognise non-self peptides and activate, functioning as helper T cells to boost the responses of other cell types of the immune system. Upon activation CD4+ T cells will differentiate into further subtypes based on cytokines within the immediate environment (Figure 2).

The TCR of CD8+ T cells binds to peptides displayed on the surface of all nucleated cells within MHC Class I. MHC class I displays peptides processed from endogenous antigens (Figure 4), which enables CD8+ T cells to survey all nucleated cells ensuring that only self-peptides are presented. In cases in which a nucleated cell has been infected with a virus, viral proteins will be processed within the Golgi Apparatus and a non-self-peptide will be presented within MHC Class I. CD8+ T cells with complementary TCRs recognise the non-self-peptides expressed in the context of MHC Class I and will activate when the appropriate co-stimulatory signal, such as CD28 engagement, is provided. CD8+ T cells release perforin, to form pores within the target cell, and granzyme to initiate apoptosis of the infected cell (Parham, 2009).

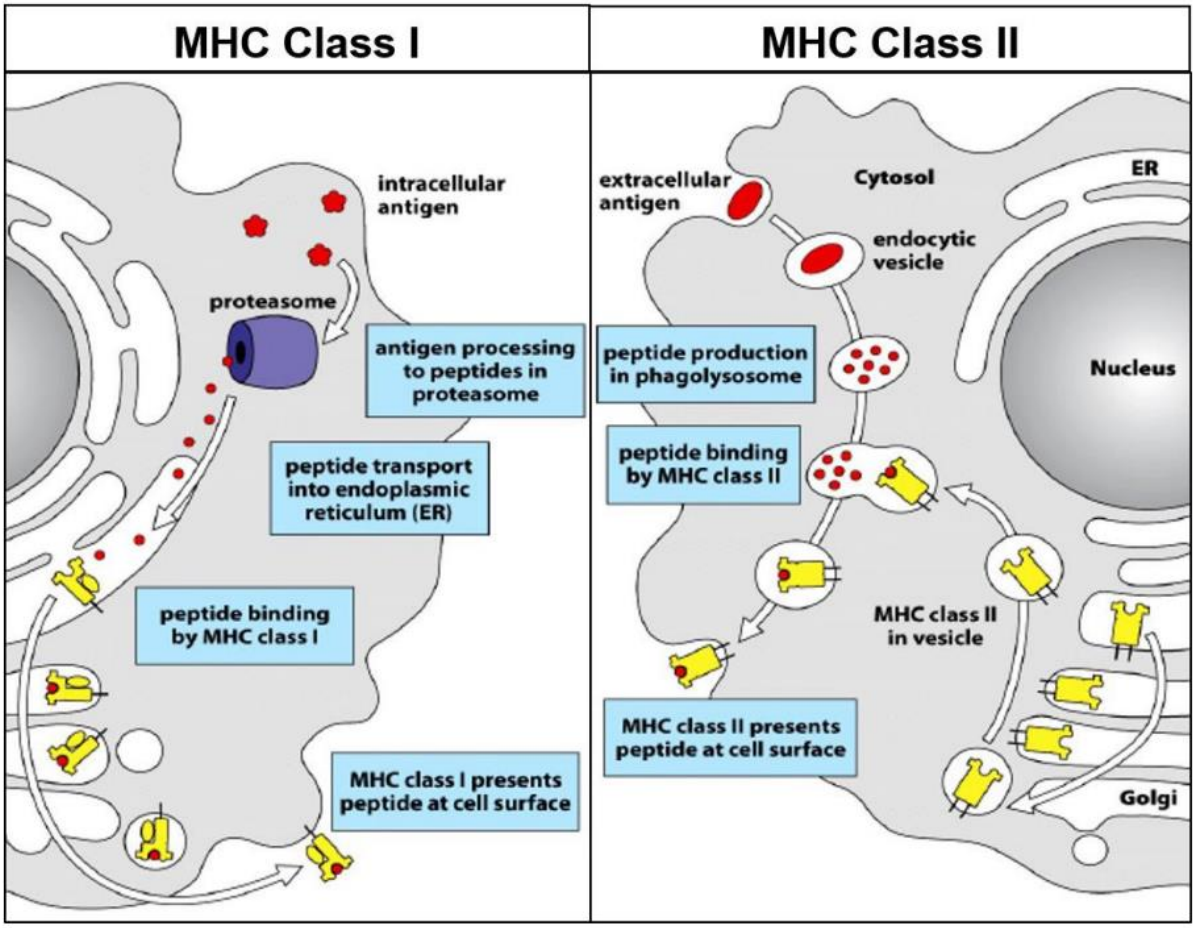

Figure 4: MHC Processing of Endogenous and Exogenous Proteins

Exogenous antigens are engulfed by antigen presenting cells and the proteins are processed within the endocytic processing pathway for expression in MHC Class II and presentation to CD4+ T cells. Within all nucleated cells, endogenous antigens are processed within the Golgi Apparatus for expression in MHC Class I for presentation to CD8+ T cells. Image reference (Parham, 2009)

1.3.4. T Cell Differentiation

Once a naïve T cell has encountered its cognate antigen in the context of MHC and become activated, it will differentiate into an effector T cell (T_{EFF}), a subset of T cell that has enhanced cytotoxic ability and proliferative capacity to rapidly kill targeted cells. A subset of activated T cells will differentiate into memory phenotype T cells, including Stem Cell Memory (T_{SCM}), Central Memory (T_{CM}) and Effector Memory T cells (T_{EM}) - each of which have distinct phenotypic and functional properties (Mahnke

et al., 2013). T_{SCM} demonstrate enhanced self-renewal properties with the ability to differentiate into T_{CM}, T_{EM} or T_{EFF} cells (Xu *et al.*, 2015). In addition to this, they are long-lived memory cells and are therefore a particularly interesting subset of T cells for cell therapies due to their ability to persist and re-populate the T cell pool upon antigenic re-stimulation, however T_{SCM} only make up around 2-4% of the total T cell population (Xu *et al.*, 2015).

T_{CM} and T_{EM} cells differ based on their expression of CCR7 and CD62L. T_{CM} express CCR7 and CD62L, which enable T_{CM} homing to secondary lymphoid tissues. Whilst T_{EM} cells are characterised by a lack of CCR7 and CD62L expression and a rapid effector function, similar to that seen in T_{EFF} (Mahnke *et al.*, 2013). T_{CM} have been shown to be capable of differentiating into T_{EM} *in vitro,* but T_{EM} are not able to differentiate into T_{CM} (Sallusto *et al.*, 1999). T_{EFF} have an increased susceptibility to exhaustion and activation induced cell death, which limits *in vivo* persistence (McLellan & Ali Hosseini Rad, 2019). Therefore, within T cell therapies, T_{EFF} are beneficial for an initial rapid cytotoxic attack on tumour cells, but memory T cell populations are critical to maintain a persistent onslaught.

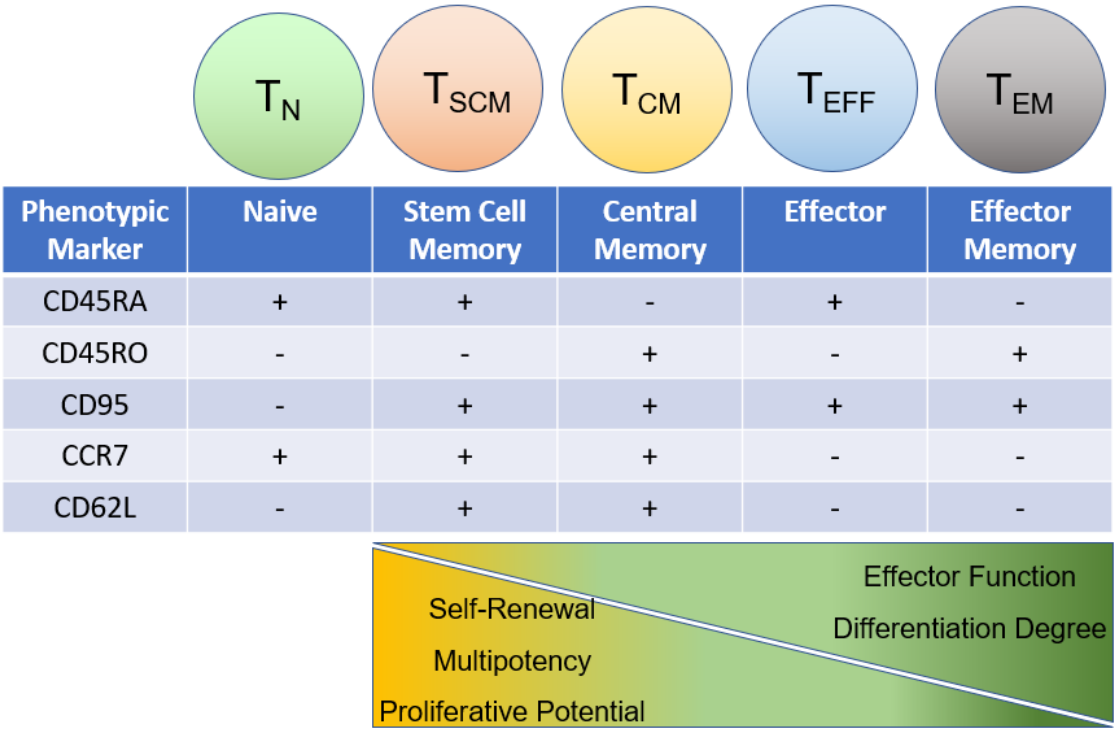

Figure 5: Differentiation of T cells

T cell subsets can be differentiated based upon the expression of phenotypic markers and distinct functionalities. Image adapted from (Xu et al., 2015)

1.4. Development of Cell Therapies

There are several stages to the development of a cell therapy product (Figure 6), with the initial focus within the discovery phase upon choosing a suitable target antigen. Target antigen choices are usually made through literature searching to identify targets that are novel, have selective or differentiated expression upon tumour cells and which are targetable by a cell therapy. The choice of target also helps to inform upon the type of cell therapy that will be utilised, whether it be CAR T or engineered TCR T cell therapy. Once a target has been selected, sufficient evidence must be gathered to link the target antigen with a desired change in disease biology enabling commitment to further investigate the development of a therapy against the selected target antigen. The milestones described are specific to GSK's development process, however the criterion for each milestone is common across industry.

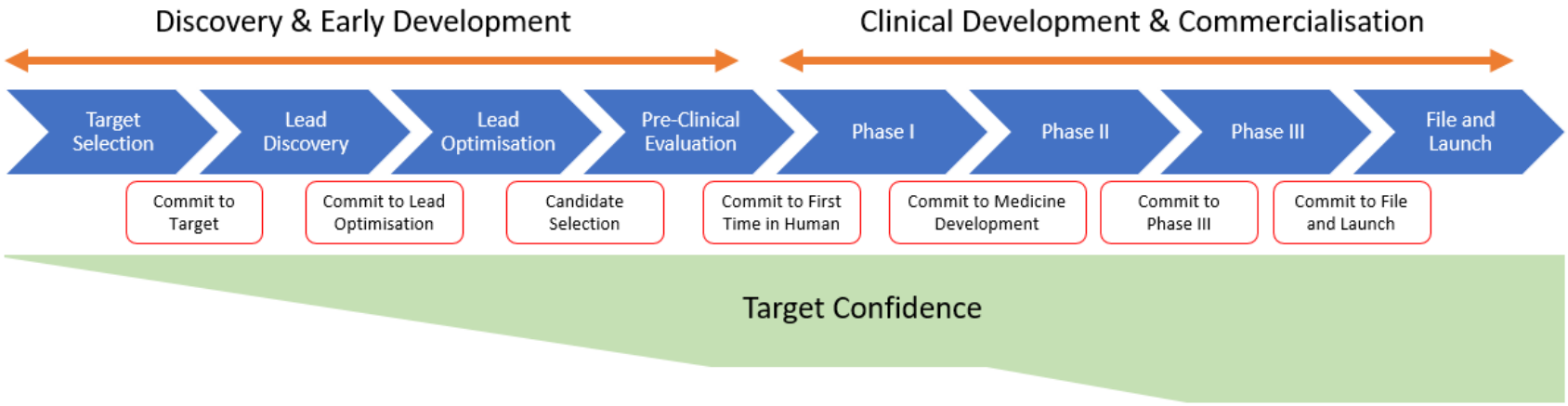

Figure 6: Drug Discovery Process

A schematic to describe the drug discovery process from early development through to clinical development and commercialisation of the product, displaying key GSK milestones through the process and the level of target confidence. Process improvements within the discovery and early development phase could help to reduce cost of goods. Once the "commit to target" milestone has been achieved, the cost of development is high as there is a large pool of candidate constructs that require screening. The "lead discovery" phase initiates the design of constructs; analysis of T cell expression and impact upon T cell viability; analysis of binding ability and functionality and assessment of off-target binding. It is within this "lead discovery" phase when there is a large pool of construct candidates that early identification of constructs with off-target binding potential could help to reduce the costs through the reduction of the number of shortlisted constructs. Once the lead candidates have been chosen, and the "commit to lead optimisation" milestone is met, investigations will focus on the optimisation of the chosen constructs. Within this phase of development, it would be beneficial to optimise processes to help to improve cell expansion and transduction efficiency, which helps to provide sufficient numbers of transduced and viable T cells for the vast number of studies required during this stage and can also help to provide key information to help optimise the large-scale manufacture of the cell product. The final stage of the discovery and early development phase is the pre-clinical evaluation of the final candidate construct, and potentially a backup construct. Within this phase, in vivo efficacy and safety studies are performed. Confidence within the chosen construct increases allowing for the "commit to first time in human" milestone to be achieved once the necessary quality criteria have been passed. Within the clinical development and commercialisation phase, the chosen candidate is optimised and passed through three phases of clinical study prior to product launch.

Once the “Commit to Target” milestone has been met, the discovery phase can continue with the generation of a pool of potential candidate constructs, CAR T or engineered TCR. At this point in development, there are a large number of potential candidates that need to be further investigated which requires a significant investment of time, resource and funding in order to successfully choose a limited number of lead constructs to progress into the “Lead Optimisation” phase of development. Within this phase, a shortlist of lead candidates is further investigated for suitability with the initiation of early *in vivo* efficacy and toxicity studies, increasing the confidence in the choice of the final candidate. Subsequent to extensive testing, a single candidate is progressed into pre-clinical evaluation progressing past the “Candidate Selection” milestone and enabling extensive safety studies to be performed in addition to optimising the manufacture of the product. At this point confidence in the target would be at a point at which a decision can be made as to whether the therapy is suitable for progression from early non-clinical development into clinical development with the commitment to progress into clinical trials through first-time-in-human studies to pivotal studies and eventual commercial launch of the product.

The discovery and early development phase of the drug discovery process for cell therapy products, including assessments and optimisation performed during the development of a cell therapy product, will be discussed in more detail below.

1.4.1. Choice of Construct (CAR vs TCR)

Both CAR T cells and engineered TCR T cells are able to re-direct the immune system to target novel cancer antigens, but the method of recognition differs between the two formats, which impacts upon the choice of antigen target.

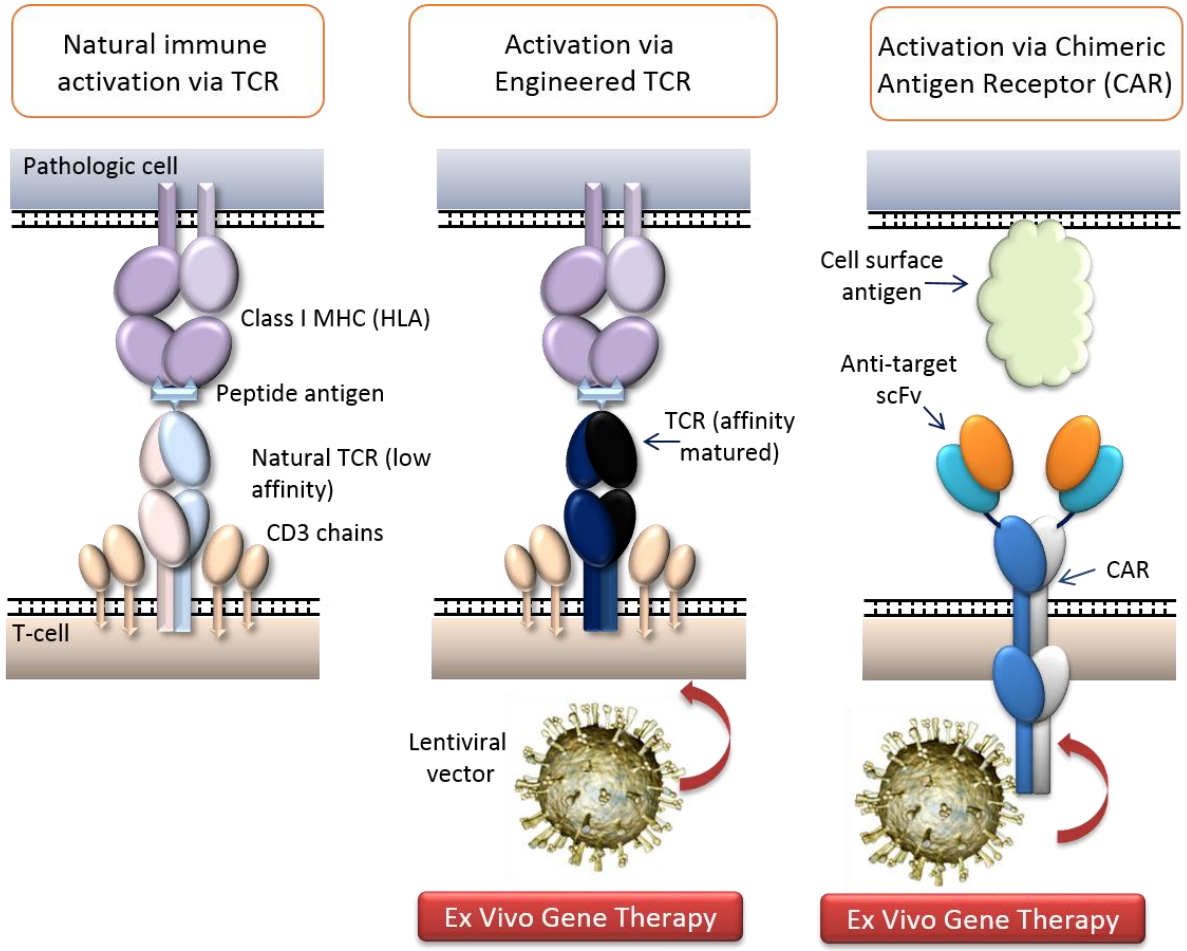

Figure 7: Natural TCR, Engineered TCR and CAR.

Natural TCRs are low affinity and bind to target peptides in the context of major histocompatibility complex (MHC) with signal transduction processing through the CD3 complex. Engineered TCRs are affinity matured TCRs expressed within T cells via lentiviral vector transduction. Signal transduction utilises the CD3 complex. CARs consist of a single chain variable fragment (ScFv) binding domain, generated through the modification of a monoclonal antibody (mAb), fused to a transmembrane domain and a signalling complex. CARs bind to cell surface antigens and do not rely on the endogenous CD3 complex for signal transduction. (Figure created at GSK).

1.4.1.1. CAR T cells

CARs are generated through the modification of a monoclonal Ab (mAb) to form an antigen recognition domain that recognises a tumour-specific antigen. The antigen recognition domains of the variable light (vL) and variable heavy (vH) chains of a mAb are re-formatted to form a Single Chain Variable Fragment (ScFv). The ScFv domain on CAR T cells enables MHC independent T cell recognition, thereby enabling T cells to directly target antigens on the surface of a tumour cell. Additional intracellular signalling domains, and co-stimulatory domains are required within the construct to enable activation of the T cell.

There have been several advancements on the CAR construct architecture (Figure 8), with first generation CAR T cells consisting of a CD3z intracellular signalling domain, whilst second and third generation CAR designs include additional co-stimulatory domains, such as CD28 (used in the Yescarta® CAR construct) and 4-1BB (used in the Kymriah® CAR construct) (Boyiadzis *et al.*, 2018). The inclusion of co-stimulatory domains enables full activation of CAR T cells by providing both of the required activation signals, which is thought to improve proliferation and persistence of CAR T cells (Kawalekar *et al.*, 2016; Guedan *et al.*, 2018).

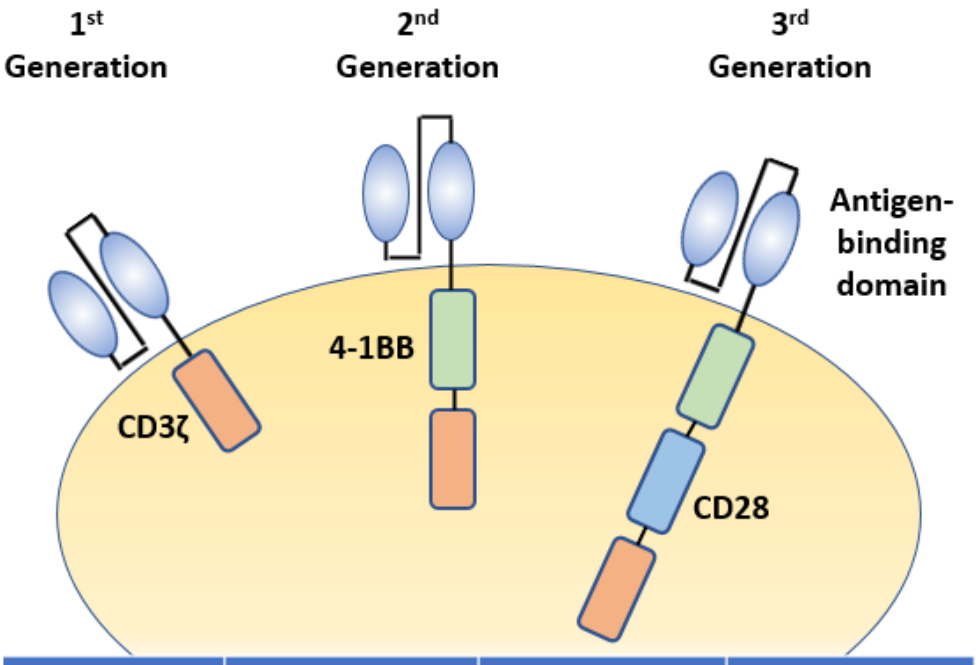

	1st Generation	2nd Generation	3rd Generation
Cytotoxicity	+	++	++
Proliferation		+	++
Persistence			+

Figure 8: Generation of CAR Constructs

First generation CARs consisted of simply a CD3z intracellular signalling domain. Additional intracellular co-stimulatory domains, such as CD28 (used in Yescarta®) or 4-1BB (used in Kymriah®) were included within second generation CAR designs to improve functionality. Third generation CAR designs include several co-stimulatory domains in the hope to improve the persistence.

Despite the successes of CAR T therapies within the haematological cancer field, there have not been such successes within the solid tumour field due to the lack of tumour specific cell surface antigens. With only 15% of a cells proteome expressed as cell membrane proteins, there is a vast number of intracellular proteins that are inaccessible to targeting by CAR T cells (He *et al.*, 2019). However, the diversity of antigens able to be targeted by CAR T cells is greater than that of engineered TCR T cells due to the ability to bind proteins, carbohydrates and glycolipid molecules (Wei

et al., 2019) – which expands the number of available tumour antigen targets to not only those in which neoantigens are expressed on the surface of tumour cells, but also to enable targeting of tumour antigens in which aberrant glycosylation, carboxylation or expression may be the differentiating factor between healthy and tumour cells.

The ideal tumour cell target antigen for CAR T therapy would be one that is highly expressed upon tumour cells, with no expression on healthy cell populations. However, tumour antigens of this sort are rare, therefore some exceptions can be made – for example targets that have high expression in tumour cells and are also expressed on healthy cells but with limited adverse effect if healthy cell killing occurs, as is the case in B cell lymphoma (Wei *et al.*, 2019); expression of targets on cancer cells that are only otherwise expressed within immunological privileged sites; differential glycosylation or carboxylation of tumour antigens compared to the equivalent antigen on healthy cells, i.e. the expression of the tumour-associated carbohydrate antigen disialylganglioside GD2 within melanoma, neuroblastoma and retinoblastoma (Berois *et al.*, 2022); and finally differential expression of antigens – for example those that are only accessible to CAR T cells within a disease state, such as isoforms of tight junction proteins, including the stomach specific isoform Claudin 18.2, which are occluded within tight junctions in healthy tissues and only accessible to CAR T cells within the disease state (Lenz *et al.*, 2022; Qi *et al.*, 2022).

To initiate contact-dependent cytotoxicity between a CAR T cell and an antigen expressing tumour cell, the formation of an immune synapse must occur. The architecture of CAR T cells, including spacer elements, can be modified to ensure proper formation of the immune synapse allowing for activation and efficient cytotoxicity. Epitope mapping enables the study of the binding points between CAR T cells and antigens to enable CAR stoichiometry to be adjusted to provide the optimal immune synapse. The study of the 3D conformation of target antigens is essential as this determines the binding of CAR T cells, it is important to assess whether homologous binding sites are shared with a non-target antigen due to similar 3D conformation, which could result in off-target binding to an unknown target. This toxicity has not yet been observed within clinical trials for CAR T cells, but has been observed for engineered TCR T cells (Brudno & Kochenderfer, 2016), such as the MAGE-A3 TCR described in more detail within sections 1.4.1.2 and 1.4.1.4.2. There is high target specificity for CAR T cells, which reduces the risk of cross-reactivity,

however, this also enables the possibility of antigen masking or downregulation by tumour cells preventing cytotoxicity and leading to failure of the therapy.

1.4.1.2. Engineered TCR T cells

Engineered TCR T cells consist of an affinity matured TCR, which can only bind to processed antigen peptides within the MHC context. Engineered TCRs are able to utilise T cell endogenous signalling pathways and do not require additional co-stimulatory domains. The utilisation of endogenous signalling pathways may improve the safety of engineered TCR T cells by restricting their activation through endogenous checkpoint inhibitors.

The advantage of engineered TCR T cells over CAR T cells is the ability to target the other 85% of the cellular proteome that is intracellularly expressed, which vastly expands the number of potential tumour specific antigens, including those that may be produced through aberrant intracellular processes occurring within tumour cells. In addition to this, the antigenic load required for activation of TCR T cells is low compared to CAR T cells. However, as engineered TCR T cells are only able to recognise peptides in the form of MHC, this does prevent their use against other antigen targets, such as carbohydrates and glycolipids. TCR T cells can only be used to treat patients with matched HLA haplotypes, reducing the number of suitable patients. Research is currently focussed upon the HLA-A*02 haplotype which is the most common haplotype within G8 countries (Bentzen & Hadrup, 2019).

Epitope mapping for TCR T cells investigates the binding of TCR T cells to the small peptide fragment presented in the context of MHC. The processing of tumour antigens required by TCR T cells could potentially increase the risk of cross-reactivity (Cameron *et al.*, 2013; Linette *et al.*, 2013) due to the presentation of only a fragment of the peptide, compared to CAR T cells which can bind larger epitopes in their native form. As was described for CAR T cells, the 3D conformation of the binding peptide within the context of MHC was also shown to be critically important for the specific binding of engineered TCR T cells. Within a trial investigating a MAGE-A3 TCR, cross-reaction with an unrelated protein, Titin, was observed (Linette *et al.*, 2013) and further studies elucidated that the peptide conformation within MHC bound by the engineered TCR

resulted nearly identical conformation, with complementarity determining region (CDR) loops and TCR crossing angles identical for the two unrelated peptides (Raman *et al.*, 2016).

This risk of cross-reactivity is increased by the innate degeneracy of TCRs. Endogenous TCRs are thought to be able to target as many as 10^6 different MHC bound peptides (Bentzen & Hadrup, 2019), with this flexibility in peptide recognition helping to prevent immune escape. The same degeneracy of peptide recognition occurs with engineered TCR T cells, which helps to reduce the risk of tumour escape due to antigen modification, but also increases the risk of off-target off-tumour binding events (Bentzen & Hadrup, 2019).

Despite the decreased risk of therapy failure due to antigen loss compared to CAR T therapies, the requirement for peptide presentation in the context of MHC for engineered TCR T cells increases the risk of tumour escape through downregulation of HLA expression (Wei *et al.*, 2019).

The ratio of endogenous to exogenous TCR alpha and beta chains is of high importance during engineered TCR production, due to the formation of TCRs through the heterodimerisation of alpha and beta TCR chains. There is a risk of heterodimerisation occurring between engineered (exogenous) TCR chains and endogenous TCR chains, which could form TCRs with unknown specificity, risking autoimmunity (He *et al.*, 2019). However, advancements have been made to reduce the risk of heterodimerisation with endogenous TCRs including mutation of the constant region of engineered TCR alpha and beta chains through the introduction of additional cysteine bridges or modification of key amino acids (He *et al.*, 2019).

1.4.1.3. Class Safety Risks

Both CAR T and engineered TCR technologies have shared safety risks due to the fact that they are therapies that utilise the adoptive transfer of genetically modified T cells. Some of the class safety risks and monitoring/mitigation strategies are provided as a summary within Table 3, with cytokine release syndrome (CRS) and immune effector cell-associated neurotoxicity syndrome (ICANS) explained in further detail within sections 1.4.1.3.1 and 1.4.1.3.2.

Table 3: Class Safety Risks

Safety Concern	Symptoms	Monitoring / Mitigation Strategy
Cytokine Release Syndrome (CRS)	Mild: Fever and Myalgia Severe: Hypotension, pulmonary œdema and severe inflammatory syndrome	Availability of tocilizumab Monitoring of cytokine levels within patients displaying symptoms
Immune Effector Cell-Associated Neurotoxicity Syndrome (ICANS)	Speech impediments, altered level of consciousness, impairment of cognitive skills, motor weakness, seizures, and cerebral edema.	Baseline and follow-up brain CT or MRI scans to be performed to monitor progression. Consultation with neurologist. Stopping of treatment if cerebral œdema that does not respond to treatment is identified. Use of Anakinra (recombinant human interleukin-1 receptor antagonist)
Haematopoietic Cytopenia / Infections	Fatigue, weakness, shortness of breath, dizziness, fever, confusion	Irradiation of transfused blood products. Availability of treatment for cytopenia and infection.
Graft vs Host Disease (GvHD)	Acute: A rash, nausea, jaundice Chronic: Dry mouth, ulcers, difficulty eating, rash, gastrointestinal ailments, shortness of breath, jaundice	Personnel available with knowledge of GvHD management and bone marrow transplantation consultants. Irradiation of transfused blood products.
Hypersensitivity	Allergic reaction, including anaphylaxis, against excipient within the cell therapy product (i.e. DMSO)	Monitoring for signs of hypersensitivity reactions before and after infusion

Table 3:Class safety risks are those associated with the type of therapy and are shared between CAR T and engineered TCR T cell therapies.

1.4.1.3.1. Cytokine Release Syndrome (CRS)

CRS is a rapid onset adverse event that has been observed within many clinical trials after infusion of CAR T products (Kochenderfer *et al.*, 2012; Grupp *et al.*, 2013; Lee *et al.*, 2015). CRS occurs due to the release of a large amount of cytokines, including IFN-γ and IL-6, with clinical symptoms ranging from mild fever-like symptoms and myalgia to severe and even life-threatening symptoms, including hypotension, pulmonary œdema and severe inflammatory syndrome (Maude & Barrett *et al.*, 2014). In the most severe cases, death has resulted, as occurred in the Juno Therapeutics CD19-CAR trial in which 5 patients died due to CRS associated cerebral œdema (Johnson & June, 2017). High levels of IFN-γ are thought to be an indication of effective CAR T cell activation, and some level of CRS may even be beneficial for efficacy with some trials correlating patients that achieved complete response with the most severe cases of CRS (Maude & Barrett *et al.*, 2014). High levels of IL-6 are believed to be an indication of macrophage activation syndrome (MAS) (Casucci *et al.*, 2015), with CRS symptoms that progressed into symptoms indicative of MAS in one CD19-CAR trial (Grupp *et al.*, 2013). The role that IL-6 plays within CRS has been further demonstrated by the amelioration of CRS through administration of the IL-6 receptor blocking mAb tocilizumab (Grupp *et al.*, 2013). Management and prediction of CRS is difficult, with contradicting results in patients treated early with corticosteroids, with some studies suggesting that partial response observed in patients was due to the early treatment of CRS (Porter *et al.*, 2011), and other studies demonstrating no impact on the efficacy of CAR T therapy (Grupp *et al.*, 2013). Current clinical recommendations are to carefully increase the dose of CAR T cells infused and provide tocilizumab to ameliorate symptoms of CRS.

1.4.1.3.2. Neurotoxicity

Neurological effects on patients have been observed in multiple clinical trials in conjunction with CRS (Maude & Frey *et al.*, 2014; Lee *et al.*, 2015; Gust *et al.*, 2017). In a study investigating neurological adverse events within 113 patients, 40% of patients suffered from a neurological adverse event, ranging from headaches and delirium to decreased consciousness and death (Gust *et al.*, 2017). Within this study,

it was found that 100% of patients that had serum levels of IL-6 over 500pg/mL developed a grade 4 neurotoxic adverse event, and suggested that systemic inflammation observed was due to CRS, which led to endothelial activation and capillary leakage allowing cytokines to enter the brain (Gust *et al.*, 2017; Shalabi *et al.*, 2018). Neurotoxicity has also been observed in response to off-target binding, for instance the MAGE-A3 engineered TCR which resulted in cerebral œdema (Morgan *et al.*, 2013) – this study is described in more detail within section 1.4.1.4.2. A neurological assessment checklist was proposed by Shalabi *et al.* (Shalabi *et al.*, 2018) for the assessment of patients during and subsequent to infusion of CAR T cells, in the hope of enabling a comparison of neurological impact observed between clinical trials. The IL-1 receptor antagonist, Anakinra, has been used clinically to manage ICANS and has been shown to be effective for the treatment of both CRS and ICANS, whilst tocilizumab has only shown efficacy in the treatment of CRS (Strati *et al.*, 2020; Cohen *et al.*, 2022).

1.4.1.4. Technology Safety Risks

The safety risks associated with the technologies differ in many aspects, but there are also shared technology risks due to the shared processes of manufacture for CAR T and TCR T cell therapies.

1.4.1.4.1. On-Target Off-Tumour Binding

As previously discussed, the ideal target would be one that is exclusively expressed upon tumour cells with no expression on healthy cells. On-target off-tumour binding describes the situation in which the cell therapy binds to the target antigen which is expressed upon healthy tissue. Some on-target, off-tumour events can be easily predicted and managed – for example with CD19-CAR T therapies, both tumour cells and healthy B cells express CD19 on their surface leading to cytotoxicity of healthy B cells and B cell aplasia. This can be sufficiently managed by providing human globulin replacement therapy in conjunction with CAR T therapy (Porter *et al.*, 2011, Brentjens *et al.*, 2013; Grupp *et al.*, 2013).

Other on-target, off-tumour binding events are not as easily predicted – with a notable case being within a clinical trial using an ErbB2 CAR T cell directed to target HER2 expressing tumours, which are often treated using the mAb Herceptin without serious adverse events. Within this trial, a third generation CAR T cell was infused into a lymphodepleted patient and within 4 hours the patient was suffering respiratory distress, which resulted in death. Researchers postulated that the ErbB2 CAR T cells recognised low levels of ErbB2 expressed on normal lung cells, resulting in activation and release of inflammatory cytokines which lead to pulmonary œdema (Morgan *et al.*, 2010). This case highlights the importance of thorough investigation of antigen expression, even low-level expression, particularly in high-risk organs and first pass organs in which CAR T cells pass through initially. It must be noted, that subsequent ErbB2 trials using second generation CAR T cells have reportedly had no such adverse event (Casucci *et al.*, 2012). This highlights that the toxicity observed with the Morgan *et al.* ErbB2 CAR T cell was specific to this CAR binder or architecture, but the reason for the toxicity is currently undetermined. This finding has enabled the continued study of ErbB2 as a target for CAR T cells.

Due to the high potency of cell therapies, it is essential to properly assess target expression throughout the body to determine the risk associated with on-target off-tumour binding. Both literature searching and well-established cell models can be utilised to investigate the expression of selected targets.

1.4.1.4.2. Off-Target Off-Tumour Binding

Off-target off-tumour binding describes situations in which a cell therapy binds to an antigen that is not the intended target that is expressed on healthy tissues. For CAR T therapies, epitope mapping and understanding how the 3D conformation of the intended antigen target impacts upon CAR binding is essential for the prediction of off-target off-tumour binding events.

Within engineered TCR T cell therapies, the prediction of off-target off-tumour binding events is more complicated due to the innate degeneracy of TCR-MHC complex specificity, which was explained in more detail within section 1.4.1.2.

In one clinical study an engineered TCR targeting Melanoma Associated Antigen A3 (MAGE-A3) bound to MAGE-A12, which was expressed at low levels in the brain – resulting in cerebral œdema, demyelination and the death of two patients (Morgan *et al.*, 2013). It is currently unknown whether MAGE-A3 specific engineered TCR T cells trafficked directly to the brain in response to low levels of MAGE-A12 expression or whether micro-metastases of MAGE-A3 expressing tumour cells in the brain caused the initial trafficking and activation of TCR T cells, resulting in additional targeting of healthy MAGE-A12 expressing cells. However, if driven by the cross reactivity with MAGE-A12 this adverse event could have been predicated with *in silico* mapping, due to the sequence homology between the two MAGE family members and demonstrated through subsequent *in vitro* studies.

A serious adverse event leading to death also occurred within another trial investigating a MAGE-A3 TCR, which was found to recognise an unrelated peptide derived from Titin, expressed within striated muscle within the heart (Linette *et al.*, 2013). Pre-clinical safety screening of the TCR product should have picked up this off-target binding event, however it was discovered that Titin was not expressed on standard cultured cardiomyocytes, with antigen expression only found on actively beating cardiomyocytes derived from inducible pluripotent stem cells (iPSC). This demonstrates the importance of suitable pre-clinical testing using well validated cell lines with accurate representation of *in vivo* protein expression.

In light of these adverse events, methods have been developed to identify the key amino acids required for TCR binding. One such method is the use of combinatorial peptide libraries in which versions of 9mer target peptide are created whereby a single amino acid is fixed whilst every other amino acid within the 9mer is modified. Through subsequent testing of TCR recognition to the newly created pool of peptides it is possible to identify the key amino acids required for binding and recognition between the TCR and peptides (Bentzen & Hadrup, 2019). An alternative method that improves upon the use of combinatorial peptide libraries by enabling the presentation of peptides within the MHC context is the use of a yeast display system, in which random peptide sequences are created and displayed within yeast cells linked to an MHC complex. TCR T cells are tested against MHC-Peptide expressing yeast cells to identify binding hits and amino acids that are key to the interaction between TCRs and MHC-complexed peptides (Bentzen & Hadrup, 2019). This method was successfully

used to identify key amino acids that were shared between MAGE-A3 and Titin derived peptides, which resulted in the off-target binding event observed within the Linette *et al.* trial (Gee *et al.*, 2018).

1.4.1.4.3. Insertional Mutagenesis

Alongside the successes observed within many cell and gene therapy clinical trials, concerns have also been raised regarding the risk of insertional mutagenesis upon integration of the vector carrying a transgene into the cell genome. This is a risk associated with both CAR T and engineered TCR T cell therapies, as both utilise viral vectors for the delivery of the transgene into T cells.

The risk of insertional mutagenesis was most notably observed within clinical trials conducted in both France and London by Hacein-Bey-Abina *et al.* (Hacein-Bey-Abina *et al.*, 2003) and Gaspar *et al.* (Gaspar *et al.*, 2004) respectively. Ten patients were recruited per study, in which HSC were transduced with a gamma retroviral vector (RVV) containing the gamma-chain of the IL-2 receptor (IL2RG) that was used to treat the monogenic disorder, X-SCID. Initially, the youngest two participants recruited to the French clinical trial developed T cell lymphoma, that was associated with insertion within the LM02 locus, leading to enhanced activation of the LM02 gene (Hacein-Bey-Abina *et al.*, 2003). Over the subsequent 2 to 6 years, a total of five patients developed T cell lymphoma as a result of the gene therapy (Check, 2005; Baum, 2007; Hacein-Bey-Abina *et al.*, 2008). Oncogenesis has not only been limited to use of RVV, with the development of hepatocellular carcinoma observed in long term rodent studies using AAV vectors (Donsante *et al.*, 2001; Chandler *et al.*, 2015; Nault *et al.*, 2015) and also within mouse studies using lentiviral vectors (LVV) with long terminal repeats (LTR) containing strong promoters (Montini *et al.*, 2009). It must be noted that both of these are animal studies, and therefore the results may not be applicable to human clinical trials. Most recently, there was a suspected incidence of Acute Myeloid Leukaemia (AML) development within a trial of BlueBird Bio's LentiGlobin™ treatment (Taylor, 2021) which uses a lentiviral vector for the treatment of Sickle Cell Disease, however the integration site was later identified to be within the VAMP4 gene, which has been shown to have no known association with AML (BlueBird Bio).

In light of these results, significant research has been performed to attempt to determine the integration profiles of different viral vectors and assess the risk of genotoxicity and tumourigenesis (Baum *et al.*, 2003; Hacker *et al.*, 2006; Bokhoven *et al.*, 2009; Montini *et al.*, 2009; Biffi *et al.*, 2011; Chandler *et al.*, 2015), with research indicating that RVV preferentially integrate near promoter/enhancer regions, whilst LVV integrate into actively transcribed regions of genes (Elleder *et al.*, 2002; Schröder *et al.*, 2002; Wu *et al.*, 2003; Mitchell *et al.*, 2004; Wang *et al.*, 2009; Šenigl *et al.*, 2017; Poletti & Mavilio, 2018). This highlights the potential difference in risk depending on the type of vector utilised within trials, as the preference to integrate near promoter/enhancer regions could result in an increased likelihood of an insertion by RVV modulating the expression of proto-oncogenes or tumour-suppressor genes, leading to oncogenic insertions. LVV integration, on the other hand, has been shown to preferentially occur within genes, which is more likely to alter the gene product than the expression of the gene. Orchard Therapeutics recently reported a case of T cell lymphoma within a patient being treated with the gamma-RVV gene therapy, Strimvelis, developed for the treatment of ADA-SCID (Orchard Therapeutics). This was the only case of insertional mutagenesis within their cell therapy product pipeline, which otherwise consists of exclusively lentiviral vector based gene therapies (Orchard Therapeutics) – which may correlate with the perceived increased risk of RVV compared to LVV. In addition to this, the risk of insertional mutagenesis is also thought to be dependent on the cell type transduced, with an increased risk of oncogenesis with HSC transduction compared to T cell transduction.

1.4.2. Choice of Viral Vector

Viruses are extremely efficient at gaining entry to host cells, which has made them an ideal candidate for the delivery of gene therapies. To convert wild-type viruses into a safe and efficient delivery method, pathogenic genes are removed whilst genes controlling replication and packaging are split over several plasmids, as shown in Figure 9 and Figure 10, which prevents the formation of replication competent viral particles. There are several types of viral vectors which have been utilised within CGT, details of some of these viral vectors are described in Table 4.

Vectors generated through the modification of gamma-RVV and LVV have been used most for *ex vivo* gene therapies, whilst AAV have been used within *in vivo* gene therapies. Within this report, the focus will be upon *ex vivo* gene therapies – therefore further details of just RVV and LVV will be provided within sections 1.4.2.1 and 1.4.2.2.

Table 4: Details of Selected Viral Vectors

Viral Vector	Enveloped or Non-Enveloped	Integrated or Episomal	Immunogenicity	Recommended Packaging Capacity	Other features
Retroviral Vectors	Enveloped	Integrates into host genome	Low	8kb	Only integrates in dividing cells
Lentiviral Vectors	Enveloped	Integrates into host genome	Low	8kb	Can integrate into non-dividing cells
Adeno-Associated Virus	Non-Enveloped	Episomal expression (low frequency of integration)	Neutralising antibodies prevent re-use	<5kb	Neutralising antibodies against wild-type AAV may prevent expression

Table 4: Characteristics for three types of viral vector commonly used within the field of cell and gene therapy. Both retroviral vectors (RVV) and lentiviral vectors (LVV) are enveloped viral vectors with the ability to integrate into the host genome. However, RVV are only able to integrate within dividing cells and LVV can integrate within non-dividing cells. There is a low risk of an immune response being generated against RVV and LVV, whereas Adeno-Associated Viruses (AAV) can initiate an immune response leading to the production of neutralising antibodies that may hamper therapeutic response. Adapted from internal GSK document (GSK, 2019).

1.4.2.1. Retroviral Vectors

Recombinant retroviral vectors, including Moloney Murine Leukaemia Virus, have been utilised in many gene therapy trials (Cavazzana-Calvo, 2000; Aiuti *et al.*, 2002; Braun *et al.*, 2014). In order to produce RVV any non-essential genes involved in producing the natural toxicity of the virus are removed and the viral genome is split across at least three plasmids to prevent viral replication. The viral proteins essential for the effective packaging of viral vectors, and integration of the viral genome into the host genome are maintained. The three-plasmid system used in the production of replication incompetent RVV is shown in Figure 9 and consists of:

1) An Envelope Plasmid

   The envelope plasmid containing the *env* gene, which encodes for the specific envelope that surrounds each viral particle. This envelope will confer varied tropism to the retroviral vector, enabling fusion with host cell membranes.

2) A Packaging Plasmid

   The packaging plasmid contains both the *gag* and *pol* genes, which encode for structure proteins including the capsid, and polymerase.

3) A Transfer Plasmid

   The transfer plasmid contains the transgene of interest between two long terminal repeat (LTR) sequences, which aid integration into the host genome.

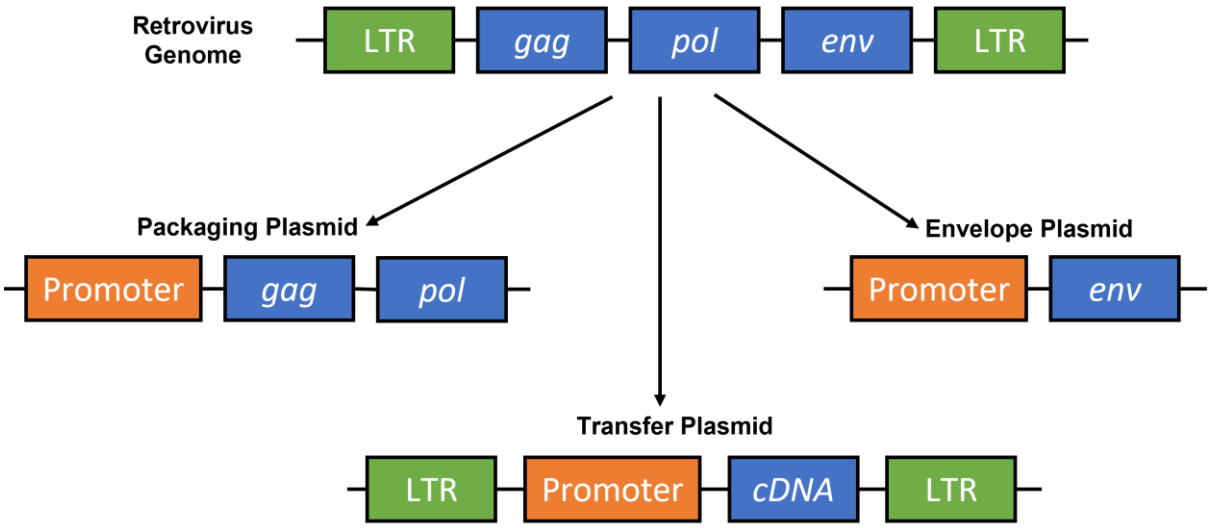

Figure 9: Production of Retroviral Vectors

The essential proteins of retroviruses are split across three plasmids to enable the production of replication incompetent retroviral vectors.

1.4.2.2. Lentiviral Vectors

Lentiviruses are a subtype of the retroviral vector family and are derived from the human immunodeficiency virus (HIV). LVV can transduce both dividing and non-dividing cells, resulting in wider application than RVV. LVVs are produced using a similar method to RVV, utilising a three-plasmid system for second generation LVV and a four-plasmid system for third generation LVV. Both the envelope plasmid and transfer plasmid used in the production of LVV are the same as RVV, as shown in Figure 10. The difference between the production of RVV and LVV comes with the packaging plasmid, which (for second generation LVVs) contains genes *rev* and *tat* in addition to *gag* and *pol*. Within second generation LVV production, the LTRs within the transfer plasmid are weak and require the expression of *tat* for effective expression of the transgene. Whereas, within third generation LVV production, the *rev* gene is separated onto a fourth plasmid and a chimeric LTR is used within the transfer plasmid eliminating the requirement for *tat*.

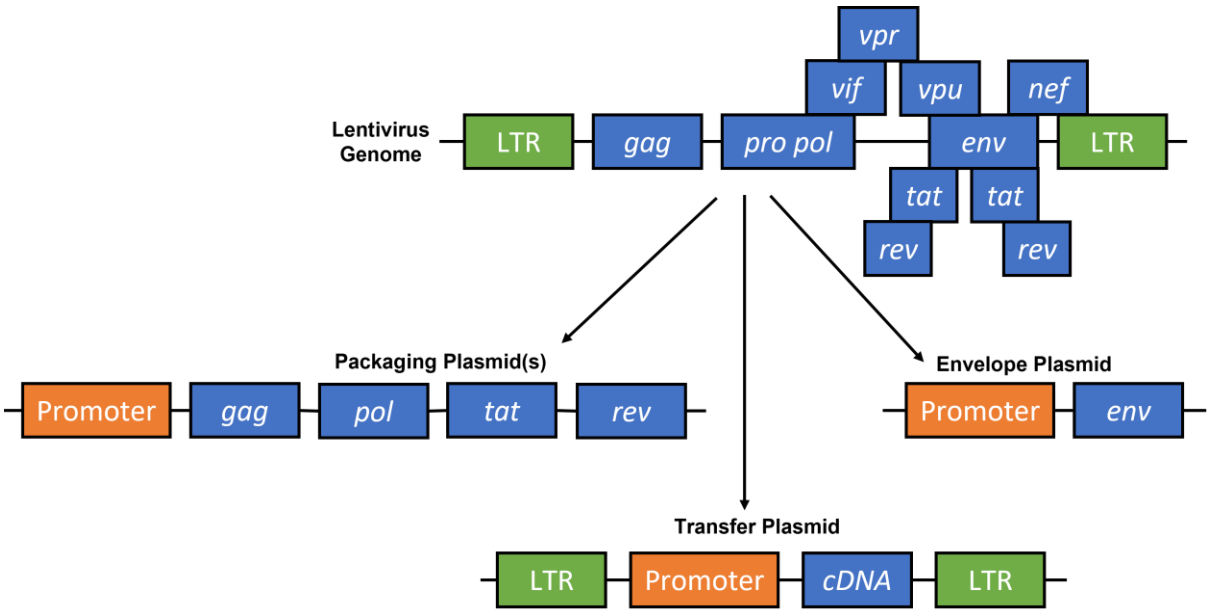

Figure 10: Production of Second Generation Lentiviral Vectors

A three plasmid system used for the production of second generation lentiviral vectors, whilst a four plasmid system is used for the production of third generation lentiviral vectors.

1.4.2.3. Production of Viral Vectors

The production of both RVV and LVV involves the co-transfection of a producer cell line, usually Human Embryonic Kidney (HEK) 293T cells, with the 3-4 plasmids (Figure 11). The splitting of essential genes across several plasmids enables the packaging of viral particles within the producer cell line without enabling the production of replication competent viral particles. Viral particles are then harvested from the supernatant, purified and concentrated. The purified viral vector particles can then be used to transduce the target cell line.

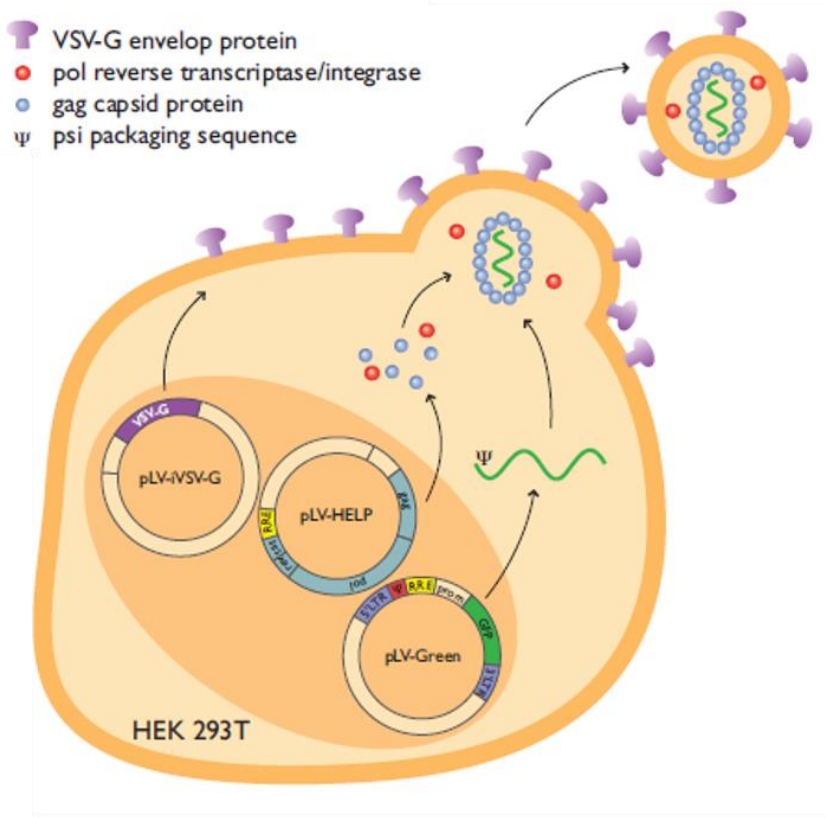

Figure 11: Production of Viral Vectors

Helper, packaging and transfer plasmids are co-transferred into a producer cell line, utilising the producer cell line to generate single stranded RNA encoding the transgene surrounded by protein capsid. These viral particles bud off the producer cell line maintaining the desired envelope, which dictates the tropism of final vector particles. Viral vector particles are harvested from cell supernatant and purified. Image Reference (Invivogen)

1.4.2.4. Lifecycle of Viral Vectors in Target Cell Lines

To integrate into a target cell line, the envelope proteins expressed on the surface of the viral particle must bind to receptors on the surface of the host cell line. It is these envelope proteins that can be modified to confer different tropism to viral vectors, by enabling the binding to various cell surface receptors. Upon binding, the envelope of the viral particles begin to fuse with the host cell membrane. Once inside the cell, the viral particle uncoats enabling the ribonucleic acid (RNA) viral genome to be reverse transcribed producing pro-viral DNA. Nuclear import transports the pro-viral DNA into the nucleus where viral integrase enables integration into the host genome (Figure 12). The gene of interest can then be expressed by the host cell. As was previously mentioned in section 1.4.1.4.3, despite similarities between RVV and LVV in the entry of host cells, the integration of pro-viral DNA differs with RVV preferentially integrating into the regions surrounding transcription start sites of genes near enhancers and promoters, and LVV preferentially integrating into actively transcribed regions (Elleder *et al.*, 2002; Schröder *et al.*, 2002; Wu *et al.*, 2003; Mitchell *et al.*, 2004; Crise *et al.*, 2005; Wang *et al.*, 2009; Ravin *et al.*, 2014; Šenigl *et al.*, 2017; Engelman & Singh, 2018; Miklík *et al.*, 2018; Poletti & Mavilio, 2018). LVV preference for integration into actively transcribed genes was also observed during transduction of mouse hepatocytes (Rittelmeyer *et al.*, 2013).

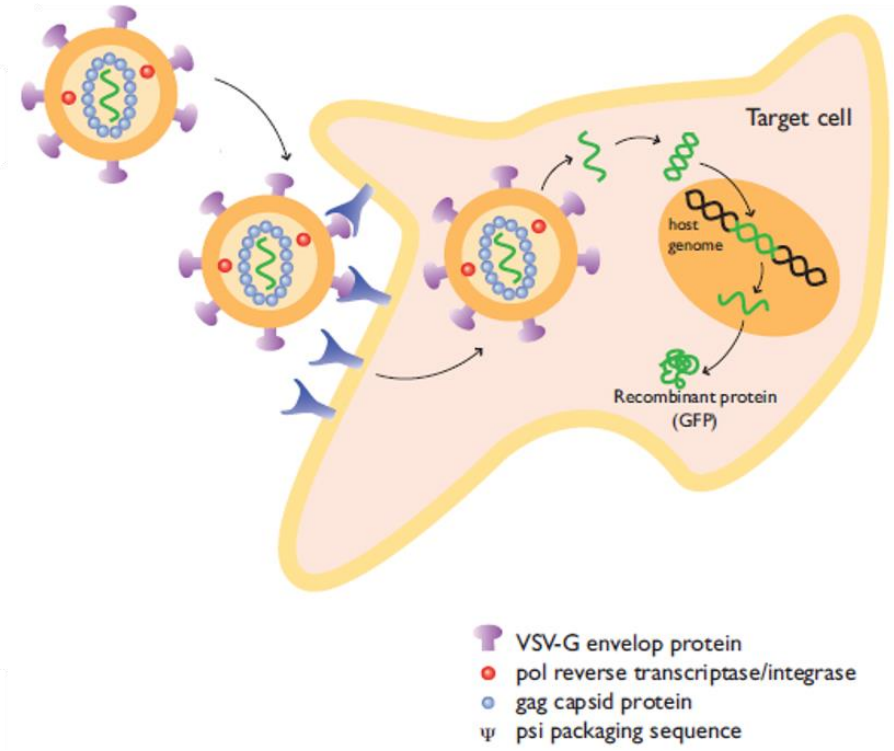

Figure 12: Binding of viral vector to target cell and integration of pro-viral DNA

Envelope proteins bind to host cell receptors, enabling membrane fusion. Once inside the host cell, the viral particle will uncoat enabling reverse transcriptase to convert single stranded RNA into pro-virus DNA, which is imported into the cell nucleus. Viral integrase aids integration of the pro-viral DNA into the host genome. Image reference (Invivogen).

1.4.2.5. Advancements Made to Viral Vectors to Reduce Insertional Mutagenesis Risk

As discussed within section 1.4.1.4.3, insertional mutagenesis is a safety risk associated with both CAR T and engineered TCR T cell therapies due to the use of viral vectors for the introduction of the transgene into the T cell genome. Research has already identified some parts of viral vector constructs believed to increase the risk of insertional activation and tumourigenesis, allowing advancements to be made to reduce the risk.

Due to the promoter and enhancer activity of the RVV LTRs, self-inactivating (SIN) viral vectors were developed. In this design, the 3' U3 region of the LTR was removed and/or modified to reduce the threat of replication competent virus mobilisation as a result of recombination between homologous regions in the vector and packaging constructs, and cis activation of neighbouring genes by the LTR (Miyoshi *et al.*, 1998) (Zufferey *et al.*, 1998). Further research performed by Zychlinski *et al.* demonstrated the SIN viral vectors alone were unable to abolish the interaction of endogenous viral enhancers with neighbouring genes upon integration (Zychlinski *et al.*, 2008). Within this research, Zychlinski *et al.* investigated the impact that switching endogenous promotors for cellular promoters, such as elongation factor 1a (EF1a) and human phosphoglycerate kinase (hPGK), had upon genotoxicity risk. This research demonstrated that weak enhancer-promoter regions (EF1a and hPGK) reduced the risk of activational transformation of neighbouring genes (Zychlinski *et al.*, 2008). These results aligned with evidence from a tumour prone mouse model that demonstrated no increased risk of tumourigenesis when hPGK promoter-enhancer viral vectors were used rather than the strong promoter-enhancer regions of gamma RVV (Montini *et al.*, 2006). To further corroborate these results, further research of leukaemic cells taken from patients of the Hacein-Bey-Abina trial (Hacein-Bey-Abina *et al.*, 2003) revealed that the activation of the LM02 gene was the result of a strong enhancer within the LTR U3 region of the RVV viral vector being used (Zhou *et al.*, 2010). LM02 gene activation was absent in cells transduced with a SIN viral vector containing the weak EF1a promoter-enhancer region (Zhou *et al.*, 2010).

Efforts made to increase the expression levels of LVV, for example with the introduction of the Woodchuck Hepatitis virus post-transcriptional regulatory element (WPRE) sequence (Zufferey *et al.*, 1999; Ramezani *et al.*, 2000), may have unintentionally increased the potential toxicity of LVV sequences. It was speculated that X gene expression in the wild type (WT) form of WPRE may increase the risk of hepatocellular carcinoma (HCC) with equine infectious anemia virus (EIAV) LVV vectors (Hacker *et al.*, 2006), however subsequent studies demonstrated that HCC also developed when EIAV LVV vectors with a truncated X gene sequence WPRE were used (Nowrouzi *et al.*, 2013).

1.4.2.6. Models for Predicting Genotoxicity

Despite the multiple studies that have been performed on clinical samples from gene therapy patients, there is still not a wide understanding of how various aspects of viral vectors may impact on the genotoxicity risk. Many groups have developed genotoxicity models to assay the risk of genotoxicity, however none of these cell-based assays or animal models have been able to accurately predict genotoxicity risk. For example, in the Hacein-Bey-Abina trial, the pre-clinical animal studies were unable to predict the genotoxicity and oncogenesis observed within the trial (Zhou *et al.*, 2016).

1.4.2.6.1. Cell Based Models for Predicting Genotoxicity

Du et al. first introduced replating cell based assays to study genes that may be involved in the immortalisation of lymphoid progenitor cells (Du *et al.*, 2005). Within this study immortalised clones, often with insertions within the EVI1 and Prdm16 genes, developed after 1 month of culture. Subsequently, a group led by Dr Ute Modlich (Modlich *et al.*, 2006; Modlich *et al.*, 2009) utilised the replating assay method to develop a screening assay, known as the *in vitro* immortalisation assay, using murine Lin negative (Lin-) bone marrow (BM) cells taken from untreated C57B16/J mice. The Lin- BM cells were plated onto retronectin coated 24 well plates for transduction with RVV at days 4 and 5 post-isolation. BM cells were expanded for two weeks prior to re-plating within a 96 well plate at a density of 100 cells per well. After a further two weeks, green fluorescent protein (GFP) positive clonal populations were counted and insertion site was analysed. Untreated cells were unable to survive this long-term culture, which demonstrated that RVV transduction provided transduced cells with a proliferation and survival advantage. This study demonstrated decreased re-plating counts and insertions with SIN RVV compared with LTR RVV. A disadvantage of this study is that it is biased for EVI1 mutations through the selection of clones that can survive a 4-week culture, which may result in other important insertion sites being missed.

Bokhoven *et al.* developed another cell culture assay used to assess the genotoxicity of RVV vectors based upon the observation that RVV vectors can introduce a gain of function mutation within the IL-3 gene to make an IL-3 dependent mouse cell line

cytokine independent (Bokhoven *et al.*, 2009). This assay set up has been able to elucidate the differences in insertion site selection for RVV and LVV vectors, as well as demonstrate how vector elements can affect insertional mutagenesis (IM) risk (Bokhoven *et al.*, 2009), however it is unable to detect mutagenesis that may occur within other gene pathways, such as p53 or pRB. For this reason, this assay is not suitable to be predictive of insertional mutagenesis in human patients, with Bokhoven *et al.* suggesting that a tumour prone mouse model may be able to better predict tumourigenesis in humans.

1.4.2.6.2. Animal Models for Predicting Genotoxicity

The lack of predictability of the cell models led to the development of multiple murine models to investigate the risk of insertional mutagenesis. Mouse transplant models are advantageous over cell culture assays due to the ability to detect a broad spectrum of transformation events (Zhou *et al.*, 2013), but they are expensive, time consuming and require a large number of animals.

Montini and co-workers developed a genotoxicity mouse model using a tumour prone mouse strain (FVB/N.129-Cdkn2atm2Rdp), with the hope of increasing the sensitivity of mouse transplant models (Montini *et al.*, 2006; Montini *et al.*, 2009). Within this study, haematopoietic progenitor cells were removed from the six week old tumour prone mice, and were transduced with SIN LVV or SIN RVV vectors prior to being transplanted into WT FBV/N.129 mice. Transplantation into a less tumour prone mouse model was performed to enable assessment of tumours developing from the transduced haematopoietic progenitor cells. The results of this study demonstrated that SIN RVV vectors were able to accelerate tumour progression in a dose dependant manner, which was not observed from SIN LVV vectors.

Mouse models of genotoxicity are often argued to be non-predictive of human genotoxicity, due to the short life span of the mice and the decreased number of transduced cells able to be re-infused back into mice. Therefore, Montini's mouse model attempts to overcome this issue by using a tumour prone mouse model, which helps to increase the sensitivity of the model to tumourigenesis by reducing the requirement for additional somatic mutations (Howe *et al.*, 2008). However, use of a

tumour prone model may be overly sensitive to certain type of insertions which could impact on genotoxicity results.

Another fœtal mouse model developed by Themis *et al.* (Themis *et al.*, 2005) involved the injection of viral vectors into the peripheral yolk sac of female MF1 mice at day 16 post-gestation, in order to transduce fœtal mouse cells (Waddington *et al.*, 2003). Injection of $2.4x10^7$ SIN configuration EIAV human Factor IX (hFIX) viral vector particles resulted in the development of palpable liver tumours in 7 out of 10 fœtal mice. Whilst injection of $1x10^7$ HIV-1-hFIX viral vector vectors had no observable adverse effects at <350-400 days. There was no evidence of tumour development in control treated mice, which demonstrated that tumourigenesis was likely due to viral vector insertion. Although this model was able to demonstrate an increased risk of genotoxicity with EIAV viral vectors compared to HIV-1 viral vectors, this model may over-estimate the likeliness of oncogenesis due to the large number of active genes during mouse development in utero. In addition to this, mouse fœtal genes may not be predictive of human active genes.

1.4.2.6.3. The Struggle to Develop a Predictive Genotoxicity Model

All of the previously described genotoxicity models have increased the knowledge of genotoxicity within gene therapy. However, there are still limitations within these genotoxicity assays which means that they may not be able to predict genotoxicity and tumourigenesis risk within humans. First, re-plating cell culture assays use mouse BM cells cultured within an artificial environment and therefore cannot be reliably used to predict genotoxicity in patients. Due to both the differences in the proliferation and differentiation controls in humans, as well as the differences in genes expressed within mouse BM cells compared to human BM cells.

Both fœtal mouse models are an improvement over the cell culture assay, as the transduced cells can grow within a natural environment. Interestingly, both animal models utilise fœtal mouse cells to demonstrate genotoxicity risk, which can increase the sensitivity of the assay. Newrzela et al. indicated that mature T cells are more resistant to oncogenic transformation by three specific oncogenes (LM02, TCL1 and TrkA), compared to HSC or early haematopoietic progenitor cells (Newrzela *et al.*,

2008). This difference in oncogenic transformation between early progenitor cells and mature T cells may be due to the increased number of active genes involved in proliferation and differentiation within early progenitors. This data also corroborates with the clinical results of Hacein-Bey-Abina's X-SCID trial, in which the two youngest patients developed leukaemia (Hacein-Bey-Abina *et al.*, 2003). This could indicate that during development there is an increased risk of insertional mutagenesis. For this reason, fœtal mouse models may be able to predict tumourigenesis within HSC but may over-estimate the risk of tumourigenesis within terminally differentiated T cells. Although, an argument can be made that all T cells transduced would also be undergoing active proliferation due to pre-stimulation with anti-CD3 and anti-CD28 antibodies, prior to transduction. For this reason, transduction of non-activated T cells may decrease the risk of insertional mutagenesis.

Overall, the development of a predictive genotoxicity assays is challenging, particularly due to the lack of understanding over why tumourigenesis is observed in some clinical trials and not others. It has also been suspected that tumourigenesis could in some cases be associated with the therapeutic gene, rather than the integration site of the viral vector. Woods et al. investigated tumourigenesis related to the therapeutic gene encoding the γ-chain of IL2RG, used for HSC therapy to treat X-SCID. A lentiviral vector encoding the IL2RG gene was used within a murine model of X-SCID, and 33% of the mice developed lymphomas within the 1.5 year study period (Woods *et al.*, 2006). Lymphomagenesis occurred in response to altered signalling through interleukin receptors and was not associated with insertional mutagenesis. Lymphomagenesis was not observed in larger animal models, and further investigation would be required to assess the relevancy of this murine model to human disease progression. Another caveat is the report that additional somatic mutations may increase the risk of tumourigenesis (Howe *et al.*, 2008), which would not be possible to control. However, genotoxicity assays may be able to highlight which genes are at higher risk of mutation upon integration of a viral vector, which may be able to be linked with common somatic mutations to indicate the overall risk of mutation with a particular gene.

Currently, the FDA requests for the Modlich *in vitro* immortalisation assay (Modlich *et al.*, 2006; Modlich *et al.*, 2009) to be performed to assess the mutagenic potential of viral vectors being used for cell therapy products, with a comparison against a positive control RVV and a positive control LVV containing the strong spleen focus-forming viral promoter used to rank whether the viral vector being assessed has a higher or lower mutagenic potential than the controls (BlueBird Bio, 2022). The caveats of this method have been previously discussed and arguments against its usefulness have been made in product filings.

1.4.3. Cell Therapy Product Manufacturing Processes

As interest in the development of cell therapy products increases, it has required the development of manufacturing procedures moving from small-scale processes suitable for the production of products for a limited number of patients into large-scale good manufacturing practise (GMP) manufacturing sufficient to supply products to a large number of patients.

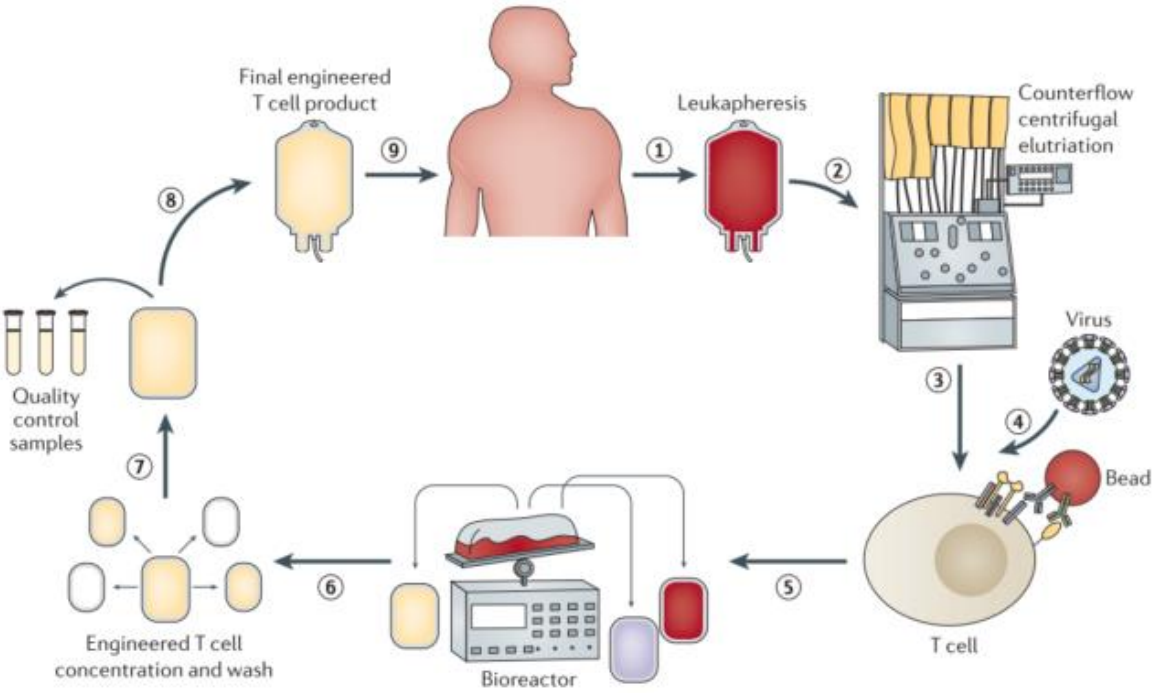

Figure 13: Manufacture of T cell Products

1) Leukocytes are obtained from patient through leukapheresis 2) T cells are purified 3) T cells are activated 4) Transduction of T cells with viral vector 5) CAR T or engineered TCR cell population is expanded through ex vivo culture 6) T cell product is formulated in the appropriate excipients 7) Quality control checks are performed to determine if the product can be released 8) Quality checked T cell product is approved for release 9) T cell product is re-infused into patient. Image reference (Fesnak, June & Levine, 2016).

The first step in the production of a cell therapy product is the acquisition of starting cell material, which most commonly is performed through apheresis within clinical settings. During apheresis, a patient is connected to a device, which uses centrifugal force and cell density to isolate the mononuclear cell layer from peripheral blood with unrequired cell components infused back into the patient. This allows cells to be harvested from a larger volume than would otherwise be possible, providing a starting material of a large number of highly concentrated lymphocytes. This is particularly useful for patients in which lymphocyte counts are low due to disease burden or prior treatments (Abou-El-Enein *et al.*, 2021). A less expensive method of lymphocyte collection, that is generally used within small-scale productions, is the collection of peripheral blood and isolation of peripheral blood mononuclear cells (PBMCs) through gradient density centrifugation; however, this method is unlikely to deliver the large number of cells required to provide the required dose of product, and requires a larger degree of open processing by skilled operators, which risks contamination of the product and would not be suitable for GMP manufacture of cell therapy products. In addition to this, gradient density centrifugation is thought to increase the risk of isolation of unwanted cellular products with similar cellular densities to lymphocytes, such as monocytes, within the starting material which have been reported to impact upon the expansion of cell therapy products (Stroncek *et al.*, 2016).

Upon collection of the starting material, the sample must be processed immediately or rapidly cryopreserved to maintain the viability of the lymphocytes. The cryopreservation of starting material is believed to reduce the quantity and viability upon thawing (Panch *et al.*, 2019), however logistically it is not always possible to initiate the manufacture of the cell product immediately, due to the location of manufacturing sites in relation to clinical sites in which apheresis is performed.

Whether using fresh or frozen starting material, the process of cell therapy production is identical, with the exception of a thawing step prior to production. Further purification of the starting material, whether through elutriation to enrich the lymphocyte population or more advanced selection processes, such as magnetic separation, to enrich for a purified T cell starting material, has been recommended based on evidence generated through research and clinical trials. The presence of contaminating cell types, including monocytes, red blood cells and granulocytes, within the starting cell material has been reported to impact upon the quality of the final cell product (Abou-El-Enein

et al., 2021). Improper selection of the starting material has even resulted in complete therapy failure due to the transduction of a contaminating leukaemic B cell within one production (Ruella *et al.*, 2018). However, it must be noted that no currently available selection processes can ensure a 100% pure T cell population. For this reason, the culture conditions implemented, such as the choice of cytokine, are permissive of T cell expansion and help to further contribute to the purity of the final product.

Generally, magnetically labelled antibodies are utilised for the positive or negative selection of T cell subsets of interest, with Miltenyi microbeads being a commonly used reagent both for the small-scale manufacture and large-scale manufacture for clinical trials within the CliniMACS Prodigy® system (Mock *et al.*, 2016; Lock *et al.*, 2017). Any reagent used for the selection of T cell subsets should be GMP grade and have no impact upon the safety or efficacy of the final product (Abou-El-Enein *et al.*, 2021).

Once the starting material has been defined and prepared, the T cell population must be activated to efficiently transduce and expand the T cell product. Methods by which T cells are activated have been optimised over the years, initially using either soluble or immobilised anti-CD3 antibodies with anti-CD28 antibodies to activate T cells via the endogenous TCR with crosslinking via CD28. However, the requirement for antibody immobilisation limited the number of T cells that could be activated at a single time (Abou-El-Enein *et al.*, 2021). The development of antibody-coated activation beads, such as Dynabeads™, overcame this issue – however, this required additional processing steps to remove the activation beads from the final product. This has also meant that Dynabeads™ are not compatible with closed processing systems, such as the CliniMACS Prodigy®, due to their large size. To overcome this issue, Miltenyi developed an anti-CD3 and anti-CD28 nanomatrix, known as TransAct™, which enabled the efficient activation of T cells with the removal of the activation reagent possible through a series of wash steps. GMP TransAct™ is available for the clinical manufacture of T cells, within the CliniMACS Prodigy®.

T cell populations are then transduced with the viral vector of choice and allowed to expand over a number of days to achieve the require dose. Small-scale culture procedures initially started with the use of multiple flat bottom culture plates for the expansion of T cells, however the amount of operator manipulation, open steps, and variability of expansion means that this method of expansion is not suitable for GMP

production of a large number of batches. The development of G-REX® culture vessels by Wilson Wolf have enabled the production of increased numbers of T cells, whilst utilising static culture within standard incubators, which has helped to advance production methods without the requirement to purchase high-cost equipment. G-REX® culture vessels have also enabled the reduction of the amount of operator manipulation required due to the use of a gas-permeable membrane to ensure sufficient perfusion of oxygen to T cells and high culture volumes enabling the reduction in the number of media changes required by maintaining sufficient nutrient levels (Bajgain *et al.*, 2014). Wilson Wolf have even recently developed a closed-system G-REX® vessel (Gagliardi *et al.*, 2019) which uses a peristaltic pump system to perform media changes when required, further reducing the need for operator manipulation and reducing contamination risk. Another large-scale culture vessel used for the clinical manufacture of T cells is the modular Xuri Wave™ system, which uses a rocking motion to ensure optimal oxygen perfusion to T cells and continual media supply to provide nutrients and prevent waste product build up (Somerville *et al.*, 2012).

Despite the ability to produce sufficient clinical grade T cell therapy products, using the aforementioned culture vessels, they have limited suitability to meet the needs of the scale of production required for the commercialisation of cell therapy products. The implementation of fully automated closed production systems is the desired outcome for the commercial manufacture of T cell therapy products, with hands-off production from apheresis product through to final expanded T cell product. All-in-one systems, such as the CliniMACS Prodigy®, are more expensive to purchase compared to modular systems, such as the Xuri Wave™, however initial costs are recouped due to the ability perform parallel manufacture of multiple batches within a single grade C cleanroom. In addition, the use of closed production systems eliminates the risk of product contamination through operator manipulation, and enables their manufacture within lower classification clean room facilities (Abou-El-Enein *et al.*, 2021). Once processes are developed, the requirement for highly skilled operators reduces, with increased requirement for operators with troubleshooting abilities rather than technical skills.

There are currently two major players within the fully automated closed production system field, with Miltenyi developing the CliniMACs Prodigy®, used within multiple

clinical trials (Mock *et al.*, 2016; Fernández *et al.*, 2019) and Lonza developing the Cocoon® platform, which has recently been successfully used within a CD19-CAR trial conducted at Sheba Medical Centre, Israel (BioPharm International, 2021). Both systems have been developed with the eventual conversion to use as an in-hospital bedside system in mind but are currently utilised within GMP compliant manufacturing hubs.

1.4.4. Critical Quality Attribute Assessment

A pharmaceutical product should always be manufactured in a manner to meet patient needs and the required product performance, with a focus on the quality of the product considered at every step of the development process. Guidelines created by the ICH provide a systematic approach to ensure that product quality is continually built throughout development and manufacturing optimisation using a quality by design (QBD) approach.

A Quality Target Product Profile (QTPP) should be defined for the product and sets the quality, safety and efficacy targets of the product enabling the creation of Critical Quality Attributes (CQAs) (European Medicines Agency, 2017). CQAs define the attributes of the product that may impact the safety or efficacy, thus impacting upon overall product quality. Once CQAs are defined, appropriate methods to test impact upon the chosen attributes can be put in place, enabling the continual assessment of the product through the development life cycle. As further information becomes available throughout development to establish whether there is a correlation between the attribute and the product quality, the CQAs can be further refined.

CQAs can be created for both the viral vector and the cell therapy product (or any other key intermediate), enabling the assessment of vector quality, prior to drug product manufacture to ensure its suitability for use to create the final cell therapy product. Examples of some CQAs for LVV and cell therapy products are provided within Table 5 and Table 6.

Table 5: Critical Quality Attributes for Assessment of Lentiviral Vectors

Category	Critical Quality Attribute	Method of Analysis
Potency	Infectious viral titre	qPCR
	Physical titre	ELISA (HIV gag p24)
	Infectivity	Ratio of qPCR & p24 ELISA
	Transgene function	RT-PCR
Identity	Transgene presence	qPCR / Sequencing
	Vector Integrity	Southern Blot
Safety	Endotoxin	Chromogenic bacterial test
	Mycoplasma	PCR
	Sterility	Culture
	Replication Competent Virus	Tissue Culture/ ELISA/ qPCR
General Characteristics	Osmolality	Osmometry
	pH	pH

Table 5: Some of the CQAs are used for the continual assessment of lentiviral vectors produced throughout the development process, whilst others are most important subsequent to the manufacture of the vector used within the final cell product manufacture, for example sterility and mycoplasma testing.

Table 6: Critical Quality Attributes for Assessment of Cell Therapy Products

Category	Critical Quality Attribute	Method of Analysis
Potency	Transduction Efficiency	Flow Cytometry
	Vector Copy Number (VCN)	qPCR
	Viability	Trypan Blue Staining
Purity	Immunophenotype	Flow Cytometry
Quantity	Cell Count	Trypan Blue Staining
	Total Cell Concentration	Trypan Blue Staining
Impurity	Mycoplasma	PCR
	Endotoxin	Clot Test
	Replication Competent Lentivirus	Tissue Culture / ELISA / qPCR

Table 6: The majority of CQAs are used for the continual assessment of cell therapy products produced throughout the development process to ensure that the quality of the final product is maintained whilst process optimisation is performed. CQAs focussed upon the impurity of the cell product are used for the assessment of final cell products during manufacturing optimisation.

CQA's enable the "scoring" of candidate constructs through their assessment in various biological and functional assays. Investigations of cell therapy products would include but not be limited to the below;

- Fold Expansion

  In some instances, the lentiviral vector used may impact upon the overall proliferation of the cell therapy product. This can occur due to tonic signalling, in which CAR or engineered TCRs are able to constitutively activate T cells in the absence of antigen – resulting in T cell exhaustion, activation induced death and low proliferation rates.

- Transduction Efficiency and Expression of CAR/TCR

  The transduction efficiency of T cells achieved by lentiviral vectors is a key component to the assessment of cell therapy candidates. Issues with expression of the CAR or engineered TCR on the surface of the T cells, due to improper trafficking or folding, will prevent its functionality. It is also of importance for the LVV to be able to achieve a reasonable level of transduction efficiency, at a minimum 10%, to ensure sufficient numbers of T cells are transduced within the final cell population to achieve the required dose of product. The multiplicity of infection (MOI) of the LVV can be increased to boost the transduction efficiency of T cells, however there is a saturation point at which no increase in LVV MOI would result in increased transduction efficiency.

- Cytotoxic Functionality

  The ability of the T cell product to efficiently kill cell lines expressing the target antigen is essential for the progression of the cell therapy product. Cytotoxicity can be assessed in a number of ways, including use of flow cytometry assays, impedance-based assays such as the xCELLigence®, visual assays such as the Incucyte and analysis of cytokine release in response to target cell binding. Candidates with the fastest or strongest cytotoxic functionality are not always the optimal candidate for progression – due to the risk of rapid cytotoxicity resulting in cytokine release syndrome within patients. Therefore, further consideration of desired killing kinetics is required prior to choice of final candidate.

- Vector Copy Number (VCN)

  The FDA recommendation is for VCN to remain below 5 copies per cell in order to reduce the risk of insertional mutagenesis; therefore, it is of importance to analyse the VCN of candidates to ensure that the LVV of choice and MOI used does not result in a VCN above this level.

1.4.5. Cost of Development

There are significant costs associated with the early development of cell therapy products, which differ to those associated with the early development of other pharmaceutical products, such as small molecules. This is due to the requirement for early-stage safety studies to be performed for cell therapy products to assess the potential for off-target off-tumour and on-target off-tumour binding events, whereas safety studies are not required until much later in development of small molecules when the pool has significantly decreased. In addition to this, due to the complexity of the manufacturing process, the costs associated with the chemistry, manufacturing and control (CMC) of the candidate are much higher for the late-stage development of cell therapy products. Well-defined safety studies and manufacturing procedures have been established for the development of small molecules, whereas the processes and FDA requirements for cell therapy products are evolving as further evidence is gathered from ongoing clinical trials. Finally, the manufacture of autologous cell therapies are not able to be scaled up in the same way as the manufacture of other pharmaceuticals where a single batch can treat multiple patients, instead a scale out of the manufacturing processes is required to enable multiple batches to be manufactured in parallel for the treatment of multiple patients, which significantly adds to the cost of manufacture.

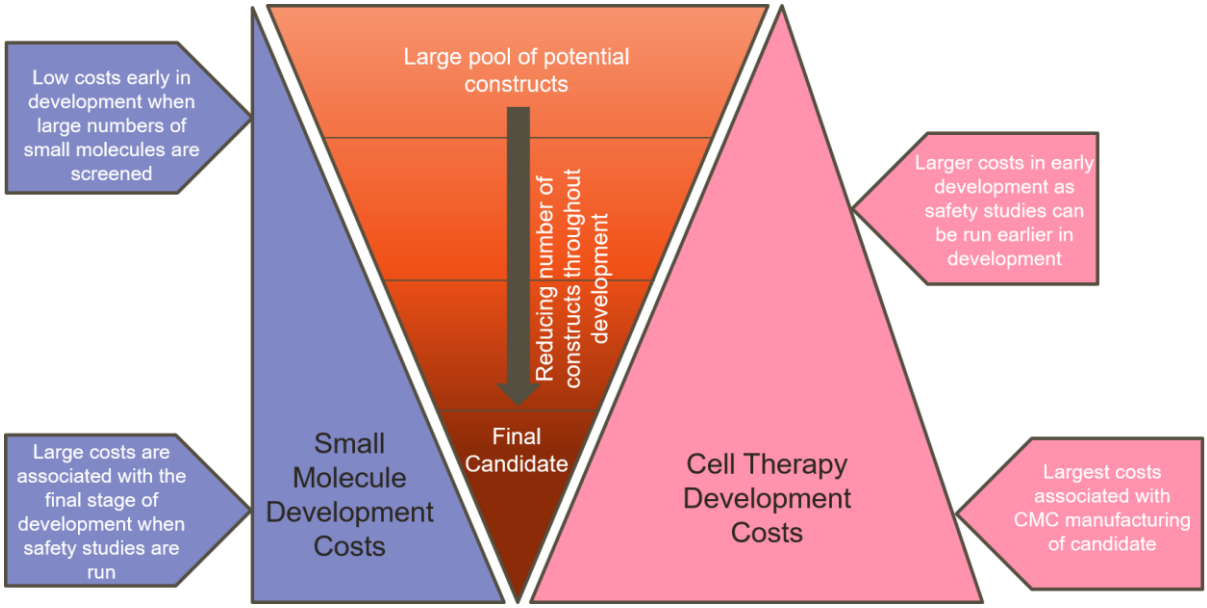

Figure 14: Comparison of Development Costs

The costs associated with the development of cell therapy products are much higher than those associated with the development of small molecule pharmaceuticals due to the requirement for safety studies early in the development process whilst the pool of candidates remains large.

In addition to the high cost of early development of cell therapy products, the cost of GMP manufacture of cell therapy products is high. This is due to a number of factors including; the high cost of reagents, such as cytokines and plasmids; the requirement for highly skilled workers; the requirement for expensive clean rooms; and the complex supply chain involving the transport of a living product from the patient to a manufacturing site and back again. These high manufacturing costs translate into a high cost of goods, with Yescarta® and Kymriah® priced at $373,000 and $475,000 per patient respectively, which significantly limits the availability of these life-saving treatments to patients (Hay & Cheung, 2019). Within the UK, approval for treatment with Yescarta® is dependent on the eligibility of patients with an estimation that between 140 to 160 patients of 4361 diagnosed with diffuse large B cell lymphoma each year would be eligible (NHS England, 2018). Of these patients, it would be essential to ensure that they have sufficient strength and clinical fitness remaining to overcome any potential adverse events that may occur during the course of treatment (Roddie, 2020).

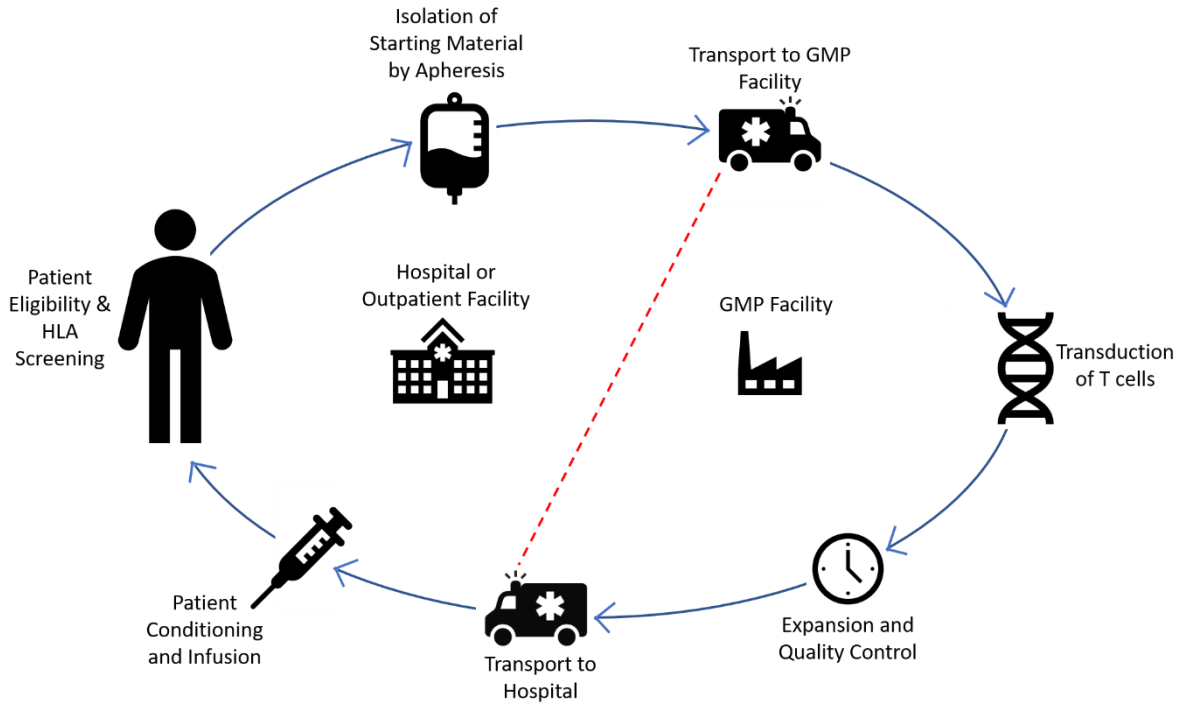

Figure 15: Manufacturing Process of Cell Therapy Products

The typical manufacturing process for commercial cell therapy products requires a significant amount of transport between clinical sites and manufacturing facilities, which increases the overall cost of goods.

A cost of goods impact analysis throughout the pre-clinical and clinical development of a cell therapy product can help to highlight aspects of the manufacturing process which add significant costs and could potentially be optimised to help reduce the final cost of goods. A model developed within GSK estimated that the total cost of development of an oncology cell therapy product, including internal project expenditure (which is the cost of staff within the organisation) and external project expenditure (which is all other costs except staff costs), would be between $500-600 million (Krishna *et al.*, 2021). Figure 16 demonstrates the breakdown of the estimated external project expenditures, with the largest proportion of those costs associated with patient cost of goods, which describe the cumulative costs associated with vein-to-vein process used to dose patients within clinical trials. The second and third largest contributors to the cost of goods are the vector and cells which includes all of the costs associated with the development, process optimisation and transfer of technology to

appropriate GMP manufacturing sites. An example of potential costs associated to a selection of the manufacturing processes will be described in more detail below.

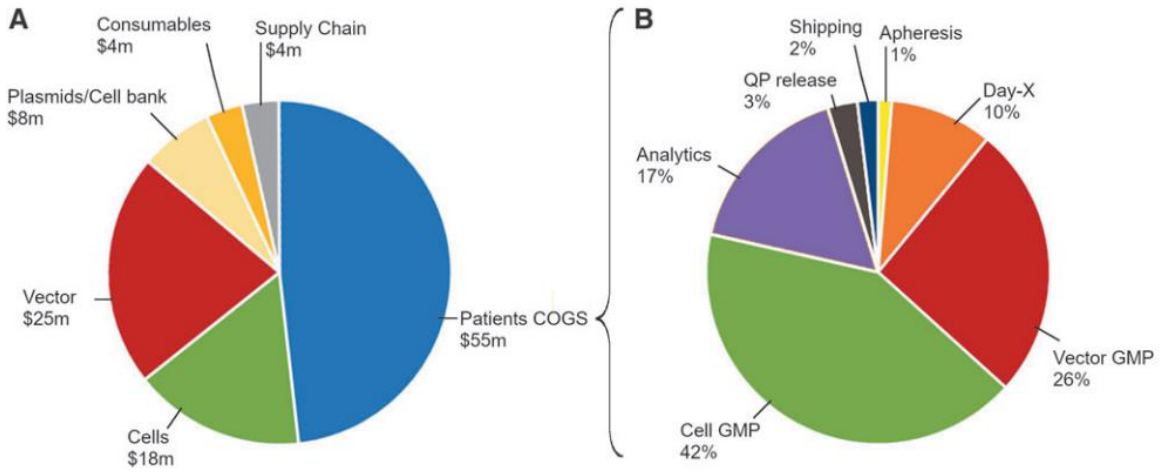

Figure 16: Breakdown of the external project expenditures contributing to the cost of goods of an oncology cell therapy product

A) The largest contributors to the cost of development of a cell therapy products include; patient cost of goods (COGs) which include all of the cumulative costs associated with manufacture of the product from vein-to-vein required for patient dosing within clinical trials; cost of vector and cell development including costs associated with technology transfer to appropriate GMP facilities; the cost of plasmid and cell bank development including stability testing and release of GMP grade products for manufacture, the cost of consumables used throughout the development process and finally supply chain costs, which include storage of product, shipment costs and development and implementation of real-time tracking systems to ensure end-to-end custody tracking of patient material. B) A breakdown of the patient COGs demonstrates that the largest costs arise from the GMP manufacture of the cells and vector. Apheresis describes the cost of cell collection, whilst "Day-X" entails the processing of apheresis material from fresh to frozen. Analytics includes all costs associated with stability testing and release of product once release criteria has been met, with cost of Qualified Person release shown as "QP Release". Image reference (Tarnowski et al., 2017)

1.4.5.1. Patient Eligibility Screening

As previously mentioned, only a selection of patients will meet eligibility criteria for treatment with cell therapy products. Tumours must be biopsied to determine whether expression of the relevant target antigen is expressed, and consideration as to the metastatic status of the tumour must be performed. This is important due to the high potency of cell therapy products, as was previously mentioned an off-target binding event with a MAGE-A3 TCR T cell product occurred potentially due to cross-reaction with MAGE-A12 expression within the brain, with limited understanding as to whether the T cells had homed into the brain due to MAGE-A3 positive micro-metastases (Morgan *et al.*, 2013). Trafficking of engineered T cells into unexpected locations within the body could result in unpredicted adverse events. In addition to this, for engineered TCR T cell therapy patients must be screened to determine if they are an HLA antigen match and suitable for the therapy. As previously mentioned, HLA matching is not required for CAR T therapies.

1.4.5.2. Isolation of Starting Material

Once eligible patients have been selected, they will need to undergo the process of harvesting the cells for manufacturing the product. This could be performed within a hospital or an outpatient facility depending on the health status of the patient. As was previously mentioned, apheresis is the preferred method of starting material isolation as it provides a high yield of cells, which can be difficult in patients that have undergone several rounds of chemotherapy (Roddie, 2020). However, there is an increased cost associated with apheresis compared to isolation of PBMCs from peripheral blood. Some patients may require extended stays within a hospital setting subsequent to apheresis due to rapidly declining health, which adds additional costs to the overall treatment of the patient. Variability in starting material has been reported to be the cause of manufacturing failure rates of up to 14% due to the inability to meet targeted dose (Bersenev, 2017). A potential mitigation strategy that could be implemented to overcome the risk of failure due to starting material variability is to perform apheresis early in a patient's treatment plan, prior to chemotherapy or other immunomodulatory drugs. However, this leads to an added complication in terms of the reimbursement of costs, with lack of clarity over who would be responsible for the cost of apheresis –

particularly in situations whereby the patient does not ever require cell therapy treatment. There would also be logistical issues, including available storage space within hospitals and the related costs of storage, which are further described in section 1.4.5.3. Further studies would also be required to determine the impact of long-term storage of apheresis material upon the quality of the final cell product.

1.4.5.3. Cryopreservation and Storage

The isolation of starting material from multiple different clinical sites, compared to a centralised hub, may also impact upon the quality of the starting material due to operator variation (Shen & van de Wiel, 2020). Firstly, apheresis requires the availability of trained personnel, and subsequent to apheresis the method of starting material storage is essential to maintain a highly viable starting material to enable the production of a high-quality cell therapy product.

The method by which starting material is processed will be dependent on whether manufacture of the cell therapy product is happening within close proximity of the clinical site in which apheresis is performed, or whether starting material requires transport to a GMP facility for manufacture. Within clinical trials, the manufacture of the cell therapy product has often been within the clinical site at which the patient is being treated, enabling a fresh apheresis product to be rapidly processed for manufacture and infused back into the patient upon completion. This method of manufacturing limits the costs associated with the cell therapy product, but also limits the reach of the product due to the requirement for patients to be within close proximity (Lipsitz *et al.*, 2017). However, with the advancement of cell therapies into a commercial setting, in which GMP compliant manufacturing methods for a large number of patients are required, production of the T cell product at the clinical site is not feasible.

Currently for the manufacture of commercial cell therapy products, starting material must be rapidly cryopreserved either at the clinical site at which apheresis is performed or at the manufacturing facility, which incurs additional costs due to the requirement of appropriate cryopreservation equipment and storage facilities. In addition to this, highly skilled operators able to perform cryopreservation are required to ensure that

product quality is maintained. Currently, this step adds potential variability to the manufacturing process due to operator variability and also equipment variability within hospitals. In addition to this, there are logistical issues with the current set up that can add to the cost of goods. Upon cryopreservation, starting material must be frozen within bags requiring storage within specialised racks within minus 150°C freezers. Due to the lack of standardisation between companies manufacturing cell therapy products, there may be a requirement for various sized racking to accommodate for the storage of a variety of cryobags. This lack of standardisation can also increase the complexity of product re-infusion to patients as equipment for the thawing of cryobags may not be standardised between different commercially manufactured products. Process standardisation between institutions may be improved by monitoring and accreditation by the Foundation for the Accreditation of Cellular Therapy (FACT), which is working to ensure quality standards are followed during cell therapy productions (Tsokas *et al.*, 2019)

With the advancement of cell therapy products, it is likely that we will see a manufacturing design in which patients attend a centralised hub for apheresis where starting material is frozen in a standardised process to ensure replicability and maintain sample quality. After which, cryopreserved samples may be shipped to a GMP site for product manufacture and quality testing prior to shipment back to a centralised hub at which point patients can be treated and monitored. This centralised hub system of manufacturing and treatment will help to reduce the cost implication associated with therapies for the hospital in which patients are being treated and will also help to standardise the process to ensure the production of high-quality cell therapy products.

1.4.5.4. Transport of Starting Material to and From Manufacturing Site

The requirement to cryopreserve both the starting material and final cell product for transport to and from the manufacturing site to extend product shelf-life and maintain quality results in the requirement for specialised transportation methods in which products can be maintained at minus 150°C. This requirement for specialised transport adds additional costs to the process of manufacture. In addition to this, human biological sample regulations must be adhered to, as starting material will be classed

as a tracked human biological sample, and the “Genetically Modified Organisms (Contained Use) Regulations 2014” must be adhered to, as the final product will be classed as a genetically modified tracked human biological sample. These two regulations are in alignment with UK laws, and additional regulations may be applicable when international shipments are required. The implementation of global real time cell tracking IT systems would be beneficial to ensure a complete chain of custody, particularly during international shipments whereby cell products may require clearance through customs authorities (Tarnowski *et al.*, 2017).

1.4.5.5. Manufacturing and Quality Control

As previously discussed within section 1.4.5, the development of fully automated closed manufacturing systems, such as the Miltenyi Biotec CliniMACs Prodigy® and Lonza Cocoon®, would enable a significant reduction in manufacturing costs. The use of closed manufacturing systems allows the manufacture of multiples batches in parallel in a lower grade of cleanroom (grade C), reducing site costs and also time, which in turn reduces costs associated with the gowning of personnel performing the production process (Lipsitz *et al.*, 2017). The use of fully automated systems would also reduce costs by decreasing the requirement for highly trained operators, and through the reduction of production failures due to decreased process variability and decreased contamination risk. It is hoped that these fully automated closed manufacturing systems could eventually be developed sufficiently to enable their use as bedside in-hospital treatment systems, similar to a dialysis machine, which could be connected directly to apheresis equipment and used by clinicians within the hospital setting to treat patients (Tarnowski *et al.*, 2017). This would significantly reduce the overall cost of goods, however there is still a way to go before the systems have been developed sufficiently to enable this solution.

1.4.6. Reduction of Cost of Goods

Some manufacturing improvements to enable the reduction of cost of goods have already been described through section 1.4.5, for example the development of centralised hubs for the treatment of patients and use of fully automated closed manufacturing systems. However, there are also some additional methods by which the cost of goods may be reduced, which can be investigated throughout the pre-clinical development of a product. Overall, it is of importance that any developments made within the pre-clinical development phase are focussed upon maintaining or advancing the quality of the final product – therefore, methods by which cost of goods could be reduced should not be performed at the detriment of product quality.

1.4.6.1. Vein-to-Vein Time

Vein-to-vein time describes the time it takes for a cell therapy product to be manufactured from the time of apheresis to the point of re-infusion. The amount of time it takes to manufacture these highly individualised cell therapies is essential for the successful treatment of patients, some of whom are in critical condition and extended time prior to treatment could risk treatment failure. Table 7 lists the disclosed manufacturing, quality control (QC) and estimated vein to vein times for a number of key companies within the cell therapy market and demonstrates the variability in production methods.

Table 7: Manufacturing Timelines

Company	Cell Product Culture Time	Quality Analytics	Estimated Vein to Vein Time
Kite Therapeutics	6 – 8 days	7 days	16-17 days
Novartis	9-10 days	9 days	22 days
Juno	Not disclosed	9 days	21-22 days
BlueBird Bio	10-11 days	Not disclosed	21-30 days
Autolus	8-12 days	4-5 days	18-20 days

Table 7: Some of the key companies involved in the production of cell therapy products have disclosed their estimated manufacturing times, including the time taken for the culture of the product, time required to perform quality control assessments and the overall estimated vein-to-vein time. Data was retrieved from GSK source on the 18th September 2019 and companies may have improved manufacturing timelines since.

One of the main aspects of the manufacturing process that can impact upon vein-to-vein time is the expansion of the cell product, with disclosed cell culture times ranging from between 6 to 12 days. One of the release criteria for cell therapy products is to have reached the required total cell number to enable appropriate dosage of the patient, which is dependent upon the expansion of the cell product during the manufacturing phase, as well as on the disease being treated: solid tumours typically require a higher dose than liquid tumours due to the challenges of the tumour microenvironment. As was already mentioned, starting material variability can impact upon the overall expansion of the product (Bersenev, 2017), which can lead to the requirement for increased cell expansion times during manufacture. This not only increases vein-to-vein time for patients, but also leads to increased manufacturing costs as cells need to be expanded for an extended amount of time. This could also lead to the inability to initiate manufacturing runs for subsequent patients, having an incremental delay on future treatments as well as the current production run. A novel CAR T platform, known as “T-Charge™”, recently developed by Novartis significantly reduces vein-to-vein time by infusing a cell product that maintains a stem-cell-like phenotype with high *in vivo* proliferative potential after just one day of *ex vivo* manufacture (Novartis), reducing the total manufacturing time down to 7 days (Stanton, 2023), which would significantly reduce manufacturing costs.

The use of either manual or automated manufacturing methods has also been shown to impact upon the rate of failure, which in turn impacts upon the cost of goods. Fully automated systems are expected to have failure rates of between 1 – 3% associated only with process failure (Lopes *et al.*, 2020), which is supported by KITE therapeutics reported failure rate of 1% (KITE Pharma, 2021). Whereas, partially automated and manual manufacture processes are estimated to have failure rates of between 3 – 15% (Lopes *et al.*, 2020) with failure rates of 10% reported for Kymriah® (Pagliarulo, 2019).

The next aspect of the manufacturing process that increases the vein-to-vein time is the requirement for extensive quality control assessment prior to release of the product. The need for quality control assessment is essential, due to cell therapies being highly individualised with a high level of variability within the production process

due to the variability of starting materials (Chabannon, 2020). In addition, there is limited experience with these products and therefore the regulatory requirements are high. An example of product assessment criteria investigated prior to product release is shown in Table 8.

Table 8: Product Release Criteria

Test	Method
CD3+ %	Flow Cytometry
Viability	Flow Cytometry
Vector Copy Number	qPCR or ddPCR
Potency	Flow Cytometry or xCELLigence®
Transduction Efficiency	Flow Cytometry
Mycoplasma	Testing methods compliant with European Pharmacopoeia (EP) General Chapter 2.6.7 and United States Pharmacopoeia (USP) General Chapter 63
Endotoxin	Testing methods compliant with EP Chapter 2.6.14 and USP Chapter 85
Sterility	Testing methods compliant with EP chapter 2.6.27
Appearance	Visual Inspection – Colourless or slightly yellow dispersion (Novartis)
Number of Transduced Cells	Calculation based on Trypan Blue Staining
Number of Vector Insertions	Vector Copy Number
Transgene Presence	PCR

Table 8: Cell therapy products must be assessed against product release criteria prior to release to the patient.

The standard pharmacopoeia recommendations for sterility testing within most countries require the culture of samples for at least 14 days – which significantly increases the quality control time, extending vein to vein time. However, rapid sterility testing methods, such as gram staining, have been utilised to enable the release of products in shortened time periods, with recommendation to test several samples taken from between 48 – 72 hours of culture (Li *et al.*, 2019). The same is true of mycoplasma testing, in which culture of samples has been the gold standard method but PCR methods are being investigated to enable rapid testing and release of the drug product within shortened timelines (Li *et al.*, 2019). In addition, the review of batch and analytical records, which are currently often handwritten, takes a significant

amount of time as records require approval by the designated qualified person (QP) prior to release of the product. Advancements in the technology utilised for the quality assessment of cell therapy products and a move to the use of electronic batch records would significantly help to reduce the overall vein to vein time.

The final aspect of the process that significantly adds to the vein-to-vein time is the delivery of the product back to the patient. This step is impacted by the manufacturing set up, as was previously discussed: if manufacturing is performed within the clinical setting, then both cost of transport and delivery time can be significantly reduced. However, this is not likely to be the case for commercially manufactured products, in which cell products are manufactured within external facilities before requiring shipment back to the clinical site. This can lead to logistical issues, particularly in cases where cell products require global shipment. For example, KITE therapeutics reported a turnaround time of 17-18 days for manufacture of ZUMA-1 within the USA, however this increased to 26 – 29 days within Europe due to the requirement of shipment between US and Europe for cell processing (Shen & van de Wiel, 2020). There are also additional regulatory requirements, with products manufactured and released within the US requiring a qualified person to re-release the produce within Europe prior to administration to the patient. The development of a centralised hub system within an increased number of countries would help to reduce transport times and therefore help to decrease the overall vein-to-vein time.

1.4.6.2. Lentiviral Vector Requirements

The cost of viral vector manufacture is also thought to be a significant contributor to the overall cost of goods of cell therapy products (Radek *et al.*, 2019). Firstly, the cost of raw materials, such as GMP grade plasmids, which are required for the manufacture of large batches of viral vectors, result in high starting costs. Then the manufacture of viral vectors, which have traditionally been performed using adherent HEK293 T cells within layered vessels, known as Cell Factories, significantly adds to these costs. Cell Factories have limited scalability, extensive manual handling requirements and typically low harvest per batch (Comisel *et al.*, 2021), therefore require a large highly

skilled workforce and increased consumable costs to achieve the required viral vector batch size.

The development of advanced methods of LVV production using suspension HEK cell lines has enabled the introduction of the use of bioreactors for the production of LVV, enabling scalability to the sizes required for commercially required doses of LVV, reducing operator manipulation and batch to batch variability. An analysis of cost savings performed by Comisel *et al.* estimated between 94-97% reduction in costs when utilising a stirred tank bioreactor compared to a 10 layer Cell Factory (Comisel *et al.*, 2021). The use of stable suspension producer cell lines, as described by Chen *et al.*, for the production of LVV would also help to significantly reduce manufacturing costs. Within this study, a producer cell line was created through the stable transfection of HEK 293T cells with a single construct encoding for all the components required for the lentiviral vector production (Chen *et al.*, 2020). The use of stable producer cell lines allows for the scale up of vector production into stirred tank bioreactors, whilst maintaining vector titres that are comparable to those achieved by transient transfection manufacture.

Improvements in the level of automation and scalability of LVV production will help to reduce the overall cost of goods of cell therapies, however there are also additional methods that could be used to reduce the requirement of LVV within the cell production method.

Firstly, improvement of the fold expansion rate of cell products during *ex vivo* culture would enable reduced starting cell numbers to be utilised, whilst still achieving the required total cell number for product release. This would help to reduce the volume of LVV required for transduction to achieve the desired MOI. Consideration of increased expansion rates upon the quality of the final cell product would need to be made, for example whether the expression of exhaustion markers such as TIM3, PD1 and LAG3 increase in response to high expansion rates?

The second method by which required volumes of LVV could be reduced is through the improvement of viral vector transduction efficiency. This would enable the use of decreased MOIs to be utilised to achieve the desired transduction efficiency, thus reducing the overall volume of LVV required for transduction. There are many reagents and methods that have been used to enhance the transduction efficiency achieved by

viral vectors. Polycationic reagents induce vector particle aggregation and enhanced binding to target cell lines through electrostatic interactions, with both polycationic liposomes (Hodgson & Solaiman, 1996) and polycationic peptides (Cornetta & Anderson, 1989) utilised to enhance the transduction efficiency of retroviral vectors. However, polycations, such as Polybrene, have been shown to be toxic to sensitive cells due to the disruption of cell membrane potential, which limits their use (Wurm *et al.*, 2010; Delville *et al.*, 2018). Bridging molecules bind to both target cell membranes and vector particles enabling co-localisation that encourages vector fusion, with recombinant fibronectin demonstrated to improve HSC transduction efficiency (Hanenberg *et al.*, 1997). A recently developed cationic peptide bridging molecule, known as Vectofusin-1®, has shown promising results for the enhancement of HSC through the production of alpha-helical nanofibrils, which promote vector and cell membrane fusion with the added benefit of being a soluble reagent that can be used within closed manufacturing systems (Radek *et al.*, 2019). Poloxamers, including synperonic F108, are able to interact with cell lipid membranes decreasing microviscosity and facilitating the transport of vector particles into target cells (Höfig *et al.*, 2012). In addition to transduction enhancing reagents, mechanical methods to promote viral vector binding, such as spinnoculation, have also been shown to improve T cell transduction efficiency particularly when used in combination with transduction enhancing reagents (Rajabzadeh *et al.*, 2021). Despite the availability of many transduction-enhancing reagents, the data on their use within genetically modified T cell products manufactured at GMP standards is limited, with many reagents shown to have toxicity issues which may be detrimental to the viability of fragile patient T cells. In addition to this, licensing costs for proprietary reagents would significantly add to the cost of manufacture which may mitigate any cost-savings achieved by reduced viral vector volume requirements.

Considerations as to how increasing transduction efficiency may impact upon the final quality of the T cell product would need to be made, for example would increased transduction efficiency result in a large frequency of T cells within the population to be transduced, or would it simply increase the number of vector copies integrating per cell – which could potentially increase the risk of oncogenic insertions into the T cell genome?

1.5. Thesis Aim

The overall aim of this thesis is to further investigate process optimisations that could reduce the cost of goods of cell therapy products being developed within GSK, with the hope that improvements could be adopted within widespread commercial manufacture of cell therapy products helping to increase the availability of these products to patients. Throughout the thesis, I have worked to ensure that high cell therapy product quality is maintained so that cost savings do not come at the detriment of the final product.

Literature searches were performed to identify areas within the development process in which optimisations could have the largest potential cost saving benefit. Within this thesis, I chose to focus my investigation into the following areas where I felt my research could make an impact:

- Investigation of the Retrogenix™ system for use as an early screening platform for the assessment of off-target binding in early development construct pools
- Investigation into methods by which T cell expansion could be improved, focusing on starting material, culture vessels and cytokine choice
- Investigation into the use of transduction enhancing compounds to improve T cell transduction efficiency

2. Materials and Reagents

2.1. Reagents

Table 9: Reagent Details

Reagent description	Supplier	Catalogue / Batch Number
Histopaque 1077	Sigma	10771
Dulbecco's PBS – without $CaCl_2$ and $MgCl_2$	GIBCO	14190-094
Solution 18	ChemoMetec	910-3018
TexMACS™ Media	Miltenyi Biotec	130-097-196
Human IL-2	Sigma	SRP3085
Human GMP IL-2	Miltenyi Biotec	170-076-147
Human IL-7	Miltenyi Biotec	130-095-362
Human IL-15	Miltenyi Biotec	130-095-764
TransAct™ Activation Reagent	Miltenyi Biotec	130-109-104/130-111-160
10x Red Blood Cell Lysis Solution	Miltenyi Biotec	130-094-183
AutoMACS® Buffer	Miltenyi Biotec	130-091-221
FcR Blocking Reagent	Miltenyi Biotec	130-059-901
CD4 Microbeads	Miltenyi Biotec	130-045-101
CD8 Microbeads	Miltenyi Biotec	130-045-201
Foetal Bovine Serum (FBS) – Heat Inactivated	GIBCO	10270106 / 10500-064
Sodium Azide	Sigma	S2002
Purified Human IgG	Life Technologies	027102
Anti-Mouse IgG Fab'(2)-Biotin Antibody	Jackson Immuno Research	115-066-072
PE Streptavidin Antibody	Miltenyi Biotec	130-106-789/5190612535
Alexa Fluor conjugated BCMA-Fc (BCMA-Fc-AF647)	In house	GRITS55881

PE conjugated anti-LNGFR Ab	Miltenyi Biotec	130-091-885
PE conjugated Dextramer	Immudex	WB2696-PE
PE conjugated Negative Control Dextramer	Immudex	WB2666-PE
Zombie NIR Live/Dead Stain	Biolegend	423106
DAPI	ThermoFisher	D1306
CryoStor CS5 Freezing Media	Sigma	C2999
Sytox AADvanced	Life Technologies	S10274/1761315
BalanCD media	Irvine Scientific	91165
10% Pluronic F-68	GIBCO	24040-032
GlutaMAX I	GIBCO	35050-038
OptiMEM	GIBCO	31985070
RPMI 1640	GIBCO	31870-025
293Fectin	Invitrogen	12347019
PEIpro	Polypus	115-010
Lipofectamine 3000	Invitrogen	L3000-001
SE Cell Line 4D Nucleofector XL Kit	Lonza	V4XC-1024
Human IFN-γ Tissue Culture Kit	MSD®	K151AEB
IFN-γ MSD® Plates	MSD®	L451AEB-1 / L451QOA-1
Diluent 1 (IFN-γ)	MSD®	R50CK
Diluent 100 (IFN-γ)	MSD®	R50AA
IFN-γ Calibrator	MSD®	C01AE
IFN-γ Detection Ab	MSD®	D21QO
Cytokine Panel 1 (Human) Multispot Kit	MSD®	N05050A-1 / Z0047325
Diluent 43	MSD®	R50AG-1/ R50AG-2
Diluent 3	MSD®	R51BA-5
Sulfotag Anti-IL-7 Detection Antibody	MSD®	D0081185

Sulfotag Anti-IL-15 Detection Antibody	MSD®	D0081363
Calibrator For Cytokine Panel 1 Kit	MSD®	A0080240
pcDNA3.1-CMV.IZW	GSK In House	GSK4051849A / N64357-12-D1
pcDNA3.1-CMV.DCC.IZW	GSK In House	GSK4051850A / N64357-12-D2
RNeasy Plus Mini Kit	Qiagen	74134
1X QuantiTech® SYBR® Green PCR Master Mix	Qiagen	1020722
Pierce RIPA Buffer	ThermoScientific	89900
Pierce BCA Assay	ThermoScientific	23225
Halt Protease Inhibitors (x100)	ThermoScientific	87785
NuPAGE 4x Sample Loading Buffer	ThermoScientific	NP0007
NuPAGE Anti Oxidant	ThermoScientific	NP0005
NuPAGE Reducing Agent (x10)	ThermoScientific	NP0009
4-12% Bis-Tris NuPAGE	ThermoScientific	NP0321BOX
20x NuPAGE MOPS SDS Running Buffer	ThermoScientific	NP0001
Chameleon Duo Pre-Stained Protein Ladder	Licor	918-60000
20x NuPAGE Transfer Buffer	ThermoScientific	NP0006
Nitrocellulose Membrane 0.2µM	ThermoScientific	LC200
Licor Odyssey Blocking Buffer	Licor	927-40000
Ponceau S	Sigma	P3504
Mouse Anti-Human DCC antibody	BD Pharmingen	554223
Goat Anti-Mouse 800 IgG (H+L) antibody	Licor	926-32210
Rabbit Anti-alpha tubulin Antibody	AbCam	Ab4074

Jet-PRIME	Polyplus-Transfection	101000027
20mM Tromethamine	Sigma-Aldrich	T6687
UltraPure Sucrose	Fisher	BPE220-1
5M Sodium Chloride (NaCl) EndoFree Tissue Culture grade	Sigma	71380
D mannitol	Sigma-Aldrich	M9546
1M HEPES	Sigma	H0887
0.5M EDTA	Invitrogen	AM9261
DMEM	GIBCO	11995073
Penicillin/Streptomycin	GIBCO	5140122
Minimum essential medium non-essential amino acid (MEM NEAA)	GIBCO	11140035
APC anti-CD3 Ab	Miltenyi Biotec	130-113-135
APC Vio770 anti-CD8 Ab	Miltenyi Biotec	130-110-681
VioBright 515 anti-LNGFR Ab	Miltenyi Biotec	130-112- 599
FITC anti-CD69 Ab	Miltenyi Biotec	130-112-612
PE anti-LDLr Ab	R&D Systems	FAB2148P
8 colour immunophenotyping kit	Miltenyi Biotec	130-120-640
7-AAD	BD Pharmingen	559925
APC-Cy7 anti-CD3 Ab	Biolegend	300438
Bv786 anti-CD8 Ab	BD Bioscience	563823
Bv650 anti-CD62L Ab	BD Bioscience	563808
PE-Cy7 anti-CD45RO Ab	Biolegend	304230
Bv421 anti-CCR7 Ab	BD Bioscience	562555
AF647 anti-CD45RA Ab	Biolegend	304154
PE anti-CD95 Ab	Biolegend	305608
Sytox AADvanced	Life Technologies	S10274
BV421 anti-CCR7 Ab	Biolegend	353208
BV510 anti-CD69 Ab	Biolegend	310939

BV711 anti-CD95 Ab	Biolegend	305644
BV785 anti-PD1 Ab	Biolegend	329930
PE-Cy7 anti-TIM3 Ab	Biolegend	345014
AF488 anti-Lag3 Ab	Biolegend	369326
BB700 anti-CD25 Ab	BD	566447
BUV395 anti-CD3 Ab	BD	564001
BUV496 anti-CD8 Ab	BD	612942
BUV737 anti-CD4 Ab	BD	612748
BV605 anti-CD45RA Ab	Biolegend	304134
AF700 anti-CD45RO Ab	BD	561136
CytoFix Fixation Buffer	BD	554655
Triton X	Sigma	X100-5ML
Synperonics F108 Poloxamer	Sigma Aldrich	07579-250G-F
Human AB Serum	Access Cell Culture	A19053 HI GI
FcX Blocking Reagent	Biolegend	422302
UltraComp eBeads Compensation Beads	Invitrogen	01-2222-42
ArC Total Antibody Compensation Bead Kit	Invitrogen	A10346
CliniMACS PBS/EDTA Buffer 3L	Miltenyi Biotec	200-070-025
2L GMP TexMACS	Miltenyi Biotec	170-076-306
10% Human Serum Albumin (HSA)	Irvine Science	9988171001
Human AB serum	Access Biologicals	A17013 HI GI
CliniMACS CD4 Reagent	Miltenyi Biotec	200-070-132
CliniMACS CD8 Reagent	Miltenyi Biotec	200-070-115
GMP TransAct	Miltenyi Biotec	170-076-156
GMP Recombinant IL-2	Miltenyi Biotec	170-076-147

2.2. Consumables

Table 10: Consumable Details

Consumable	Supplier	Catalogue Number
Leukosep Tubes	Greiner Bio-One	227290
Pasteur pipettes	Fisher	10652842
50mL centrifuge tube	Corning	430290
V bottom 96-well plates	Greiner Bio-One	651201
A8 NucleoCounter® Slides	ChemoMetec	942-0003
24-well Flat Bottom Suspension Plates	Greiner Bio-One	662102
48-well Flat Bottom Cell Culture Plates	Greiner Bio-One	677180
U bottom 96-well plates	Costar	3799
96-well Plate V Bottomed	Thermo Scientific	10565131
24-well G-REX® Plate	Wilson-Wolf	80192M
6-well G-REX® Plates	Wilson-Wolf	80240M
10M G-REX®	Wilson-Wolf	80110S
100M G-REX®	Wilson-Wolf	RU81100
RNAse Free Sterile Eppendorf Tubes	Eppendorf	H179516O
Nalgene 1.5mL Cryogenic vials	ThermoScientific	5000-1020
FluidX 0.9 mL external thread dual coded cryovial	Brooks	68-1000-10N
xCELLigence® E-Plate 96 PET	Agilent	300600910
Transfer Coupler	Miltenyi Biotec	130-018-601
96-well DeepWell™ Plate	Nunc™	278605
RNeasy Spin Column	Qiagen	
MicroAmp® Fast Optical 96-well Reaction Plate	Applied BioSystems	4346907
96-well flat bottom plate	Corning	10695951
6-well flat bottom plate	Corning	10578911

2.3. Equipment

Table 11: Equipment Details

Equipment	Supplier	Asset / Catalogue Number
Centrifuge (Multifuge X3R)	Thermo Scientific	2T32270
High speed centrifuge Avanti J-20 XP	Beckman Coulter	-
AutoMACS® Proseparator	Miltenyi Biotec	-
NucleoCounter® NC250	Chemometec	900-0251
Incubator (for Cell Culture)	Panasonic	2T31755
Plate Washer	BioTek	2T31219
Plate Shaker	Heidolph	17122
MACSQuant® Analyser 10	Miltenyi	21707
MSD® Sector 600 Imager	MSD®	29252
CytoFLEX S Flow Cytometer	Beckman Coulter	079682
StepOnePlus Real Time PCR System	Applied Biosystems	16811
NanoDrop ND-1000 Spectrophotometer	Thermo Fisher	17020
C1000 Touch® Thermal Cycler	BioRad	2T33050
iBlot 2	Invitrogen	-
Odyssey Imager	Licor	-
NuPAGE Electrophoresis Xcell SureLock Mini Cell System	Invitrogen	-
Xcell II Blot Module	Invitrogen	-
EVOS Microscope	ThermoFisher	-
CryoMed Controlled Rate Freezer (CRF)	ThermoFisher	300106537
Fortessa X-20 Flow Cytometer	BD	R658226R1073
ViCell XR	Beckman Coulter	-
XCELLigence® RTCA SP	ACEA	-
PlasmaTherm Thawing Device	Barkey	-
CoolCell™	Corning	432006

2.4. Biologicals

2.4.1. Primer Sets

Table 12: Primer Sets

Primer	Sequence 5'→ 3'	Tm (˚C)	Length (bp)	Accession #
DCC.19-20.F	AGCCAATGGGAAAATTACTGCTTAC	60	25	NM_005215.4
DCC.20.R	AGGTTGAGATCCATGATTTGATGAG	59	25	
ACTB.F	GAGCTACGAGCTGCCTGACG	63	20	NM_001101.5
ACTB.R	GTAGTTTCGTGGATGCCACAGGACT	64	25	

2.4.2. Vectors

Table 13: Vector Details

Vector Name	Batch Number	Titre (TU/mL)	Vector Size (kB)	Packaging System	MOI Used	CAR T Cells Produced Used in Figure #	Name of T Cell Population
BCMA-030	N44162-8-1	5.74E08	8.1	ViraSafe™	2.75	Figure 39	BCMA-CAR T
BCMA-030	N44162-8-1	5.74E08	8.1	ViraSafe™	2.4	Figure 41, Figure 42	BCMA-CAR T
CD19-CAR (ZsGreen Tag)	N67693-12-V2	1.31E09	Unknown	ViraSafe™	1	Figure 57, Figure 59	CD19-CAR T
CD19-CAR (LNGFR Tag)	N67693-15-1	1.23E09	Unknown	ViraSafe™	3	Figure 58, Figure 67, Figure 69, Figure 70, Figure 71	CD19-CAR T
ZsGreen	N65039-5-V1	1.39E08	Unknown	pK	1	Figure 59	ZsGreen
Vector A	N67693-10-V1	1.69E09	10.1	ViraSafe™	5	Figure 41, Figure 42	CAR-A T
Vector B	N67693-10-V2	8.56E08	10.1	ViraSafe™	5	Figure 41, Figure 42	CAR-B T

	N67693-15-V3	1.32E09	Unknown	ViraSafe™	3	Figure 58, Figure 67, Figure 69, Figure 70, Figure 71	CAR-B T
Vector C	B18173	7.57E07	Unknown	pK	2	Figure 75, Figure 76, Figure 77, Figure 78, Figure 79, Figure 80	TCR-C T
Vector D	B18142	1.85E08	Unknown	pK	1	Figure 75, Figure 76, Figure 77, Figure 78, Figure 79, Figure 80, Figure 83, Figure 84	TCR-D T
Vector X	N63420-29-V2	1.94E08	10.2	ViraSafe™	5	Figure 42	CAR-X T
Vector Y	N63420-43-V1	7.09E08	9.2	pK	3	Figure 48, Figure 49	CAR-Y T
Vector Z	N63420-43-V3	5.34E08	9.2	pK	3	Figure 48, Figure 49	CAR-Z T

Table 13: Details of the lentiviral vectors used for the transduction of T cells, including lentiviral vector titre (transduction units per mL) and MOI used for each experiment. Vector size is calculated from LTR to LTR.

One of two different vector packaging systems, either commercially available ViraSafe™ packaging plasmids (Figure 17) or in-house generated PK packaging plasmids (Figure 18), were utilised in the production of lentiviral vectors, as described in Table 13. Both are third generation four-plasmid packaging systems, consisting of an envelope plasmid encoding VSV-G, a packaging plasmid encoding *gag* and *pol*, a *rev* encoding plasmid and the transfer plasmid encoding the CAR or engineered TCR construct.

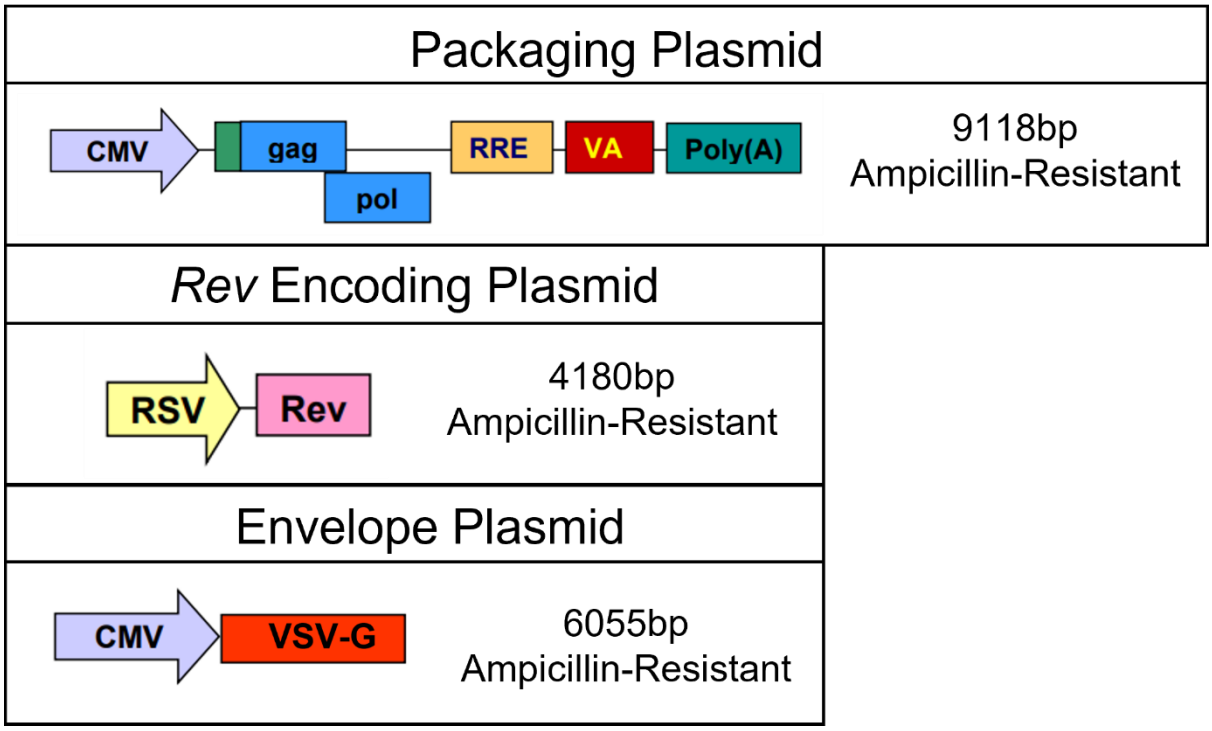

Figure 17: ViraSafe™ Packaging System

The third generation ViraSafe™ lentiviral packaging system (Cell BioLabs, Inc., #VPK-206) provides three of the four plasmids required for lentiviral vector production. A codon wobble is incorporated within the gag sequence to reduce sequence homology and increase safety and vector particle production is boosted by the inclusion of an adenovirus VA_I element. Image adapted from (Cell BioLabs, Inc., 2009)

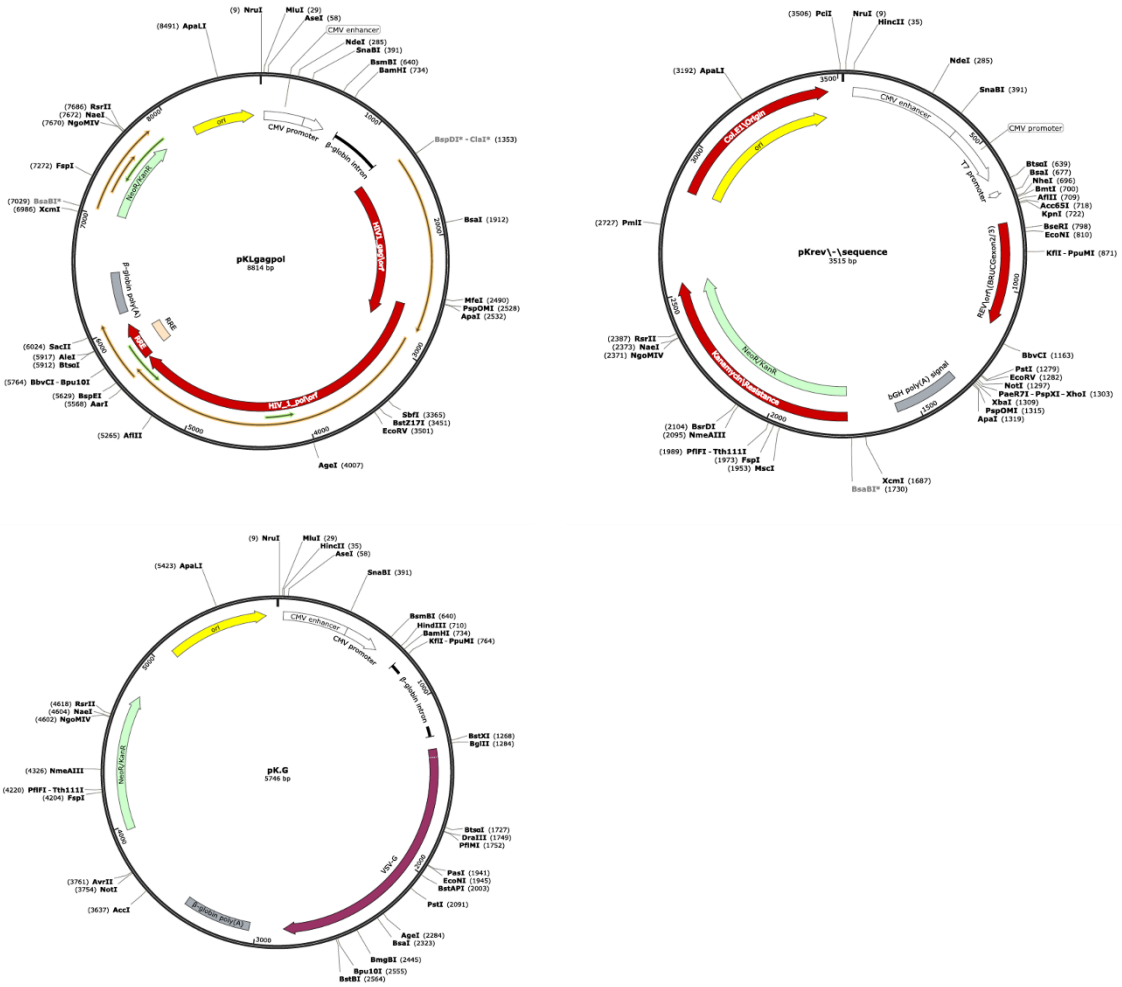

Figure 18: pK Packaging System Plasmid Maps

The third generation pK lentiviral vector packaging system was designed in-house at GSK, with three packaging plasmids to be utilised alongside the transfer plasmid (encoding the CAR or engineered TCR construct of interest) for the production of replication-incompetent lentiviral vectors.

2.4.3. Cell Lines

Table 14: Cell Line Information

Cell Line Name	Supplier	Catalogue/ BioReg Number	Use	Media Components
LentiX HEK293T	Clontech	632180	Adherent HEK vector production	DMEM with 1% (v/v) pen/strep, 10% (v/v) FBS, 1% (v/v) MEM NEAA
HEK293Tsa	GSK	GSK3880943A	Suspension HEK vector production	BalanCD HEK 293 with 2% (v/v) Glutamax and 1% (v/v) Pluronic F68
COSMC Jurkat	GSK	-	Negative control cell line for use in co-culture experiment (3.12)	RPMI with 10% (v/v) heat inactivated FBS
Wild Type Jurkat	GSK	114406	Positive control cell line for use in co-culture experiment (3.12)	RPMI with 10% (v/v) heat inactivated FBS
H441	GSK	119470	Target antigen negative and HLA-A*02 positive cell line for use in xCELLigence® assay (3.10.1)	RPMI with 10% (v/v) heat inactivated FBS and 1% (v/v) Glutamax
H1755	GSK	144415	Target antigen positive and HLA-A*02 positive cell line for use in xCELLigence® assay (3.10.1)	RPMI with 10% (v/v) heat inactivated FBS and 1% (v/v) Glutamax
H647	GSK	144210	Target antigen negative and HLA-A*02 negative cell line for use in xCELLigence® assay (3.10.1)	RPMI with 10% (v/v) heat inactivated FBS and 1% (v/v) Glutamax

2.4.4. Human Biological Samples

The human biological samples were sourced ethically and their research use was in accord with the terms of the informed consents under an independent ethical review board (IRC/EC) approved protocol. Human biological samples, obtained from healthy donors, used within this thesis were sourced from Research Donors (Cambridge Bioscience), Clinical Trials Laboratory Service (CTLS), now owned by BioIVT, or HemaCare USA.

3. Methods

3.1. Lentiviral Vector Manufacture

Small-scale production of lentiviral vector was performed as described briefly below. LentiX HEK293T cells (for adherent HEK vector production) or HEK293Tsa cells (for suspension HEK vector production) were seeded into T175 flasks and cultured in the appropriate medium (as described in Table 14) overnight to achieve a confluency of 70-80%. HEK cells were transfected with the appropriate transfer, packaging and helper plasmids, using Jet-PRIME reagent (Polyplus-Transfection, #101000027) to aid transfection. After 4-6 hours, a media change was performed. If a fluorescent protein encoding CAR vector was produced, the expression of GFP/ZsGreen was assessed via a fluorescent microscope after 24 hours to confirm transfection. This step was not possible for constructs lacking a fluorescent tag. Two days post-transfection, vector containing supernatant was removed from the flasks, and concentrated by ultracentrifugation through a 20% sucrose cushion (20% (w/v) UltraPure sucrose (Fisher, #BPE220-1), 100mM NaCl (Sigma, #71380), 20mM HEPES (Sigma, #H0887) and 1mM EDTA (Invitrogen, #AM9261)). Vector pellets were resuspended in TSSM buffer (20mM tromethamine (Sigma-Aldrich, #T6687), 100mM sodium chloride, 10mg/ml UltraPure sucrose and 10mg/mL D mannitol (Sigma-Aldrich, #M9546)), aliquoted and stored at -80°C.

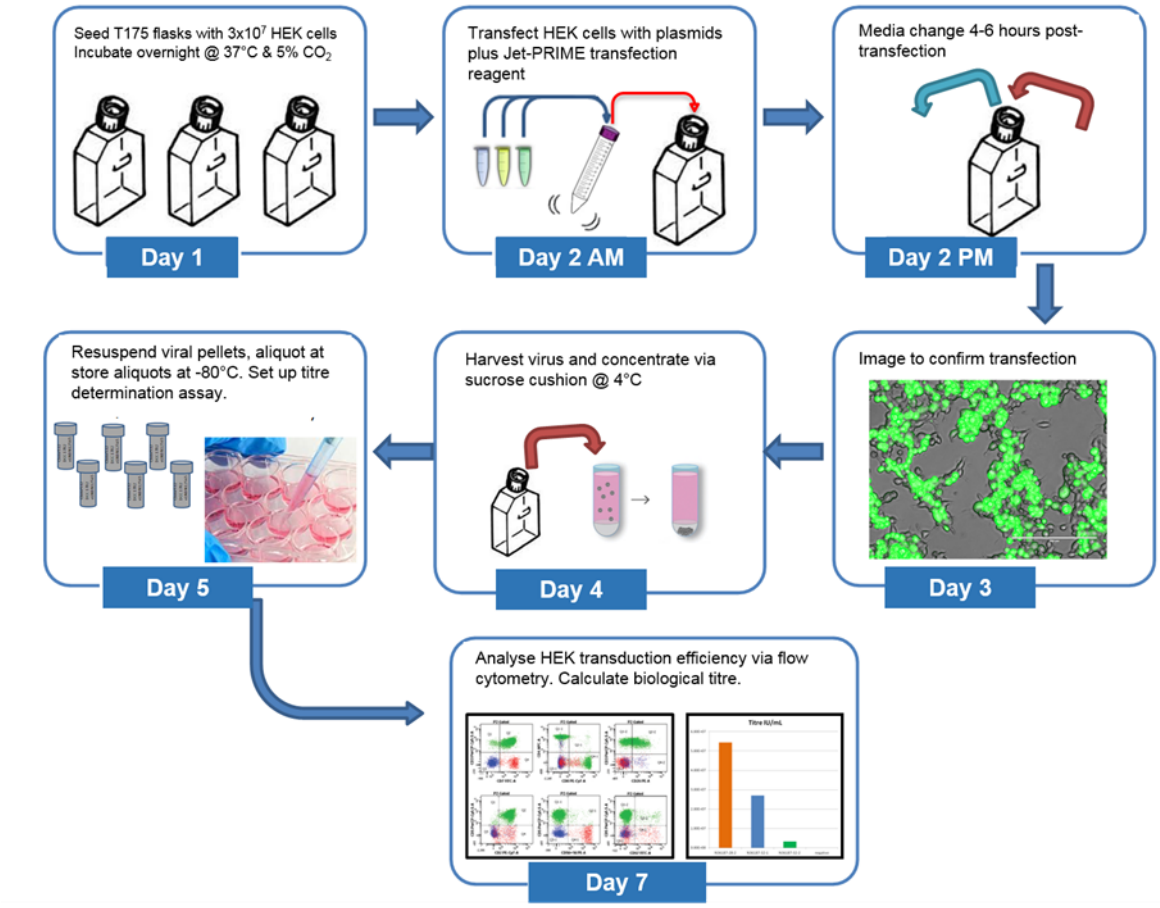

Figure 19: Lentiviral Vector Production

Lentiviral vector stocks were produced over 7 days, with HEK transduction efficiency analysed to calculate biological titres.

Once vector stocks were produced, a vial was thawed and the biological titre (transduction units (TU)/mL) was calculated through the transduction of HEK cells using Equation 1.

Equation 1:

$$Titre = \frac{\#\ of\ cells\ transduced \times \%\ GFP\ or\ CAR\ positive\ cells\ \times Dilution\ Factor}{Transduction\ Volume\ (mL)}$$

Several dilution factors of lentiviral vector were tested, and the titre was only calculated from the dilution factors where the frequency of GFP/LNGFR/CAR/TCR expressing cells was between 3 – 30%, as determined by flow cytometry. For the vectors described in Table 13; an AlexaFluor 647 tagged BCMA-FC protein was used to analyse the expression of the BCMA-030 CAR; a PE anti-LNGFR antibody was used for Vectors A, B and X to analyse the expression of a P2A linked LNGFR tag; an anti-Fab'(2) antibody was used to analyse the expression of the CAR construct for vectors Y and X; and a PE conjugated Dextramer reagent was used to analyse expression of the engineered TCR for vectors C and D.

3.2. T cell Manufacture (Small-scale)

A simple representation of the process used for the small-scale manufacture of T cell products is shown within Figure 20. Initially, cell populations must be isolated from peripheral blood and activated with TransAct™ activation reagent for between 24-48 hours. Activated T cell populations are transduced with lentiviral vectors and expanded over a 10-day process prior to harvest and use within biology assays. The steps are described in more detail within the following sections.

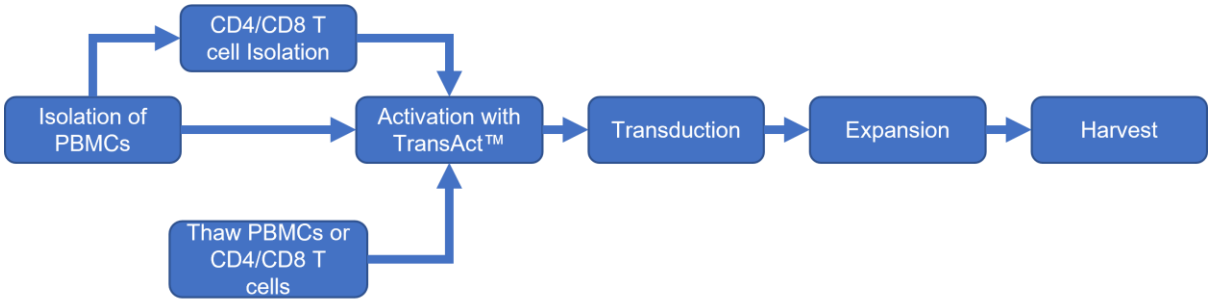

Figure 20: Small-scale T cell Production Flow Chart

PBMCs and CD4/CD8 T cells are isolated from peripheral blood, or thawed from frozen stocks, before being activated with TransAct™ activation reagent for between 24-48 hours. T cells are then transduced with lentiviral vector stocks and expanded for up to 10 days prior to harvest for use within biology assays.

3.2.1. Gradient Density Centrifugation – PBMC Isolation

15mL of Histopaque 1077 (Sigma, #10771) was added to Leukosep tubes (Greiner Bio-one, #227290) at room temperature (RT) before the tubes were centrifuged at 1000g for 1 minute, in accordance with the manufacturer's instructions. Whole peripheral blood isolated from healthy donors was diluted 1:1 with Dulbecco's PBS (GIBCO, # 14190-094) and added to each Leukosep tube, with a maximum of 33mL of diluted blood added to each tube. Leukosep tubes were centrifuged at 800g for 15 minutes at RT with no/slow brake to ensure that buffy coat layers are not disturbed. The cloudy mononuclear layers, visible in the mid-upper part of the tube, were

removed using a Pasteur pipette (Fisher, #10652842) and transferred into 50mL centrifuge tubes (Corning, #430290). Up to three buffy coat layers from the same donor were transferred into a single 50mL centrifuge tube, in order to ensure sufficient removal of remaining Histopaque and plasma from the cell pellets. Cell pellets were washed three times – tubes were topped up to the 50mL mark with PBS, centrifuged at 400g for 10 minutes, supernatant removed and cell pellets were flicked to aid re-suspension of cell pellets. Prior to centrifugation on the final wash step, a 20µL sample of cell solution was removed and counted using the NC-250™ NucleoCounter® (ChemoMetec), following the protocol described in section 3.4.

Depending on the experimental set up, isolated PBMCs were either progressed to CD4+ and CD8+ T cell isolation (as described in section 3.2.3) or activated and transduced following the method described in section 3.2.5.1.

3.2.2. Red Blood Cell Lysis

Red blood cell (RBC) lysis was performed when RBC contamination remained subsequent to gradient density centrifugation and a PBMC population was required, therefore the remaining RBCs would not be removed through CD4/CD8 T cell isolation. Sufficient numbers of PBMCs were transferred into a 50mL centrifuge tube and centrifuged at 300xg for 10 minutes before pouring off supernatant. 10x RBC Lysis Solution (Miltenyi Biotec, #130-094-183) was diluted with room temperature (RT) tissue-culture grade water to generate a 1x RBC lysis solution. Cell pellets were resuspended in 25mL of 1x RBC lysis solution and mixed well before incubating at RT for 10 minutes. The cell solution was centrifuged at 300xg for 10 minutes and the supernatant was discarded before cell pellets were resuspended in an appropriate volume of TexMACS™ media (Miltenyi Biotec, #130-097-196).

3.2.3. CD4/CD8 Isolation

Subsequent to the isolation of PBMCs from peripheral blood, following the protocol described in section 3.2.1, the cell solution was further enriched (when required) to isolate for either CD4+ or CD8+ T cells alone, or a mixed population of CD4+ and CD8+ T cells. Cell pellets were resuspended with 80µL of cold AutoMACS® buffer (Miltenyi Biotec, #130-091-221) and 20µL of FcR blocking reagent (Miltenyi Biotec, #130-059-901) for every 10^7 cells before being mixed and incubated at RT for 5 minutes. At this point, the appropriate microbeads were added depending on the T cell population required:

- CD4+ T cell isolation: 20µL of CD4 microbeads (Miltenyi Biotec, #130-045-101) for every 10^7 cells
- CD8+ T cell isolation: 20µL of CD8 microbeads (Miltenyi Biotec, #130-045-201) for every 10^7 cells
- CD4+ and CD8+ T cell isolation: 20µL of CD4 microbeads for every 10^7 cells and 20µL of CD8 microbeads for every 10^7 cells

The samples were mixed well and then incubated for 15 minutes at 4°C, at which point the AutoMACS® Pro-Separator (Miltenyi Biotec) was set up with the appropriate buffers, according to the manufacturer's instructions. Subsequent to the incubation, the cells were washed with 1mL of cold AutoMACS® buffer for every 10^7 cells centrifuging at 300xg for 10 minutes. Supernatants were poured off and cell pellets were resuspended in 500µL of AutoMACS® buffer for every 10^8 total cells.

At this point, the samples were transferred to the AutoMACS® proseparator and the "PosselS" protocol was used for a sensitive positive selection of the magnetically labelled T cells. Within this protocol, the sample was loaded into the AutoMACS® proseparator and sequentially run through two columns sat within magnets which are turned on for cell separation. Non-magnetically labelled cells were eluted as the negative fraction, with the columns being washed thoroughly with AutoMACS® buffer. Once non-magnetically labelled cells were eluted, the magnets turned off and the magnetically labelled cells were flushed out of the columns as the positive fraction.

The positive fractions were then washed twice by adding up to 15mL of PBS, centrifuging at 300xg for 10 minutes and discarding the supernatant. These wash

steps are important to remove any remaining EDTA, contained within the AutoMACS® buffer, which interferes with the activation of T cells. Samples were then resuspended in an appropriate volume of TexMACS™ media and counted on the NC-250™ NucleoCounter®, following the protocol described in section 3.4. T cell samples were then either cryopreserved for later use as described in section 3.2.8 or activated and transduced following the protocols described in sections 3.2.5.2 and 3.2.6 respectively.

3.2.4. Thawing of Human Blood Cells

Frozen stocks of peripheral blood mononuclear cells (PBMCs) or purified CD4/CD8 T cells were thawed at 37°C in a water bath for up to 40 seconds until a small ice chip remained. 500µL of cold TexMACS™ media was pipetted into each cryovial to aid the thawing process and the whole volume was pipetted into a 15mL tube containing 12.5mL of cold TexMACS™ media. Tubes were centrifuged at 300xg for 10 minutes, washed with 14mL of cold TexMACS™ media and centrifuged as previously. Cell pellets were resuspended in 5mL of warm TexMACS™ media and counted using the NC-250™ NucleoCounter®, following the method described in section 3.4. PBMCs and T cells were then cultured and activated following the method described in section 3.2.5.1 and 3.2.5.2 respectively, prior to transduction as described in section 3.2.6.

3.2.5. Activation

3.2.5.1. PBMCs

Isolated PBMCs were resuspended in TexMACS™ media, supplemented with 100 International Units (IU) per ml IL-2 (Sigma, #SRP3085) and a 1:100 dilution of TransAct™ T cell activation reagent (Miltenyi Biotec, #130-109-104/130-111-160), at a density of $1x10^6$ cells per mL. $1x10^6$ cells were plated into each well of a 24-well flat bottom cell culture plate (Greiner Bio-One, #662160) and incubated in a humidified incubator at 37°C with 5% CO_2 for two days.

T cells were harvested from flat bottom cell culture plates, re-counted following the method described in section 3.4, resuspended to a density of $1x10^6$ cells/mL in TexMACS™ media supplemented with 100 IU/mL IL-2, and re-plated into flat bottom cell culture plates adding $1x10^6$ cells per well. The appropriate number of wells were transduced with the appropriate lentiviral vectors following the method described in section 3.2.6, with the addition of a spinnoculation step where cells were centrifuged for 2 hours at 32°C before being incubated at 37°C with 5% CO_2 for two days.

3.2.5.2. T cells

CD4/CD8 T cells were resuspended in TexMACS™ media, supplemented with the cytokine cocktail of choice (either 100IU/mL IL-2 or a combination of 10ng/mL IL-7 (Miltenyi Biotec, #130-095-362) and 10ng/mL IL-15 (Miltenyi Biotec, #130-095-764)) and a 1:100 dilution of TransAct™ T cell activation reagent, at a density of $1x10^6$ cells per mL.

T cells were plated either directly into 24-well G-REX® plates (Wilson-Wolf, #80192M) and 6-well G-REX® plates (Wilson-Wolf, #80240M), adding $1x10^6$ cells or $4x10^6$ cells per well respectively prior to transduction, or were seeded into 24-well flat bottom culture plates at a density of $1x10^6$ cells/mL for 24 hours prior to harvest and counting, following the protocol described in section 3.4, and then seeded into 24-well and 6-well G-REX® plates, adding $1x10^6$ cells or $4x10^6$ cells per well respectively prior to transduction.

3.2.6. Transduction

The required volume of lentiviral vector to transduce known numbers of T cells at a specific multiplicity of infection (MOI) was calculated using Equation 2.

Equation 2:

$$\text{Volume of Lentiviral Vector Required } (\mu L) = \frac{Total\ number\ of\ T\ cells\ to\ transduce\ x\ MOI}{Vector\ titre\ (TU/mL)}\ x\ 1000$$

The appropriate volume of lentiviral vector was removed from the -80°C storage location and thawed on ice for 10 minutes. Vials of lentiviral vectors were pooled together where appropriate and the required volume of lentiviral vector for the required MOI was added into each well of the culture plate. Cells were incubated at 37°C with 5% CO_2 within a humidified incubator for 48 hours.

3.2.7. Expansion of T Cell Products

3.2.7.1. Standard 24-well Flat Bottom Culture Plates

Subsequent to transduction of T cells, T cells cultured within standard 24-well flat bottom culture plates must be split to a density of between $7.5x10^5$ – $1x10^6$ cells/mL every 2 – 3 days to ensure sufficient nutrient availability for expansion. In order to do so, a representative well of the culture plate for each donor was mixed and a sample was removed for counting, following the protocol described in section 3.4. This provided an estimated cell count for each donor, with all other wells for the same donor being split based on this estimation. T cells were split by the addition of media to bring the cell density down to the recommended density, with half of the cell solution transferred into a new well if required. The appropriate volume of cytokine was added to each well subsequent to cell splitting to ensure the appropriate final concentration of cytokine was maintained throughout the culture procedure.

Table 15: Standard 24-well flat bottom culture plate production process

Day of Experiment	Suggested Day of Week	Activity
Day -1	Tuesday	Isolation of CD4/CD8 T cells (if performed) and activation of cell populations
Day 0	Wednesday	Harvest, replating and transduction of cell populations
Day 2	Friday	Cell splitting with cytokine addition
Day 5	Monday	Cell splitting with cytokine addition
Day 7	Wednesday	Cell splitting with cytokine addition
Day 9	Friday	Cell splitting with cytokine addition
Day 12	Monday	Harvest Day

Table 15: An example of a standard flat bottom culture plate T cell production method

3.2.7.2. 24-well and 6-well G-REX® Plates

After 48 hours of transduction, T cells were transferred into G-REX® plates with either $1x10^6$ cells transferred into each well of a 24-well G-REX® plate or $4x10^6$ cells transferred into each well of a 6-well G-REX® plate, depending on the number of T cells transduced. The appropriate volume of TexMACS™ media, as described in Table 16, was added to each well with sufficient volume of the appropriate cytokines added to achieve 100 IU/mL IL-2 or 10ng/mL of IL-7 and IL-15.

Table 16 : G-REX® Plate Details

Plate Type	Total Volume (mL) per well	Volume (mL) of media to remove at media change
24-well G-REX®	8mL	6.5mL
6-well G-REX®	35mL	30mL

Table 16: Volume of TexMACS™ media required for 24-well or 6-well G-REX® plates

Cells were incubated at 37°C with 5% CO_2 within a humidified incubator for 72 hours. After 72 hours, the appropriate volume of either fresh IL-2 or IL-7/IL-15 was added to each well to ensure a final concentration of 100 IU/mL or 10ng/mL respectively. Cells were incubated at 37°C with 5% CO_2 within a humidified incubator for 48 hours.
After a further 48 hours (at day 7 post-transduction), a media change was performed. G-REX® plates were carefully removed from the incubator and a strippette was used to remove 6.5mL of TexMACS™ media from each well of 24-well G-REX® plates, or 30mL of TexMACS™ media from each well of 6-well G-REX® plates. Care was taken to ensure that the strippette did not disturb the T cells settled at the bottom of each well. The appropriate volume of warm TexMACS™ media supplemented with either 100 IU/mL IL-2 or 10ng/mL IL-7/IL-15 was added into each well of the G-REX® plates. Cells were incubated at 37°C with 5% CO_2 within a humidified incubator for 48 hours. After 48 hours (Day 9 post-transduction), the appropriate volume of IL-2 (100 IU/mL) or IL-7/IL-15 (10ng/mL) was added to each well. Cells were incubated at 37°C with 5% CO_2 within a humidified incubator for 72 hours.

After a further 72 hours (Day 12 post-transduction), T cells were harvested from G-REX® plates by mixing with a strippette and transferring the cell solution into the appropriately sized centrifuge tube. Duplicate wells were pooled together. At this point, samples of cell solution were removed for counting on the NC-250™ NucleoCounter® (as described in section 3.4) and transduction efficiency analysis (as described in section 3.5).

Table 17: 24-well and 6-well G-REX® Production Process

Day of Experiment	Suggested Day of Week	Activity
Day -1	Tuesday	Isolation of CD4/CD8 T cells (if performed) and activation of cell populations
Day 0	Wednesday	Transduction of cell populations
Day 2	Friday	Transfer to G-REX® and top up to full media volume
Day 5	Monday	Cytokine feed
Day 7	Wednesday	Media Change
Day 9	Friday	Cytokine feed *(optional day for early harvest)*
Day 12	Monday	Harvest Day

Table 17: An example of the production process used for 24-well and 6-well G-REX® T cell productions

3.2.7.3. 10M and 100M G-REX® Plates

CD4/CD8 T cells selected using a CliniMACs Prodigy® by colleagues within the Cell and Gene Therapy Process Development team were transferred over for use within this experiment. T cells were counted using the NC-250™ NucleoCounter® following the protocol described in section 3.4. T cells were centrifuged at 300xg for 8 minutes and resuspended to the appropriate cell density for seeding ($1.5x10^6$ cells/mL) in TexMACS™ media containing the appropriate concentration of cytokine, either 10ng/mL or 40ng/mL of IL-7/IL-15. 10mL of cell solution was seeded into the 10M G-REX® vessels (Wilson-Wolf, #80110S) and 100mL of cell solution was seeded into the 100M G-REX® vessels (Wilson-Wolf, #RU81100). The appropriate volume of TransAct™ Activation Reagent (10µL per $1x10^6$ cells) was added into each vessel directly and mixed well. Vessels were incubated within a humidified incubator at 37°C for 24 hours.

After 24 hours of activation, T cells were transduced by adding the appropriate volume of lentiviral vector to achieve an MOI of 1.7 (as calculated in section 3.2.6) directly to the G-REX® vessels and cell solution was mixed well before being incubated within a humidified incubator at 37°C for a further 24 hours.

After a further 24 hours, sufficient media containing the appropriate concentration of cytokine (either 10ng/mL or 40ng/mL of IL-7/IL-15) was added to each vessel to bring the total volume up to the maximum for each culture vessel: 100mL total volume for a 10M G-REX® vessel and 1L total volume for a 100M G-REX® vessel. Vessels were incubated for a further 48 hours within a humidified incubator at 37°C.

At days 4, 7 and 10, samples of media were removed from the mid-section of the culture vessels and stored at -80°C for later analysis of cytokine concentration by Meso Scale Discovery® (MSD®). Cells were mixed within the culture media to enable a sample to be removed for cell count, following the protocol described in section 3.4. The appropriate volume of IL-7/IL-15 was added into vessels in which continual cytokine addition was performed throughout the culture procedure, to provide a final concentration of 10ng/mL.

Table 18: 10M and 100M G-REX® Production Process

Day of Experiment	Suggested Day of Week	Activity
Day 0	Monday	Activation of selected T cells
Day 1	Tuesday	Transduction of T cells
Day 2	Wednesday	Media top up
Day 4	Friday	Cell Count, Supernatant Sampling and addition of cytokine (where necessary)
Day 7	Monday	Cell Count, Supernatant Sampling and addition of cytokine (where necessary)
Day 10	Thursday	Cell Count, Supernatant Sampling and harvest of cultures

Table 18: An example of the production process used for 10M and 100M G-REX® T cell productions

3.2.8. Freezing of T cells

T cell populations were counted on the NC-250™ NucleoCounter® (section 3.4). Cells were centrifuged at 300g for 10 minutes and supernatants were poured off. Cell pellets were resuspended with the appropriate volume of CS5 freezing media (Sigma, #C2999) to achieve cell densities of between $1x10^7$ – $1x10^8$ cells/mL. Cell solution was rapidly aliquoted into Nalgene 1.5mL cryovials (ThermoScientific, #5000-1020) adding between 0.5 – 1mL of cell solution per vial (depending on the experiment).

Depending on the experiment, cryovials were then frozen by one of two methods.

1) CoolCell™ Freezing Container (Corning, #432006)

   Cryovials were transferred into a CoolCell™ freezing container and stored within a -80°C freezer for 24 hours, prior to samples being transferred to a -150°C chest freezer.

2) CryoMed Controlled Rate Freezer (CRF) (ThermoFisher, # SN300106537)

   Cryovials were transferred into the CRF and the following freezing profile was used to control the freezing of cells:

   - Hold at 4.0°C
   - Ramp 1.0°C/min until Chamber = -7.0°C
   - Ramp 60.0°C/min until Chamber = -50.0°C
   - Hold at -50.0°C for 1.0 minutes
   - Ramp 9.0°C/min until Chamber = -25.0°C
   - Ramp 2.0°C/min until Chamber = -40.0°C
   - Ramp 5.0°C/min until Chamber = -100.0°C
   - End – Hold at -100.0°C until samples were transferred to -150°C chest freezer.

3.3. Large-scale Clinical Manufacturing Process on the CliniMACS Prodigy®

The large-scale production of clinical grade T cells on the CliniMACS Prodigy® was performed by colleagues within the Process Development Cell and Gene Therapy department (GSK), with isolated CD4/CD8 T cells provided for use within experiments described within section 3.13.

For completeness, the large-scale CliniMACS Prodigy® manufacturing process is briefly described within section 3.3. A simplified flow chart of the CliniMACS Prodigy® manufacturing process shown in Figure 21.

Figure 21: Large-scale Manufacturing Process of T cell Products on CliniMACS Prodigy®

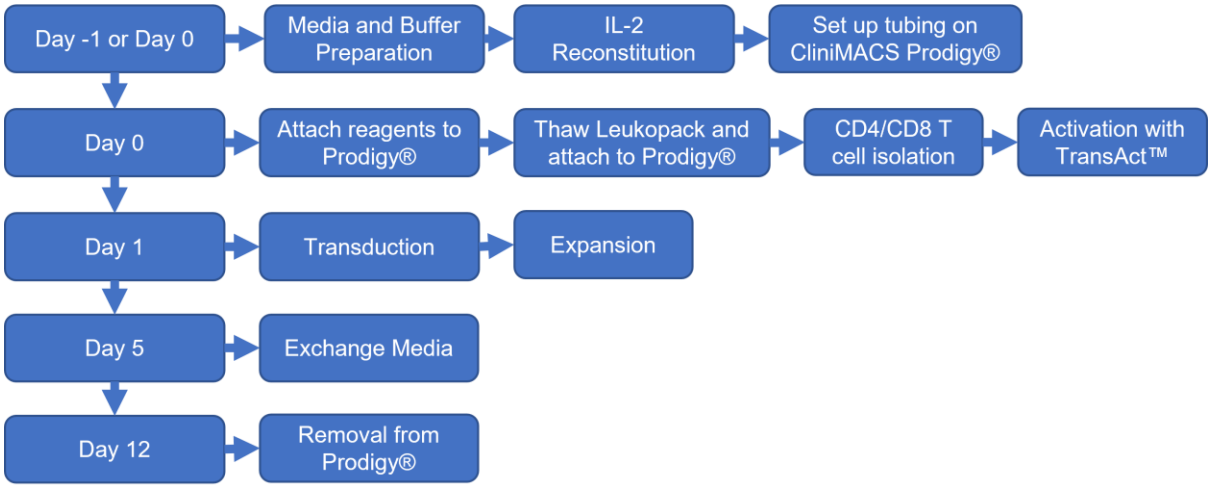

Figure 21: Flow chart demonstrating the large-scale manufacturing process of T cell products on the CliniMACS Prodigy®

3.3.1. Media Preparation

GMP grade CliniMACS® buffer (Miltenyi Biotec, #200-070-025) supplemented with human serum albumin (HSA) (Irvine Science, #9988171001) and TexMACS media (Miltenyi Biotec, #170-076-306) supplemented with Human AB serum (Access Biologicals, #A17013 HI GI) and IL-2 (Miltenyi Biotec, #170-076-147) was prepared within a biological safety cabinet with components added into buffer and media bags using transfer couplers (Miltenyi Biotec, # 130-018-601) and luer-lock syringes to maintain sterility. Components of buffer and media are listed within Table 19.

Table 19: Components of Clinical Grade Buffer and Media for CliniMACS Prodigy®

Media	Day of Preparation	Day of Use	Components	Number of Bags Prepared Per Prodigy®
CliniMACS Buffer + HSA	Day -1 or Day 0	Day 0	3L bag of CliniMACS Buffer + 0.5% (v/v) HSA	1
TexMACS® Media + Human AB Serum + IL-2	Day -1 or Day 0	Day 0	2L bag of GMP TexMACS® + 5% (v/v) human AB serum + 100IU/mL IL-2	2
TexMACS® Media + IL-2	Day 5	Day 5	2L bag of GMP TexMACS® + 100IU/mL IL-2	3

Table 19: *Clinical grade buffer and media was prepared within a biological safety cabinet to maintain sterility.*

3.3.2. GMP IL-2 Reconstitution

The number of international units (IU) within the GMP IL-2 vial was calculated using Equation 3, with the IL-2 content and specific activity defined within the product insert.

Equation 3:

$$Number\ of\ IU\ per\ Vial = IL2\ Content\ (mg)\ x\ Specific\ Activity\ (IU/mg)$$

A stock solution of $2x10^6$ IU/mL IL-2 was prepared by reconstituting lyophilised IL-2 with the appropriate volume of TexMACS™ media, calculated using Equation 4.

Equation 4:

$$Volume\ of\ TexMACS\ media\ (mL) = \frac{Number\ of\ International\ Units\ (IU)}{2x10^6}$$

3.3.3. Tubing Set Installation (Day -1 or Day 0)

The tubing set was installed following the manufacturer's instructions on the CliniMACS Prodigy® on either day -1 or day 0 of the clinical manufacturing process, using the "T cell engineering – large scale (TCE-LS)" protocol.

3.3.4. Thawing of Leukopack (Day 0)

The Plasmatherm thawing device (Barkey) was warmed up to 37°C and a leukopack was placed within the centre of the device for 3 minutes.

3.3.5. CliniMACS Prodigy® Set Up (Day 0)

The manufacturer's instructions displayed on the CliniMACS Prodigy® were followed to attach two bags of TexMACS media (supplemented with 5% (v/v) human AB serum and 100IU/mL IL-2), one bag of CliniMACS buffer (supplemented with 0.5% (v/v) HSA) and GMP grade CD4 and CD8 microbeads to the Prodigy®. The CliniMACS Prodigy® was set to prime whilst a leukopack was thawed. Once thawed the leukopack was sterile welded onto the Prodigy® allowing transfer of the sample into the application bag. The process of CD4/CD8 selection was then continued following the manufacturer's instructions on the CliniMACS Prodigy®. Once the CD4/CD8 selection was completed, a proportion of T cells were transferred into a separate bag for removal from the CliniMACS Prodigy® and freezing following the method described in section 3.2.8. Remaining T cells were maintained on the CliniMACS Prodigy®, GMP grade TransAct™ activation reagent was attached, and T cells were activated for 24 hours. After which T cells were transduced and expanded following the method described in sections 3.3.6 and 3.3.7.

3.3.6. Transduction (Day 1)

Viral vector stocks were thawed at RT for 30 minutes before being diluted in 10mL of TEXMACS media (supplemented with 5% (v/v) Human AB serum and 100IU/mL IL-2). The bag of diluted viral vector was sterile welded onto the CliniMACS Prodigy® and manufacturer's instructions were followed to continue with the transduction of T cells.

3.3.7. Expansion and Harvest

At day 5, media bags were exchanged with bags of TexMACS media supplemented with IL-2 only, and the expansion process was continued following the manufacturer's instructions. At the end of the process, transduced T cells were removed from the CliniMACS Prodigy®, samples were removed for analysis as required and T cells were frozen following the protocol described in section 3.2.8.

3.4. T cell Counting and Viability Assessment (NC-250™ NucleoCounter®)

20µL samples of cell solution were plated into a V bottom polypropylene plate (Greiner Bio-One, #651201) and 1µL of solution 18 (ChemoMetec, #910-3018) was added to each well and mixed well. 10µL of cell solution was loaded into each segment of an A8 NucleoCounter® slide (ChemoMetec, #942-0003) and the "T cell viability and counting" protocol was used to provide a viable cell count per mL and frequency of viable cells. The NucleoCounter® excludes RBCs from the cell count.

Fold expansion of cell populations was calculated by division of the final total cell number by the starting cell number, as shown in Equation 5.

Equation 5:

$$Fold\ Expansion = \frac{Total\ Final\ Cell\ Number}{Starting\ Cell\ Number}$$

3.5. Transduction Efficiency Analysis

3.5.1. Detection of ZsGreen Expression (T cells)

ZsGreen was used as a detection marker for transduction efficiency within transduced T cell populations (Figure 57, Table 39). Approximately $2x10^5$ cells were plated into a V bottom polypropylene plate, and sufficient volume of FACS buffer (PBS + 2% (v/v) FBS (GIBCO, #10270106/10500-064) + 0.05% (v/v) sodium azide (Sigma, #S2002)) was added to each well to bring the total volume up to 200µL per well. The plate was centrifuged at 400g for 5 minutes and supernatants were flicked off. Cell pellets were resuspended with 100µL of 1µg/mL DAPI solution (ThermoFisher, #D1306), prior to analysis on either the CytoFLEX S flow cytometer (Beckman Coulter) or MACSQuant® Analyser 10 flow cytometer (Miltenyi Biotec), with the intent to acquire a minimum of 10,000 live events per sample

Data was analysed using FlowJo™ software (version 10.1, BD Life Sciences), with gating strategy for T cells shown in Figure 22. Results were plotted in GraphPad Prism software (Version 6.07 for Windows, La Jolla California USA).

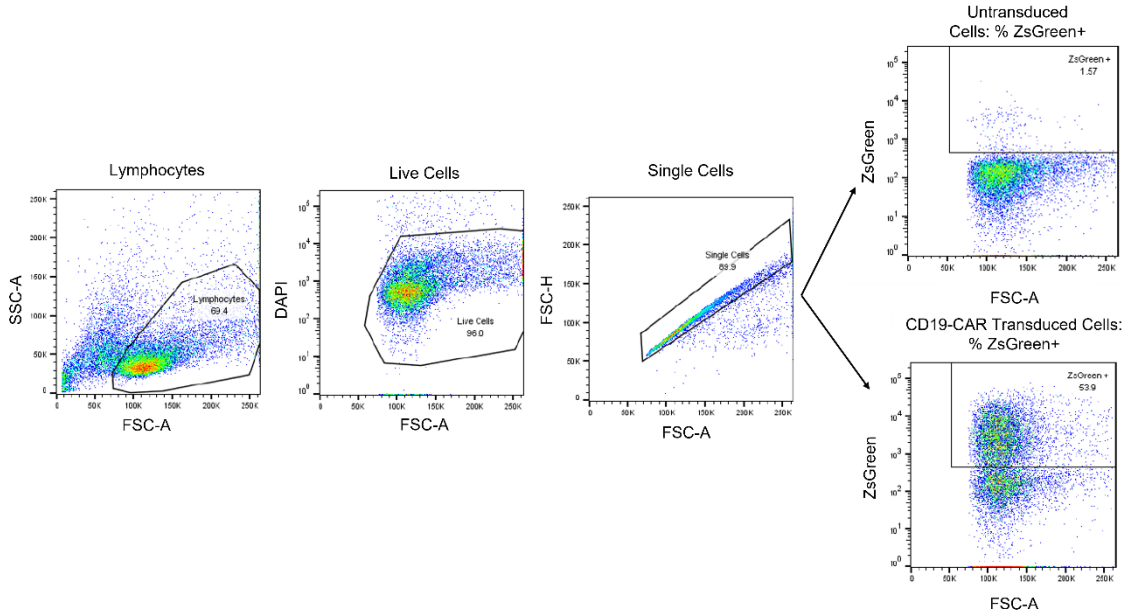

Figure 22: Gating Strategy for the Detection of ZsGreen Expression in T cells

Forward and side scatter were used to gate around the lymphocyte population. Within the lymphocyte population DAPI staining enabled gating around the DAPI negative live cell population. Within the live cell population, forward scatter height and forward scatter area were used to remove doublets from the analysis. Finally, ZsGreen expression enabled the gating around the ZsGreen positive T cells, with the gate set using an untransduced T cell population as a negative control.

3.5.2. Detection of ZsGreen Expression (HEK Cells)

ZsGreen was used as an indicator of transfection efficiency within HEK cells (Figure 44, Figure 46A, Table 35). The methodology used for analysis of ZsGreen expression within HEK cells was the same as that described for T cells within section 3.5.1. Data was analysed using FlowJo™ software (version 10.1, BD Life Sciences), with gating strategy for T cells shown in Figure 23. Results were plotted in GraphPad Prism software (Version 6.07 for Windows, La Jolla California USA)

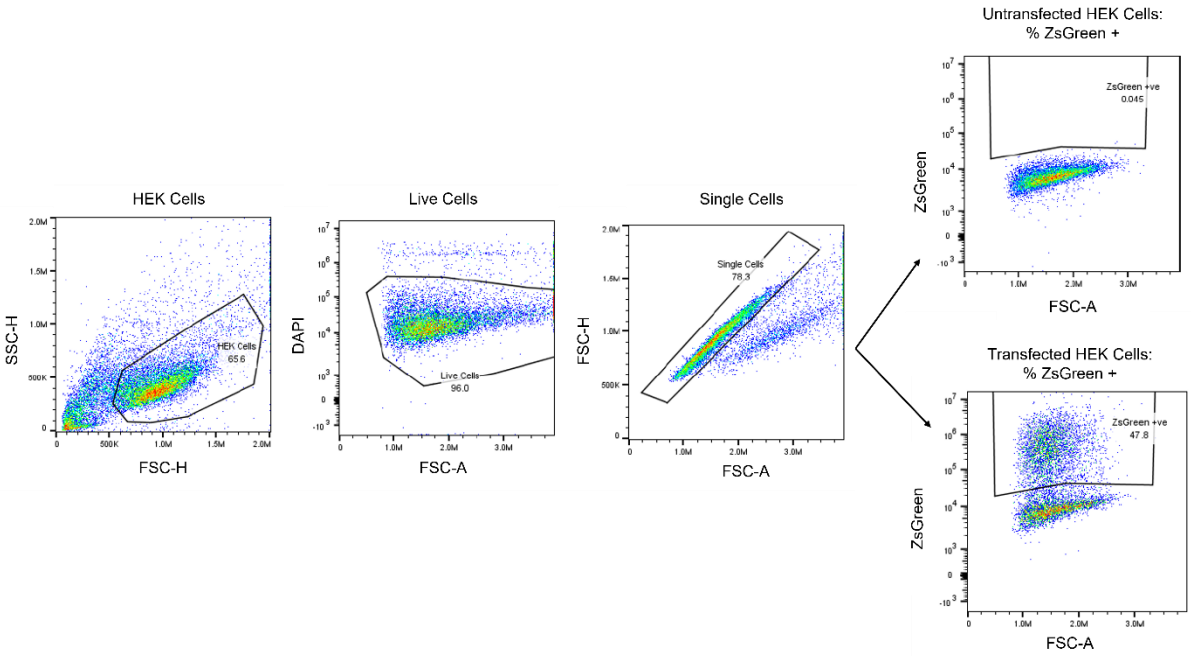

Figure 23: Gating Strategy for the Detection of ZsGreen Expression in HEK cells

Forward and side scatter were used to gate around the HEK cell population, gating out debris. Within the HEK cell population, DAPI staining enabled gating around the DAPI negative live cell population. Within the live cell population, forward scatter height and forward scatter area were used to remove doublets from the analysis. Finally, ZsGreen expression enabled the gating around the ZsGreen positive HEK cells, with the gate set using an untransfected HEK cell population as a negative control.

3.5.3. Detection of BCMA-CAR Expression

BCMA-CAR expression on the surface of transduced T cells was analysed by flow cytometry using an AF647 tagged BCMA-FC protein (GSK, #GRITS55881), which bound specifically to the BCMA-CAR construct. Approximately $2x10^5$ cells were plated into a V bottom polypropylene plate, and sufficient volume of FACS buffer was added to each well to bring the total volume up to 200µL per well. The plate was centrifuged at 400g for 5 minutes and supernatants were flicked off. Purified human IgG (hIgG) (Life Technologies, #027102) was diluted 1:125 in FACS buffer to generate a working solution of 40µg/mL. Cell pellets were resuspended in 50µL of diluted hIgG and incubated at RT for 5 minutes. The plate was centrifuged at 400g for 5 minutes and

supernatants were flicked off. AF647 tagged BCMA-FC protein was diluted 1:140 in FACS buffer and cell pellets were resuspended in 50µL of diluted BCMA-FC-AF647 and incubated for 30 minutes at RT in the dark. After incubation, the cells were washed three times – FACS buffer was added to bring the total volume up to 200µL, centrifuged at 400g for 5 minutes and supernatants were flicked off. DAPI was diluted 1:200 in FACS buffer to produce a working solution of 1µg/mL. Cell pellets were resuspended in 100 - 200µL of 1µg/mL DAPI solution. Samples were analysed on the MACSQuant® Analyser 10 Flow Cytometer, with the intent to acquire a minimum of 10,000 live events per sample. Data was analysed using FlowJo™ software, with gating strategy shown in Figure 24. Results were plotted onto graphs using GraphPad Prism.

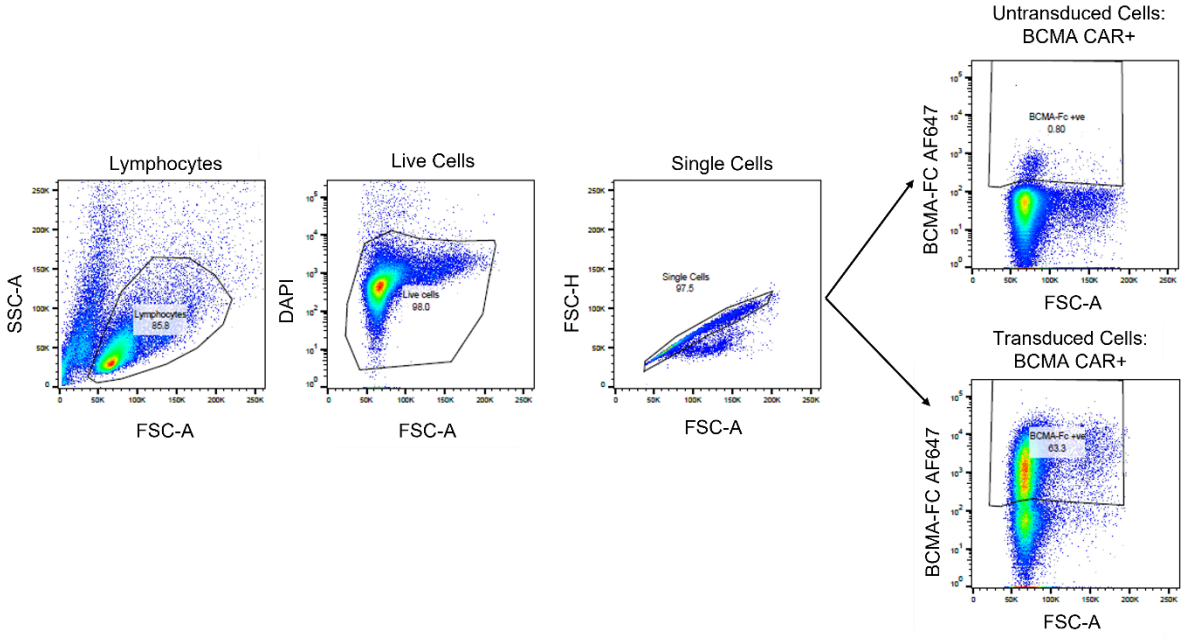

Figure 24: Gating Strategy for Detection of BCMA-CAR Expression

Forward and side scatter were used to gate around the lymphocyte population. Within the lymphocyte population DAPI staining enabled gating around the DAPI negative live cell population. Within the live cell population, forward scatter height and forward scatter area were used to remove doublets from the analysis. Finally, BCMA-FC AF647 staining enabled the gating around the BCMA-CAR positive T cells, with the gate set using an untransduced T cell population as a negative control.

3.5.4. Detection of LNGFR Expression

3.5.4.1. Within Total T cell Population

Expression of the CD19-CAR (vector batch #N67693-15-1), CAR-A, CAR-B and CAR-X were analysed by flow cytometry using PE conjugated anti-LNGFR Ab (Miltenyi Biotec, #130-091-885), which bound specifically to an LNGFR tag on the CAR construct. Approximately $2x10^5$ cells were plated into a V bottom polypropylene plate, and sufficient volume of FACS buffer was added to each well to bring the total volume up to 200µL per well. The plate was centrifuged at 400g for 5 minutes and supernatants were flicked off. Purified human IgG (hIgG) was diluted 1:125 in FACS buffer to generate a working solution of 40µg/mL. Cell pellets were resuspended in 50µL of diluted hIgG and incubated at RT for 5 minutes. The plate was centrifuged at 400g for 5 minutes and supernatants were flicked off. PE conjugated anti-LNGFR Ab was diluted 1:50 in FACS buffer and cell pellets were resuspended in 50µL of diluted PE anti-LNGFR Ab and incubated for 15 minutes at 4°C. After incubation, the cells were washed three times – FACS buffer was added to bring the total volume up to 200µL, centrifuged at 400g for 5 minutes and supernatants were flicked off. DAPI was diluted 1:200 in FACS buffer to produce a working solution of 1µg/mL. Cell pellets were resuspended in 100 - 200µL of 1µg/mL DAPI solution. Samples were analysed on the MACSQuant® Analyser 10 Flow Cytometer, with the intent to acquire a minimum of 10,000 live events per sample. Data was analysed using FlowJo™ software, with gating strategy shown in Figure 25. Results were plotted onto graphs using GraphPad Prism.

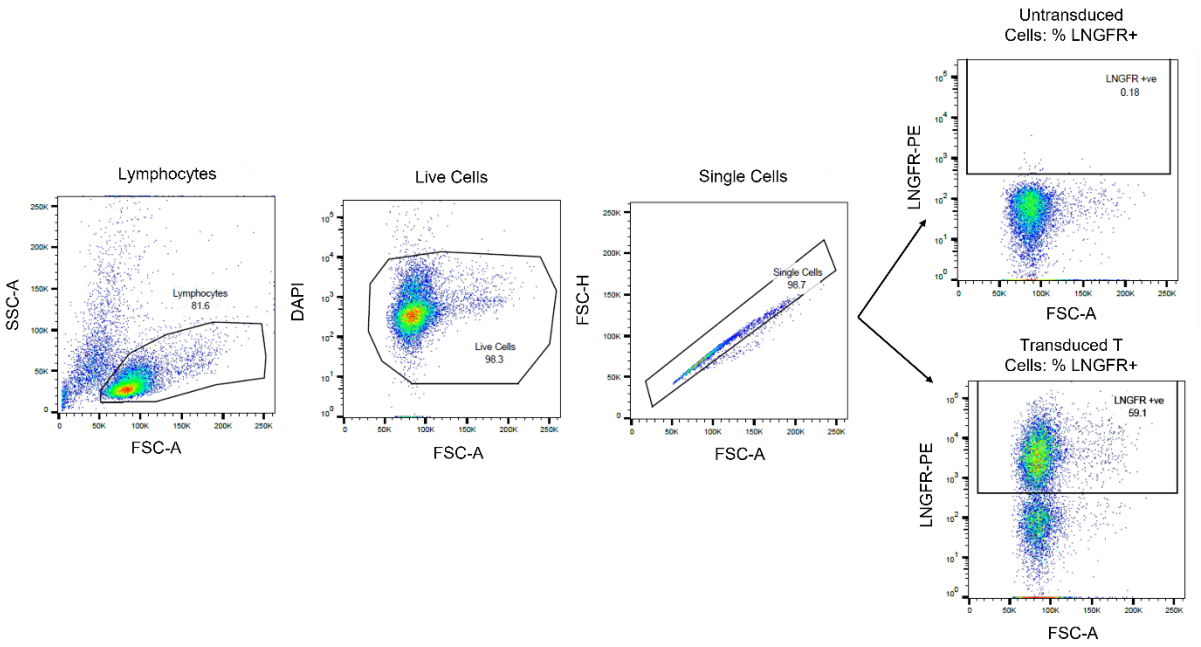

Figure 25: Gating Strategy for Detection of LNGFR Expression

Forward and side scatter were used to gate around the lymphocyte population. Within the lymphocyte population DAPI staining enabled gating around the DAPI negative live cell population. Within the live cell population, forward scatter height and forward scatter area were used to remove doublets from the analysis. Finally, LNGFR-PE staining enabled the gating around the LNGFR positive T cells, with the gate set using an untransduced T cell population as a negative control.

3.5.4.2. Within CD4+ and CD8+ T cell Populations

Within Figure 58, LNGFR expression was determined within the CD4+ and CD8+ T cell populations, therefore the staining methodology used differed slightly to that described within section 3.5.4.1.

Approximately $5x10^4$ cells per sample were plated into a 96-well V bottom polypropylene plate and centrifuged at 300g for 5 minutes before supernatants were removed. Cell pellets were resuspended in 40µL of 40µg/mL human IgG solution and incubated for 10 minutes at RT. 10µL of antibody mastermix was added to each well, with antibodies diluted in FACs buffer as described in Table 20. Cells were incubated at RT for 15 minutes in the dark. Fluorescence Minus One (FMO) wells were set up at the same time to enable accurate gating of samples during the analysis stage.

Table 20: LNGFR Staining Mastermix

Fluorophore	Antibody	Dilution
APC-Cy7	CD3	53.3
Bv786	CD8	26.6
VioBright 515	LNGFR	50.0

Table 20: Dilution of antibodies required for the LNGFR staining mastermix

Cells were washed three times with 200µL of FACS buffer and centrifugation at 300g for 5 minutes. Cell pellets were resuspended in 100µL of diluted Sytox AADvanced (Life Technologies, #S10274) (1 in 2000 dilution in FACS buffer) and incubated for 10 minutes at RT prior to analysis on the CytoFLEX S Flow Cytometer, with the intent to acquire a minimum of 20,000 live events per sample.

Data was analysed using FlowJo™ software, with gating strategy shown in Figure 26.

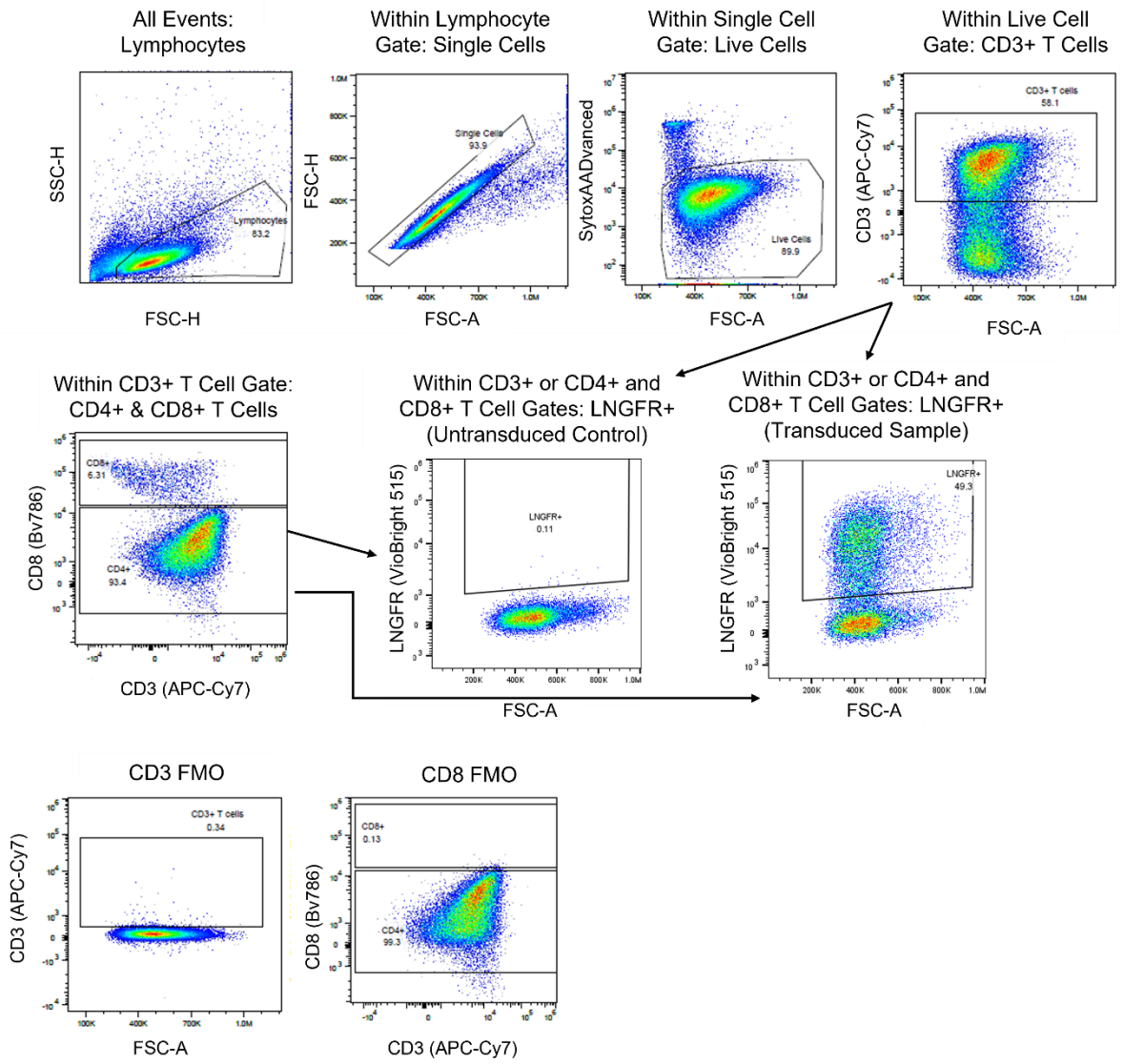

Figure 26: Gating Strategy for the Analysis of LNGFR Expression within CD3+, inferred CD4+ and CD8+ T cell Populations

Forward and side scatter were used to gate around the lymphocyte population. Within the lymphocyte population, forward scatter height and forward scatter area were used to remove doublets from the analysis. Within the single cell population, DAPI staining enabled gating around the DAPI negative live cell population. Within the live cell population, APC-Cy7 stained CD3+ T cells were gated and within the CD3+ T cell gate, APC-Cy7 anti-CD3 Ab and Bv786 anti-CD8 Ab were used to define the inferred CD4+ T cell population (CD3+ & CD8-) and the CD8+ T cell population (CD3+ & CD8+). Within either the CD3+, inferred CD4+ or CD8+ T cell populations, VioBright 515 anti-LNGFR Ab vs forward scatter was used to gate around the LNGFR positive T cells, using an untransduced sample as a negative control to set the gate. CD3 and CD8 FMO wells were used to accurately gate around the T cell populations.

3.5.5. Detection of CAR Expression (Vectors Y and Z)

The expression of CAR-Y and CAR-Z on the surface of transduced T cells was analysed by flow cytometry using a primary anti-Fab'(2)-Biotin Ab (Jackson ImmunoResearch, #115-066-072), which binds to the Fab region of the CAR construct, and a secondary PE-Streptavidin (Miltenyi Biotec, #130-106-789), which binds to biotin on the primary Ab. Approximately $2x10^5$ cells were plated into a V bottom polypropylene plate, and sufficient volume of FACS buffer was added to each well to bring the total volume up to 200µL per well. The plate was centrifuged at 400g for 5 minutes and supernatants were flicked off. Purified hIgG was diluted 1:125 in FACS buffer to generate a working solution of 40µg/mL. Cell pellets were resuspended in 50µL of diluted hIgG and incubated at RT for 5 minutes. The plate was centrifuged at 400g for 5 minutes and supernatants were flicked off. Anti-Fab'(2)-Biotin Ab was diluted 1:250 in FACS buffer and cell pellets were resuspended in 50µL of diluted anti-Fab'(2)-Biotin Ab and incubated for 45 minutes at 4°C. After incubation, the cells were washed twice – FACS buffer was added to bring the total volume up to 200µL, centrifuged at 400g for 5 minutes and supernatants were flicked off. PE-Streptavidin was diluted 1:500 in FACS buffer, and cell pellets were resuspended in 50µL of diluted PE-Streptavidin and incubated for 45 minutes at 4°C. Cells were washed three with FACS buffer and stained with 100µL of 1µg/mL DAPI solution prior to analysis on the MACSQuant® Analyser 10 Flow Cytometer, with the intent to acquire a minimum of 10,000 live events per sample. Data was analysed using FlowJo™ software, with gating strategy shown in Figure 27. Results were plotted onto graphs using GraphPad Prism.

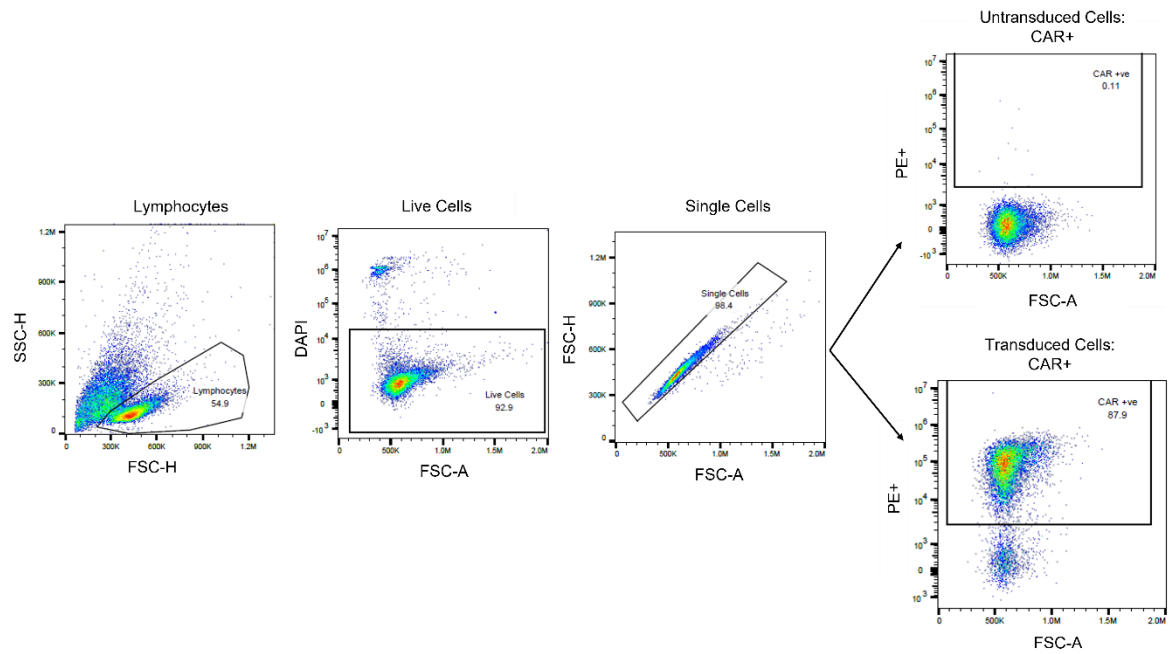

Figure 27: Gating Strategy for Detection of CAR Expression

Forward and side scatter were used to gate around the lymphocyte population. Within the lymphocyte population DAPI staining enabled gating around the DAPI negative live cell population. Within the live cell population, forward scatter height and forward scatter area were used to remove doublets from the analysis. Finally, PE-Streptavidin staining enabled the gating around the CAR positive T cells, with the gate set using an untransduced T cell population as a negative control.

3.5.6. Detection of Engineered TCR Expression (Vectors C and D)

The expression of engineered TCR-C and TCR-D on the surface of transduced T cells was analysed by flow cytometry using a PE conjugated dextramer reagent (Immundex, #WB2696-PE) which contains multiple binding sites enabling the specific binding of engineered TCR expressing T cells. Between $5x10^5$ and $1x10^6$ cells per sample were plated into a 96-well plate, and sufficient volume of PBS was added to each well to bring the total volume up to 200µL per well. The plate was centrifuged at 300g for 5 minutes and supernatants were flicked off. Cell pellets were resuspended in 50µL of Zombie Near Infrared live-dead stain (Biolegend, #423106), diluted 1 in 1000 in PBS, and incubated with 15 minutes at RT. 150µL of PBS was added to each well, the plate was centrifuged at 300g for 5 minutes and supernatants were flicked off. 10µL of PE

conjugated dextramer reagent or PE conjugated negative control dextramer (Immundex, #WB2666-PE) was added to wells as appropriate and cells were incubated for 25 minutes at RT. Cell pellets were washed twice with 200µL of FACs buffer, centrifuging at 300g for 5 minutes each time. Cell pellets were resuspended in 100µL of FACs buffer and analysed on the Fortessa X-20 Flow Cytometer (BD), with the intent to acquire a minimum of 50,000 events per sample.

Data was analysed using FlowJo™ software, with gating strategy shown in Figure 28. Results were plotted onto graphs using GraphPad Prism.

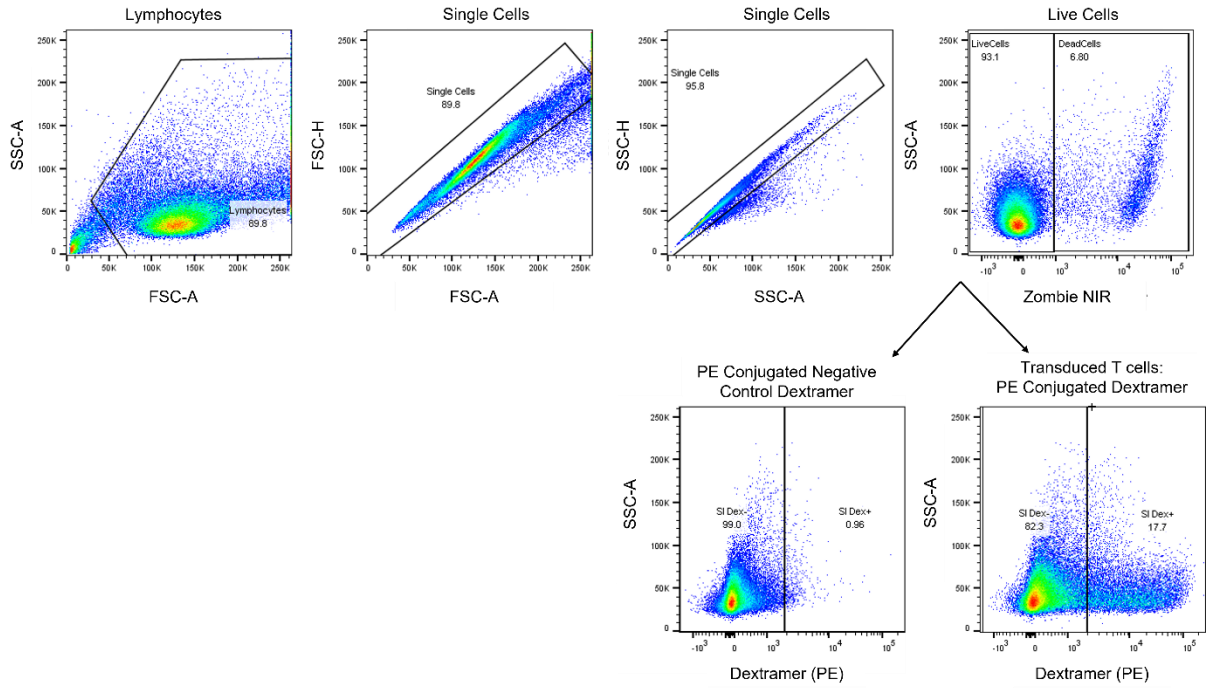

Figure 28: Gating Strategy for Detection of Engineered TCR Expression

Forward and side scatter were used to gate around the lymphocyte population. Both forward scatter height vs forward scatter area and side scatter height vs side scatter area were used to remove doublets from the analysis. Within the single cell population, Zombie NIR negative T cells were gated as live cells. Finally, dextramer positive T cells were gated as engineered TCR expressing T cells, with the gate set using PE conjugated negative control dextramer stained T cells.

3.6. Activation Status Analysis

3.6.1. Analysis of LDLr and CD69 Expression

The frequency of CD4 and CD8 T cells and expression of low-density lipoprotein receptor (LDLr) and CD69 activation markers within the cell populations was analysed by flow cytometry. $2x10^5$ cells from each sample were transferred into a 96-well V bottom polypropylene plate and sufficient volume of FACs buffer was added to each well to bring the total volume up to 200µL. The plate was centrifuged at 400xg for 5 minutes and the supernatants were flicked off. Cell pellets were resuspended in a 40µg/mL working solution of purified hIgG. Cells were incubated for 5 minutes at room temperature, before being centrifuged at 400xg for 5 minutes and supernatants flicked off. Sufficient volume of antibody mastermix, for 50µL per sample, was made up in FACs buffer with antibodies diluted as shown in Table 21.

Table 21: Activation Status Analysis Antibody Mastermix

Fluorophore	Target	Manufacturer	Catalogue Number	Dilution
APC	CD3	Miltenyi Biotec	130-113-135	75
APC-Vio770	CD8	Miltenyi Biotec	130-110-681	75
FITC	CD69	Miltenyi Biotec	130-112-612	50
PE	LDLr	R&D Systems	FAB2148P	10

Table 21: Dilution of antibodies within the activation status analysis mastermix

Samples were incubated for 30 minutes at RT in the dark, before being washed three times with FACs buffer making the total volume up to 200µL, centrifuging at 300xg for 5 minutes and flicking off the supernatants. Cell pellets were resuspended in 100µL of a 1µg/mL working solution of DAPI.

Due to the potential for spill-over of fluorescence between the channels, particularly between FITC and PE, single stain control wells were set up to enable the creation of a compensation matrix within the CytoFLEX S software, allowing for correction of fluorescence spill-over prior to analysis of the samples. Single stain control wells were

analysed on the CytoFLEX S Flow Cytometer (Figure 29), allowing the setup of a compensation matrix (Figure 30), which was applied prior to the analysis of the remaining samples. The set-up of the compensation matrix was successful, with orange and red highlighted compensation values not a concern as these channels (APC-A700, KO525 and ECD) were not used within this analysis. Samples were acquired with the intent to capture a minimum of 10,000 live events per sample. Data was analysed using FlowJo™ software, with gating strategy shown in Figure 31. Results were plotted onto graphs using GraphPad Prism.

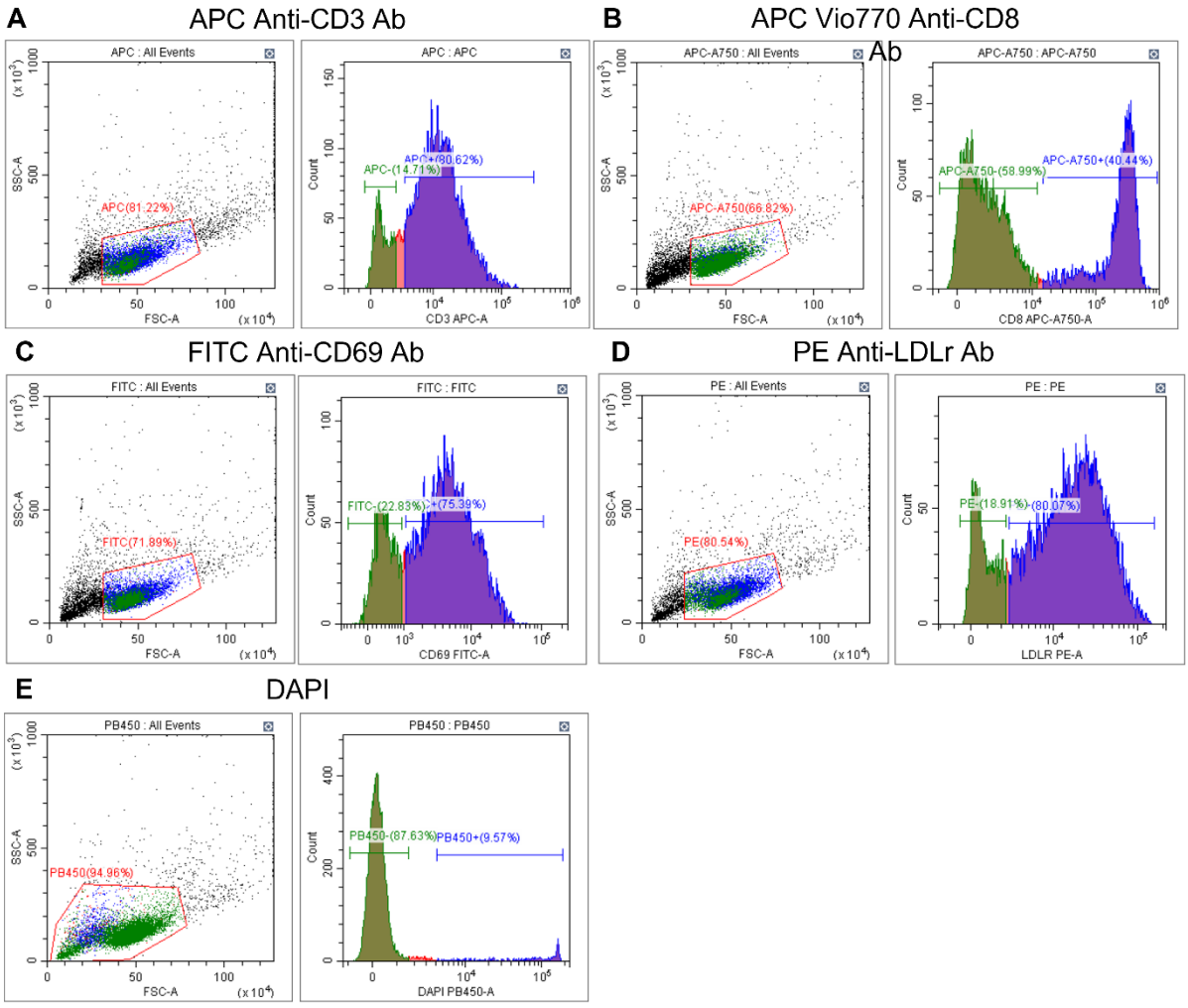

Figure 29: Single Stain Control Well Analysis for Compensation Matrix Setup

Prior to analysis of samples on the CytoFLEX S flow cytometer, single stain control wells were analysed to enable the creation of a compensation matrix enabling the correction of fluorescence spill-over.

Autofl.	Channel	-FITC%	-PerCP...	-APC%	-APC-A700%	-APC-A750%	-PB450%	-KO525%	-Violet 660%	-Violet 786%	-PE%	-ECD%	-PC5.5%	-PC7%
17.94	FITC		0.00	0.30	0.00	0.00	0.67	0.00	0.00	0.00	0.20	0.00	0.00	0.00
0.00	PerCP	19.81		5.16	0.00	0.13	4.03	0.00	0.00	0.00	19.00	0.00	0.00	0.00
2.94	APC	0.63	0.00		0.00	4.05	0.12	0.00	0.00	0.00	0.35	0.00	0.00	0.00
0.00	APC-A700	0.56	0.00	108.55		6.27	0.44	0.00	0.00	0.00	0.17	0.00	0.00	0.00
4.76	APC-A750	0.17	0.00	17.08	0.00		0.13	0.00	0.00	0.00	0.10	0.00	0.00	0.00
157.10	PB450	0.32	0.00	0.12	0.00	0.00		0.00	0.00	0.00	0.00	0.00	0.00	0.00
0.00	KO525	56.63	0.00	6.99	0.00	0.00	2569.16		0.00	0.00	3.31	0.00	0.00	0.00
0.00	Violet660	1.05	0.00	3.94	0.00	0.12	26.03	0.00		0.00	0.84	0.00	0.00	0.00
0.00	Violet786	0.40	0.00	1.46	0.00	3.57	7.14	0.00	0.00		0.28	0.00	0.00	0.00
5.52	PE	0.33	0.00	0.13	0.00	0.00	0.14	0.00	0.00	0.00		0.00	0.00	0.00
0.00	ECD	1.12	0.00	1.69	0.00	0.05	0.53	0.00	0.00	0.00	126.88		0.00	0.00
0.00	PC5.5	1.58	0.00	50.74	0.00	2.19	0.62	0.00	0.00	0.00	32.84	0.00		0.00
0.00	PC7	0.49	0.00	3.92	0.00	19.24	0.11	0.00	0.00	0.00	1.88	0.00	0.00	

Figure 30: Compensation Matrix

Analysis of single stain control wells enabled creation of a compensation matrix, within the CytoFLEX S software, to be applied prior to sample analysis. The orange and red values within the matrix, highlight channels where a large amount of compensation was required – however, these were not of concern as the channels impacted (APC-A700, KO525 and ECD) were not used within this analysis.

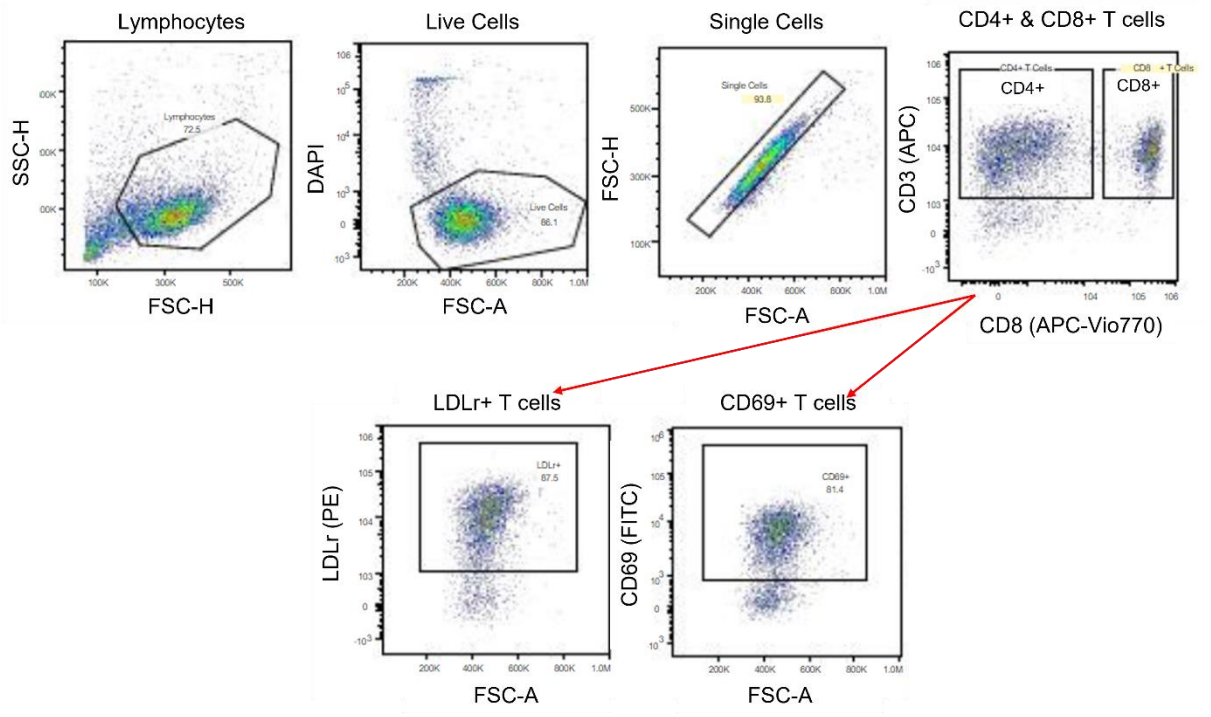

Figure 31: Gating Strategy for Detection of LDLr and CD69 Expression

Forward and side scatter were used to gate around the lymphocyte population. Within the lymphocyte population, DAPI staining enabled gating around the DAPI negative live cell population. Within the live cell population, forward scatter height and forward scatter area were used to remove doublets from the analysis. APC anti-CD3 Ab and APC-Vio770 anti-CD8 Ab was used to gate around inferred CD4+ T cells (CD3+ & CD8-) and CD8+ T cells (CD3+ & CD8+). Within the single cell, inferred CD4+ and CD8+ T cell gates, expression of LDLr and CD69 was analysed, with gates set using FMO controls.

3.7. Cell Population Purity

The 8 colour immunophenotyping kit (Miltenyi Biotec, #130-120-640) was used for the analysis of different immune cell populations on the day of cell isolation. Prior to the staining of the samples, a compensation matrix was set up on the MACSQuant® Analyser 10 Flow Cytometer to ensure that the samples were compensated appropriately when using this multi-colour kit. In order to set up the compensation matrix, the following protocol was used. Firstly, $1x10^6$ cells were transferred into six FACS tubes, centrifuged at 300xg for 5 minutes and the supernatant was removed. Cell pellets were resuspended in 100µL of FACS buffer. Each tube had one of the below antibodies added:

- 10µL of VioBright 667 Anti-CD4 Ab
- 10µL of APC-Vio770 Anti-CD8 Ab
- 10µL of PE-Vio770 Anti-CD19 Ab
- 10µL of VioBright 515 Anti-CD56 Ab
- 1µL of 7-AAD
- Blank – No stain added

Cells were incubated for 10 minutes at 4°C, before being washed with 2mL of FACS buffer, centrifuged at 300xg for 5 minutes and the supernatant poured off. The cell pellets were resuspended in 500µL of FACS buffer and analysed on the MACSQuant® Analyser 10 Flow Cytometer, following compensation matrix set up steps as per the manufacturer's instructions. Subsequent to compensation matrix setup, $5x10^5$ cells from each sample were plated into a 96-well V bottom polypropylene plate and topped up to a total volume of 250µL with FACS buffer. The plate was centrifuged at 300xg for 5 minutes, supernatants were flicked off and cell pellets were resuspended in 100µL of FACS buffer. 10µL of the 8 colour immunophenotyping antibody cocktail (components listed within Table 22) and 1µL of 7-AAD was added to each well and samples were incubated at 4°C for 10 minutes. Samples were washed twice by adding sufficient volume of FACS buffer to bring the total volume to 200µL per well, centrifuging at 300xg for 5 minutes and flicking off the supernatants. Cell pellets were resuspended in 100µL of FACS buffer and analysed on the MACSQuant® Analyser 10 Flow Cytometry acquiring 10,000 live events per sample, applying the compensation matrix settings that were previously set up to the instrument settings.

Table 22: Components of 8 colour immunophenotyping antibody cocktail

Antibody	Fluorophore	Clone
Anti-CD3	PE	REA613
Anti-CD4	Vio®Bright 667	REA623
Anti-CD8	APC-Vio770	REA734
Anti-CD14	VioBlue®	REA599
Anti-CD16	Vio Bright 515	REA423
Anti-CD19	PE-Vio 770	REA675
Anti-CD45	VioGreen™	REA747
Anti-CD56	VioBright 515	REA196

Table 22: The antibodies included within the 8 colour immunophenotyping antibody cocktail target cell markers enabling the differentiation of cell populations and determination of cell population purity.

Data was analysed using FlowJo™ software, with gating strategy shown in Figure 32. Results were plotted onto graphs using GraphPad Prism.

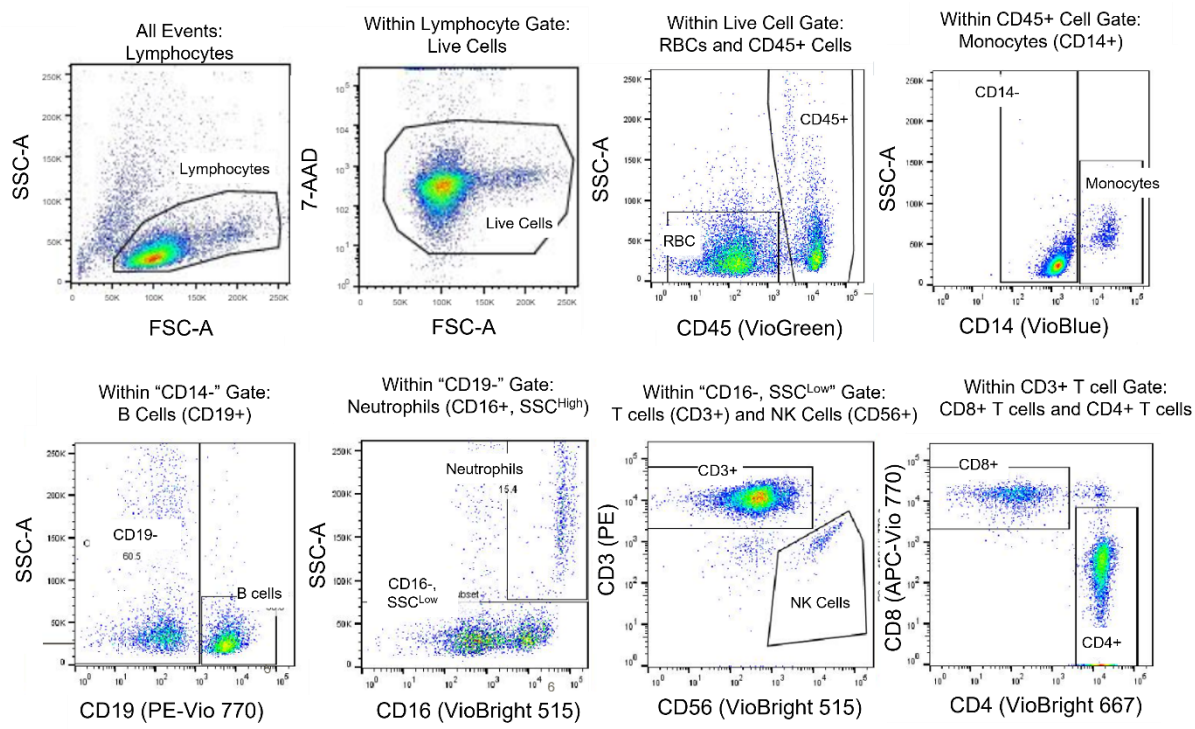

Figure 32: Gating Strategy for Cell Population Purity Analysis

Forward and side scatter were used to gate around the lymphocyte population. Within the lymphocyte population, 7-AAD staining enabled gating around the 7-AAD negative live cell population. Within the live cell population, side scatter and CD45 staining were used to gate around the CD45+ cells and the CD45- RBCs. Within the CD45+ cell gate, CD14 staining was used to gate around CD14+ monocytes. Within the CD14 negative gate, CD19 staining was used to gate around the CD19+ B cells. Within the CD19 negative gate, side scatter and CD16 staining was used to gate around the CD16+ SSC^{High} Neutrophils. Within the CD16-, SSC^{Low} gate, CD3 and CD56 staining were used to gate around the CD3+ T cells and the CD56+ NK cells. Finally, within the CD3+ gate, CD8+ T cells and CD4+ T cells were gated using CD8 and CD4 staining.

3.8. Differentiation Phenotype Analysis

The method of analysis of differentiation differed between Figure 70 and Figure 80, as methodology optimisation was performed allowing for a standardised method (as described for Figure 80) to be used going forward. For completeness, both methods are described below. The phenotypic markers used to define each T cell subset are shown within Table 23. Subsequent to methodology optimisation, the Fortessa X-20 flow cytometer was used instead of the CytoFLEX S flow cytometer, which enabled the use of a wider range of fluorophores due to the increased number of channels for fluorescence detection. This enabled the greater separation of cell populations, making gating and identification of differentiated T cell populations more accurate. The use of BV605 anti-CD45RA Ab and AF700 anti-CD45RO Ab within the optimised method improved the separation between these two populations, enabling more accurate gating. This improvement to the methodology may have increased the frequency of CD45RA+ cells identified within Figure 70. The decision was also taken to increase the minimum number of live events recorded to 50,000, in order to improve the gating of rarer cell populations. It was determined that CD62L was not required for the identification of T cell subsets, therefore this antibody was not included within the analysis method described within section 3.8.2.

Table 23: Phenotypic Markers of T cell Subsets

T cell Subset	Phenotypic Markers
Naïve (T_N)	CD45RA+, CD95-, CCR7+, (CD62L-)
Effector	CD45RA+, CD95+, CCR7-, (CD62L-)
Stem Cell Memory	CD45RA+, CD95+, CCR7+, (CD62L+)
Central Memory	CD45RO+, CD95+, CCR7+, (CD62L+)
Effector Memory	CD45RO+, CD95+, CCR7-

Table 23: T cell subsets were defined based on the expression of the listed phenotypic markers.

3.8.1. Differentiation Analysis (Figure 70)

Approximately $5x10^4$ cells per sample were plated into a 96-well V bottom polypropylene plate and centrifuged at 300g for 5 minutes before supernatants were removed. Cell pellets were resuspended in 40µL of 40µg/mL human IgG solution and incubated for 10 minutes at RT. 10µL of antibody mastermix was added to each well, with antibodies diluted in FACs buffer as described in Table 24. Cells were incubated at RT for 15 minutes in the dark.

Single stain control wells and Fluorescence Minus One (FMO) wells were set up at the same time to enable the setup of a compensation matrix and to enable accurate gating of samples during the analysis stage.

Table 24: Differentiation Antibody Master Mix

Fluorophore	Antibody	Dilution
APC-Cy7	CD3	53.3
Bv786	CD8	26.6
Bv650	CD62L	13.3
PE	CD95	26.6
PE-Cy7	CD45RO	6.6
Bv421	CCR7	8.3
AF647	CD45RA	8.3

Table 24: The required dilution of antibodies used within differentiation mastermix

Cells were washed three times with 200µL of FACS buffer and centrifugation at 300g for 5 minutes. Cell pellets were resuspended in 100µL of diluted Sytox AADvanced (Life Technologies, #S10274) (1 in 2000 dilution in FACS buffer) and incubated for 10 minutes at RT prior to analysis on the CytoFLEX S Flow Cytometer, with the intent to acquire a minimum of 20,000 live events per sample.

Data was analysed using FlowJo™ software, with gating strategy shown in Figure 34. The phenotypic markers used to define each of the T cell populations are shown within Table 23. Results were plotted onto graphs using GraphPad Prism.

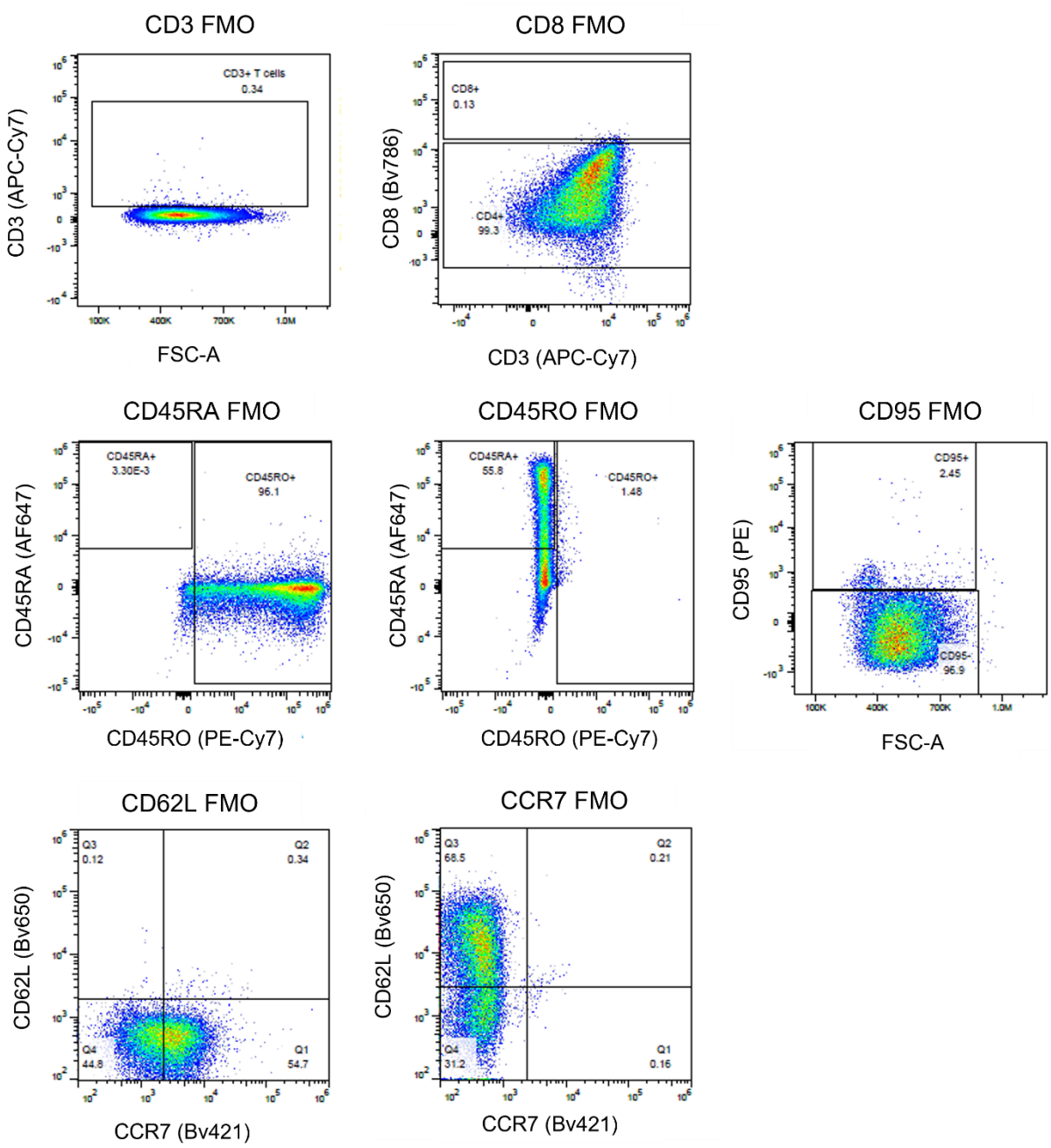

Figure 33: FMO Control Flow Plots

Flow gates were set based on FMO controls for each fluorophore to ensure accurate gating of samples.

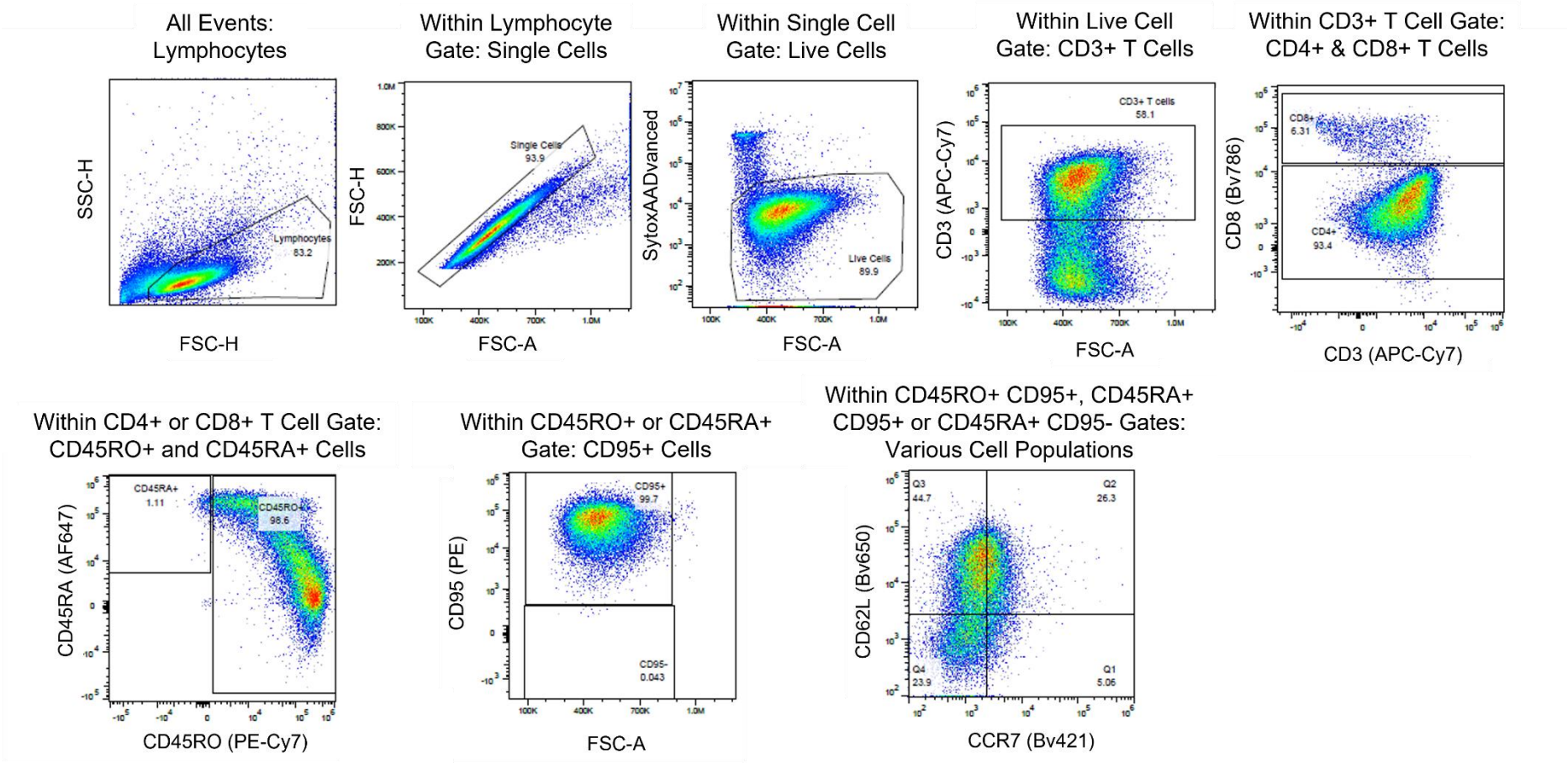

Figure 34: Flow cytometry gating strategy for the analysis of T cell differentiation phenotype (Figure 70)

Within the inferred CD4+ and CD8+ T cell populations, the phenotypic markers CD45RO, CD45RA, CD95, CD62L and CCR7 were used to define the T_{EM}, T_{CM}, T_N, T_{SCM} and T_{EFF} populations. FMO controls were used to determine where gates should be set.

3.8.2. Differentiation Analysis (Figure 80)

Between $5x10^5$ and $1x10^6$ cells per sample were plated into a 96-well plate, and sufficient volume of PBS was added to each well to bring the total volume up to 200µL per well. The plate was centrifuged at 300g for 5 minutes and supernatants were flicked off. Cell pellets were resuspended in 50µL of Zombie Near Infrared live-dead stain, diluted 1 in 1000 in PBS, and incubated with 15 minutes at RT. 150µL of PBS was added to each well, the plate was centrifuged at 300g for 5 minutes and supernatants were flicked off. Cell pellets were resuspended in 50µL of FcX blocking reagent (Biolegend, #422302) and incubated for 15 minutes at RT. Cell pellets were washed with 150µL of FACS buffer and stained with 50µL of the Stain 1 mastermix (components described in Table 25) and incubated for 30 minutes at RT.

Single stain control wells and Fluorescence Minus One (FMO) wells were set up at the same time to enable the setup of a compensation matrix and to enable accurate gating of samples during the analysis stage.

Table 25: Stain 1 Mastermix

Fluorophore	Antibody	Dilution
BV421	CCR7	80
BV510	CD69	200
BV711	CD95	100
BV785	PD1	80
PE-Cy7	TIM3	80
AF488	Lag3	160
BB700	CD25	100
BUV395	CD3	100
BUV496	CD8	200
BUV737	CD4	200

Table 25: Required dilution of antibodies used within the stain 1 mastermix

Table 26: Stain 2 Mastermix

Fluorophore	Antibody	Dilution
BV605	CD45RA	100
AF700	CD45RO	50

Table 26: Required dilution of antibodies used within the stain 2 mastermix

Cell pellets were washed with 150µL of FACS buffer and resuspended in 100µL of 1x CytoFix Fixation buffer (BD, #554655) (containing 4% v/v formaldehyde) before incubating for 30 minutes at RT. Cell pellets were washed two times with 200µL of FACS buffer and stained with 50µL of the Stain 2 mastermix (components described in Table 26) and incubated for 30 minutes at RT. Cell pellets were washed one time with 150µL of FACS buffer, and resuspended in 100µL of FACS buffer before analysing on the Fortessa X-20 Flow Cytometer, with the intent to acquire a minimum of 50,000 events per sample.

Data was analysed using FlowJo™, with gating strategy shown in Figure 36. Gates were set based on FMO controls for each fluorophore, as shown in Figure 35. The phenotypic markers used to define each of the T cell populations are shown within Table 23. Results were plotted onto graphs using GraphPad Prism and Spotfire (version 7.11, TIBCO).

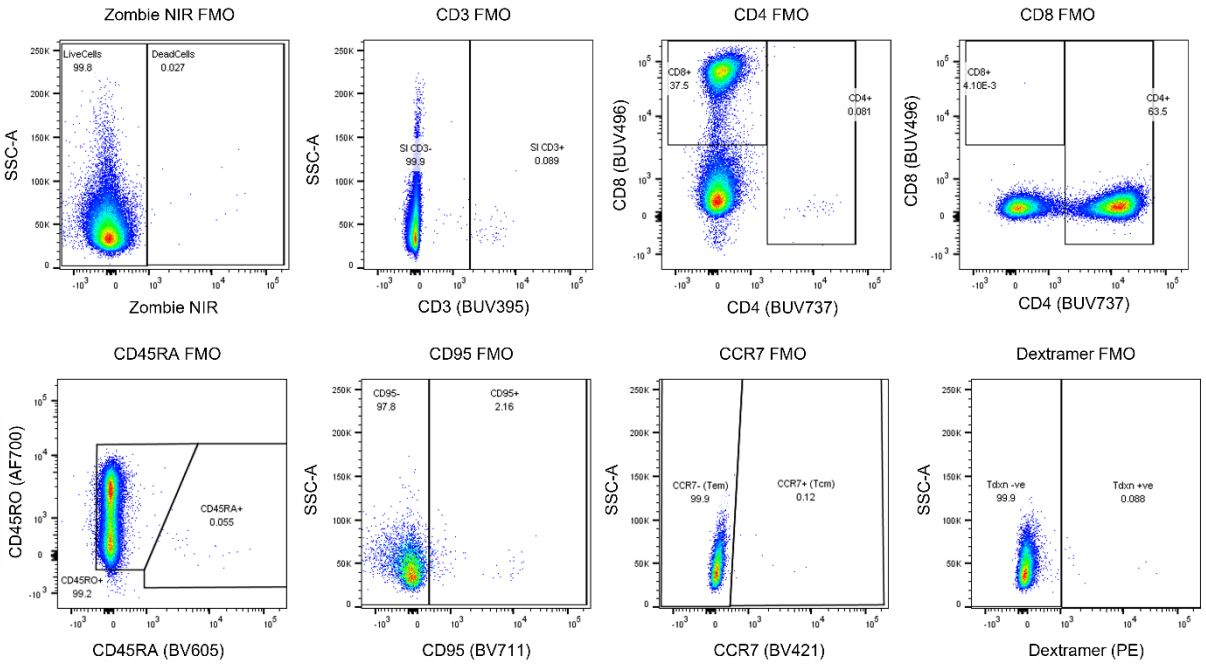

Figure 35: FMO Control Flow Plots

Flow gates were set based on FMO controls for each fluorophore to ensure accurate gating of samples.

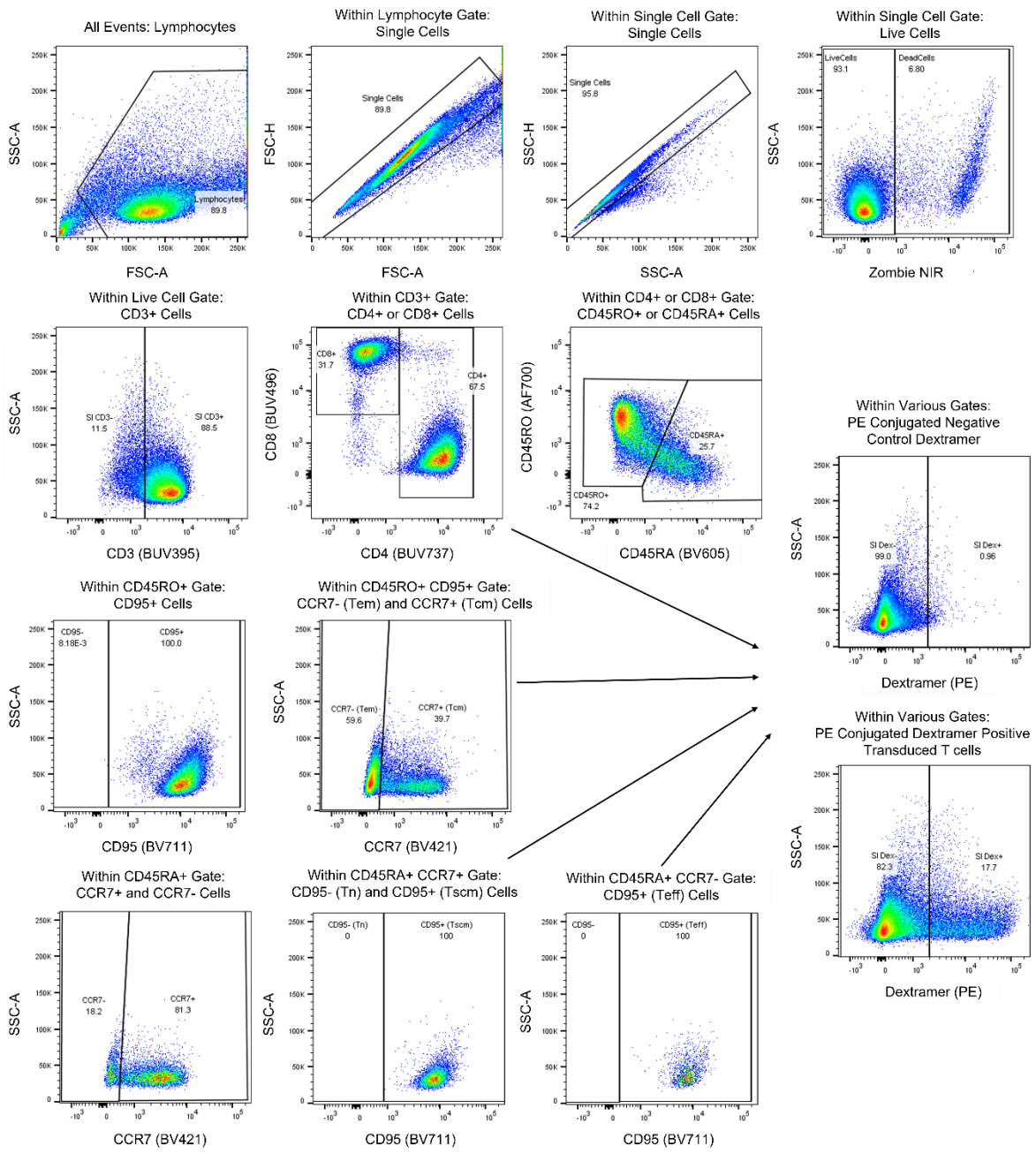

Figure 36: Flow cytometry gating strategy for the analysis of T cell differentiation phenotype (Figure 80)

Within the CD4+ and CD8+ T cell populations, the phenotypic markers CD45RO, CD45RA, CD95 and CCR7 were used to define the T_{EM}, T_{CM}, T_N, T_{SCM} and T_{EFF} populations. Dextramer positive stained cells from each population were gated as engineered TCR expressing T cells, with the gate set using PE conjugated negative control dextramer stained T cells.

3.9. Retrogenix™

Plasma membrane protein array data was analysed at Retrogenix™ with binding assessed by imaging for fluorescence and quantitated for transduction efficiency using ImageQuant software (GE). Levels of background binding were determined using areas of untransfected HEK293 cells. A protein 'hit' was defined as duplicate spots showing a raised signal compared to background levels. This was achieved by visual inspection using the images gridded on the ImageQuant software. Hits were classified as strong, medium, weak, or very weak depending on the intensity of the duplicate spots.

3.10. Functional Testing

3.10.1. Cytotoxicity (xCELLigence® Assay)

Analysis of antigen-specific cell killing by transduced T cells was performed using the xCELLigence® (ACEA). A background equilibration step was performed by added 50µL of pre-warmed xCELLigence® media (RPMI (GIBCO, #31870-025)+ 10% (v/v) FBS + 1% (v/v) Glutamax (GIBCO, #35050-038)) to each well of the xCELLigence® E-plate (Agilent, #300600910) before placing the plates within the xCELLigence® cradles for a background sweep to be performed. Antigen positive and antigen negative cell lines were resuspended to a density of $4x10^5$ cells/mL in xCELLigence® media, with 50µL added to each of the appropriate wells of the xCELLigence® plates to seed $2x10^4$ target cells per well. Plates were left at RT for 45 minutes to allow target cell lines to evenly settle across the well before being placed into the xCELLigence® cradles for initiation of assay reading.

Transduced and untransduced T cell populations were thawed on the same day as target cell seeding, following the protocol described within 3.2.4, allowing for populations to recover for 24 hours prior to addition to xCELLigence® plates. Prior to recovery, each transduced T cell population was normalised, via addition of untransduced T cell populations treated with the same compound, to within 5% of the transduction efficiency of the relevant untreated transduced control population for each

donor. Once normalised, T cell populations were seeded into 24-well G-REX® plates and incubated for 24 hours at 37°C with 5% CO_2.

After allowing for 24-hour target cell proliferation and T cell recovery, T cell populations were harvested from culture vessels, counted as described in section 3.4, and resuspended to a density of $2x10^5$ cells/mL in xCELLigence® media. The xCELLigence® assay was paused, and 100µL of T cell solution ($2x10^4$ cells) were added to the appropriate wells of the xCELLigence® plate. 100µL of media only or 0.1% Triton X solution (Sigma, #X100-5ML) were added to no killing and 100% lysis control wells respectively. xCELLigence® plates were returned to the appropriate xCELLigence® cradles and plates were incubated for a further 48 hours, with assay measurements performed every hour. After approximately 24 hours and 48 hours, the assay was paused and 50µL of supernatant was carefully removed from each well and transferred into 96-well V bottom polypropylene plates before being stored at -80°C for later MSD® analysis of IFN-γ production.

Analysis of xCELLigence® data was performed within the RTCA xCELLigence® software (version 2.3.0), in which calculation of the KT_{50} values were determined. Calculation of the KT_{50} ratio of compound treated populations compared to untreated transduced T cell populations was performed within Microsoft Excel™ (version 2002).

3.10.2. MSD®

Analysis of cytokines in the cell culture supernatant was performed using MSD®, with a human IFN-γ tissue culture kit (MSD®, K151AEB) used for the analysis of IFN-γ production within Figure 49 and a human cytokine panel 1 kit (MSD®, #N05050A-1) used for the analysis of IL-7 and IL-15 concentration within Figure 72. Supernatants, stored at -80°C, were thawed at RT. Samples and calibrators were prepared as per manufacturer's instructions and 25µl of each sample were added to the MSD® plate. Calibrators were added in duplicate. Plates were sealed and incubated at RT with shaking for between 1.5 to 2 hours. Plates were washed 3 x with PBS + 0.5% (v/v) Tween (Sodexo) using the plate washer (BioTek). Detection antibody was diluted to a 1x solution in the appropriate diluent according to the MSD® kit used. Following the addition of 25µl of 1x detection antibody, the plates were sealed and incubated at room temperature with shaking for between 1.5 hours to 2 hours. Plates were washed as before. 150µl of 2 x read buffer was added to each well before reading on the Sector 600 Imager (MSD®).

MSD® data was analysed using XLFit version 5.3.1.3 software (XLFit model 204 and 4 parameter nonlinear regression) to calculate IFN-γ, lL-7 and IL-15 concentrations in pg/mL based on the results of the standard curve included in each experiment.

3.11. HEK Transfection

In order to validate an off-target binding hit between CAR-X and the Netrin-1 receptor (DCC), which was identified through Retrogenix™ screening, suspension HEK cells were transfected with a DCC expressing plasmid. DCC expression was confirmed by flow cytometry analysis of ZsGreen expression (section 3.5.2), qPCR analysis of DCC gene expression (section 3.11.2) and western blot analysis of DCC protein expression (section 3.11.3). DCC-expressing HEK cells were used within the co-culture experiment described within section 3.12.

3.11.1. Transfection

Three methods of HEK transfection were frequently used within GSK and were shown to be successful, therefore optimisation of the transfection method was not performed. Instead, the three transfection reagents (PEIpro (Polypus, #115-010), 293Fectin (Invitrogen, #12347019) and Lipofectamine 3000 (Invitrogen, #L3000-001)) were tested with two different amounts of the plasmid DNA (4µg and 8µg) for the transfection of HEK cells. ZsGreen expression analysis (section 3.5.2), via flow cytometry, was used to confirm successful HEK cell transfection and enable the method resulting in the highest transfection efficiency to be chosen for use in the subsequent HEK cell transfection (Figure 46A).

HEK293Tsa cells were harvested from culture vessels, centrifuged, resuspended in HEK293Tsa media (components described within Table 14) and counted on the ViCell XR (Beckman Coulter). Cells were resuspended at $4x10^6$ cells/mL and $2x10^6$ cells were plated into a 96-well DeepWell™ plate (Nunc™, #278605).

For PEIpro transfection, the required volume of optiMEM media (GIBCO, #31985070) and plasmid DNA were transferred into a 1.5mL Eppendorf tube and incubated at RT for 5 minutes. The required volume of PEIpro transfection reagent was added to the tube and mixed gently before incubating for 30 minutes at RT. The transfection mixture was then added dropwise into the appropriate wells of the 96 well DeepWell™ plate (Table 27). The required volumes of reagents for PEIpro transfection are listed in Table 28.

For 293Fectin transfection, the required volume of optiMEM media was transferred into two different tubes – Tube A for DNA and Tube B for transfection reagent. The appropriate volume of plasmid DNA was added into Tube A and the appropriate volume of 293Fectin transfection reagent was added into Tube B. Both tubes were mixed gently and incubated for 5 minutes at RT. The optiMEM-DNA mixture was added into the optiMEM-293Fectin mixture and mixed by flicking the tube before being incubated for 30 minutes at RT. The transfection mixture was then added dropwise into the appropriate wells of the 96 well DeepWell™ plate (Table 27). The required volumes of reagents for 293Fectin transfection are listed in Table 29.

For Lipofectamine 3000 transfection, the required volume of optiMEM media was transferred into two different tubes – Tube A for DNA and Tube B for transfection reagent. The appropriate volume of plasmid DNA was added into Tube A and then the appropriate volume of P3000 was added into the optiMEM-DNA mixture in Tube A. The appropriate volume of Lipofectamine 3000 was added into Tube B. Both tubes were mixed gently and incubated for 5 minutes at RT. The optiMEM-DNA-P3000 mixture was added into the optiMEM-Lipofectamine 3000 mixture and mixed by flicking the tube before being incubated for 15 minutes at RT. The transfection mixture was then added dropwise into the appropriate wells of the 96 well DeepWell™ plate (Table 27). The required volumes of reagents for Lipofectamine 3000 transfection are listed in Table 30.

Subsequent to the addition of each transfection reagent, the HEK cells were incubated in a 37°C shaker incubator with 210rpm and 5% CO_2 for 72 hours. The transfection efficiency of the HEK cells was analysed by flow cytometry analysis of ZsGreen expression following the protocol described in section 3.5.2.

Table 27: Plate Plan for HEK Transfection Method Assessment

			PEIpro			293Fectin			Lipofectamine 3000			
	1	**2**	**3**	**4**	**5**	**6**	**7**	**8**	**9**	**10**	**11**	**12**
A												
B			UT	UT		UT	UT		UT	UT		
C												
D			ZsG (4µg)	ZsG (8µg)		ZsG (4µg)	ZsG (8µg)		ZsG (4µg)	ZsG (8µg)		
E												
F			DCC (4µg)	DCC (8µg)		DCC (4µg)	DCC (8µg)		DCC (4µg)	DCC (8µg)		
G												
H												

Table 27: HEK cells were transfected with three different transfection reagents (PEIpro, 293Fectin or Lipofectamine 3000) and two plasmid DNA amounts (4µg or 8µg) within a 96 well DeepWell™ plate before being analysed for transfection efficiency by flow cytometry analysis of ZsGreen expression. UT = untransfected HEK cells, ZsG = ZsGreen transfected HEK cells and DCC = DCC-ZsGreen transfected HEK cells

Table 28: PEIpro Transfection Mixture Components

PEIpro Transfection Mixture		**Untransfected**	**ZsGreen Transfected**	**DCC Transfected**
4µg Plasmid Condition	**DNA Volume (µL)**	0	8.8	8.8
	PEIpro Volume (µL)	17.6	17.6	17.6
	OptiMEM Volume (µL)	202.4	193.6	193.6
8µg Plasmid Condition	**DNA Volume (µL)**	0	17.6	17.6
	PEIpro Volume (µL)	35.2	35.2	35.2
	OptiMEM Volume (µL)	184.8	167.2	167.2

Table 28: The volumes of the reagents required for the transfection of HEK cells using two amounts of DNA plasmid (4µg and 8µg) and the PEIpro transfection method

Table 29: 293Fectin Transfection Mixture Components

293Fectin Transfection Mixture			Untransfected	ZsGreen Transfected	DCC Transfected
4µg Plasmid Condition	Tube A	DNA Volume (µL)	0	8.8	8.8
		OptiMEM Volume (µL)	110	101.2	101.2
	Tube B	293Fectin Volume (µL)	17.6	17.6	17.6
		OptiMEM Volume (µL)	92.4	92.4	92.4
8µg Plasmid Condition	Tube A	DNA Volume (µL)	0	17.6	17.6
		OptiMEM Volume (µL)	110	92.4	92.4
	Tube B	293Fectin Volume (µL)	35.2	35.2	35.2
		OptiMEM Volume (µL)	74.8	74.8	74.8

Table 29: The volumes of the reagents required for the transfection of HEK cells using two amounts of DNA plasmid (4µg and 8µg) and the 293Fectin transfection method

Table 30: Lipofectamine 3000 Transfection Mixture Components

Lipofectamine 3000 Transfection Mixture			Untransfected	ZsGreen Transfected	DCC Transfected
4µg Plasmid Condition	Tube A	DNA Volume (µL)	0	8.8	8.8
		P3000 Volume (µL)	17.6	17.6	17.6
		OptiMEM Volume (µL)	92.4	83.6	83.6
	Tube B	Lipofectamine 3000 Volume (µL)	13.2	13.2	13.2
		OptiMEM Volume (µL)	96.8	96.8	96.8
8µg Plasmid Condition	Tube A	DNA Volume (µL)	0	17.6	17.6
		P3000 Volume (µL)	35.2	35.2	35.2
		OptiMEM Volume (µL)	74.8	57.2	57.2
	Tube B	Lipofectamine 3000 Volume (µL)	26.4	26.4	26.4
		OptiMEM Volume (µL)	83.6	83.6	83.6

Table 30: *The volumes of the reagents required for the transfection of HEK cells using two amounts of DNA plasmid (4µg and 8µg) and the Lipofectamine 3000 transfection method*

3.11.2. qPCR Analysis of DCC Gene Expression

SYBR® Green-based real time qPCR was used for relative quantification of the DCC mRNA expression. First, RNA was extracted with the RNeasy Plus Mini kit (Qiagen, #74134) following the manufacturer's instructions. Cells were harvested and lysed in 350µL Buffer RLT Plus. The gDNA was removed by transferring the lysate onto a gDNA eliminator spin column. The RNA was precipitated following addition of 1 volume of 70% ethanol to the flow-through and the sample was transferred onto a RNeasy spin column and washed with 700µL Buffer RW1 and twice with 500µL Buffer PRE. The RNA was eluted into 40µL of RNase-free water and quantified using a NanoDrop 1000 spectrophotometer (ThermoFisher). The total RNA was then reverse transcribed into cDNA using the Superscript™ IV First-Strand Synthesis System according to manufacturer's guidelines. Briefly, 1µg of total RNA was mixed with 1µL of 10 mM dNTP mix, 1µL of oligo(dT) and adjusted to 13µL with diethylpyrocarbonate (DEPC)-treated water. The RNA/primer mixture was incubated at 65˚C for 5 minutes and then immediately chilled on ice for at least 1 minute. To the annealed RNA, 7µL of a reaction mixture containing 4µL of 5X SSIV Buffer, 1µL of 100 mM DTT, 1µL of Ribonuclease Inhibitor and 1µL of SuperScript™ IV Reverse Transcriptase (200 U/µL) was added. The RT negative controls contained similar reagents with the substitution of the 1µL of SuperScript™ IV Reverse Transcriptase with 1µL of DNase/RNase-free water. The combined reaction was incubated at 55˚C for 10 minutes followed by a 10-minute incubation at 80˚C for enzyme inactivation. Incubation steps were carried out onto a C100 Touch™ Thermal Cycler (BioRad). The cDNA samples were then diluted at a range of 1:10 to 1:80 for quantitative PCR (qPCR). Transgene-derived *DCC* was quantified and normalised against endogenous *ACTB* which was used as reference control. Primer sets are listed in section 2.4.1. At least 1 primer from each primer set spans the junction of two exons for mRNA specificity. Each qPCR reaction contained 5µM of each primer, 1X QuantiTech® SYBR® Green PCR Master Mix (Qiagen, #1020722) and 3µL of the diluted cDNA, adjusted to 20µL with DNase/RNase-free water. Thermal cycling reaction conditions were 10 minutes at 95˚C, 40 cycles of 15 seconds at 95˚C, 30 seconds at 60˚C 30 seconds at 72˚C, with the addition of a melting curve to detect specific amplification products (60˚C - 95˚C). The qPCR reactions were performed in MicroAmp® Fast Optical 96-Well Reaction Plate (Applied Biosystems) on StepOnePlus Real-Time PCR System instrument linked to QuantStudio Real-Time

PCR System software (Applied Biosystems). The Ct threshold was automatically set and Ct values were exported in a .csv file and analysed in Microsoft Excel™ with the 2-ΔCT method and visualised in GraphPad Prism 5.0.4.

3.11.3. Western Blot Analysis of DCC Protein Expression

Cell pellets were lysed on ice in 50µL of RIPA buffer (Thermoscientific, #89900) with protease inhibitors (ThermoScientific, #87785), with three 5 minute incubations and 30 seconds of vortexing between each incubation. The cell lysates were centrifuged for 15 minutes at 13,000g for 4°C before lysates were transferred to fresh tubes, ensuring no cell debris was transferred. A Pierce BCA assay (ThermoScientific, #23225) was performed according to the manufacturer's protocol for total protein quantification. Samples were incubated at 37°C for 30 minutes. Three readings of the standards were performed on the Nanodrop 1000 (ThermoFisher) to generate a standard curve, and two reading for each cell lysis sample was performed and converted to mg/mL. Mastermixes for four wells were prepared for each sample for 5µg total protein to be loaded per 10µL of mix. Reducing agent (ThermoScientific, #NP0009) and LDS loading buffer (ThermoScientific, #NP0007) were added to the required amount of cell lysate and then made up to 40µL with water. Loading samples were incubated at 70°C for 10 minutes.

NuPAGE SDS Electrophoresis was the performed according to the manufacturer's protocol. 10µL of protein ladder (Licor, #918-60000) was added to the first well, and 10µL of each sample were added to subsequent wells of a 10 well 4-12% Bis-Tris Gel (ThermoScientific, #NP0321BOX). The gel was run for 50 minutes at 200v in MOPS (ThermoScientific, #NP0001) with antioxidant agent (ThermoScientific, #NP0005) added. Nitrocellulose membrane (ThermoScientific, #LC200), filter paper and blotting pads were soaked in transfer buffer (ThermoScientific, #NP0006) for 30 minutes and SDS gels were incubated in transfer buffer for 3 minutes. A transfer sandwich was set up in an Xcell II transfer module (Invitrogen) and the gel was transferred for 1 hour at 30 V and 170 mA.

The membranes were washed in PBS followed by ddH_20, before being stained with Ponceau S (Sigma, #P3504) to check that proteins were transferred correctly.

Ponceau S was then washed off with three 5 minutes PBS washes with shaking. Membranes were blocked in 5mL Odyssey blocking buffer (Licor, #927-40000) for 1 hour.

The primary mouse anti-human DCC antibody (BD Pharmingen, #554223) and the secondary goat anti-mouse 800 IgG (H+L) antibody and rabbit anti-alpha tubulin antibody (AbCam, #Ab4074) were diluted in Odyssey blocking buffer 30 minutes prior to use. Membranes were incubated in 5mL primary antibody overnight at 4°C with shaking, before being washed three times in 5mL PBS/Tween for 5 minutes with shaking. Membranes were incubated in 5mL secondary antibody for 1 hour at room temperature with shaking, before being washed three times in 5mL PBS/Tween for 5 minutes with shaking. Membranes were then imaged using the Odyssey imager (Licor) and analysed on Lite Studio software (Licor, Version 3).

3.12. Co-culture of CAR T cells and Transfected HEK Cells

HEK cells were transfected with 8µg of plasmid using 293Fectin and were incubated for 48 hours at 37°C following the protocol described in section 3.11.1.

48 hours post-transfection, HEK cells (untransfected, ZsGreen transfected and DCC-IRES-ZsGreen transfected), WT Jurkat cells and COSMC Jurkat cells were harvested, counted, washed with PBS and then resuspended to a cell density of $2x10^6$ cells/mL in RPMI media.

CAR T cells were thawed at 37°C for up to 40 seconds until a small ice chip remained. 500µL of cold TexMACS™ media was pipetted into each cryovial to aid the thawing process and the whole volume to pipetted into a 15mL tube containing 12.5mL of cold TexMACS™ media. Tubes were centrifuged at 300xg for 10 minutes, washed with 14mL of RT TexMACS™ media and centrifuged as previously. Cell pellets were resuspended in 5mL of warm TexMACS™ media and counted using the NC-250™ NucleoCounter®. Cell were resuspended to a density of $1x10^6$ cells/mL, and sufficient volume of IL-2 (final concentration 100 IU/mL) was added to the cell solution. PBMCs were plated into flat bottom 24-well cell culture plates adding $1x10^6$ cells per well and were incubated in a humified incubator at 37°C with 5% CO_2 for 24 hours.

After a recovery period of 24 hours, T cells were harvested from 24-well plates, re-counted and $6x10^6$ cells from each cell population were transferred into 15mL tubes. Cells were washed with PBS twice and resuspended in RPMI media to achieve a cell density of $2x10^6$ cells/mL.

100µL ($2x10^5$ cells per well) of cell lines and 100µL ($2x10^5$ cells per well) of T cells were plated into 96-well flat bottom plates (Corning, # 10695951), separating the four donors across four plates. The conditions set up within the co-culture experiment were; T cells alone; untransfected HEK cells + T cells; ZsGreen transfected HEK cells + T cells; DCC transfected HEK cells + T cells; COSMC Jurkat cells + T cells; WT Jurkat cells + T cells; and all cell lines cultured alone. Plates were incubated within a humidified chamber at 37°C with 5% CO_2 for 48 hours.

Samples of CAR T cells were analysed for CAR expression, following the protocol described in section 3.5.5. Samples of cell lines were analysed for ZsGreen expression by flow cytometry following the protocol described in section 3.5.2. Cell pellets of cell lines were analysed for DCC gene expression by qPCR following the protocol described in section 3.11.2 and for DCC protein expression by Western Blot following the protocol described in section 3.11.3.

After 48 hours, plates were removed from the incubator, centrifuged at 300g for 5 minutes and 100µL of supernatant was removed from each well and transferred into 96-well V bottom plates. The plates were sealed and supernatants frozen at -80°C until MSD® analysis was performed, following the protocol described in section 3.10.2.

3.13. Compound Treatment of T cell Populations

For experiments described within section 4.3, T cell populations required treatment with compounds chosen from GSK's compound library or with Synperonics F108 Poloxamer (Sigma Aldrich, #07579-250G-F). The T cell production process followed for these productions is as below.

Firstly, isolated CD4/CD8 T cell populations, provided by the Process Development Cell and Gene Therapy department (GSK) from CliniMACS Prodigy® isolated stocks, were thawed following the protocol described in section 3.2.4. T cells were counted following the protocol described in section 3.4 and resuspended in TexMACS™ media, supplemented with 100IU/mL of IL-2, 5% (v/v) human AB serum (Access Cell Culture, #A19053 HI GI) and a 1:100 dilution of TransAct™ T cell activation reagent, at a density of $1x10^6$ cells per mL. T cells were plated into 96-well flat bottom culture plates (Corning, #10695951) for activation and incubated for 24 hours at 37°C within a humidified incubator with 5% CO_2. After 24 hours of activation, T cells were harvested from the culture plates, re-counted using the NC-250™ NucleoCounter® (as previously described) and resuspended to a cell density of $1x10^6$ cells per mL within TexMACS™ media supplemented with 100IU/mL of IL-2 and 5% (v/v) human antibody serum. T cells were replated into 24-well flat bottom cell culture plates with either $1x10^6$ or $1.5x10^6$ cells added per well, depending on the number of T cell available. The appropriate volume of each compound was added to each well to achieve a final compound concentration of 100µM. Cells were incubated for 2 hours at 37°C within a humidified incubator with 5% CO_2, after which sufficient volume of either lentiviral vector C or D was added to the appropriate wells to transduce T cells, as described within section 3.2.6. Cells were incubated for 24 hours at 37°C within a humidified incubator with 5% CO_2. After 24 hours, T cells were harvested from culture plates and transferred into sterile 5mL FACS tubes before being centrifuged for 5 minutes at 300g. Supernatant was removed and cell pellets were resuspended in TexMACS™ media supplemented with 100IU/mL of IL-2 and 5% (v/v) human AB serum to a cell density of approximately $1x10^6$ cells/mL. T cell samples were transferred to a 24-well G-REX® plate with approximately $1x10^6$ cells added per well and were incubated for 48 hours at 37°C within a humidified incubator with 5% CO_2. Sufficient media (TEXMACS™ + 100IU/mL IL-2 + 5% (v/v) human AB serum) was added to each well

of the 24-well G-REX® plate to achieve a total final volume of 7mL, before T cells were incubated for 72 hours at 37°C within a humidified incubator with 5% CO_2. A media change was performed at this point, with 6mL of media carefully removed using a strippette and wells topped up with 6mL of TEXMACS™ media supplemented with 100IU/mL of IL-2 only. T cells were incubated for 48 hours at 37°C within a humidified incubator with 5% CO_2. Sufficient volume of IL-2 was added to each well to achieve a final concentration of 100IU/mL and T cells were incubated for 48 hours at 37°C within a humidified incubator with 5% CO_2. After which T cells were harvested and frozen down, using the CryoMed Control Rate Freezer, following the protocol described in section 3.2.8.

3.14. Integration Site Analysis

Integration Site Analysis was performed using SLiM-PCR methodology that was developed in collaboration with GeneWerk, and is based upon the methodology first described by Firouzi *et al.* (Firouzi *et al.*, 2014). Full details of the methodology cannot currently be disclosed due to confidentiality and IP restrictions, however further information can be obtained through a published poster by Benedicenti *et al.* (Benedicenti *et al.*, 2022).

Data analysis was performed by Martijn Brugman (Associate Director, Analytics Cell and Gene Therapy, GSK) using R analysis software packages, further details are provided within section 4.3.3.2.

3.15. Statistical Analysis

Unless otherwise stated, statistical analysis was performed by Charlotte Kay within GraphPad Prism (Version 6.07). Within the statistical analyses performed, it was assumed that data sets followed a normal distribution, and the appropriate parametric statistical test was chosen dependent on the analysis required (Table 31).

Paired T tests were used to determine whether the mean change for paired data sets were significantly different from 0. The null hypothesis was defined as “the mean of the paired differences equals 0 in the population”, whilst the alternative hypothesis was defined as “the mean of the paired differences does not equal 0 in the population”. The significance level was set to 0.05 meaning that p-values lower than 0.05 demonstrated that the mean of the paired differences did not equal 0 in the population, and therefore the null hypothesis could be rejected.

Non-paired T tests were used within experiments in which I wanted to compare the means of two groups that did not have matched samples. The null hypothesis was defined as “the means for the two populations were equal”, whilst the alternative hypothesis was defined as “the means for the two populations were not equal”. The significance level was set to 0.05, therefore at p-values less than 0.05 the null hypothesis was rejected as this demonstrated that the difference between the means of the two sets of samples being compared was significantly different.

One-way ANOVA was used within experiments in which I wanted to compare the means of multiple groups, with paired and non-paired ANOVA tests used as appropriate. The null hypothesis was defined as “there is no difference between the groups and equality between means”, whilst the alternative hypothesis was “there is a difference between the means of the groups”. Further to this, Tukey’s multiple comparison test was used to perform multiple pair-wise comparisons determining whether there was a significant difference between the mean of all possible pairs of data. Whilst Dunnett’s multiple comparison test was used to perform pairwise comparison of each condition against a set control (untreated transduced control) within Figure 79. The significance level for both multiple comparison tests was set to 0.05, therefore at p-values less than 0.05 the null hypothesis was rejected as this

demonstrated that there was a significant difference between the means of the groups compared. Significance cut-offs are defined within Table 32.

Table 31: Choice of Statistical Test for Figures

Figure Number	Parametric Data	Matched Data	Analysis Required	Statistical Test
Figure 48	Yes	Yes	Fresh vs Frozen Transduction Efficiency	Paired T Test (Two-Tailed)
Figure 58	Yes	Yes	CD4 vs CD8 T cells	Paired T test (Two-Tailed)
Figure 59	Yes	No	Multiple comparison of the mean of each group	One-Way ANOVA with Tukey's multiple comparisons
Figure 62	Yes	No	Flat Bottom vs G-REX – Fold Expansion	Unpaired T Test (Two Tailed)
Figure 63	Yes	No	24 well vs 6 well – Fold Expansion	Unpaired T Tested (Two Tailed)
Figure 64	Yes	No	10M vs 100M – Fold Expansion	Unpaired T test (Two-Tailed)
Figure 65	Yes	No	24 well vs 6 well vs Prodigy – Fold Expansion	One-Way ANOVA with Tukey's multiple comparisons
Figure 66	Yes	No	24 Well vs 6 Well and IL-2 vs IL-7 & IL-15 – Fold Expansion	One-Way ANOVA with Tukey's multiple comparisons
Figure 67	Yes	Yes	IL-2 vs IL-7/IL-15 – Transduction Efficiency	Paired T Test (Two-Tailed)
Figure 71	Yes	Yes	IL2 vs IL7/15 IFN-y Production	Paired T Test (Two-Tailed)
Figure 79	Yes	No	Compare each condition against the untreated transduced control	One-way ANOVA using Dunnets Multiple Comparison Test

Table 31: Statistical analysis of the figures within the table above were performed within GraphPad Prism, with the appropriate statistical test being chosen depending on the data sets to be compared. All analyses were performed by Charlotte Kay.

Table 32: Significance Cut-off Definitions

Symbol	Definition or P-value
ns	Non-significant
*	P<0.05
**	P≤0.01
***	P≤0.001
****	P≤0.0001

Table 32: Within all statistical analysis, the significance cut-offs and symbols within this table were used.

3.15.1. IFN-γ concentration (Figure 49)

For statistical analysis of IFN-γ concentrations within Figure 49, IFN-γ concentrations were exported to Microsoft Excel™ for pre-processing, prior to statistical analysis within JMP Statistical Analysis software (version 15). Nicholas Galwey (Statistics Leader, Research Statistics, GSK) is credited for the choice of statistical model and analysis within JMP. A mixed model of statistical analysis was performed fitted with the below specifications:

- Response Variable: $\log_{10}$ (IFN-γ concentration)
- Fixed Effect Terms (Conditions in which we would like to observe variation): Transduction + Cell.Type + Transduction:Cell.Type
- Random Effect Terms (Impact of random variation): Donor + Transduction:Cell.Type:Donor

The term ‘Transduction:Cell.Type:Donor’ represents sets of observations from the same Transduction:cell.type:Donor combination: i.e. 3 observations per set in the present experiment. Random variation of 37.9% was observed between donors and 54.38% random variation was observed between sets of

'Transduction:Cell.Type:Donor'. The impact of random variation was accounted for within the statistical model. Significant differences ($p < 0.0001$) was observed with all of the fixed effect terms, namely Transduction, Cell Type and Transduction*Cell.Type. The mean Log_{10} IFN-γ concentration for the four donors was calculated for each of the "Transduction*Cell.Type" conditions and back-transformed to provide mean IFN-γ concentrations with lower and upper confidence intervals. The mean IFN-γ concentrations were plotted within GraphPad Prism (Version 6.07) with lower and upper confidence intervals displayed as error bars and data displayed on a Log_{10} scale. Multiple comparisons of key co-culture conditions were performed within JMP statistical analysis software to determine the significance of the fold change of IFN-γ concentration between the conditions. Key significance results were plotted onto Figure 49, with the results of all comparisons performed displayed in Table 37.

3.15.2. Cytokine Impact Upon Cell Phenotype (Figure 69 and Figure 70)

The choice of statistical model used to determine the impact of cytokines upon the T cell phenotype within Figure 69 and Figure 70 is credited to Nicholas Galwey (Statistics Leader, Research Statistics, GSK), who also performed the analysis within JMP Statistical Analysis software (version 15). A mixed model of statistical analysis was performed fitted with the below specifications:

- Fixed Effect Terms (Conditions in which we would like to observe variation): "Cytokine" + "CAR Construct" + "Cytokine*CAR Construct"
- Random Effect Terms (Impact of random variation): "Donor ID"

Calculated significance values were plotted onto graphs produced within GraphPad Prism (Version 6.07).

4. Results

4.1. Chapter 1: Pre-Production – Choice of Construct

4.1.1. Introduction

As was previously discussed within section 1.4.5, there is a high cost associated with the early development of CGT constructs, both CARs and engineered TCRs, due to the large pool of potential constructs that need to be assessed to determine their suitability against key quality attributes. These attributes can include, but are not limited to, the transduction of T cells, the impact on expansion and viability, the functionality and the specificity of the constructs.

The assessment of the majority of key quality attributes in early-stage development does not increase development costs significantly. However assessment of the specificity of the constructs which helps inform the potential safety of the construct adds significant costs to the development process as the available assays are expensive to run on such a large number of constructs. The introduction of a specificity screening assay early in the development phase of CGT products could potentially help to decrease the early development costs by enabling constructs with reduced specificity, and therefore increased safety risks, to be discarded early within development before extensive safety studies are performed. This would help to reduce investments in high-risk candidates, whilst also improving the quality of the pool of candidates progressed by increasing the chances of selecting only highly specific constructs.

Literature and database searches are used for a large proportion of the CGT pre-clinical safety packages for the investigation of potential on-target off-tumour or off-target off-tumour binding events, which were described in more detail within sections 1.4.1.4.1 and 1.4.1.4.2. On-target off-tumour binding can be identified through searching for gene and protein expression within both healthy and diseased tissue to identify potentially “at risk” organs and tissues. Information from mAb studies can also help to identify on-target off-tumour binding risks, although it is important to note that

low expression of proteins in healthy tissue, which may not be detected with mAbs, can cause major toxicity if bound by CAR T cells – as was shown within the Morgan anti-ErbB2 trial (Morgan *et al.*, 2010). Previous mAb campaigns can also identify potential off-target binding events, but mAbs may not bind to off-target hits with the same affinity as CAR T cells.

In vivo models can be utilised to assess the risk of off-target toxicities, however in addition to the high costs associated with *in vivo* studies, there are also a myriad of disadvantages with the use of animal models for pre-clinal safety studies within CGT, including; the potential difference in expression of proteins between species; lack of CAR cross-reactivity; requirement for a surrogate CAR for the species which may produce irrelevant results that are not applicable to the lead CAR; and potential issues with accurate expression of human proteins within transgenic mouse models (Zhao *et al.*, 2019; Duncan *et al.*, 2022).

In vitro profiling of CAR T cells provides the most comprehensive assessment of off-target binding, with a variety of possible screening assays that could be performed. For example, CAR T cells can be screened against primary cell lines derived from critical organs to assess if any CAR toxicity is observed. However, standard cultured cell lines may not be representative due to lack of or altered expression of key proteins, as was found in the Linette MAGE-A3 study (Linette *et al.*, 2013). Other potential assessments involve the use of parental mAbs for immunohistochemistry screening, with the caveat that the parental mAb may not be predictive of CAR T cell binding.

A limited number of companies have developed *in vitro* technologies to screen for off-target binding events, with the potential caveats of each available system still being scrutinised to assess the technology's suitability for inclusion within pre-clinical safety packages. Cellzome and Retrogenix™ are currently leading the pack for *in vitro* off-target screening of CAR T cells, with off-target screening of engineered TCR T cells posing additional complications, due to the requirement for antigen presentation within MHC.

Cellzome have developed a platform to screen for off-target binding through the use of ScFv immobilised onto beads, which are then co-incubated with cell lysates and free antigen. The inclusion of free antigen into the mixture enables competitive inhibition of the binding of off-target peptides, with only off-target peptides of higher

affinity than the expected target competitively binding to the ScFv. The bead-immobilised ScFvs with bound peptide are then analysed through mass spectrometry to identify the bound peptide. There are a number of caveats with this method.

Firstly, the use of ScFvs for screening rather than CAR T cells. Although the binding domains of the ScFv and CAR construct are identical, consideration as to how the immunological synapse impacts upon binding would be required. The potency of a CAR T cell response against an antigen expressing target is impacted by the avidity of the CAR T cell, which describes the T cell's cumulative binding strength. CAR T avidity is determined by both the affinity and level of expression of the ScFv upon its surface (Fujiwara *et al.*, 2020), in addition to the level of antigen expression upon the target cell (Jayaraman *et al.*, 2020). Some studies have demonstrated that modification of ScFv affinity can improve CAR specificity, particularly in cases where target antigens are differentially expressed on both healthy and tumour cells (Liu *et al.*, 2015). However, the modification of ScFvs may not translate to a modification of CAR T avidity due to structural differences between a soluble ScFv and a ScFv anchored to a T cell through the hinge and transmembrane domains (Fujiwara *et al.*, 2020). Modifications to a ScFv could also impact upon the level of expression upon the surface of a CAR T cell, which would impact upon the avidity. Finally, differences between CAR T avidity and soluble ScFv affinity would also impact upon the on and off rates of binding to antigen expressing cell lines, with reports that decreased affinity with faster dissociation constants could result in rapid serial killing and improved therapeutic response (Jayaraman *et al.*, 2020). Therefore, the screening of ScFvs may not be able to provide results that are translatable to CAR T cells.

Additionally, screening against cell lysates leads to a potential increase in identified off-target binding events, as intracellular proteins (which would not otherwise be targeted by CAR T cells) could be identified. Screening against peptides and linear proteins may increase the number of false positives through the exposure of epitopes that would not usually be presented, but conversely may also increase the number of false negatives as the peptides and proteins would not have the correct 3D conformation. Both the 3D conformation and post-translational modifications, such as glycosylation, can impact upon the epitopes expressed on proteins and potential binding sites available.

Retrogenix™, on the other hand, have developed a plasma membrane protein cell microarray which has been used routinely for screening of mAbs against a panel of over 5000 full-length clones encoding for approximately 4000 different plasma membrane proteins and protein variants. The huge library of plasma membrane proteins is expressed through the reverse transfection of a HEK293 cell monolayer cultured over spots of cDNA encoding the protein of interest with a bicistronic green fluorescent protein (GFP), which enables confirmation of transfection (Figure 37). The Retrogenix™ technology has been modified and optimised for the screening of CAR T cells, using a Far Red stain to tag CAR T cells and track their binding to specific spots on the microarray. The advantage of the Retrogenix™ platform is that proteins are expressed on the cell surface, with the potential for post-translational modifications and proper folding of the proteins. This is dependent however upon whether HEK cells are able to perform the appropriate post-translational modifications for the target of interest, for example a target protein usually expressed within the brain may not be able to be properly processed by kidney cells. The Retrogenix™ platform has reportedly been utilised by BlueBird Bio and KITE Pharma for the assessment of CD19-CAR and BCMA-CAR T cells respectively.

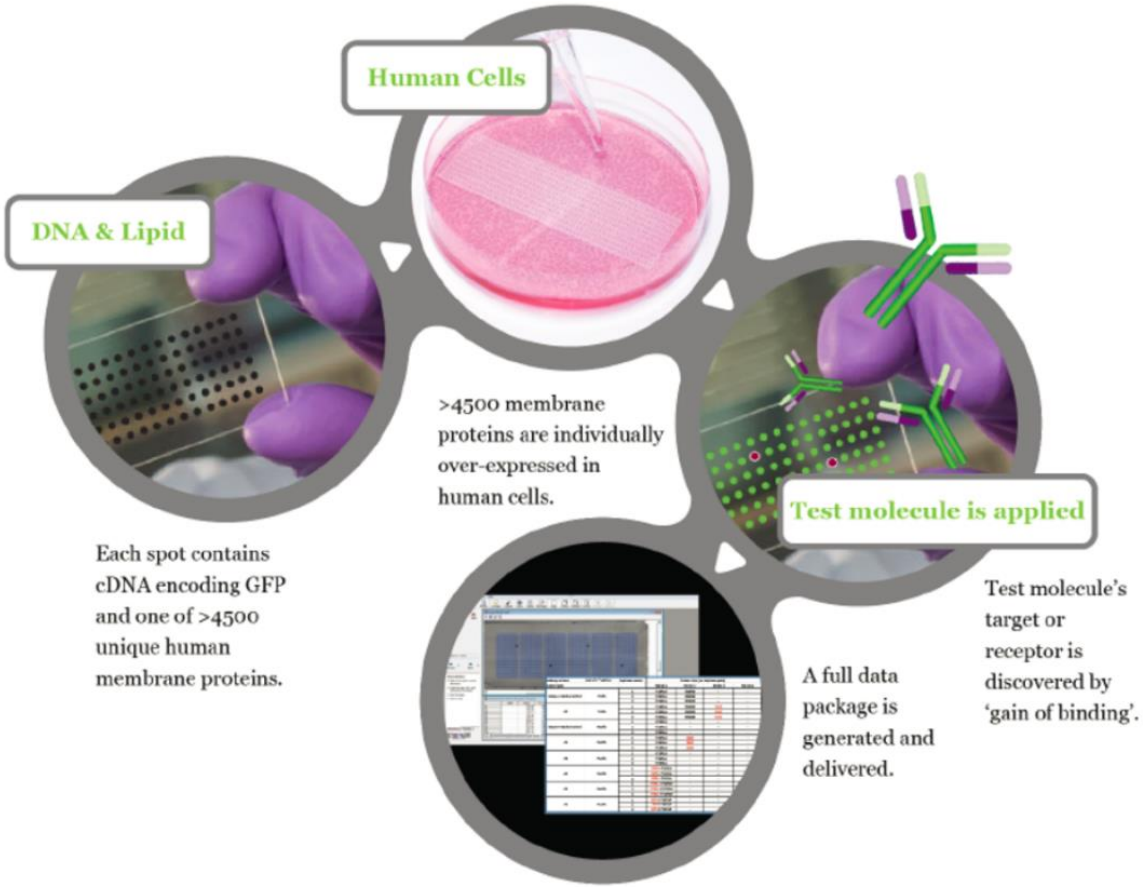

Figure 37: Retrogenix™ Technology

cDNA encoding for over 5500 human plasma membrane proteins is spotted onto microarray slides and HEK cells are grown in a monolayer over the slide. HEK cells are reverse transcribed and express the corresponding plasma membrane protein on their surface. CAR T cells stained with a membrane dye are added to the slides, before unbound CAR T cells are washed off. The slides are imaged, and CAR T binding sites are analysed. Image Reference: (Freeth, 2019)

4.1.2. Hypothesis and Study Aims

The hypothesis of this study is that the Retrogenix™ platform would be suitable for inclusion within the early development phase of CGT products to enable the progression of highly specific candidates, reducing early development costs by reducing the pool of constructs undergoing extensive safety assessment.

In order to evaluate the Retrogenix™ platform, a number of studies were performed to assess the suitability of the platform and identify potential caveats. The aims of these studies were to:

- Evaluate the impact that donor variability has upon the binding results, including background binding, to assess the potential risk of missed binding hits due to donor variability.

- Assessment of binding of CAR T cells populations to their known targets, and at least one known off-target binding event to investigate the accuracy of binding hit identification.

- In house validation of any unknown off-target binding events identified by Retrogenix™ to determine whether off-target binding hits identified translate to CAR T activation and cytokine production.

4.1.3. Results

4.1.3.1. Study 1: Investigation of Donor Differences

The Retrogenix™ technology relies on the specific binding of CAR T cells to transfected HEK293 cells cultured onto a microarray slide; however, some non-specific binding of T cells may occur, resulting in false positives that may lead to a CAR T candidate being discarded. An initial study was performed to assess the level of background binding of T cells from three donors to microarray slides. As shown in Figure 39, binding to known T cell interactors, including PVR, CD244, TNFSF4, ICOSLG and CD86, occurred with all three donors tested. In addition to this, when BCMA targeting CAR T cells were screened, a specific interaction was observed against BCMA expressing HEK293 cells. The transduction efficiency of the CAR T cell populations was between 50 – 62% for the three donors, as shown in Table 33. These differences in transduction efficiency of CAR T populations did not correlate with the intensity of the binding spot observed, with the spot intensity appearing similar across all three donors. There was a visible difference in the level of background binding of T cell populations to the slides, with increased graininess observed particularly with Figure 39F. This graininess on the slide is due to T cells sticking non-specifically to untransfected HEK293 cells grown on the microarray slide, which appears to become more prevalent when CAR T cells are used compared to untransduced (UT) T cells.

Table 33: Transduction Efficiency of CAR T cells

Donor ID	T cell Population	Frequency of BCMA-CAR Expressing T cells (%)
12021	Untransduced	0.37
	BCMA-CAR	62.19
30865	Untransduced	0.93
	BCMA-CAR	50.58
90928	Untransduced	1.03
	BCMA-CAR	55.83

Table 33: Untransduced and BCMA CAR transduced T cell populations produced from three healthy donors were analysed for transduction efficiency via flow cytometry using BCMA-FC protein tagged with AF647 following the methodology described in 3.5.3.

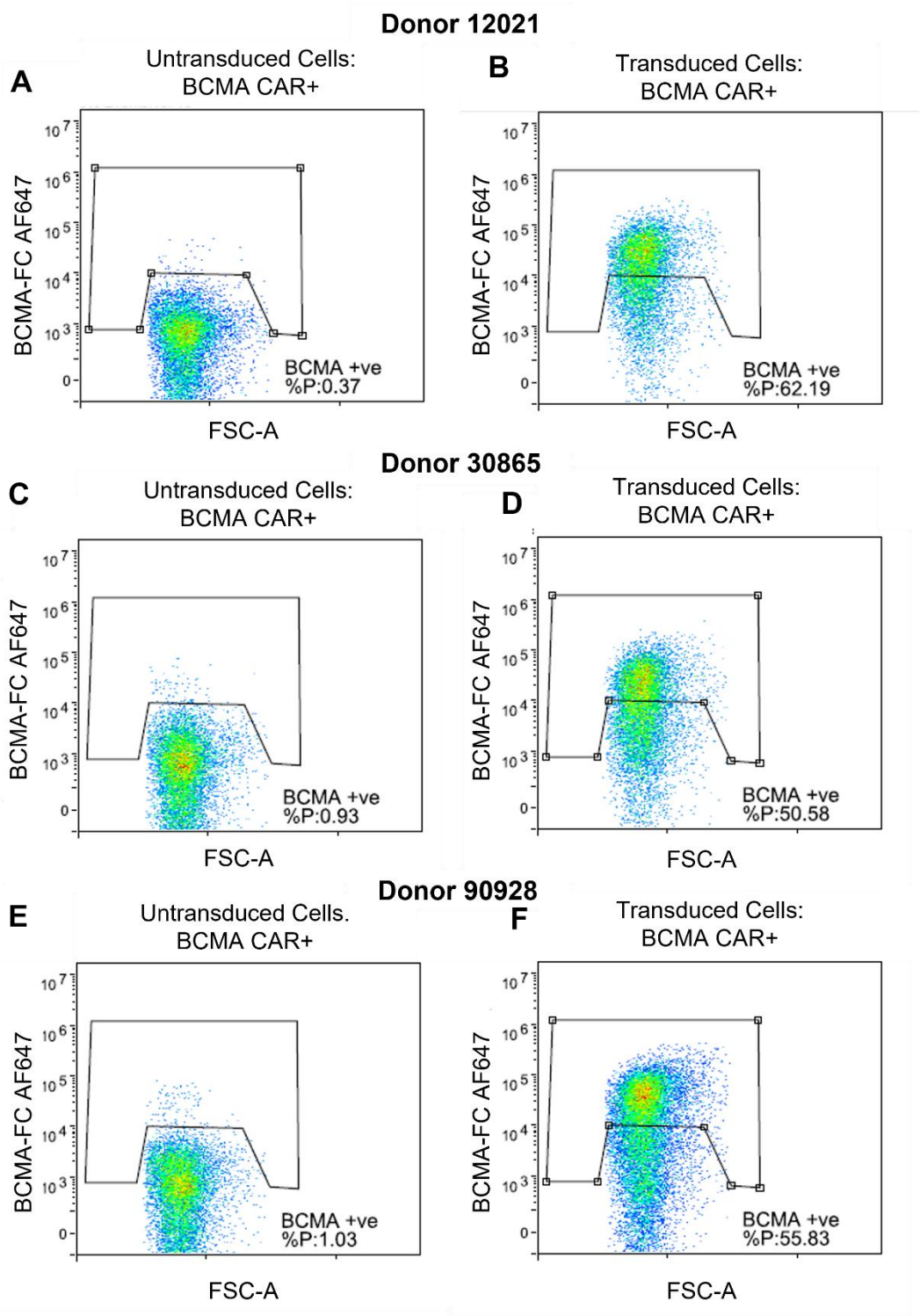

Figure 38: BCMA CAR Transduction Efficiency Analysis Flow Plots

A) Untransduced and B) BCMA CAR transduced T cells from donor 12021, C) Untransduced and D) BCMA CAR transduced T cells from donor 30865, E) Untransduced and F) BCMA CAR transduced T cells from donor 90928. T cells were analysed for BCMA CAR expression via flow cytometry using an AF647 tagged BCMA-FC protein

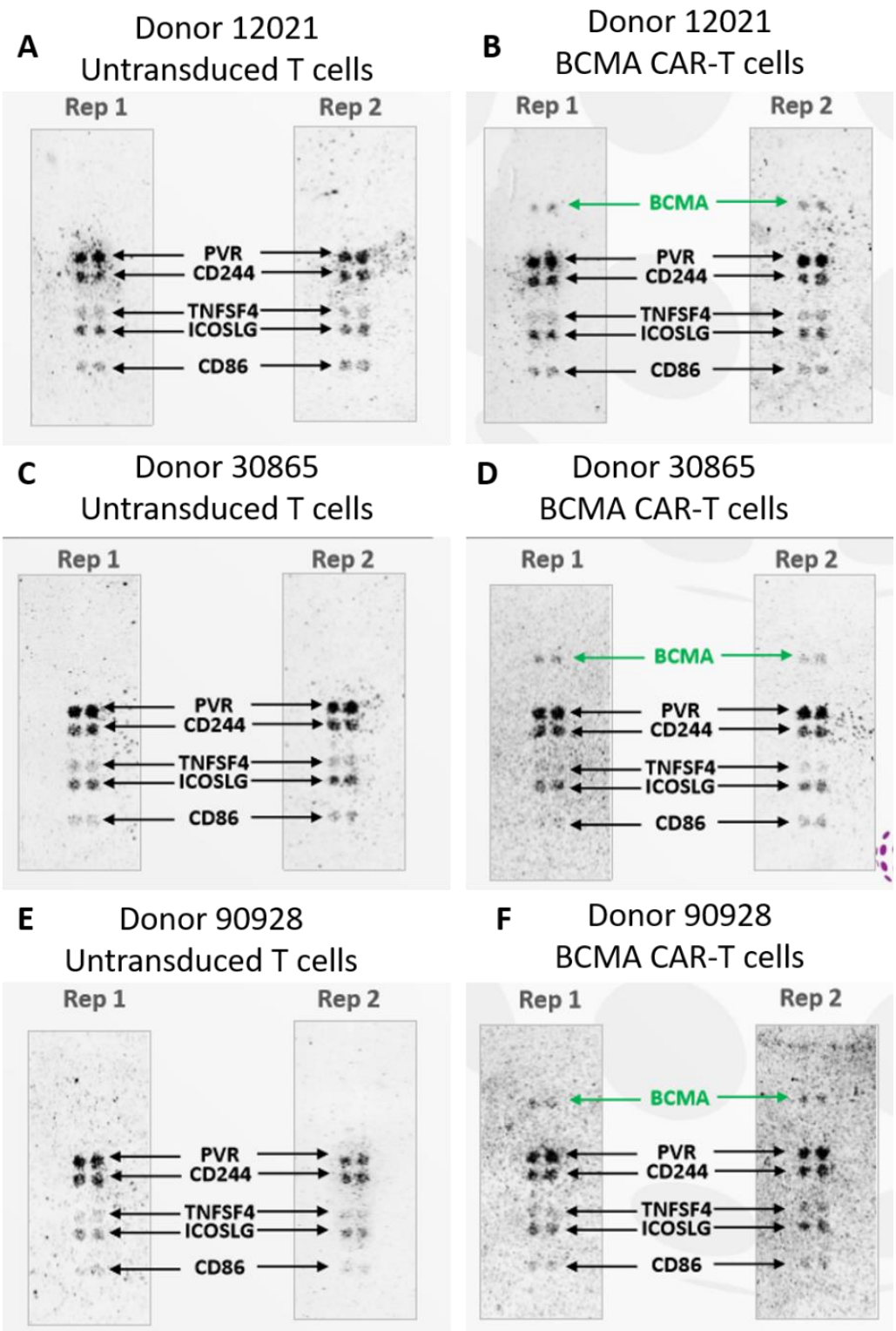

Figure 39 : Plasma Membrane Protein Array: Analysis of Donor Differences

A) Donor 12021 Untransduced T cells, B) Donor 12021 BCMA CAR T cells, C) Donor 30865 Untransduced T cells, D) Donor 30865 BCMA CAR T cells, E) Donor 90928 Untransduced T cells, F) Donor 90928 BCMA CAR T cells

4.1.3.2. Study 2: CAR Assessment

In order to further validate the Retrogenix™ platform, four CAR T cell populations (BCMA-CAR T cells, CAR-A T cells, CAR-B T cells and CAR-X T cells) and one untransduced T cell population were produced from donor 90928. Initially, a pre-screen was performed, with BCMA-CAR, CAR-A, CAR-B and untransduced T cells, to assess the binding of the CAR T cells to known target proteins (Figure 41). The known targets from BCMA-CAR T cells, CAR-A T cells and CAR-B T cells were all identified. A higher intensity spot was identified with BCMA-CAR T cells within the pre-screen (Figure 41) than when screened within the donor pilot study (Figure 39). At a transduction efficiency of 63% (Table 34), it was not expected that the spot intensity would differ to the binding spot intensity observed with donor 12021, which had a transduction efficiency of 62% in the donor pre-screen (Table 33).

CAR-A T cells and CAR-B T cells both bind to the same known target, described as “Target 1” in Figure 41C and Figure 41D, with CAR-A T cells reportedly shown to have higher binding affinity than CAR-B T cells within previous *in vitro* studies (data not shown). Some differences within the intensity of the binding spots observed against Target 1 can be seen, with higher spot intensity for CAR-A T cells (Figure 41C) than CAR-B T cells (Figure 41D).

Untransduced T cells, BCMA-CAR T cells, CAR-A T cells, CAR-B T cells and a new CAR T cell population (CAR-X T cells) targeting a novel antigen, were screened against the whole Retrogenix™ library of over 4500 surface membrane proteins. Any binding hits that were observed within the primary screen were re-screened within a confirmation screen, in which cDNA from the relevant proteins was re-spotted onto a single slide for transfection of HEK293 cells alongside known T cell interactors and the known target proteins (Figure 42). The results package provided by Retrogenix™ identified two off-target hits with CAR-X, a medium intensity hit against the Netrin 1 Receptor (DCC) (described as “Off-Target 1”) and a very weak to weak intensity hit against SELPLG (described as “Off-Target 2”). The definition of spot intensity was defined by Retrogenix, with spots defined as very weak to weak intensity given a low confidence rating of being a true binding hit.

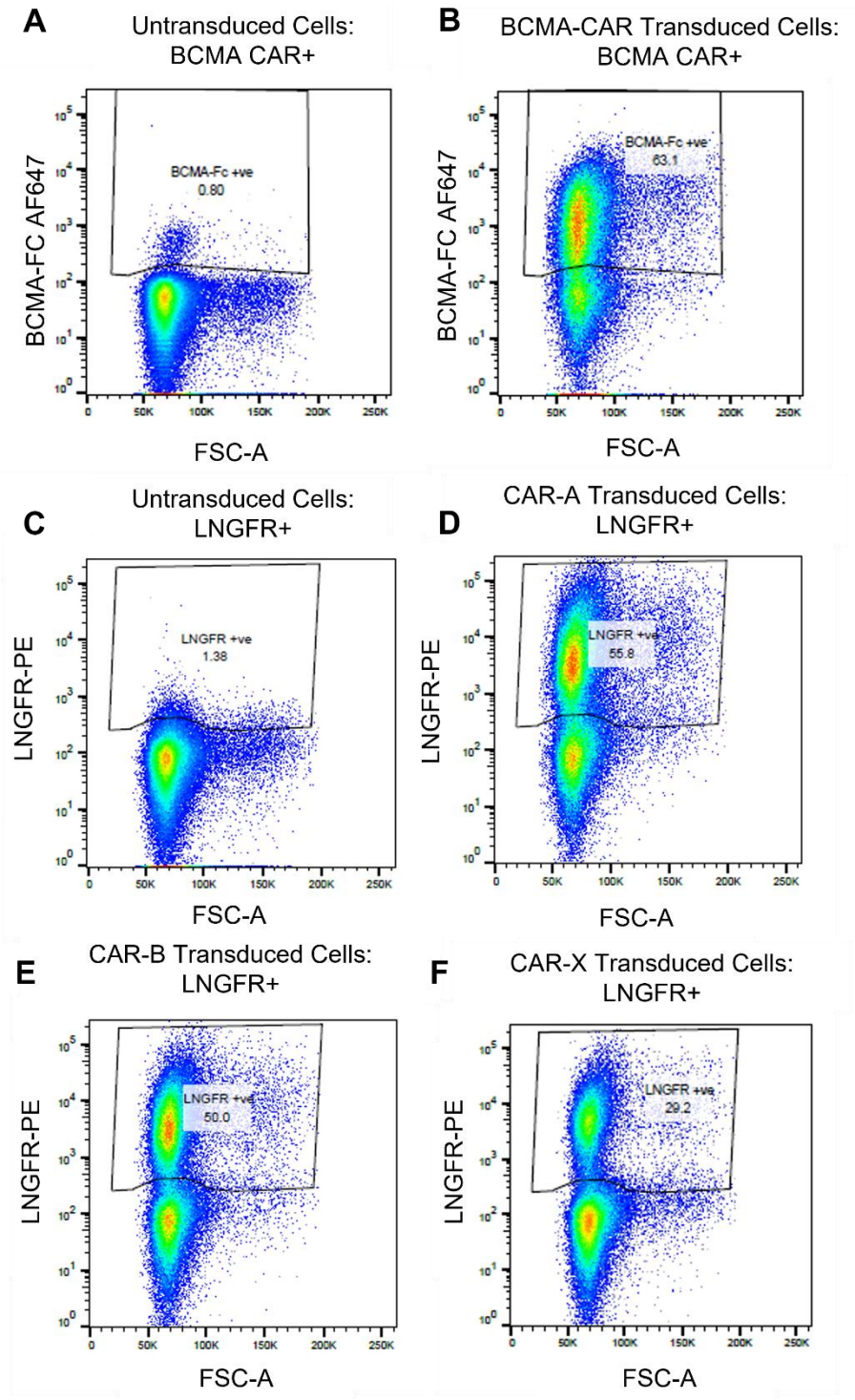

Figure 40: CAR T Transduction Efficiency Flow Plots

Untransduced T cells and four CAR T cell populations produced from healthy donor 90928 were analysed for transduction efficiency by flow cytometry. A) Untransduced and B) BCMA-CAR transduced T cells were analysed for BCMA-CAR expression, C) Untransduced, D) CAR-A, E) CAR-B and F) CAR-X transduced T cells were analysed for CAR expression via analysis of the expression of an LNGFR tag.

Table 34: Transduction Efficiency of CAR T cells

Donor ID	T cell Population	Frequency of BCMA-CAR Expressing T cells (%)	Frequency of LNGFR Expressing T cells (%)
90928	Untransduced	0.8	1.4
	BCMA-CAR	63.1	-
	CAR-A	-	55.8
	CAR-B	-	50.0
	CAR-X	-	29.2

Table 34: *Untransduced T cells and four CAR T cell populations produced from healthy donor 90928 were analysed for transduction efficiency by flow cytometry. BCMA CAR T cells were analysed using BCMA-FC AF647 tagged protein (method described in section 3.5.2). CAR-A, CAR-B and CAR-X expressing T cells were analysed using PE LNGFR antibody (method described in section 3.5.4).*

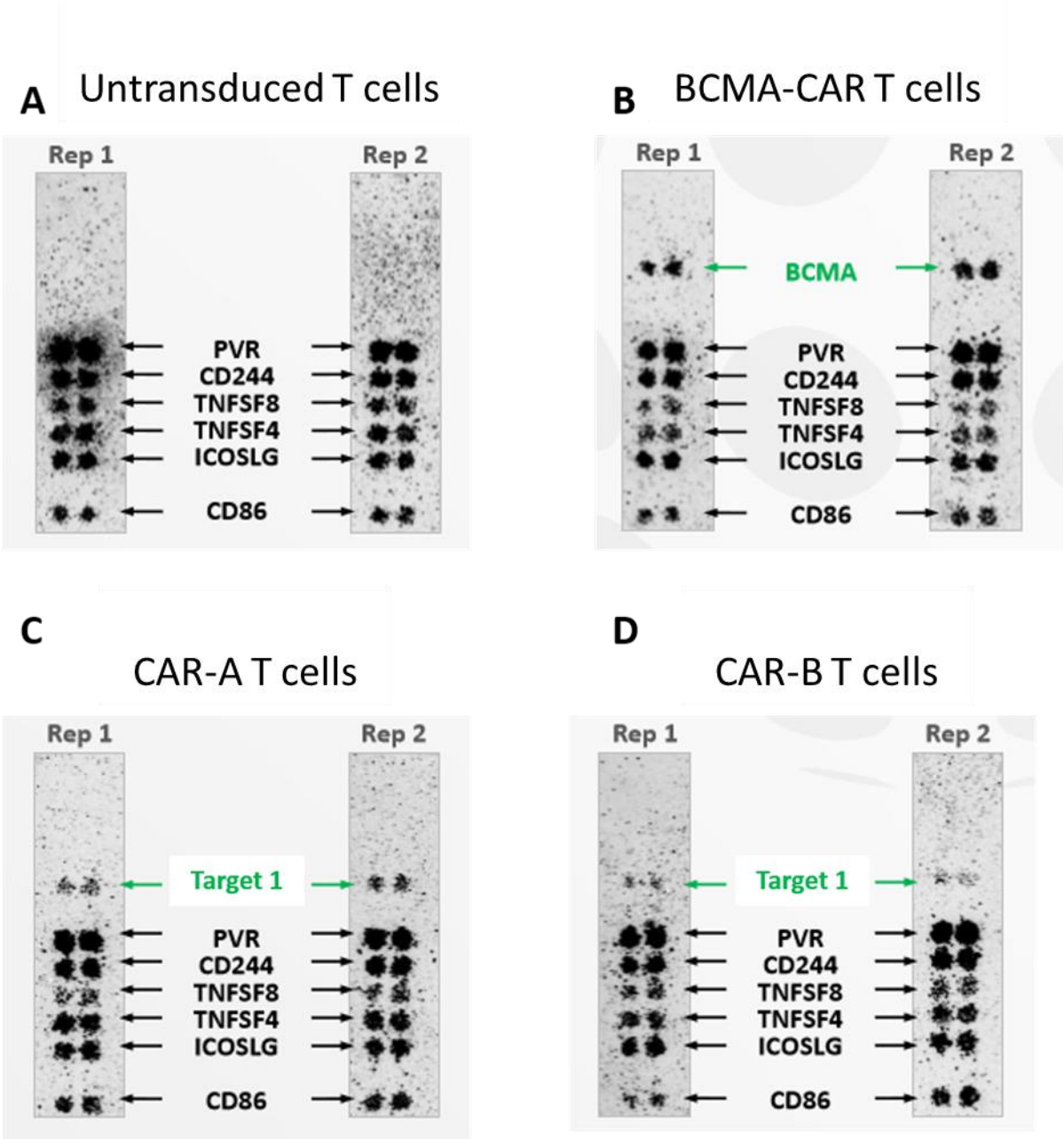

Figure 41 : Plasma Membrane Protein Array: Pre-screen Study of CAR T Cell Populations

Untransduced T cells and CAR T cell populations produced from donor 90928 were pre-screened against known T cell interactors and known targets. A) Untransduced T cells, B) BCMA CAR T cells, C) CAR-A T cells, D) CAR-B T cells

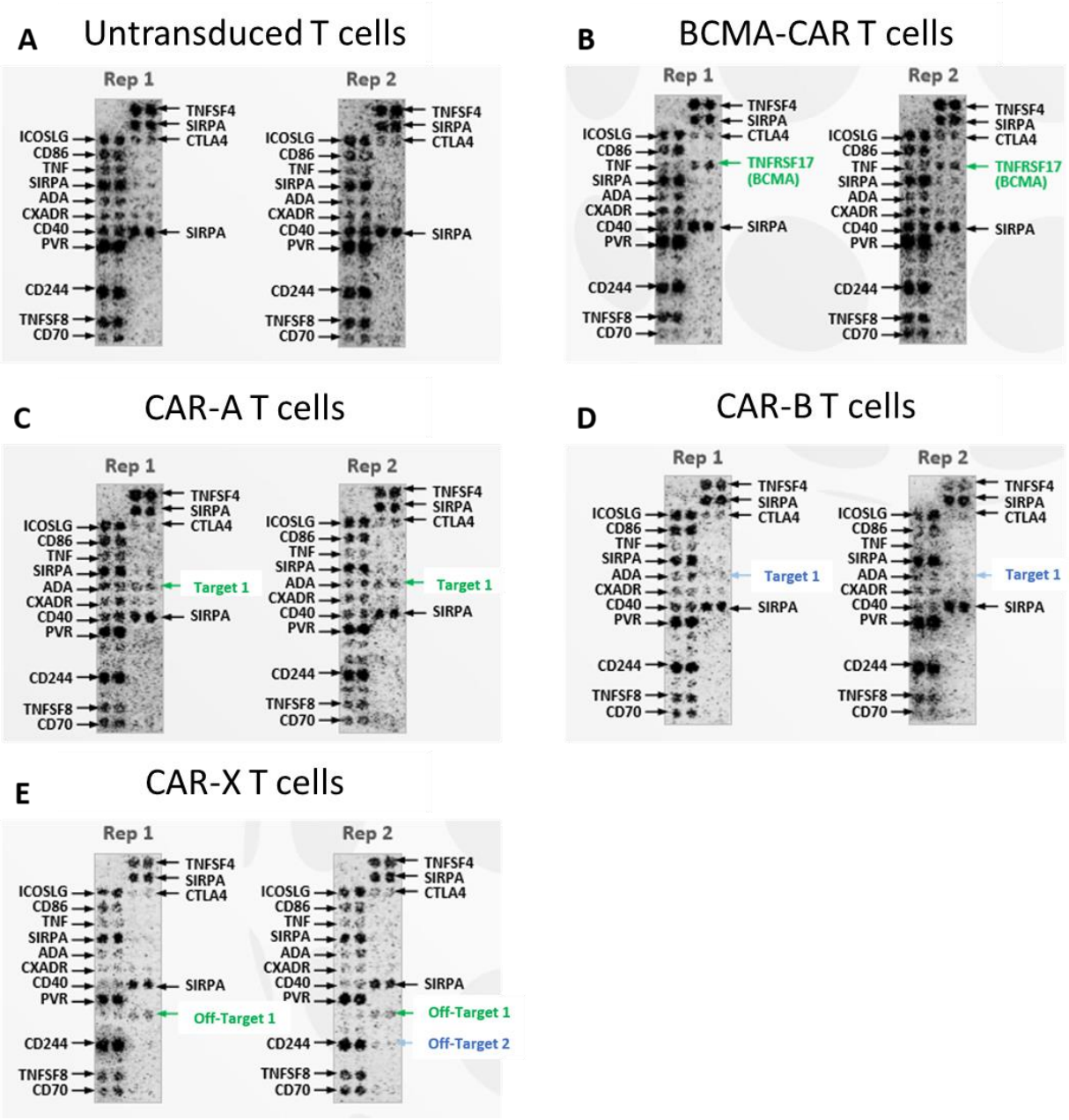

Figure 42 : Plasma Membrane Protein Array: Confirmation Screen of CAR T cell populations

Untransduced T cells and four CAR T cell populations were produced from donor 90928 and screened against the whole Retrogenix™ surface protein library. Hits were re-spotted onto a slide with known T cell interactors and known targets. A) Untransduced T cells, B) BCMA CAR T cells, C) CAR-A T cells, D) CAR-B T cells, E) CAR-X T cells

4.1.3.3. Study 3: In House Validation of Hit

4.1.3.3.1. Plasmid Design

In light of the results of the Retrogenix™ screen, further in house validation of the DCC binding hit observed with CAR-X was performed to determine whether the binding events correlated with activation of CAR T cells. In order to assess this, a DCC.IRES.ZsGreen plasmid was designed to enable transfection of suspension HEK cells in house (Figure 43), in addition to a ZsGreen-only control plasmid.

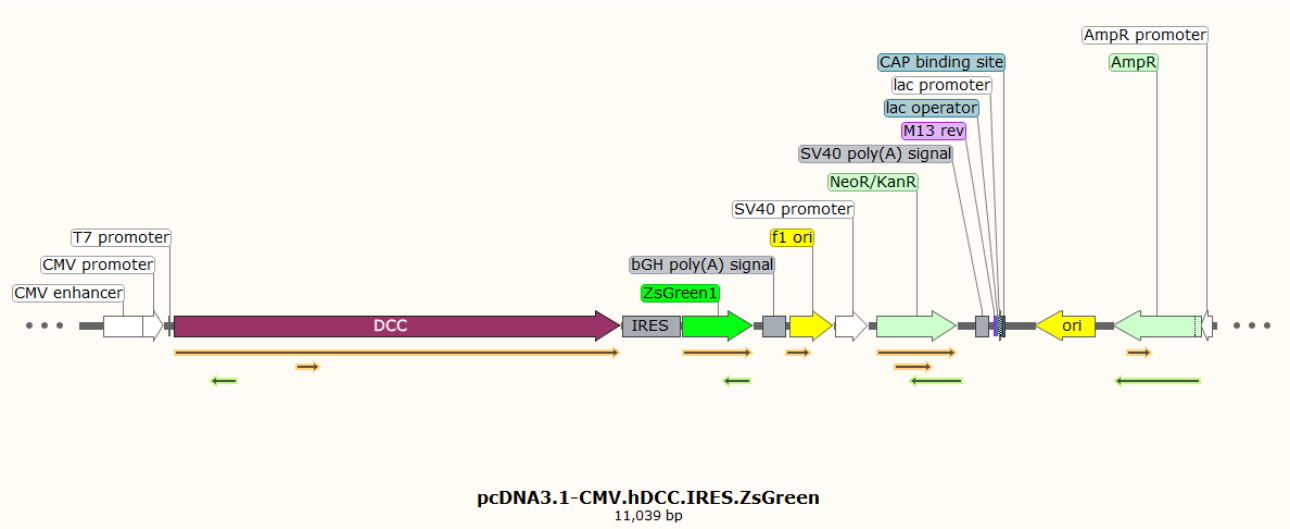

Figure 43 : DCC Plasmid Design

The DCC plasmid was designed with ZsGreen expressed from an RNA element known as an internal ribosome entry site (IRES) to enable detection of transfection efficiency

4.1.3.3.2. Suspension HEK Cell Transfection

In order to ensure a good level of transfection in suspension HEK cells, in house optimised transfection methods were evaluated with the transfection efficiency assessed through detection of ZsGreen expression via flow cytometry. Three commercially available transfection reagents, PEIpro, 293Fectin and Lipofectamine, were all evaluated using plasmid amounts of 4µg and 8µg (Figure 44). This study allowed a decision to be made as to which method would be used going forward and was only performed one time as optimisation of these transfection methods had already been performed within GSK. The highest transfection efficiency was observed with the use of 293Fectin and 8µg of ZsGreen control plasmid or DCC-IRES-ZsGreen plasmid, with frequencies of ZsGreen expressing HEK cells of 37.3% and 33.5% respectively (Table 35).

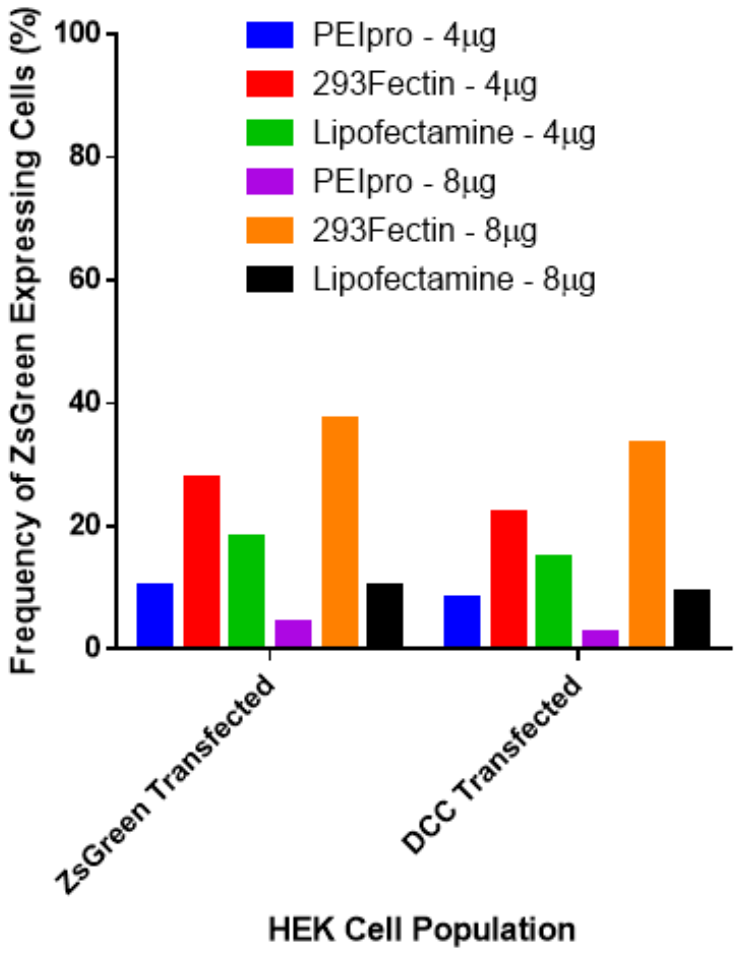

Figure 44 : Suspension HEK Transfection

Three transfection reagents were tested with two concentrations of plasmid to decide on the optimal method for the transfection of suspension HEK cells (method as described in section 3.11.1). *The transfection efficiency of HEK cells was analysed through analysis of the frequency of ZsGreen expressing HEK cells using flow cytometry (n=1)*

Table 35: Suspension HEK Cell Transfection – Frequency of ZsGreen Expressing Cells

Transfection Reagent (Plasmid Amount)	Frequency of ZsGreen Positive Cells (%)	
	ZsGreen Plasmid	DCC-ZsGreen Plasmid
PEI-Pro (4µg)	10.3	8.3
293Fectin (4µg)	27.8	22.2
Lipofectamine (4µg)	18.3	14.9
PEI-Pro (8µg)	4.4	2.5
293Fectin (8µg)	37.3	33.5
Lipofectamine (8µg)	10.1	9.2

Table 35: The frequency of ZsGreen positive HEK cells within each of the conditions used for transfection of suspension HEK cells was analysed using flow cytometry (method as described in section 3.5.2).

Transfection of suspension-adapted HEK cells prior to co-culture set up was successful, with transduction efficiency determined by flow cytometry (Figure 45 and Figure 46A), DCC gene expression determined by qPCR (Figure 46B) and DCC protein expression determined by Western Blot (Figure 46C).

The expression of ZsGreen within ZsGreen-only control plasmid transfected HEK cells and DCC-IRES-ZsGreen plasmid transfected HEK cells was 48% and 34% respectively (Figure 45 and Figure 46A). The expression of ZsGreen indicates the frequency of successfully transduced HEK cells but does not confirm expression of DCC on the surface of the HEK cells.

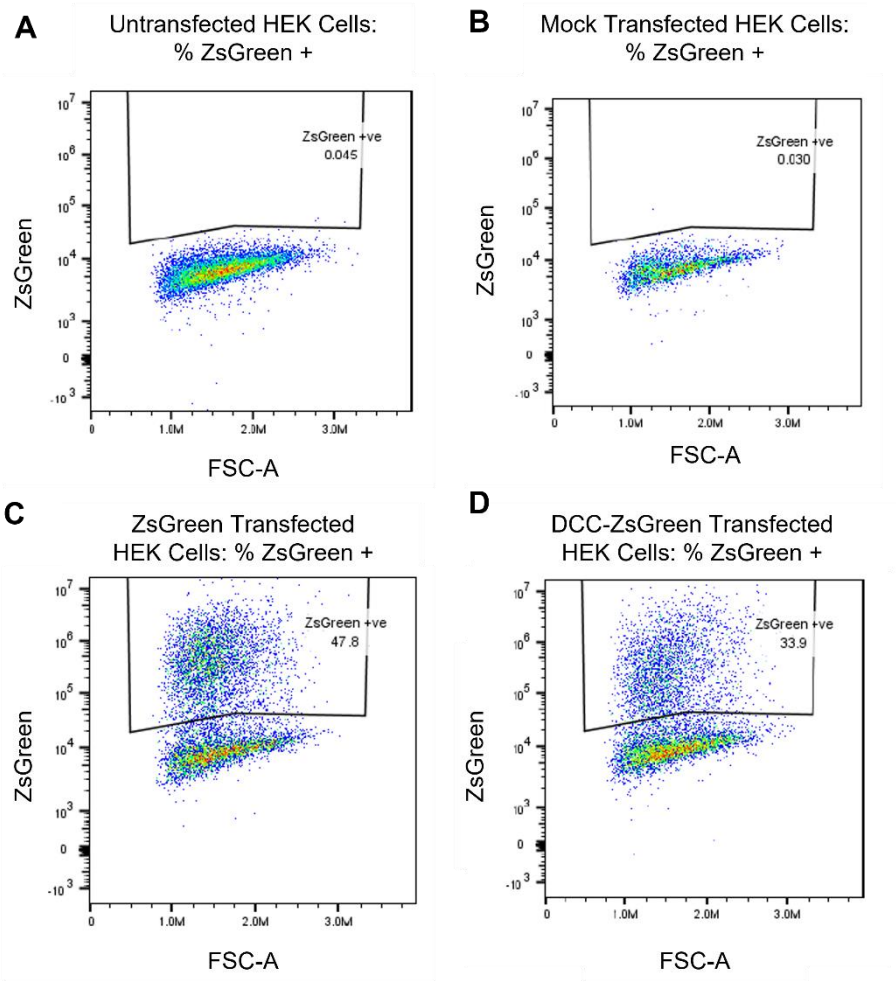

Figure 45: Analysis of ZsGreen Expression within Transfected HEK Cell Populations

A) Untransfected, B) Mock transfected, C) ZsGreen transfected and D) DCC-ZsGreen transfected HEK cell populations were analysed via flow cytometry for the expression of ZsGreen as an indication of transfection efficiency

qPCR analysis of the transfected HEK cells demonstrated high expression of the DCC gene within the DCC-ZsGreen transfected HEK cells at day 3 post-transfection compared to the housekeeping gene ACTB. The expression of the DCC gene decreased by day 5 post transfection, however expression was still higher than the expression of the DCC gene within the endogenous DCC-expressing positive cell line A673 (Figure 46B).

Western blot analysis demonstrated that the DCC protein was expressed within the DCC-IRES-ZsGreen transfected HEK cells at both day 3 and day 5 post-transfection, with a band running within the molecular weight range predicted by Becton Dickinson (168-175kDa). IMR-32 cells were recommended by Becton Dickinson as the DCC positive control cell line; however, no band was observed for this cell line (Figure 46C).

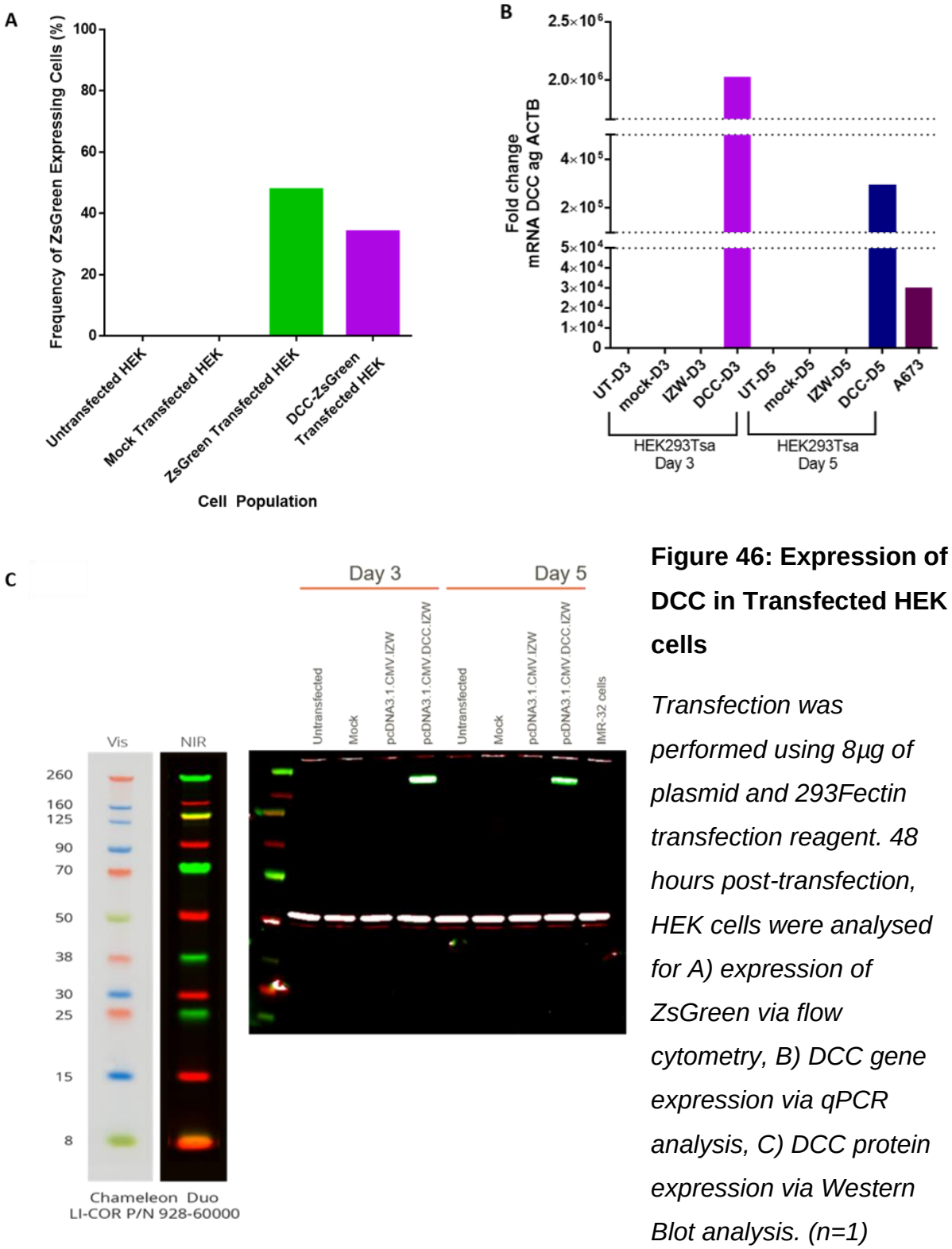

Figure 46: Expression of DCC in Transfected HEK cells

Transfection was performed using 8µg of plasmid and 293Fectin transfection reagent. 48 hours post-transfection, HEK cells were analysed for A) expression of ZsGreen via flow cytometry, B) DCC gene expression via qPCR analysis, C) DCC protein expression via Western Blot analysis. (n=1)

4.1.3.3.3. Production of CAR T cells

Two lentiviral vectors were used to transduce T cells for use in this study, CAR-Y, which has the same target as CAR-X used in section 4.1.3.2 and is equivalent except for the removal of a low affinity nerve growth factor receptor (LNGFR) tag used for the detection of CAR expression; and CAR-Z, which differs from CAR-Y by a single amino acid in the variable light chain of the ScFv. T cells isolated from four healthy donors were transduced with the two lentiviral vectors and transduction efficiency of the T cell populations was determined through the detection of CAR expression using an anti-Fab antibody (Figure 47 and Figure 48). All CAR T cells populations were over 69% CAR-expressing with similar transduction efficiencies between CAR-Y and CAR-Z CAR T cell populations for each donor (Table 36). A comparison of the transduction efficiency of CAR T cell populations tested prior to freezing and post-thaw was performed, and no significant difference in transduction efficiency was observed.

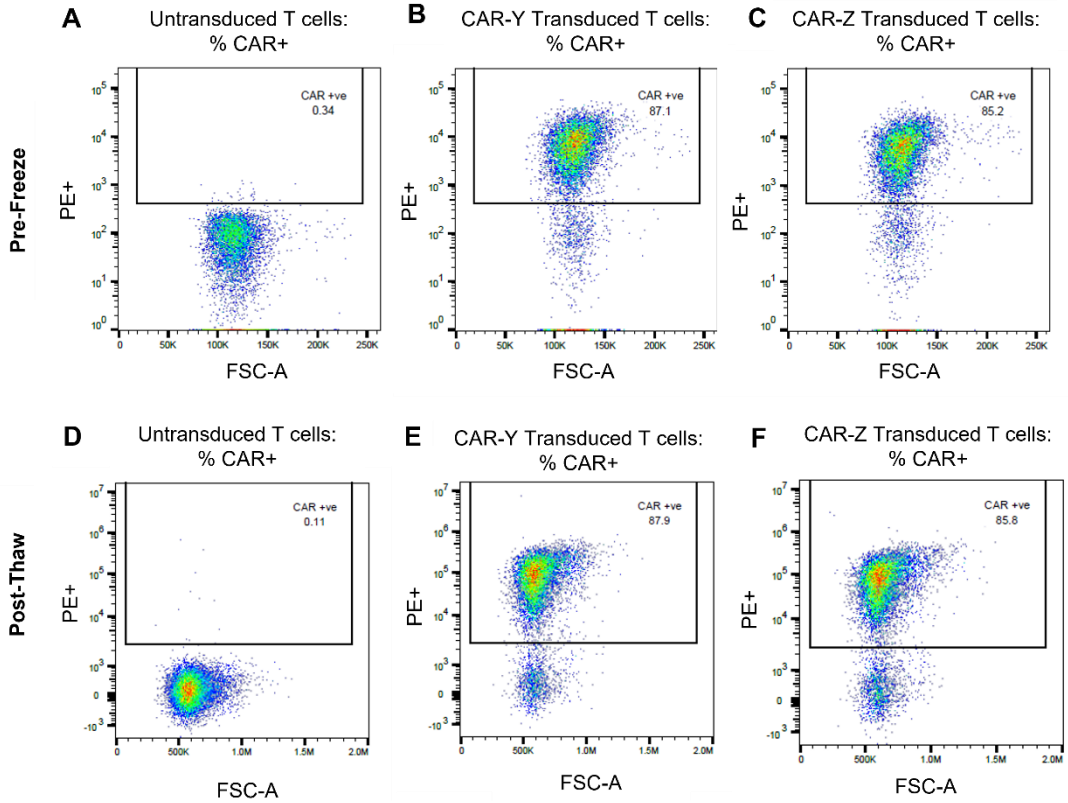

Figure 47: Pre-Freeze and Post-Thaw Transduction Efficiency of T cell Populations

Representative flow plots showing the transduction efficiency analysis both pre-freeze and post-thaw of untransduced, CAR-Y transduced and CAR-Z transduced T cell populations from donor PR19C128729

Table 36: Transduction Efficiency of CAR T cells

Donor ID	T Cell Population	Frequency of CAR+ T cells (Pre-Freeze)	Frequency of CAR+ T cells (Post-Thaw)
PR19C128729	Untransduced	0.34	0.11
	CAR-Y	87.10	87.90
	CAR-Z	85.20	85.80
PR19E128767	Untransduced	0.98	0.15
	CAR-Y	82.20	84.70
	CAR-Z	78.60	81.70
PR19X128768	Untransduced	0.53	0.08
	CAR-Y	72.60	72.90
	CAR-Z	69.30	69.30
PR19W128773	Untransduced	0.69	0.19
	CAR-Y	80.00	80.30
	CAR-Z	77.00	77.80

Table 36: Untransduced, CAR-Y and CAR-Z T cell populations were produced from four healthy donors. Transduction efficiency of T cell populations was performed both pre-freezing and post-thawing using anti-Fab Ab for the detection of CAR expression.

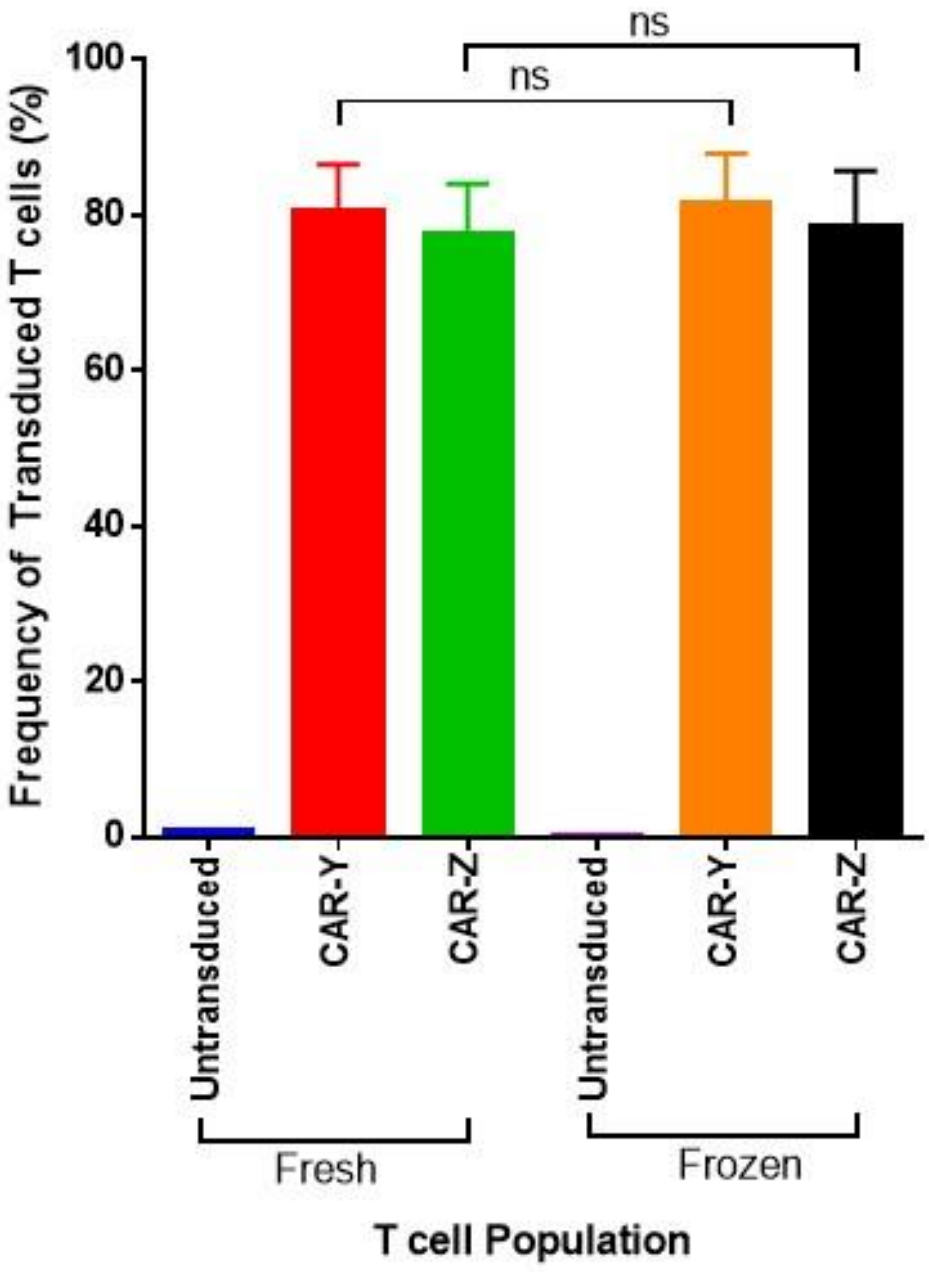

Figure 48 : CAR T Transduction Efficiency

Untransduced T cells, CAR-Y and CAR-Z CAR T cells were produced from four healthy donors and analysed for transduction efficiency through use of an anti-Fab Ab to detect CAR expression. Analysis of transduction efficiency was performed prior to freezing ("Fresh") and post-thaw ("Frozen"). A paired two-tailed T test was performed to determine if there was a significant difference in transduction efficiency between pre-freeze T cells or post-thaw T cells. CAR-Y p-value = 0.16. CAR-Z p-value = 0.20. ns=not significant. (n=4). Error bars display mean with SD.

4.1.3.3.4. Co-culture of CAR T cells and Transfected HEK cells

CAR-Y and CAR-Z CAR T cells were co-cultured with target cell lines, including untransfected HEK cells, ZsGreen transfected HEK cells, DCC transfected HEK cells, COSMC Jurkat cells (negative control cell line) and wild-type (WT) Jurkat cells (positive control cell line). Cell lines were co-cultured at a 1:1 ratio for 48 hours, subsequent to which supernatant was removed and analysed for production of IFN-γ by MSD® assay.

As shown in Figure 49, a peak in IFN-γ production was observed when CAR T cell populations were co-cultured with both DCC transfected HEK cells and with the positive control cell line, WT Jurkat cells. There was a small increase in background levels of IFN-γ production when CAR T cell populations were co-cultured with untransfected and ZsGreen transfected HEK cells.

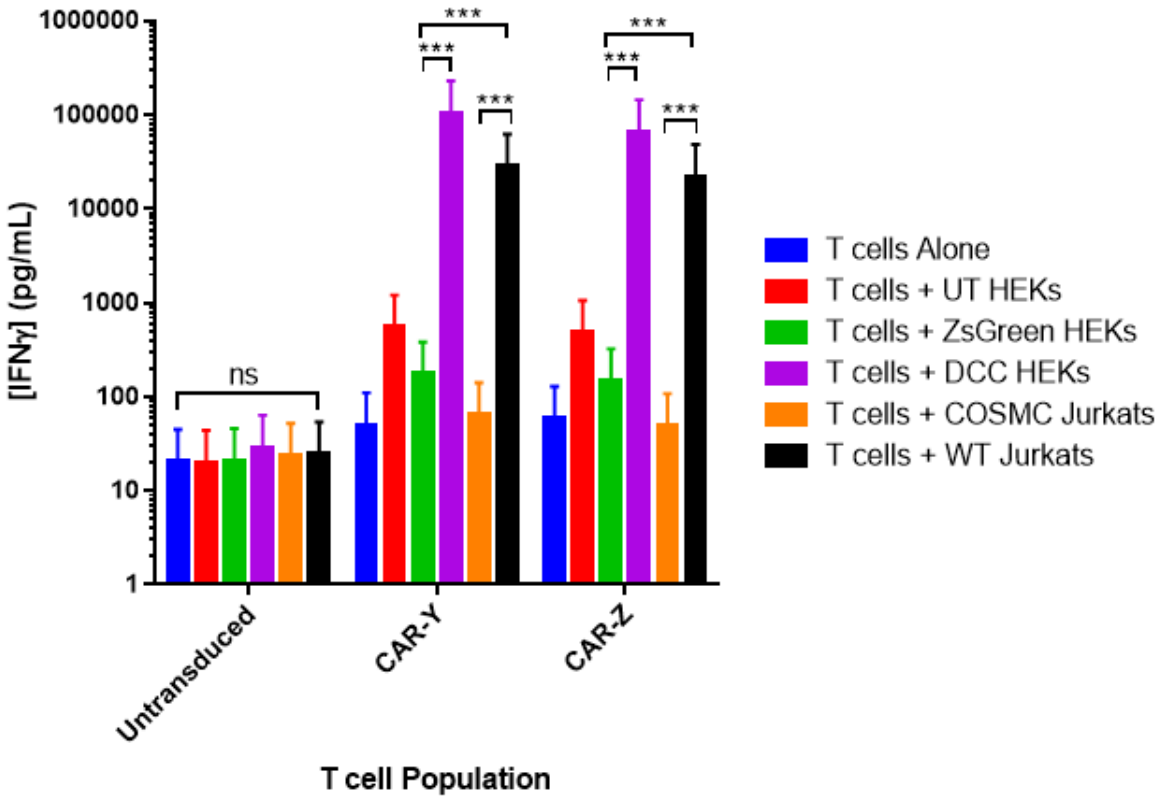

Figure 49 : Co-Culture of CAR T Cells and Target Cells – Analysis of IFN-γ Production by MSD®

*CAR T cells were co-cultured with target cell populations, including untransfected HEK cells, ZsGreen transfected HEK cells, DCC.IRES.ZsGreen transfected HEK cells, COSMC Jurkat cells (negative control) and wild-type (WT) Jurkat cells (positive control). A significant increase in IFN-γ production was observed when CAR-Y and CAR-Z CAR T cells were co-cultured with DCC transfected HEK cells and with the WT Jurkat positive control cell line. Significance determined using a mixed model with response variable log10 (IFN-γ concentration), fixed effect terms "Transduction" + "Cell Type" + "Transduction:Cell Type", and random effect terms "Donor + Transduction:Cell Type: Donor", where the term Transduction:Cell Type: Donor represents sets of observations from the same Transduction, Cell Type, Donor combinations (i.e. triplicate values per set). *** = P = <0.001. ns = not significant. Error bars display mean with upper and lower limit confidence intervals across 4 donors with triplicate wells set up for each set. Data is displayed on a Log10 Scale. Not all significance values are displayed, the significance of all comparisons performed are shown in Table 37.*

A selection of comparisons between co-culture conditions was performed using a mixed statistical model to determine the significance of the fold change in IFN-γ concentration. The comparisons performed are described in Table 37. There was no significant difference in IFN-γ concentration produced by untransduced T cells in any of the co-culture conditions that were compared. There was a significant difference ($p = <0.001$) in IFN-γ concentration produced for both CAR-Y and CAR-Z T cells when co-cultured with DCC HEK cells compared to when co-cultured with either ZsGreen transduced HEK cells or untransfected (UT) HEK cells, with the highest fold change in IFN-γ concentration observed between DCC HEK cells and ZsGreen HEK cells at 600.9 and 448.75 for CAR-Y and CAR-Z T cells respectively. A comparison between ZsGreen HEK cells and UT HEKs was performed to determine whether there was a significant difference in the IFN-γ concentration produced between the two negative controls, with p values of 0.0105 and 0.0083 for CAR-Y and CAR-Z T cells respectively. This demonstrated that there was a significant difference within the IFN-γ concentration produced between the two negative controls, however with upper confidence intervals of 0.76 and 0.73 the ratio was close to 1 demonstrating that there was a minimal difference between the levels. This provided the confidence to use ZsGreen HEK cells as the negative controls for comparisons as shown on Figure 49. Finally, a comparison was performed between the IFN-γ concentration produced between the positive control (WT Jurkats) and the negative control (COSMC Jurkats) which demonstrated a significant difference in the IFN-γ concentration ($p = < 0.001$) between these two conditions, with a fold change in IFN-γ concentration of 440.96 and 452.58 for CAR-Y and CAR-Z T cells respectively.

Table 37: Significance of Multiple Comparisons Performed on IFN-γ Concentrations Produced With Different Co-Culture Conditions

Comparisons of IFN-γ Concentrations Produced with Different Co-Culture Conditions		P Value	Significance Symbol	Fold Change in IFN-γ Concentration	Upper Confidence Interval	Lower Confidence Interval
Untransduced T cells	DCC HEK vs ZsGreen HEK	0.45	ns	1.39	3.31	0.59
	WT Jurkat vs ZsGreen HEK	0.70	ns	1.18	2.80	0.50
	WT Jurkat vs COSMC Jurkat	0.94	ns	1.03	2.46	0.44
	ZsGreen HEK vs UT HEK	0.95	ns	1.03	2.45	0.43
	DCC HEK vs UT HEK	0.41	ns	1.43	3.41	0.60
	WT Jurkat vs UT HEK	0.65	ns	1.21	2.89	0.51
CAR-Y T cells	DCC HEK vs ZsGreen HEK	4.00E-20	***	600.90	1428.30	252.80
	WT Jurkat vs ZsGreen HEK	3.00E-16	***	162.52	386.30	68.37
	WT Jurkat vs COSMC Jurkat	3.00E-19	***	440.96	1048.14	185.52

	ZsGreen HEK vs UT HEK	1.05E-02	*	0.32	0.76	0.13
	DCC HEK vs UT HEK	1.00E-16	***	190.99	453.96	80.35
	WT Jurkat vs UT HEK	2.00E-12	***	51.65	122.78	21.73
CAR-Z T Cells	DCC HEK vs ZsGreen HEK	3.00E-19	***	448.75	1066.65	188.79
	WT Jurkat vs ZsGreen HEK	6.00E-16	***	149.97	356.47	63.09
	WT Jurkat vs COSMC Jurkat	3.00E-19	***	452.58	1075.77	190.41
	ZsGreen HEK vs UT HEK	8.30E-03	**	0.31	0.73	0.13
	DCC HEK vs UT HEK	1.00E-15	***	137.15	326.00	57.70
	WT Jurkat vs UT HEK	7.00E-12	***	45.84	108.95	19.28

*Table 37: Significance of fold change in IFN-γ concentration between multiple comparisons of co-culture conditions. Values determined as mean of four donors with triplicate samples for each condition. Significance determined using a mixed model with response variable log10 (IFN-γ concentration), fixed effect terms "Transduction" + "Cell Type" + "Transduction:Cell Type", and random effect terms "Donor + Transduction:Cell Type: Donor", where the term Transduction:Cell Type: Donor represents sets of observations from the same Transduction, Cell Type, Donor combinations (i.e. triplicate values per set). *** = P = <0.001. ** = P <0.01. * = P <0.05. ns = non-significant.*

4.1.4. Discussion

The aim of this set of studies was to evaluate the Retrogenix™ platform for inclusion within early development phase of CGT products in order to reduce the number of candidate constructs progressing to extensive safety studies.

The Retrogenix™ cell surface protein microarray has been used regularly for the screening of monoclonal antibodies for confirmation of known target binding and identification of potential off-target binding. However at the time of writing this thesis, the use of Retrogenix™ for screening of CAR T cells has only been utilised by a limited number of companies, including BlueBird Bio and KITE Pharma.

Optimisation of the Retrogenix™ platform for screening of CAR T cells has included an investigation into the number of CAR T cells to be used for each screen, as well as the washing techniques to try to limit non-specific binding. The level of non-specific binding of T cells from three different donors was investigated in Figure 39 and demonstrated that there was some variability between the three donors – with increased levels of graininess on the background of the microarray slides demonstrating the binding of T cells to untransfected HEK293 cells grown as a monolayer across the whole microarray slide. The level of graininess was variable across all three donors, and even differed between the two replicates of the same conditions. Overall, non-specific binding of CAR T cells did not impact upon the observed results and would not be considered to be a risk to hit identification.

Within the second assessment, CAR T cell populations were produced from T cells isolated from donor 90928 and were initially screened against known target proteins, as shown in Figure 41. The transduction efficiency of BCMA-CAR T cells generated from donor 90928 for study 1 and study 2 differed by just 7% , with 55.8% and 63.2% BCMA-CAR expression respectively (Table 33 & Table 34), and was almost identical to the transduction efficiency of BCMA-CAR T cells from donor 12028 (62%) within study 1 (Table 33). However, within the second study, the intensity of the binding spot against BCMA was more intense. This increased intensity of spot intensity is unlikely to be due to the small increase in BCMA-CAR T cells within the cell population but demonstrates that the expression of protein on the surface of HEK293 cells could differ

between two studies. For this reason, Retrogenix™ do not recommend comparison of data generated within different screens.

This variability in the expression of protein on the HEK293 cell surface demonstrates a major caveat with the Retrogenix™ technology, with the detection of protein expression reliant on the expression of GFP that is encoded bicistronically with the surface protein cDNA. This confirms transfection, however there is not a method to directly quantify the expression of the protein on the surface of the HEK cells. This results in there being no possibility to compare the expression of the protein between two separate screens. In addition, this means the affinity of CAR T binding to proteins cannot be assessed within screens – as any differences within spot intensity observed may be due to differences in the level of protein expression, rather than differences in CAR T affinity. This highlights a disadvantage in the Retrogenix™ platform compared to the Cellzome platform, which utilises a method of competitive inhibition to identify off-target binding hits which are of higher affinity than the target binding.

Some evidence of differences in binding spot intensity, potentially due to differences in the CAR T cells affinity to the known target, were observed with CAR-A T cells and CAR-B T cells. Both CAR T cell populations were known to bind to the same target (defined as “Target 1”), with CAR-A T cells reportedly having a higher binding affinity to Target 1 than CAR-B T cells based on the results of previous *in vitro* studies (data not shown). Within Figure 41C and Figure 41D and Figure 42C and Figure 42D, the binding spot against Target 1 was observed to be more intense with CAR-A T cells than CAR-B T cells. This highlights that some qualitative information on the affinity of CAR T cells may be possible when CAR T cell populations are screened concurrently, although further confirmations would be required as differences in protein expression between spots on the same screen would still be possible.

The inability to directly assess the expression of protein on the surface of HEK cells also results in the possibility of false negatives. There is the potential that GFP could be expressed to a low level, indicating successful transfection, however the protein may not have been expressed properly on the HEK cell surface. The possibility of false negatives was demonstrated within Study 2 during the screening of the two CAR T populations, CAR-A & CAR-B. The binding of both CAR-A & CAR-B T cells to the

known target (Target 1) was demonstrated in both the pre-screen and confirmation screen (Figure 41 & Figure 42). However, CAR-A was independently demonstrated to bind to an additional off-target family member of the known target (data not shown). This off-target binding event was not identified through the Retrogenix™ screening platform, which may be due to incorrect protein expression or incorrect protein folding, resulting in masking of the epitope.

As shown in Figure 42, off-target binding was observed with CAR-X with one medium intensity binding event observed against the netrin 1 receptor (DCC) and one weak-very weak binding event observed within SELPLG. Due to the inconsistency of the binding to SELPLG, as shown by a binding spot visible in only one of the replicate slides, this binding hit was described as very low confidence by Retrogenix™ and project prioritisation within GSK meant that this binding hit was not followed up with further investigations. Instead, resourcing was prioritised on the investigation of the binding event between CAR-X and DCC, with further in house validation performed to determine whether this was a true binding event that could lead to the activation of CAR T cells and subsequent cytokine production. Although it was not possible to follow-up with the very weak to weak intensity SELPLG binding hit within this investigation, it would have been of interest to have investigated this further to determine whether these very weak to weak intensity hits identified within an *in vitro* screening assay would lead to the activation of CAR T cells, both in *in vitro* follow-up assays and within an *in vivo* setting. Instances in which very low levels of expression of a target antigen within a healthy tissue have led to detrimental activation of a CAR T product, such as within the Morgan *et al.* anti-ErbB2 CAR T trial (Morgan *et al.*, 2010) in which low expression of ErbB2 within the lungs led to CAR T activation and pulmonary œdema, demonstrate that even very low intensity binding could result in a potent activation of CAR T cells. This highlights the importance of understanding the avidity of a T cell interaction with a target antigen, as low density expression of a high affinity target and high density expression of a low affinity target can have an equal avidity. Therefore, despite the appearance of low intensity binding with SELPLG, the potential of a high avidity interaction within an *in vivo* setting may still be possible and could lead to activation of CAR T cells and the safety risks associated with off-target off-tumour binding.

In order to validate the off-target binding event identified by Retrogenix™, a DCC plasmid was produced and HEK cell transfection was performed enabling a method of HEK cell transfection to be chosen for the co-culture experiment – with at least 30% of the HEK cell population demonstrating expression of ZsGreen. Due to the lack of availability of a suitable anti-DCC antibody, it was not possible to confirm the expression of DCC on the surface of the transfected HEK cells, however DCC gene and protein expression was also confirmed by qPCR and Western blot analysis respectively (Figure 46).

As previously described, two CAR T cell populations were utilised for the co-culture experiment, CAR-Y and CAR-Z, with activation of both CAR T cell populations when co-cultured against DCC expressing HEK cells confirmed through the production of significant levels of IFN-γ above background levels (Figure 49). Higher levels of IFN-γ were produced when CAR-Y and CAR-Z were co-cultured with DCC expressing HEK cells than when co-cultured with the positive cell line (wild type Jurkat cells). This validated the results observed with Retrogenix™ confirming that DCC was a real off-target binding hit for both CAR-Y and CAR-Z CAR T cell populations.

Through the evaluation of the Retrogenix™ platform, I have been able to build confidence in the technology by demonstrating that the off-target positive binding hit (DCC) identified through the microarray screen did correspond with actual binding and activation of CAR T cells. The major caveat to this platform is the potential for false negatives, due to improper expression of proteins on the surface of HEK293 cells. This issue with correct protein expression is prevalent in all of the current technology platforms, with the main limitation of the Cellzome platform being the presentation of proteins as peptides within the cell lysate, which may impact the conformational structure of proteins and thus the potential epitopes expressed. The expression of plasma membrane proteins in the context of a cell provides the Retrogenix™ platform with a large advantage over the Cellzome platform by potentially enabling the proper folding of proteins in their native form - providing a more realistic presentation of potential epitopes. However, issues still may persist which impede proper protein expression – for example, improper folding of the protein within the HEK cell line leading to incorrect expression of epitopes, and incorrect glycosylation of the proteins. The glycosylation state of proteins is particularly important for CAR T cells which detect neoantigens expressed only in tumour cells due to errors in protein

glycosylation. The post-translational modifications possible within HEK293 cells may differ to that of an antigens native cell type – leading to the potential to miss important off-target binding events.

The potential for false negatives was demonstrated through the lack of binding of CAR-A to a known off-target family member of the target protein and remains to be further investigated through comparison of binding results observed with the parental mAb and CAR-A T cells. The ability to assess off-target binding of CARs in the context of a CAR T cell is beneficial and may narrow down the number of positive hits that require investigation, however it appears there is also the potential that important off-target binding hits are being missed. It would be of interest to perform a comparison between the binding hits observed with the parental mAb and CAR-A to help elucidate the differences in binding observed with different reagents and enable a decision to be made on whether parental mAbs or CAR T cells should be utilised in further screens with Retrogenix™.

This investigation has demonstrated that the Retrogenix™ platform is a useful method to screen CAR T cells for early-stage assessment of CAR specificity by identifying constructs with potential off-target binding hits. The technology is currently unsuitable to be used as a definitive off-target binding screen for pre-clinical safety studies, due to the potential for false negatives. However, the Retrogenix™ technology is powerful in enabling the screening of multiple CAR T cell populations to narrow down the number of candidates to follow through with additional pre-clinical safety studies. The potential for false negatives would not be as detrimental if the technology were to be used at the early development stage, as any constructs would still need to be progressed into more extensive safety assessments where potential false negatives would hopefully be identified. Further improvements to the Retrogenix™ technology would be required to enable it to be used as a key part of later pre-clinical safety packages. These improvements would include the detection and quantification of protein expression on the surface of HEK cells and confirmation of correct glycosylation of proteins or ability to offer proteins with abnormal glycosylation patterns.

One disadvantage of using the Retrogenix™ platform for early development screening is that there would be a risk that a significant number of CAR constructs could be

removed from the candidate pool due to identification of off-target binding by the Retrogenix™ technology that would not have been fully confirmed by additional hit confirmation studies, such as the co-culture experiment performed in section 4.1.3.3.4. However, Retrogenix™ does now offer additional hit confirmation studies, at additional cost, which utilise flow cytometry to further confirm and increase confidence that any hits identified were true hits.

Another disadvantage to the Retrogenix™ technology is the fact that it would only be able to be utilised within the early development of CAR constructs, as the technology is not suitable for the screening of engineered TCRs, where peptides require presentation in the context of MHC. A different method of screening engineered TCRs would be required to significantly reduce early development costs within a Cell and Gene Therapy department where both CAR constructs and engineered TCRs are actively investigated.

Overall, the inclusion of the Retrogenix™ screening technology as part of the early development stage of research would need to be dependent on the potential cost saving that could be expected. There are two different approaches that could be taken for the screening of CAR constructs at an early stage;

A) Cut-down Screen

   Includes the assessment of background binding and a single shot screen against the protein library, consisting of over 5500 plasma membrane proteins – at a cost of ~£5000 per construct. Note; costing information was obtained in 2018 and may be subject to change due to the recent acquisition of Retrogenix™ by Charles River.

B) Full Screening

   Includes assessment of background binding, a single shot screen against the full protein library, consisting of over 5500 plasma membrane proteins and a confirmation screen in which identified hits are spotted in duplicate and retested against the protein library – at a cost of ~£15,000 per construct. Note: costing information was obtained in 2019 and may be subject to change due to the recent acquisition of Retrogenix™ by Charles River.

For early development screening, the cut-down screen approach would be most suitable at approximately £5000 per construct to be tested. This is still a significant cost at the early development stage, meaning that the Retrogenix™ platform could only realistically be used to further narrow down a shortlist of candidates. However, this would still contribute to a beneficial cost saving by enabling the reduction of the number of constructs being progressed into *in vivo* studies and additional safety studies. Through ensuring that only the highest quality candidate constructs are progressed, GSK can continue to strive to improve the ethics of animal study design by enabling the reduction in the number of animals required for *in vivo* studies, which would also help to reduce the costs associated with these studies that can typically range between £50,000 to £100,000 depending on the mouse model used.

4.2. Chapter 2: Manufacturing – Improving Product Quality

4.2.1. Introduction

As previously described, the expansion of the T cell product is critical to achieve the appropriate dosage for treatment of the patient. The dosage of Kymriah® to be used for the treatment of paediatric and young adult B cell ALL is 0.2 to $5x10^6$ CAR positive viable T cells per kg of bodyweight for patients under 50kg, and 0.1 to $2.5x10^8$ CAR positive viable T cells per kg of body weight for patients over 50kg. The dose used in the treatment of adult relapsed or refractory diffuse large B cell lymphoma is 0.6 to $6x10^8$ CAR positive viable T cells (FDA/CBER).

In addition to this, within the product release criteria for Kymriah®, it is stated that the product must have a high purity CD3+ T cells. If the final product doesn't meet the release criteria, then it must be given to the patient off-label with manufacturing costs then unable to be reimbursed. The culture conditions for expansion are selectively permissive for T cells, and therefore expansion also results in increased purity of the drug product compared to immediately post-selection of CD4+/CD8+ cells.

The expansion of the T cells is not only essential to ensure a sufficient dose is provided to the patient, but also increased expansion rates could help to reduce the volume of lentiviral vector required for the production of the T cell product – thus lowering the cost of goods, as the cost of lentiviral vector is considered to significantly contribute to the overall manufacturing costs of cell and gene therapy products (Comisel *et al.*, 2021). Improved expansion rates of the product may help to reduce the vein-to-vein time by reducing the number of days of expansion required, enabling faster treatment of the patient and reducing manufacturing costs.

Different methods of manufacture of T cell products have been utilised within clinical trials, enabling an insight into the aspects of manufacture which may lead to failures within the manufacturing process. Due to the large scope of the manufacturing process, I have chosen to concentrate my research on three aspects of the manufacturing process that I feel may have the largest impact upon improving the quality of the final T cell product. Firstly, the chosen starting material, as previously mentioned in section 1.4.3, can impact upon the expansion of the final product.

Secondly, the method of culture of T cells, which can differ in small-scale production runs compared to large-scale production runs, with trials utilising small-scale G-REX® culture vessels (Bajgain *et al.*, 2014; Lonez *et al.*, 2017) through to large Wave™ bioreactors (Somerville *et al.*, 2012) for the production of T cells. Finally, the choice of cytokine used within the culture media, which can impact upon the final product phenotype and the rate of expansion (Geginat *et al.*, 2001) .

4.2.2. Hypothesis and Study Aims

The hypothesis of this set of studies is that changes in product manufacturing methods would help to increase cell expansion without negatively impacting upon other CQAs, such as transduction efficiency and phenotype.

The aims of the studies described within this chapter are:

- To investigate the impact that starting material has upon cell expansion and final product quality, analysing cell activation, fold expansion and transduction efficiency.
- To investigate the impact that method of culture has upon the fold expansion of the final product
- To investigate the impact that the choice of cytokine during culture has upon cell expansion and final product quality, analysing fold expansion, transduction efficiency and T cell phenotype

4.2.3. Results

4.2.3.1. Impact of Starting Material

For the clinical manufacture of a T cell product, the starting material is typically obtained from patients through apheresis, which was explained in more detail within section 1.4.3, providing a lymphocyte enriched peripheral blood mononuclear cell (PBMC) population. Whereas, within research, whole peripheral blood is obtained from healthy donors. Subsequent to collection of the blood, it is generally processed in a manner to remove contaminating red blood cells (RBCs) and platelets, which may be through use of gradient density centrifugation (as described in section 3.2.1) as was performed within clinical trials NCT00012207 (Till *et al.*, 2008) and NCT01886976 (Guo *et al.*, 2016). Other trials utilise automated cell washers, such as the Haemonetics® CellSaver® (Braintree, USA) to remove apheresis buffer and other impurities from the PBMC population (Levine, 2015), before continuing with the processing of the PBMC population with the main aim to reduce the number of contaminating RBCs and platelets, which can cause clumping of the subsequent product or impact upon the clinical efficacy of the final product (Fesnak & Lin *et al.*, 2016).

The resulting PBMC population generally consists of mixture of lymphocytes (T cells, B cells and NK cells), monocytes, granulocytes and dendritic cells. Some clinical trial protocols have proceeded with activation of the PBMC population through use of anti-CD3 monoclonal antibodies to enable the preferential expansion of activated T cells within the cell population (Itzhaki *et al.*, 2020), whilst others continue with additional isolation techniques to further purify the starting cell population (Brentjens *et al.*, 2013; Grupp *et al.*, 2013). Within some studies utilising PBMCs as the starting material, a high rate of failure due to insufficient cell numbers produced during expansion of the product was reported and linked to a high frequency of monocyte contamination within the PBMC population (Stroncek *et al.*, 2016; Allen *et al.*, 2017). It has also been reported that monocyte contamination may impact upon the functionality of the final product (Ino *et al.*, 2001). In light of this finding, Stroncek *et al* carried out a study

investigating the use of a plastic adherence step to eliminate monocytes but found that this method did not completely eliminate manufacturing failures (Stroncek *et al.*, 2017). Further to this, the group tested the use of counter flow elutriation to purify lymphocytes from monocytes and granulocytes and found that improved purification of the starting material resulted in increased expansion of the T cell product and reduced the rate of manufacturing failures (Stroncek *et al.*, 2017). Similarly, a study by Singh *et al.* found that the presence contaminating NK cells may impact upon the culture of the T cell product (Singh *et al.*, 2013).

With these studies in mind, it puts weight to the argument that a selection step to purify T cells prior to activation and transduction may improve the manufacturing process. A variety of the isolation procedures have been utilised within clinical trials, with the CliniMACs Prodigy® (Miltenyi Biotec) used regularly for the isolation of CD4+ and CD8+ T cells using magnetically labelled microbeads (Mock *et al.*, 2016; Lock *et al.*, 2017), which have the benefit of degrading within the culture media eliminating the requirement of additional steps to remove the selection antibodies from the final formulation (Miltenyi Biotec). Further studies have investigated the potential of product improvements through use of defined compositions of T cell populations which require more extensive selection methods, including defining the ratio of CD4+ to CD8+ T cells as performed within the clinical trial NCT-01865617 (Turtle, Hanafi, Berger & Gooley *et al.*, 2016) or isolating particular T cell subsets of interest, such as central memory T cells (Vormittag *et al.*, 2018).

Within this chapter, I will investigate the impact that the starting cell population has upon the activation, transduction and expansion of the T cell product. This will enable optimisation of the choice of starting material used within *in vitro* research and will provide translatable data to help optimise methods that could ensure that final cell products have the key quality attributes and achieve the required expansion rate for product release.

The method chosen for the purification of the T cell populations was use of anti-CD4 microbeads (Miltenyi Biotec, #130-045-101) and anti-CD8 microbeads (Miltenyi Biotec, #130-045-201) and use of the AutoMACS® Pro-Separator to mimic the

selection process that occurs within the CliniMACs Prodigy® in GSK's clinical manufacturing process. Prior to selection, gradient density centrifugation of peripheral whole blood was performed to isolate the PBMC population. The PBMC population was subsequently treated with anti-CD4 or anti-CD8 microbeads or a combination of anti-CD4 and anti-CD8 microbeads before proceeding with isolation using the AutoMACS® Pro-Separator. A sample of each cell population was removed and analysed using an 8 colour immunophenotyping kit (Miltenyi Biotec, #130-120-640) to determine the purity of the sorted T cell populations.

Despite use of gradient density centrifugation for the removal of contaminating RBCs, a high frequency is still evident when a sample of the negative fraction from donor PR20F384542 is analysed (Figure 50A). These contaminating RBC are removed from the isolated T cell populations through use of the anti-CD4 and anti-CD8 microbeads (Figure 50B), with only 0.22% remaining which is within the limits of error for this analysis.

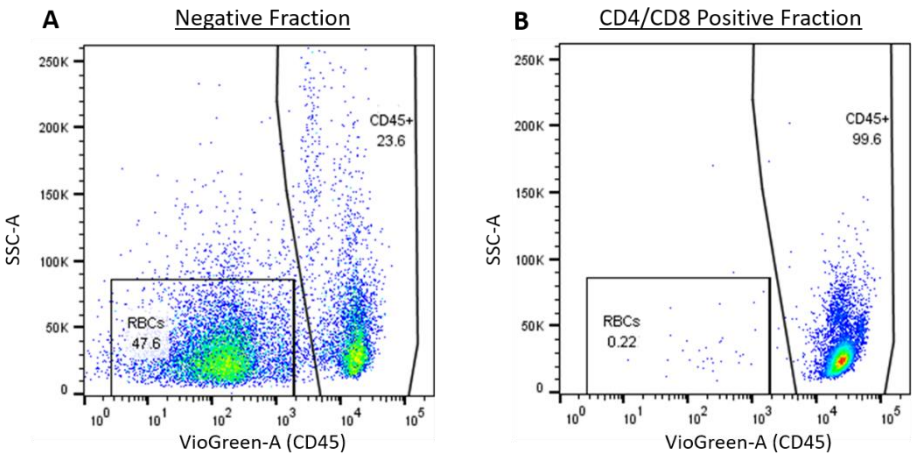

Figure 50: Red Blood Cell (RBC) contamination with T cell Populations

A) Despite Ficol Density Gradient Centrifugation being performed to remove contaminating RBC from T cell populations, a high frequency still remains as shown within the negative fraction taken from donor PR20F384542. B) The population of contaminating RBCs is diminished when isolation of T cells using anti-CD4 and anti-CD8 microbeads is performed.

As shown in Figure 51 and Figure 52, the use of anti-CD4 and anti-CD8 microbeads provides high purity T cell populations. There was a larger frequency of contaminating monocytes when anti-CD4 microbeads were used during the isolation, with an average of 6.7% and 8.6% for the CD4+/CD8+ T cell population and the CD4+ T cell population respectively. The average frequency of monocyte contamination within the CD8+ T cell population was 0.27%. This is due to the low level expression of CD4 on the surface of monocytes (Filion *et al.*, 1990), resulting in the isolation of a small frequency of contaminating monocytes alongside the CD4+ T cells. The frequency of B cells, NK cells and neutrophils was under 1% for all of the isolated T cell populations, demonstrating that the presence of these cell types would not impact upon the final T cell product. The isolation of either CD4+ or CD8+ T cells separately enabled the production of highly pure T cell populations, particularly when isolating CD8+ T cells where monocyte contamination is not an issue. The use of Miltenyi microbeads enabled the production of an average of 88% pure CD4+ T cell population and 94% pure CD8+ T cell population.

It had been planned for three donors to be analysed within the following set of experiments to enable statistical analysis of the results, however due to a production error, the processing of cell populations from a third donor failed thus the experiments had to continue with only two of the three donors.

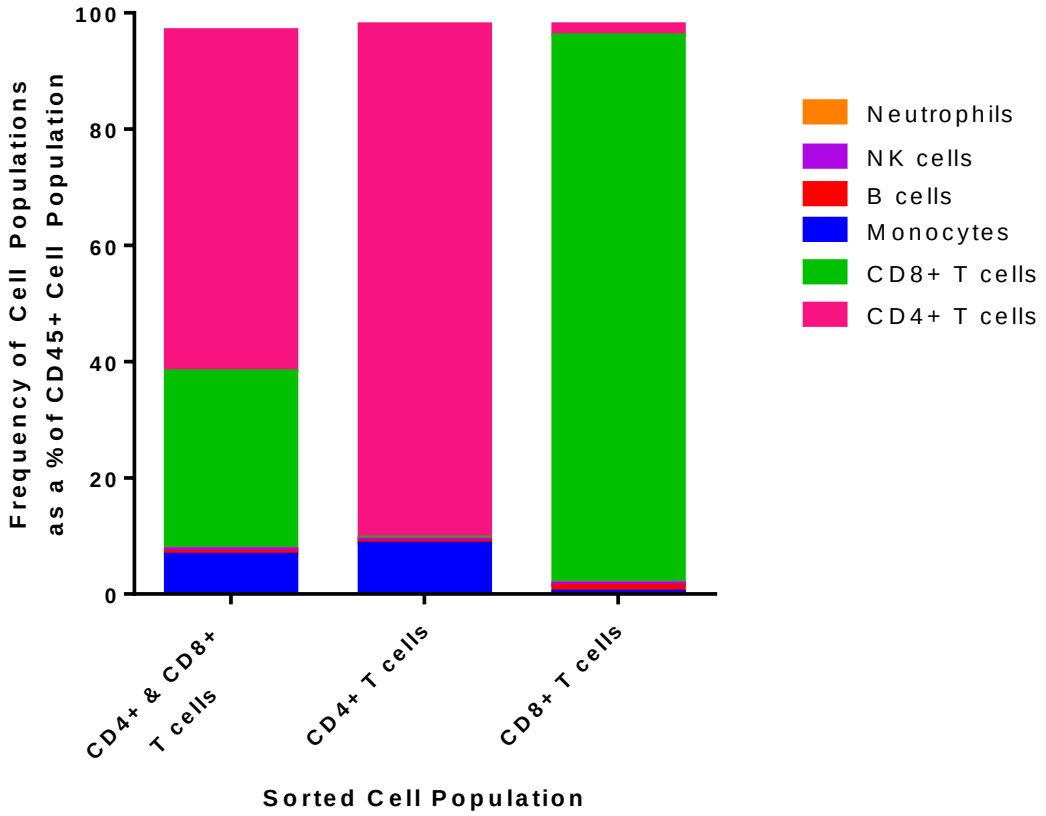

Figure 51: Purity of Sorted T cell Populations

Average frequency of each cell population (neutrophils, NK cells, B cells, monocytes, CD8+ T cells and CD4+ T cells) as a percentage of the CD45+ cell population are displayed. T cell populations were sorted using anti-CD4 and anti-CD8 microbeads with the AutoMACS® Pro-separator. (n= 2).

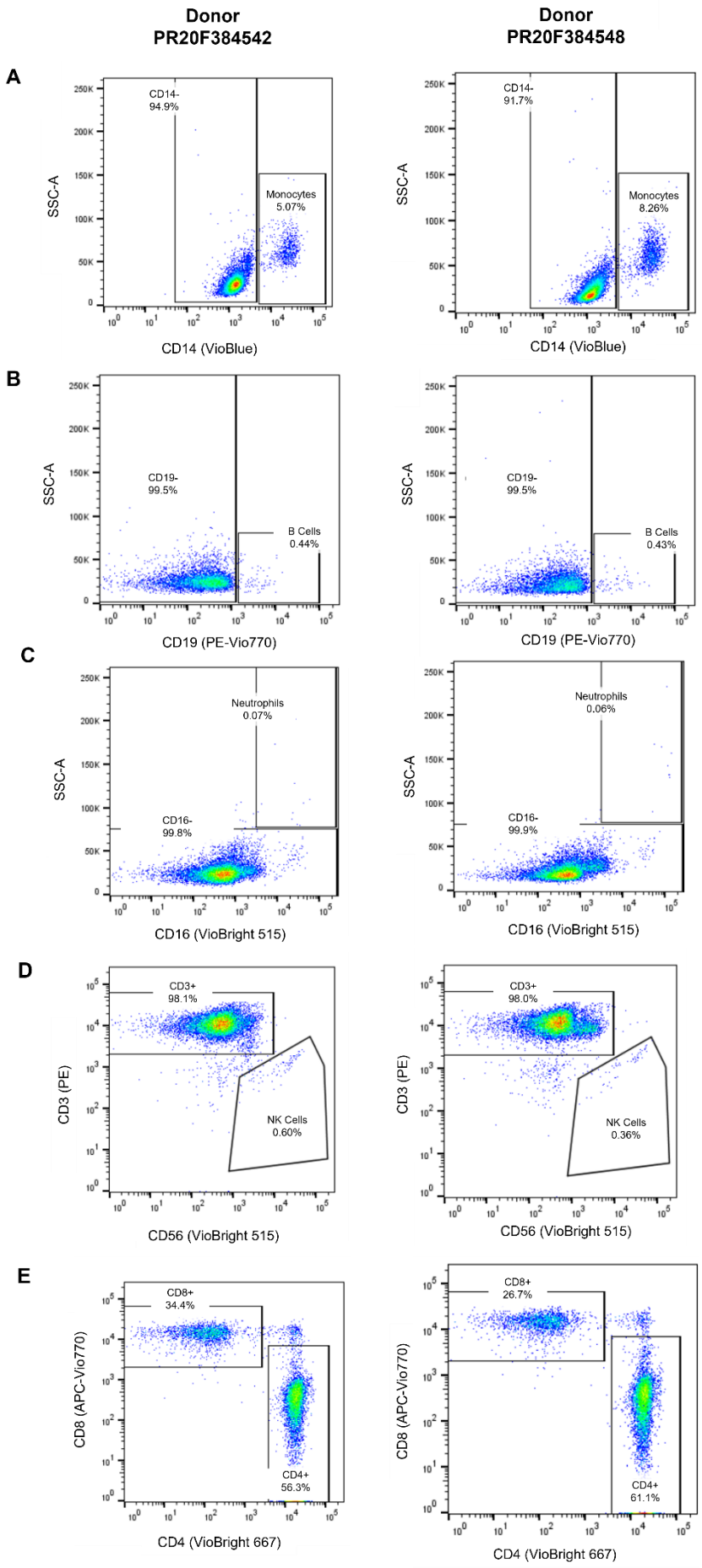

Figure 52: CD4/CD8 Sorted T cell Population Purity Flow Plots

Flow plots show the frequency of cell types within a CD4+ & CD8+ sorted T cell population for donor PR20F384542 (left panel) and PR20F384548 (right panel). T cell populations were sorted using a combination of CD4+ and CD8+ microbeads and cell populations were analysed for purity using an 8 colour immunophenotyping flow cytometry kit. Flow plots show the frequency of A) Monocytes, B) B Cells, C) Neutrophils, D) NK Cells and E) CD4+ and CD8+ T cells as a frequency of the CD45+ cell population.

Table 38: Frequency of Cell Populations as a Percentage of CD45+ Cell Population

		Sorted Cell Population		
Frequency of Cell Population as a % of CD45+ Cell Population		**CD4+/CD8+ T cells**	**CD4+ T cells**	**CD8+ T cells**
CD4+ T cells	PR20F384542	56.30	90.50	1.29
	PR20H384548	61.10	86.10	2.48
	Average	*58.70*	*88.30*	*1.89*
CD8+ T cells	PR20F384542	34.40	0.32	94.70
	PR20H384548	26.70	0.25	93.80
	Average	*30.55*	*0.29*	*94.25*
Monocytes	PR20F384542	5.07	6.33	0.11
	PR20H384548	8.26	10.80	0.43
	Average	*6.67*	*8.57*	*0.27*
B cells	PR20F384542	0.44	0.37	1.01
	PR20H384548	0.43	0.31	0.89
	Average	*0.44*	*0.34*	*0.95*
NK cells	PR20F384542	0.60	0.49	0.42
	PR20H384548	0.36	0.25	0.56
	Average	*0.48*	*0.37*	*0.49*
Neutrophils	PR20F384542	0.07	0.03	0.06
	PR20H384548	0.06	0.08	0.05
	Average	*0.07*	*0.06*	*0.05*

Table 38: An 8 colour immunophenotyping kit (Miltenyi Biotec) was used to analyse the frequency of cell populations as a frequency of the CD45+ cell population (following the method described in section 3.7) subsequent to T cell isolation using the AutoMACS® pro-separator. The frequency of each cell type for each donor (PR20F384542 and PR20H384548) are shown, along with the average for the two results.

Subsequent to the isolation of the T cell populations, the T cells were activated with TransAct™ activation reagent for 24 hours. Despite being reported to be able to transduce non-dividing cells, Vesicular Stomatitis Virus G Protein (VSV-G) pseudotyped lentiviral vectors are unable to transduce quiescent T cells (Amirache *et al.*, 2014), due to the requirement for expression of Low Density Lipoprotein Receptor (LDLr) expression on T cells to enable vector particle binding. The use of TransAct™ activation reagent (CD3 and CD28 nanomatrix) increases the expression of LDLr on the surface of T cells, thus enabling efficient transduction. After 24 hours of activation, the expression of an early activation marker (CD69) and LDLr was analysed on the T cell populations to determine whether differences in activation status (and thus potentially transduction efficiency) could occur within the different T cell populations.

As shown in Figure 53, a similar level of LDLr and CD69 expression is observed across all of the T cell populations apart from the isolated CD8+ T cell population, which has a decreased expression of both CD69 and LDLr. This data is only taken from two donors; therefore the significance of this result could not be calculated. In order to determine the significance of the results observed, this experiment would need to be repeated with a larger number of donors.

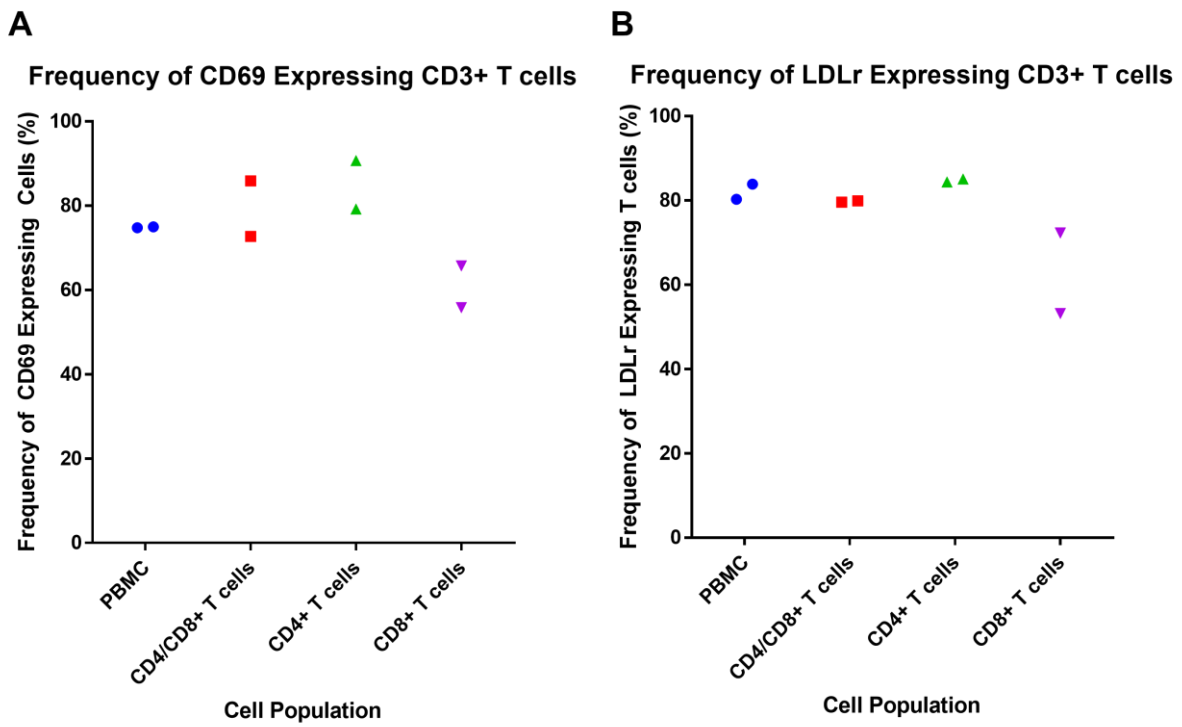

Figure 53: CD69 and LDLr expression in isolated T cell populations

Four cell populations (PBMCs, CD4/CD8+ T cells, CD4+ T cells and CD8+ T cells) were activated with TransAct™ activation reagent for 24 hours prior to flow cytometry analysis of the expression of A) CD69 and B) LDLr. (n=2).

Each cell population was stained for the expression of CD4 and CD8, in addition to LDLr and CD69, enabling analysis of the differential expression of activation markers within the CD4+ and CD8+ T cell subsets within each cell population. This demonstrated that the expression of both CD69 and LDLr was lower in the CD8+ T cell populations than the CD4+ T cell populations (Figure 55A and Figure 55B). Analysis of the median fluorescence intensity (MFI) of the staining for both CD69 and LDLr enabled determination of the relative expression of each marker on each cell, with the data showing that there was lower expression of CD69 and LDLr on each CD8+ T cell as well as a lower frequency of the overall cell population expressing the activation markers, when compared to CD4+ T cells (Figure 55C and Figure 55D). As this data was only produced using two donors, the significance of the differences could not be calculated. It would have been beneficial to repeat this experiment with further donors to determine the significance of these results, however due to portfolio prioritisation at GSK I was unable to repeat this study.

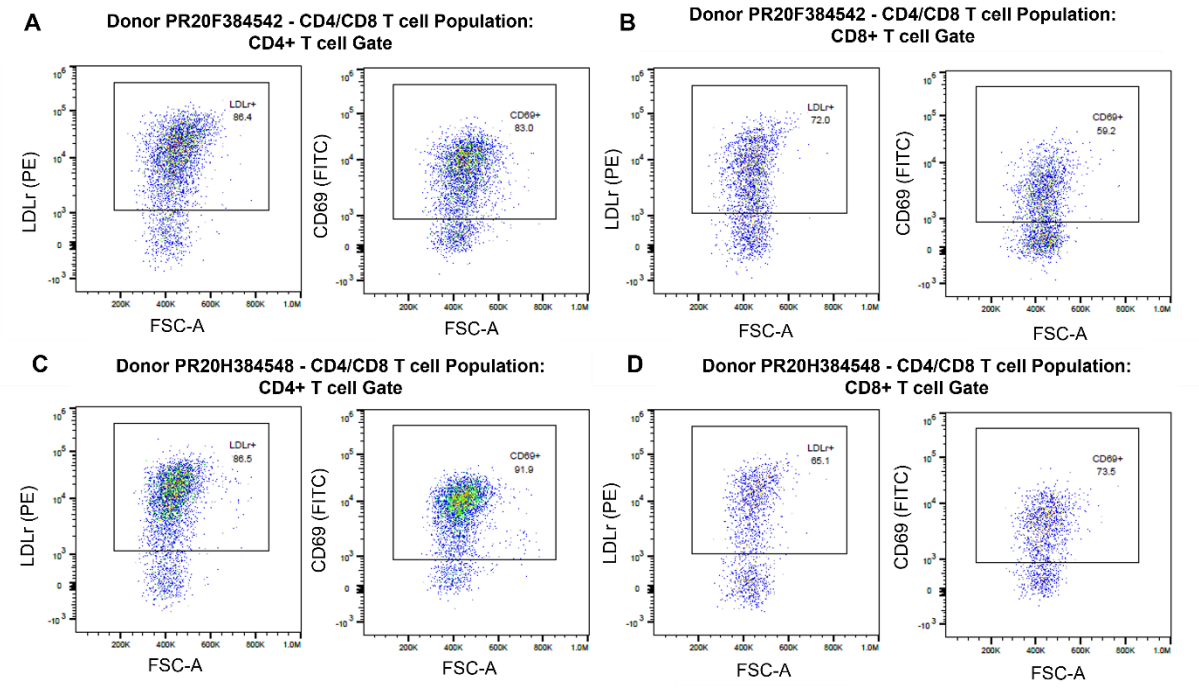

Figure 54: Representative Flow Plots of CD69 and LDLr Expression

The frequency of CD69 and LDLr positive T cells was analysed within both the CD4+ and CD8+ T cell population for each of the four cell populations (PBMCs, CD4/CD8+, CD4+ and CD8+). Representative flow plots are shown for the CD4/CD8+ population for each donor, A) Donor PR20F384542 – expression within CD4+ gate, B) Donor PR20F384542 – expression within CD8+ gate, C) Donor PR20H384548 – expression within CD4+ gate, B) Donor PR20H384548 – expression within CD8+ gate. Full gating strategy is shown within Figure 31.

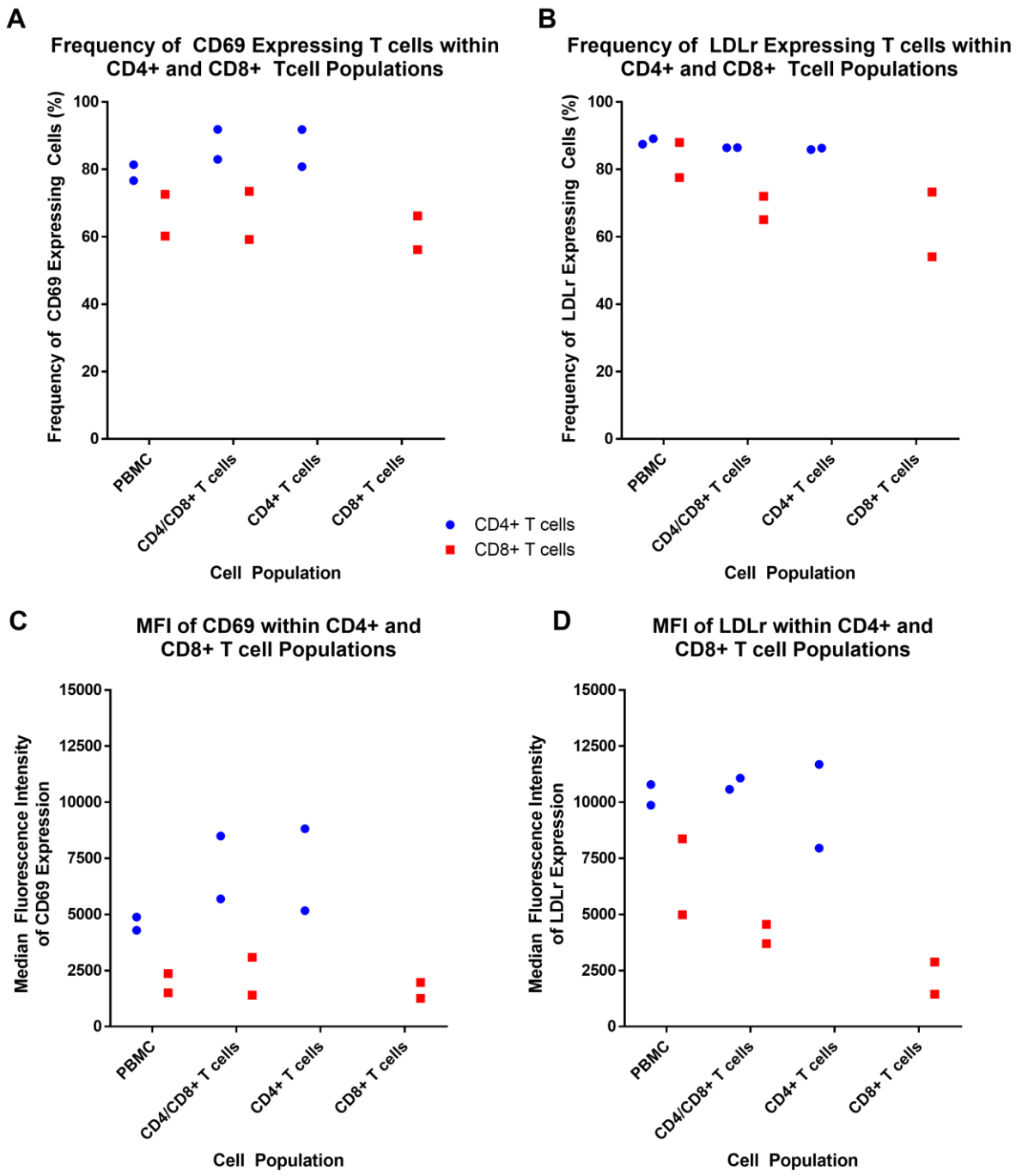

Figure 55: Frequency and Median Fluorescence Intensity (MFI) of CD69 and LDLr within CD4+ and CD8 T cells within Each Cell Population

Each cell population was stained for the expression of CD4 (shown in blue) and CD8 (shown in red) in addition to CD69 and LDLr, enabling determination of the expression of the activation markers within each T cell subset. A) Frequency of CD69 expression, B) Frequency of LDLr expression, C) MFI of CD69 and D) MFI of LDLr. (n=2).

With both a decreased frequency of CD8+ T cells expressing the two activation markers and a lower number of the receptor per cell at the time of transduction, it would be anticipated that the lowest transduction efficiency would be observed within the CD8+ isolated T cell population.

The results demonstrated a large difference in the transduction efficiency of T cells for donor PR20F384542, with the highest transduction efficiency within the PBMC population (65.6%) and the lowest transduction efficiency within the CD8+ population (41.4%) (Figure 57A and Table 39). These results correlated well with the CAR MFI results for this donor, with the highest CAR MFI observed within the PBMC population and the lowest CAR MFI observed within the CD8+ T cell population (Figure 57B). Interestingly, there was a difference in the transduction efficiency between the PBMC and CD4/CD8+ T cell population at 65.6% and 53.9% respectively, despite the fact that the frequency of LDLr expressing CD3+ T cells was very similar between the two populations (Figure 53B). When investigating the differences in the frequency and MFI of LDLr expression within the CD4 and CD8 populations within these two populations (Figure 55B and Figure 55D), it suggests that this difference in the transduction efficiency of the two populations may be due to differences within the LDLr expression within the CD8+ population, in which there is a similar frequency of LDLr expression and LDLr MFI for the CD4+ population when comparing PBMCs and CD4/CD8 T cells, but a lower frequency of LDLr expression and LDLr MFI for the CD8+ population within the CD4/CD8 T cells compared to the PBMC population.

The results of donor PR20H384548 were not as conclusive – the transduction efficiency of the PBMC, CD4/CD8+ and CD4+ T cell populations were very similar at 37.5%, 36.6% and 40.2% respectively, with the transduction efficiency of the CD8+ T cell population only marginally lower at 33% (Figure 57A and Table 39). The MFI of the cell populations for donor PR20H384548 were also very similar to one another (Figure 57B and Table 39). This highlights the large amount of variability that can be seen between the transduction of different donor T cells, irrespective of additional extenuating circumstances such as differences in pre-treatment of the donors. Analysis of a larger number of donors would be required to determine whether there is a significant difference in the transduction efficiency of the T cell populations generated from different starting populations.

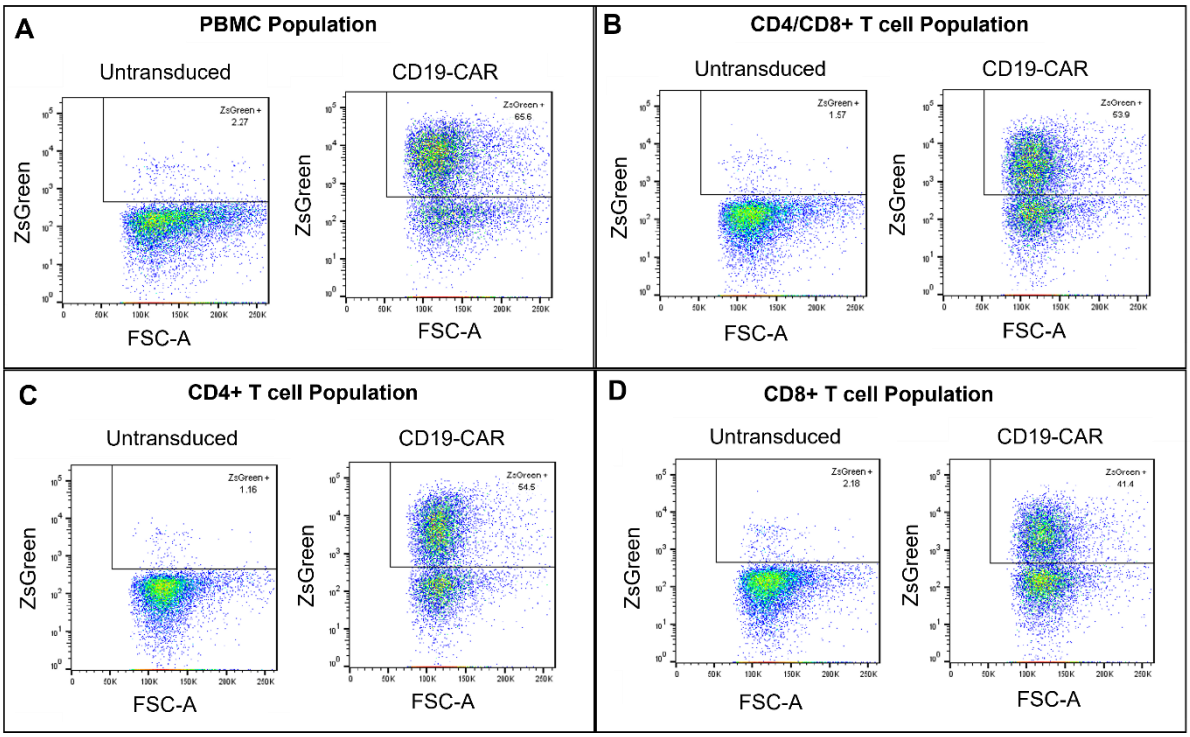

Figure 56: Flow Cytometry Analysis of ZsGreen Expression in Four Cell Populations from Donor PR20F384542

Analysis of ZsGreen expression of untransduced and CD19-CAR transduced cell populations was performed via flow cytometry, with ZsGreen gates set based on a representative untransduced sample. A) PBMC population, B) CD4/CD8+ T cell population, C) CD4+ T cell population and D) CD8+ T cell population. The full gating strategy is shown in Figure 22.

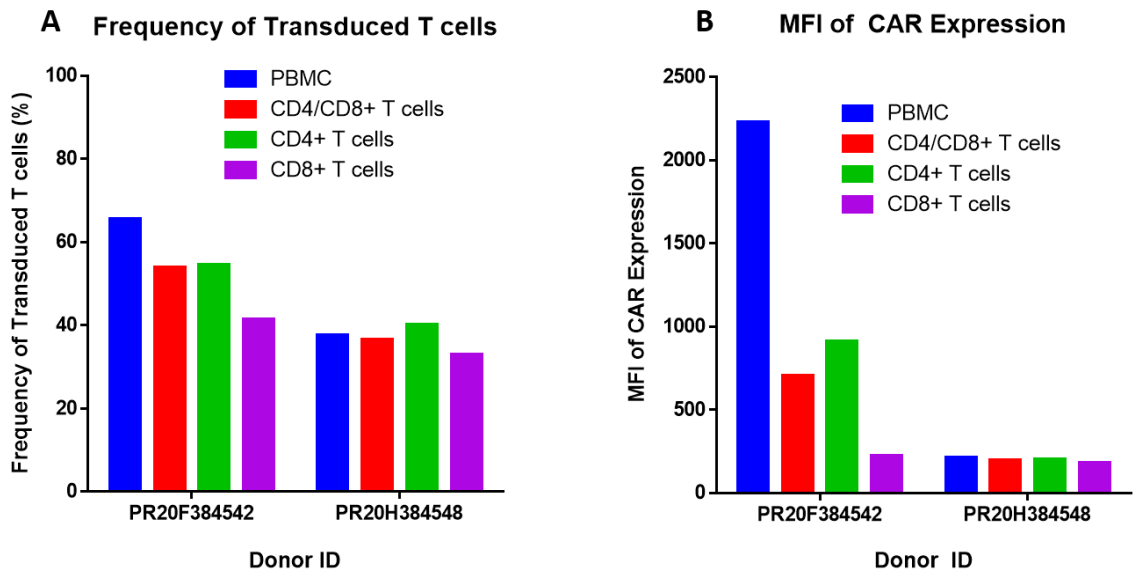

Figure 57: Transduction Efficiency and MFI of T cell populations

Four different starting cell populations from two donors (PR20F384542 and PR20H384548) were transduced with a CD19-CAR lentiviral vector and cultured for nine days prior to the analysis of transduction efficiency, via analysis of the detection marker ZsGreen, following the method described in section 3.5.1. A) The frequency of transduced T cells B) The MFI of ZsGreen expression within the single cell population was analysed to determine the relative expression of CD19-CAR per cell.

Table 39: Transduction Efficiency and Median Fluorescence Intensity of Transduced T cells

Donor ID	Cell Population	Frequency of ZsGreen Expressing T cells within the Live, Single Cell Population (%)	Median Fluorescence Intensity of ZsGreen within the Live, Single Cell Population
PR20F384542	PBMC	65.6	2230
	CD4/CD8	53.9	705
	CD4	54.5	908
	CD8	41.4	224
PR20H384548	PBMC	37.5	214
	CD4/CD8	36.6	198
	CD4	40.2	200
	CD8	33.0	180

Table 39: *T cell populations were transduced with a CD19-CAR containing a ZsGreen detection marker enabling analysis of transduction efficiency at day 9 post-transduction. The MFI of ZsGreen expression was analysed within the live, single cell population to determine the median expression of CD19-CAR per cell.*

As portfolio prioritisation at GSK prevented me from repeating this set of studies in a larger number of donors, I analysed additional data from combined CD4+ and CD8+ T cell transductions to determine if decreased transduction efficiency within CD8+ T cell populations was observed with an increased number of donors (Table 40). As shown in Figure 58A, a significant difference in the transduction efficiency of CD4+ and CD8+ T cells was observed ($p<0.0001$). In addition to this, analysis of the MFI of the CAR expression within the CD4+ and CD8+ T cell populations demonstrated a significantly lower MFI within the CD8+ T cell population ($p<0.0001$), demonstrating that there is not only lower frequency of CD8+ T cells transduced, but also that the expression of the CAR construct per cell is lower for CD8+ T cells than CD4+ T cells (Figure 58B).

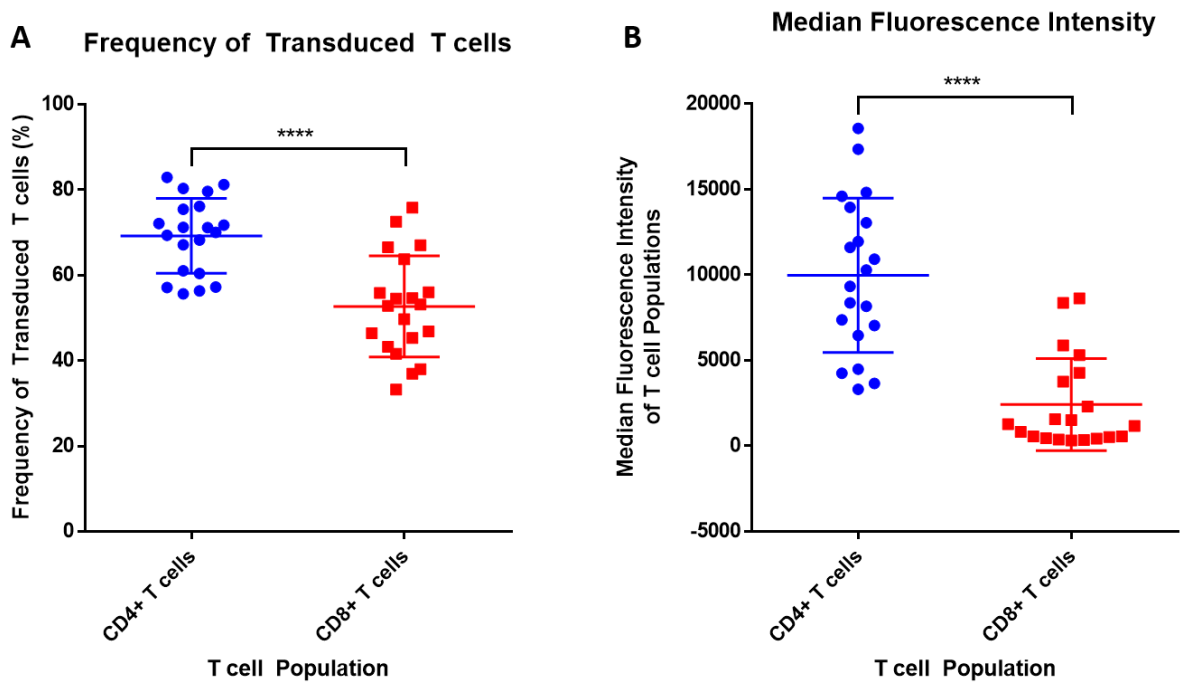

Figure 58: Differences in Transduction Efficiency of CD4+ and CD8+ T cells

*T cells from 5 healthy donors were transduced as pooled CD4+ and CD8+ T cell populations with CAR expression determined by flow cytometry detection of an LNGFR tag (following the method described in section 3.5.4.2). A paired two-tailed T test was used to calculate the significance of the difference between the two groups, with a total of 20 pairs from 5 donors (4 samples per donor). **** = p<0.0001. Error bars display mean and SD.*

Table 40: Transduction Efficiency and Median Fluorescence Intensity of Transduced T cells

Donor ID	Sample Number	Frequency of Transduced CD4+ T cells (%)	MFI of CD4+ T cells	Frequency of Transduced CD8+ T cells (%)	MFI of CD8+ T cells
PR19C133904	1	57.2	4481	41.6	423
	2	60.4	8168	46.8	549
	3	76.1	10917	67.0	5304
	4	80.3	18559	66.5	5869
PR19K133900	1	57.1	4246	36.9	344
	2	61.0	7041	43.2	449
	3	81.2	13949	63.7	4274
	4	72.1	10274	54.5	1502
PR19T133635	1	71.2	8354	54.6	2298
	2	69.3	14590	56.0	3760
	3	82.9	13039	75.8	8354
	4	79.6	17348	72.5	8621
PR19T133651	1	71.1	11944	46.4	547
	2	67.1	14822	45.3	517
	3	75.4	11600	55.8	1557
	4	68.2	9327	53.1	1261
PR19W133916	1	55.6	3308	33.2	316
	2	56.3	3644	38.0	373
	3	71.7	7365	49.7	813
	4	70.0	6450	52.8	1165
Average		***69.2***	***9971***	***52.7***	***2415***
Standard Deviation		***8.8***	***4514***	***11.8***	***2692***

Table 40: T cells from 5 healthy donors were transduced as pooled CD4+ and CD8+ T cell populations with four samples set up per donor. CAR expression determined by flow cytometry detection of an LNGFR tag and expression of CD3 and CD8 was used to define inferred CD4+ T cells (CD3+ and CD8-) and CD8+ T cells (CD3+ and CD8+) (following the method described in section 3.5.4).

Next, I wanted to investigate the impact that starting material was having upon the expansion of the T cell product, with particular interest in the impact upon the CD8+ T cell population in which a decreased transduction efficiency was observed. In order to investigate this, the fold expansion of the different T cell populations was calculated from transduction day to day 9 post-transduction. Within each cell population, there were three different transduction conditions (untransduced, ZsGreen transduced and CD19-CAR transduced) for each of the two donors (PR20F384542 and PR20H384548).

Table 41: Fold Expansion and Viability of T cell Populations

Cell Population	Transduction Condition	Donor ID	Fold Expansion	Viability (%)
PBMC	Untransduced	PR20F384542	26	93.8
		PR20H384548	25	93.5
	ZsGreen	PR20F384542	29	92.7
		PR20H384548	24	93.4
	CD19-CAR	PR20F384542	39	91.0
		PR20H384548	28	94.5
CD4 & CD8 T cells	Untransduced	PR20F384542	21	92.7
		PR20H384548	21	95.1
	ZsGreen	PR20F384542	22	93.9
		PR20H384548	21	94.0
	CD19-CAR	PR20F384542	27	94.0
		PR20H384548	24	95.2
CD4 T cells	Untransduced	PR20F384542	17	93.6
		PR20H384548	23	95.2
	ZsGreen	PR20F384542	13	94.2
		PR20H384548	13	94.8
	CD19-CAR	PR20F384542	20	94.6
		PR20H384548	26	94.4
CD8 T cells	Untransduced	PR20F384542	24	89.7
		PR20H384548	30	91.9
	ZsGreen	PR20F384542	24	84.7
		PR20H384548	29	90.1
	CD19-CAR	PR20F384542	23	88.1
		PR20H384548	32	90.3

Table 41: The fold expansion and viability of T cell populations was assessed at day 9 post-transduction. Within each cell population (PBMCs, CD4/CD8 T cells, CD4 T cells and CD8 T cells) there were three transduction conditions (untransduced, ZsGreen transduced and CD19-CAR transduced) and two donors (PR20F384542 and PR20H384548).

In order to combine the data sets for each transduction condition and analyse the impact of T cell population upon fold expansion and viability irrespective of transduction condition (as shown in Figure 59), I first had to confirm that the transduction conditions were not impacting upon the fold expansion or viability of the T cells within each cell population group. To investigate this, I performed a two-way ANOVA with Tukey's multiple comparison test enabling the pair-wise comparison of the means of each transduction condition within each cell population. This demonstrated that transduction condition was not significantly impacting upon the difference in fold expansion or viability within each T cell population, therefore I continued with my analysis of cell population impact upon fold expansion and viability grouping the results of the transduction conditions.

As shown in Figure 59A, there was a significant difference between the fold expansion of PBMCs vs CD4+ T cells ($P=\leq 0.01$) and CD4+ T cells vs CD8+ T cells ($P=\leq 0.05$). The lowest average fold expansion observed within the CD4+ population (18.7) and the highest fold expansion observed within the PBMC population (28.5). No significant difference in fold expansion was identified during comparisons of the other T cell populations. Interestingly, the CD4+ population had one of the highest levels of expression of LDLr and CD69 activation markers on the day of transduction (Figure 55), which did not result in an increased rate of expansion of the CD4+ T cell population. The viability of the T cell populations (Figure 59B) was measured at the end of the culture process and demonstrated a significant difference between all of the T cell populations vs the CD8+ T cell population ($P=\leq 0.001$). The lowest average viability was observed within the CD8+ T cell population at 89.1%, whilst the viabilities of the PBMC, CD4/CD8 T cell and CD4+ T cell populations were similar averaging 93.2%, 94.2% and 94.5% respectively.

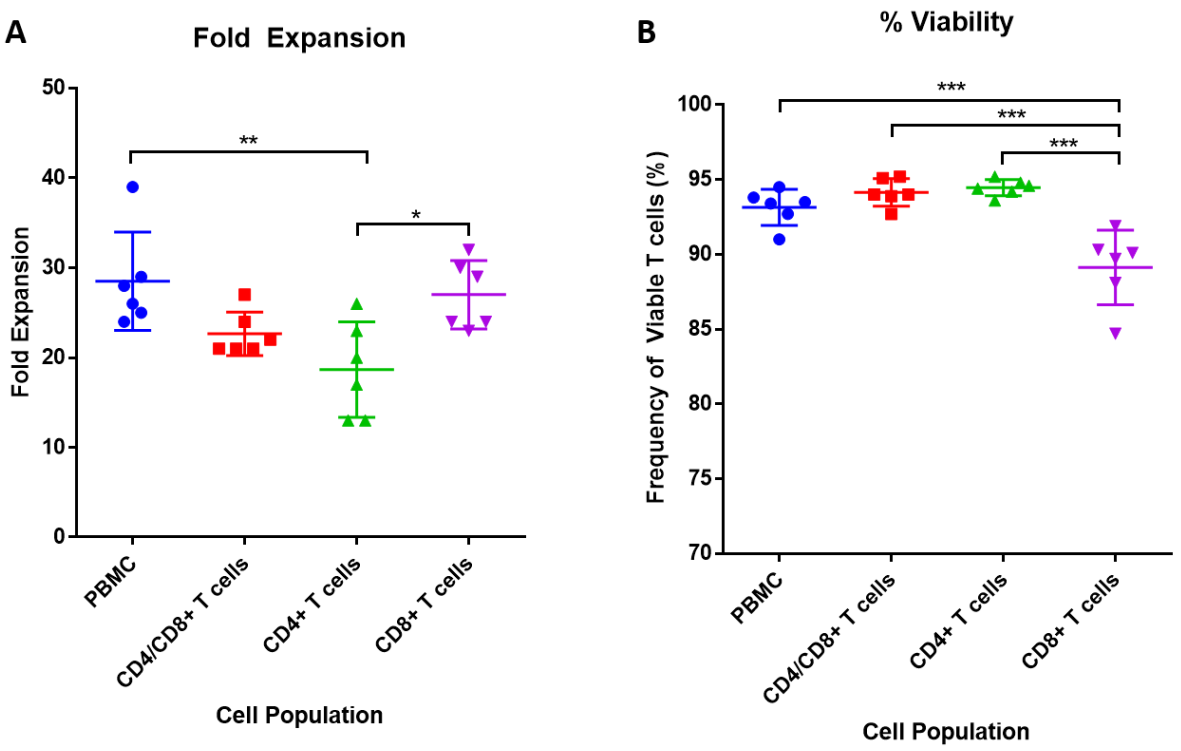

Figure 59: Fold Expansion and Viability of Different T cell populations

*Four different starting populations (PBMC, CD4/CD8+ T cells, CD4+ T cells and CD8+ T cells) from two donors were left untransduced or transduced with either a ZsGreen or CD19-CAR encoding lentiviral vector. The T cells were cultured for 9 days post-transduction, at which point the T cell populations were harvested and counted to calculate A) the fold expansion of the populations across the culture procedure and B) the viability of the T cell populations at the end of the culture procedure. n = 6 (2 donors each with three transduction conditions). Error bars display mean with SD. Significance was determined a one-way ANOVA with Tukey's multiple comparison test. *= P≤0.05. **=P≤0.01.***=P≤0.001. Non-significant results have been left blank.*

4.2.3.1.1. Discussion of Starting Material Data

The results obtained demonstrate that there is a trend for a lower expression of CD69 and LDLr within the CD8+ T cell population, irrespective of whether the CD8+ T cells are isolated and activated alone or isolated and activated within a pooled population, i.e. as PBMCs or a mixed CD4/CD8+ T cell population. When correlating this observation with the transduction efficiency of the different T cell populations, there was not a clear pattern due to a large variation between the two healthy donors. This data set would need to be repeated on a larger pool of donors to enable determination of significance of the differences, as the variation between donors has a large influence on the variation of the results. Donor to donor variation, even with healthy donors, plays a massive role in the results gathered – which highlights the importance of large donor pools, particularly when moving onto the use of patient T cells where additional sources of variation, such as pre-treatment, would add an additional level of complexity to the analysis of the results.

It was of interest that a large difference in the frequency and MFI of LDLr expression was observed between the CD4+ and CD8+ populations within the PBMC and CD4/CD8 T cell populations, which also correlated with an impact on transduction efficiency for donor PR20F384542. It would have been anticipated that the presence of contaminating cell types would have hampered the transduction of T cells within the PBMC population, with the potential that LVV could stick to other cell types reducing the availability for T cells. However, the results demonstrated a higher transduction efficiency within the PBMC population compared to the isolated CD4/CD8+ T cell population, with higher LDLr expression on CD8+ T cells within the PBMC population.

When investigating the differences between MFI and transduction efficiency of CD4+ and CD8+ T cells transduced in pooled populations, it was clear that there was a significant difference in the transduction efficiency and MFI between the two populations. This indicates that transduction of a pooled CD4/CD8 T cell population will lead to the preferential transduction of CD4+ T cells, but also that the number of CARs expressed on the surface of the CD4+ T cells would be higher than that of the CD8+ T cells. As the CD8+ T cells are essential for the efficient cytotoxicity of the tumour cells (Raskov *et al.*, 2021), it would potentially be of increased benefit to boost

the transduction efficiency specifically within the CD8+ population to ensure that significant numbers of cytotoxic T cells are available for tumour killing. One method that has been investigated within clinical trials for B cell ALL is the use of defined 1:1 ratio of transduced CD4+ and CD8+ T cells within the final product (Gardner *et al.*, 2016; Turtle, Hanafi, Berger & Gooley *et al.*, 2016). The study performed by Turtle *et al.* demonstrated the feasibility of producing CAR T products consisting of a 1:1 ratio of transduced T cells – with only three out of thirty patients unable to receive CAR T product at the defined ratio. This demonstrates the requirement for flexibility within release criteria, for some patients it may not be possible to use defined CD4:CD8 ratios – in which case the product should be provided without a defined ratio to allow the opportunity to treat the patient. The results of this study demonstrated that the defined ratio CAR T product was highly effective, even at reduced cell dosages. Although a reduced cell dose would be beneficial due to the potential reduction in manufacturing time and therefore reduced vein-to-vein time, there are additional complications that would mitigate any potential cost savings, including an increase in manufacturing costs due to the requirement of an additional cell selection step and use of two devices for the expansion of the two T cell populations. There may also be additional analytical costs and logistical costs to ensure that the mixture of the two cell types is performed correctly.

Further studies need to be performed to determine whether use of defined ratios of CD4+ and CD8+ T cells within cell therapy products could improve the safety of the final product. This is a difficult aspect to investigate as the patient's response is also dependent upon disease burden and tumour antigen expression.

If time had permitted, it would have been of interest to investigate potential differences in the cytotoxic potential of the four different T cell populations (PBMCs, CD4/CD8, CD4+ and CD8+). Within this study, I would have normalised the transduction efficiency of the CD3+ population to equal the population with the lowest transduction efficiency (in this case the CD8+ population). The normalised T cell populations would have then been co-cultured with a target antigen-expressing cell line for the assessment of cytotoxic potential through the use of an xCELLigence® assay. This would have enabled the elucidation of differences in the cytotoxic potential between

the four populations. It would have also been of interest to investigate the expression of exhaustion markers, such as PD1, TIM3 and LAG3, to determine whether one of the four populations expressed a higher level of exhaustion markers which could impact upon the cytotoxic functionality of the cell product (Zhang, Zhao & Huang, 2020).

Within this set of experiments, the investigation of the impact that the starting material had upon the fold expansion of the T cell population contradicted the hypothesis and results observed from other studies in which decreased fold expansion when using PBMCs as the starting material was observed (Stroncek *et al.*, 2016). It was hypothesised that a decreased fold expansion of the PBMC population would be observed, due to the presence of monocytes, compared to isolated T cell populations. However, within this study, the PBMC population demonstrated the highest fold expansion, whilst the isolated CD4+ T cell population demonstrated the lowest fold expansion. These differences in fold expansion did not appear to be due to differences in viability of the population, with no significant difference in the viability of PBMCs and CD4+ T cells identified. In addition to this, the CD4+ population had the highest average viability at day 9, despite having the lowest fold expansion. It could be that the presence of monocytes within the PBMC population was lower than expected due to the culture process used, and therefore did not impact upon the expansion as much as expected. If this study were to be repeated, it would be of interest to set up PBMC populations with varying frequencies of contaminating monocytes to determine the level at which an impact on fold expansion is observed. If time had permitted and this study could have been set up, it would have also been beneficial to compare the cytotoxic function of the transduced PBMC populations with differing frequencies of monocyte contamination to determine whether the presence of monocytes would also impact upon the cytotoxic function of the final drug product.

Overall, the choice of starting material did not appear to have a large impact upon the fold expansion or transduction efficiency of the final drug product within these studies. Further studies could be performed to investigate whether contaminating cells (such as B cells and NK cells) within the PBMC population would have been transduced and maintained within the final drug product to consider the impact that this may have upon the safety of the final drug product, including the potential contribution to adverse events within patients. Resistance to CAR therapy has been induced through the

accidental transduction of a contaminating leukaemic B cell (Ruella *et al.*, 2018), therefore the presence of contaminating cell types during production could lead to therapy failure.

The main conclusion gathered from this set of studies is the observation that there is a significant difference in the transduction efficiency of CD4+ and CD8+ T cell populations when transduced within a pooled T cell population. This could have a significant impact upon the efficacy and safety of the final drug product – further consideration would be required to determine whether it would be optimal to define the ratio of CD4+ and CD8+ T cells, as has been performed within some clinical trials (Turtle, Hanafi, Berger & Gooley *et al.*, 2016). However, this would add additional complications to the manufacture of an already complex product. For instance, CD4+ and CD8+ T cells would need to be separately isolated and transduced before being infused at an appropriate dosage to ensure the correct number of transduced CD4+ and CD8+ T cells were infused. This may result in a significant proportion of patient drug products being “out of specification” due to insufficient numbers of CD8+ T cells to achieve the defined ratio. In many instances, it would be more beneficial to provide the patient with a drug substance of undefined ratio, than not have sufficient cell numbers for an effective dose. However, this would result in a manufacturing deviation and a requirement to discuss dosing the patient with an unreleased product with the regulators which would result in significant operational and reputational risks to the manufacturing company.

4.2.3.2. Impact of Culture Vessel

Based on the data gathered from section 4.2.3.1, it appeared that the choice of starting material, either PBMCs or pooled CD4+ & CD8+ T cell populations, did not impact on the expansion of the T cell product. Therefore, I progressed investigations into the next aspect of the manufacturing process, which was the method of T cell expansion, investigating whether the choice of culture vessel could impact upon the quality of the final product. Either PBMCs or pooled CD4+ & CD8+ T cell populations were used within this set of experiments.

The methods used for the expansion of T cell populations differ depending on the scale of the production required, with small-scale productions often utilised for *in vitro* research and large-scale production methods utilised when large numbers of T cells are required for clinical trial or *in vivo* studies. Within research and clinical trials, a variety of culture vessels (as shown in Figure 60) have been utilised ranging from the traditional use of flat bottom culture plates, into the use of new plate designs, including Wilson Wolf's G-REX® culture plates (Bajgain *et al.*, 2014), and finally into large-scale culture systems, such as Wave™ bioreactor systems (Somerville *et al.*, 2012) or the CliniMACs Prodigy® (Mock *et al.*, 2016). Within this chapter, I have investigated the expansion of T cells within a variety of culture vessels, and further explored the translatability of small-scale production methods to large-scale productions.

Figure 60: Culture Vessels Used for the Production of T cell Therapy Products

A) 24-well G-REX® plate, B) 10M G-REX® vessel, C) 100M G-REX® vessel are three of the vessel types available from Wilson Wolf for small to medium scale T cell productions. D) Sartorius BioStat Wave™ Bag and E) Miltenyi CliniMACs Prodigy® are culture systems available for large-scale productions.

Initially, the small-scale culture process of PBMCs and T cells involved the use of 24-well cell culture treated flat bottom plates with T cells cultured in TexMACS™ media containing 100 IU/mL of IL-2. T cells were maintained at a density of $1x10^6$ cells/mL with splitting of the T cell populations performed every 2 to 3 days to prevent overgrowth and lack of nutrients, which would hamper the expansion of the T cell populations. Figure 61 shows the total cell number and viability of PBMCs from four donors cultured within 24-well cell culture plates over a 12-day culture period The PBMCs from the four donors only expanded between 2 to 7 fold over the 12-day culture period, which is a slow rate of expansion. The small reduction in cell viability at day 5 was suspected to have been caused by over-growth.

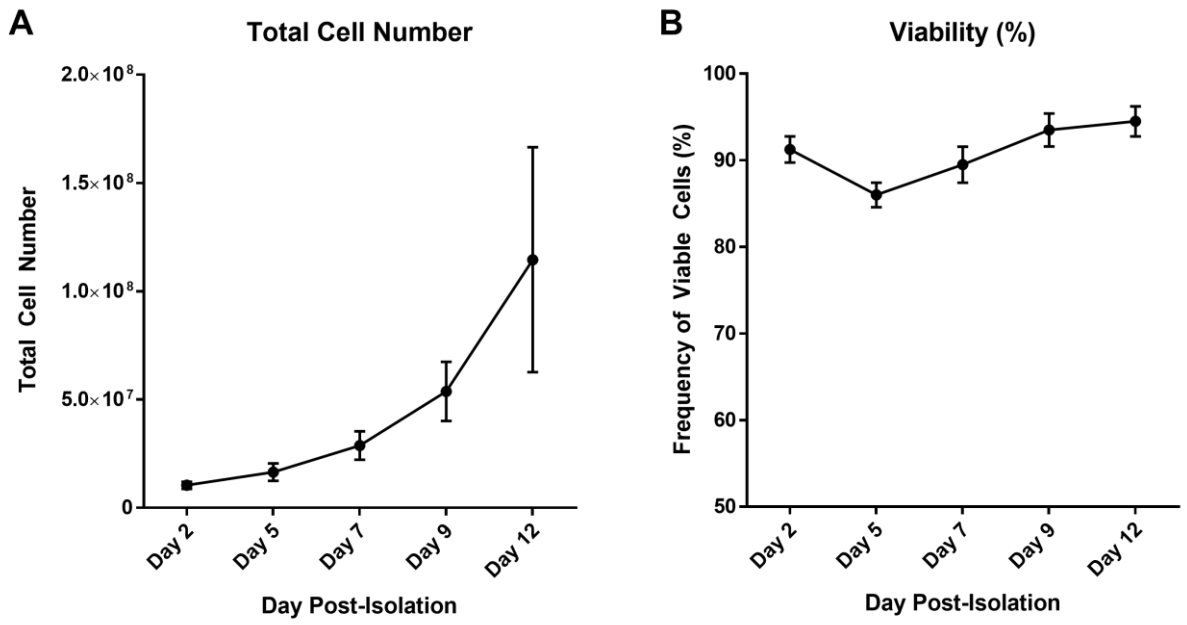

Figure 61: Expansion and Viability of PBMCs

PBMCs from four donors were cultured in 24-well flat bottom culture plates. Cell counts were taken every two days when cells were split to track the expansion and viability of the PBMC populations. A) Over 12 days of culture, PBMCs only expanded between 2- and 7-fold which is a low rate of expansion. B) The viability of the cells dropped at day 5, which is likely due to overgrowth of the culture. Error bars display SD (n=4).

Due to the low rate of expansion observed with 24-well cell culture plates, it was essential to optimise other culture vessels, in order to produce sufficient T cell numbers for additional research studies. G-REX® plates have been demonstrated to achieve superior expansion of T cells compared to conventional culture methods (Bajgain *et al.*, 2014; Marín Morales *et al.*, 2019), and are scalable for clinical manufacturing, with Celyad using the G-REX® system to produce sufficient CAR T numbers within a clinical trial (Lonez *et al.*, 2017). The fold expansion of cells was calculated, using Equation 6, as the total number of cells plated at the start of the culture differed between the standard 24-well plate ($2x10^6$ cells/well) and the 24-well G-REX® plate (minimum of $5x10^5$ cells/well).

Equation 6:

$$Fold\ Expansion = \frac{Final\ viable\ cell\ count}{Starting\ viable\ cell\ count}$$

Figure 62B demonstrates significantly higher fold expansion of T cells (P=0.0003) within the 24-well G-REX® plate, with an average of 140-fold expansion, compared to the fold expansion observed with the standard 24-well culture plates (2-7 fold expansion).

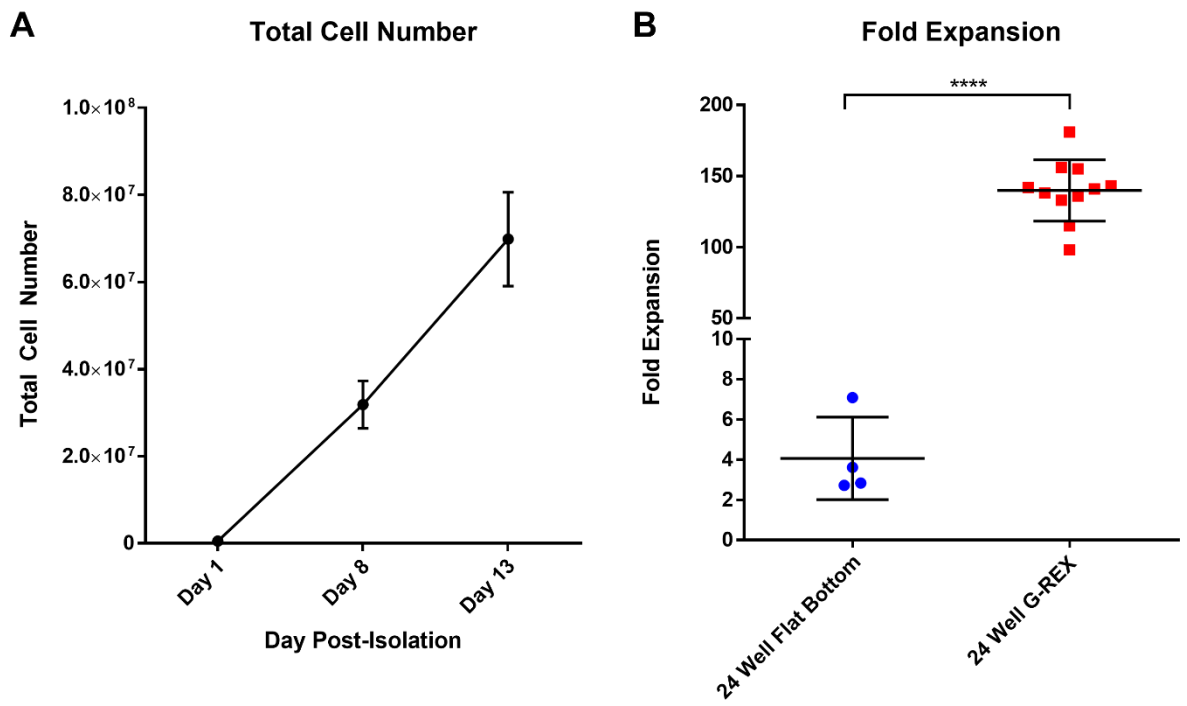

Figure 62: Expansion of T cells within 24-well flat bottom culture plate and 24-well G-REX® plate

*A) Cell populations were cultured in 24-well G-REX® plates for 10 days (transferred to G-REX® on day 3 post-isolation) with average fold expansion reaching 140 fold. B) Comparison of the fold expansion over the culture period demonstrated significantly better fold expansion of PBMCs in G-REX® plates. Error bars display SD. n=4 for 24-well flat bottom plates. n=11 for 24-well G-REX® plates. A non-paired two-tailed T test was performed to analyse significance. **** indicates that P ≤0.0001.*

The results demonstrated that use of G-REX® plates for the culture of T cells would significantly increase the fold expansion of the T cell cultures, with increased numbers of T cells enabling larger research studies to be planned and executed.

G-REX® culture vessels consist of a gas-permeable membrane upon which the T cells sit. This enables the T cells to have direct access to oxygen, reducing the time it takes for oxygen to perfuse through the whole media volume to get to the T cells (Ludwig). The direct access to oxygen enables increased expansion rates of the T cells. This differs to the method used by systems such as the Wave™ bioreactor system, in which rocking of the T cells is performed to ensure adequate perfusion of oxygen to the T

cells (Somerville *et al.*, 2012). In addition to this, G-REX® plates hold a large volume of media, compared to standard 24-well flat bottom culture plates, enabling continual delivery of nutrients, rather than requiring frequent media changes, with convection thought to enable the continual movement of warm media from the walls of the G-REX® vessel to the cooler core of the vessel aiding with the delivery of nutrients to the T cells settled across the membrane without disturbance (Bajgain *et al.*, 2014).

As seen in Figure 61, there was a drop in viability at day 5 within the standard flat bottom culture plate, which was suspected to be due to overgrowth of T cells and lack of nutrients. The large volumes of media within the G-REX® plates, 8mL per well for 24-well G-REX® and 35mL per well of 6-well G-REX®, would prevent this lack of nutrients. The reduced amount of operator interaction with the T cells, compared to the frequent media changes required for standard culture plates, also reduces the risk of contamination and operator to operator variability in the culture of T cells.

Depending on the experiment size, either 24-well or 6-well G-REX® plates were utilised for the culture of T cells. A comparison of the fold expansion observed with the two culture methods over a number of experiments was performed to determine if there was a significant difference in the expansion of T cells observed. Within a 24-well G-REX® plate, $1x10^6$ cells were seeded into each well (1mL per well) with the media volume topped up to a total of 8mL 48 hours post-transduction. Whereas, $4x10^6$ cells were seeded into each well of a 6-well G-REX® plate (4mL per well) with the media volume topped up to 35mL 48 hours post-transduction. As shown in Figure 63, the range of fold expansions observed is large due to donor variability, with some particularly high fold expansion rates (316-fold) observed within 24-well G-REX® plates. However, there is no significant difference between the fold expansion for the two culture vessels, with an average fold expansion of 60.2 and 68.6 for 24-well and 6-well G-REX® plates respectively.

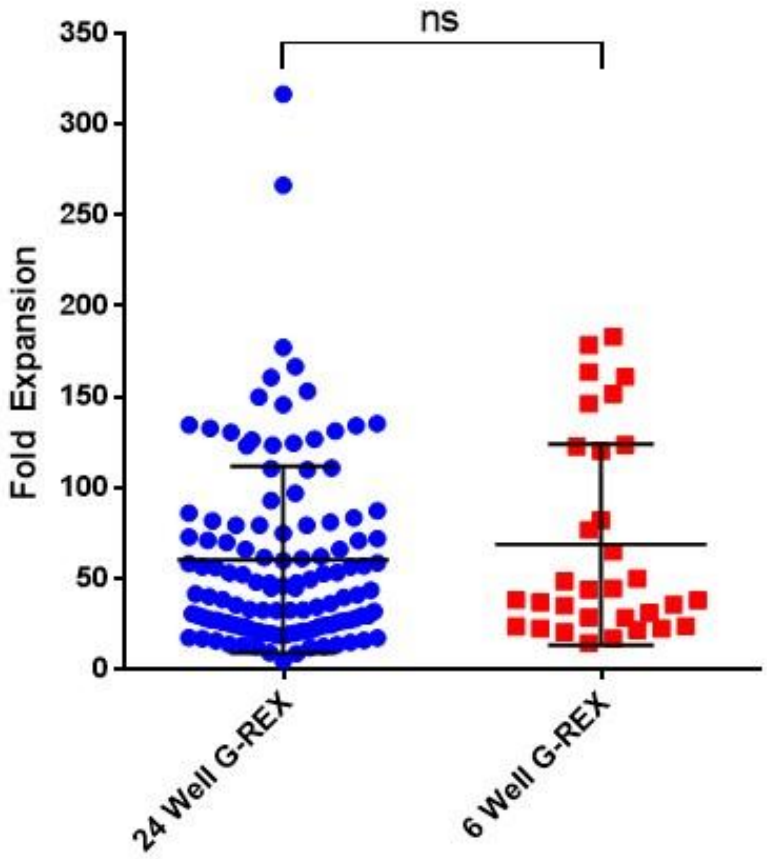

Figure 63: Comparison of 24-well and 6-well G-REX® plates.

PBMCs or CD4+/CD8+ pooled T cells were seeded at the appropriate density into either 24-well or 6-well G-REX® plates with cell counts performed at the end of the culture period to determine the fold expansion of the T cell populations. All T cell populations were cultured using IL-2 throughout the culture procedure. n=121 for 24-well G-REX® (21 donors) and n=32 for 6-well G-REX® (11 donors). A non-paired two-tailed T test was performed to determine the significance of the difference in fold expansion. ns = not significant. Error bars display mean and SD.

An additional advantage to the use of G-REX® culture vessels is the scalability of smaller vessels to larger vessels with a direct linear correlation in the fold expansion of T cells grown in the 10M, 100M and 500M G-REX® vessels when T cells are seeded proportionally to the surface area of the vessels, with surface areas of 10 cm^2, 100cm^2 and 500cm^2 for the 10M, 100M and 500M G-REX® vessels respectively (Bajgain *et al.*, 2014). This enables culture conditions and seeding densities optimised at small-scale to be utilised within the larger scale production of T cells.

An investigation into the scalability of T cell productions into larger 10M and 100M G-REX® vessels was performed. T cells were seeded at $1.5x10^6$ cells per cm^2, with a total of $1.5x10^7$ cells seeded into the 10M G-REX® vessels and $1.5x10^8$ cells seeded into the 100M G-REX® vessels. Due to the large number of isolated CD4+ and CD8+ T cells required for the seeding of all conditions within this experiment, T cells from a single donor were obtained from a selection of a leukopack performed on the CliniMACs Prodigy®.

As shown in Figure 64, there was no significant difference (p = 0.3) in the fold expansion obtained with the 10M and 1000M G-REX® plates after 10 days of culture, with average fold expansion values of 28.8 and 31.9 respectively. This demonstrated that there was direct scalability between the 10M and 100M G-REX® culture vessels when T cells are seeded based on the surface area of the culture vessel.

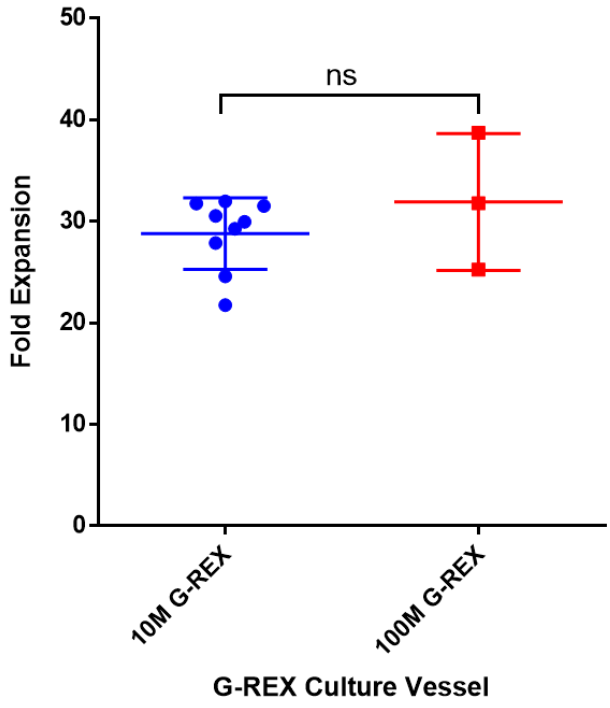

Figure 64: 10M vs 100M G-REX® Culture Vessels

CD4+ and CD8+ T cells were seeded into 10M and 100M G-REX® plates at a seeding density of $1.5x10^6$ cells/cm^2, with $1.5x10^7$ cells seeded into the 10M culture vessels (10cm^2 surface area) and $1.5x10^8$ cells seeded into the 100M culture vessels (100cm^2 surface area). 40ng/mL of IL-7/IL-15 was added to the media at the start of the 10-day culture procedure, with no additional media exchanges or cytokine additions performed. A non-paired two-tailed T test was performed to determine the significance of the difference in fold expansion between the two groups. n=9 for the 10M G-REX® and n=3 for the 100M G-REX® culture vessel. All replicates were from the same donor. Error bars display mean with SD. ns = not significant.

There were several differences in the methodology used for the culture of T cells within the small-scale G-REX® production vessels (24-well and 6-well G-REX® plates) (Figure 63) and the large-scale production vessels (10M and 100M G-REX® vessels) (Figure 64), which meant that a direct comparison of these culture vessels was not possible. Firstly, during small-scale productions, the T cells were seeded at a lower seeding density per cm^2 ($5x10^5$ cells/cm^2 seeded into 24-well G-REX® plates and $4x10^5$ cells/cm^2 seeded into 6-well G-REX® plates) compared to the seeding density used for the 10M and 100M G-REX® vessels ($1.5x10^6$ cells/cm^2). The seeding densities for the small-scale production method were historically optimised within the cell and gene therapy department at GSK based on the lowest seeding density recommended by Wilson Wolf, which is $1.25x10^5$ cells/cm^2 for both 24- and 6-well G-REX® plates. Secondly, the culture period was 10 days for T cells within 10M and 100M G-REX® vessels, whilst it was 13 days for T cells within 24-well and 6-well G-REX® plates.

To further investigate the scalability of the small-scale production methods to large-scale production methods, I compared data gathered from experiments in which T cells were cultured with IL-2 at small-scale to data generated by the Cell and Gene Therapy Cell Process Development team who utilise the CliniMACs Prodigy® for the expansion of T cells with IL-2.

Initial data sets, as shown in Figure 65, demonstrate that although the average fold expansion rate within the CliniMACs Prodigy® T cell productions was slightly lower than that of the G-REX® plate productions, there was no significant difference, with average fold expansion rates of 60.2, 68.6 and 39.4 respectively. This indicates that data generated on the fold expansion of T cells within small-scale experiments would be informative for CliniMACs Prodigy® production runs, allowing optimisation of expansion methods at small-scale and reducing the cost and scale of those optimisation experiments.

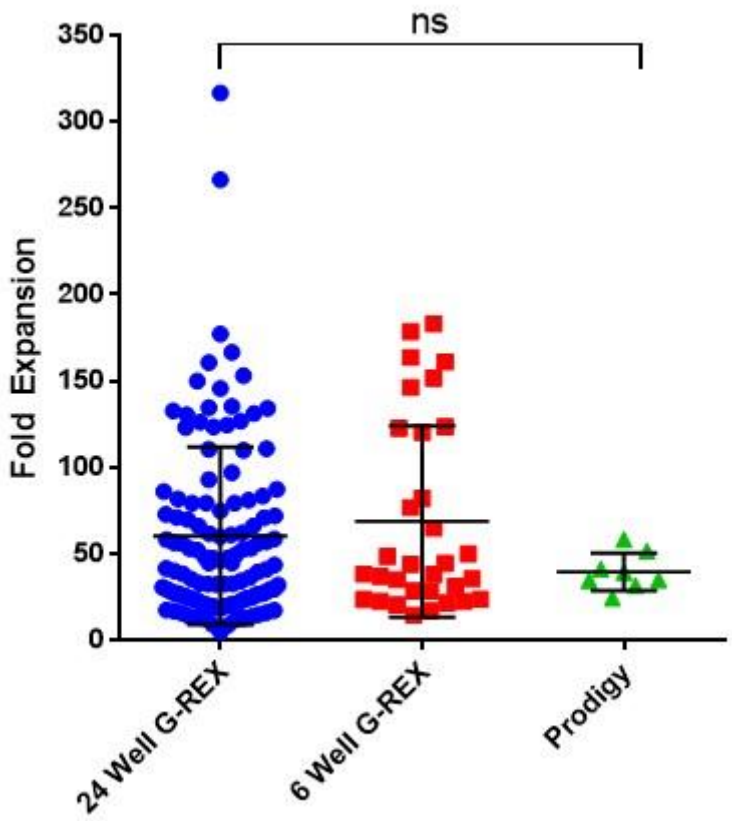

Figure 65: G-REX® vs Prodigy® Data

Fold expansion of CD4+/CD8+ T cell populations was analysed after a 12-day culture process with IL-2, with T cells processed using either the small-scale production method within 24-well or 6-well G-REX® plates, or the large-scale production method using the CliniMACs Prodigy®. Significance was determined using a one-way ANOVA with Tukey's multiple comparison test. ns = not significant. n=121 for 24-well G-REX® (21 donors), n=32 for 6-well G-REX® (11 donors) and n=8 for CliniMACs Prodigy® (6 donors). Error bars display mean with SD.

4.2.3.2.1. Discussion of Culture Vessels

The use of G-REX® plates significantly improved the fold expansion of T cell populations compared to the traditional flat bottom plate culture method of T cells. In addition to this the reduction in manipulation of the T cells helped to reduce the risk of contamination throughout the culture process and also standardised T cell productions. This was particularly beneficial as it enabled the prediction of the number of T cells that would be required at the start of a production to enable delivery of the required number of T cells for project work.

The fold expansion of T cells cultured using IL-7/IL-15 within 24-well and 6-well G-REX® plates was tracked over multiple experiments and no significant difference in the fold expansion between these vessels was observed. In addition to this, a comparison of the two large scale culture vessels (10M and 100M G-REX® culture vessels), also demonstrated no significant difference in fold expansion – however, it must be highlighted that only one donor was used for the comparison of 10M and 100M G-REX® culture vessels due to the high starting number of cells required, which may be the reason for the reduced average fold expansion observed during this experiment (28.8 and 31.9 for 10M and 100M G-REX® culture vessels respectively), as fold expansion is impacted by donor to donor variability. It would be of benefit to track fold expansion of T cells within 10M and 100M G-REX® culture vessels in a larger number of donors in order to get a more accurate measure of the average fold expansion.

It would be of interest to determine whether the lower seeding densities used for the 24-well and 6-well G-REX® plates ($5x10^5$ cells/cm^2 and $4x10^5$ cells/cm^2 respectively) could have improved the fold expansion within 10M and 100M G-REX® culture vessels, which were seeded at $1.5x10^6$ cells/cm^2. A decreased seeding density per cm^2 could lead to improved fold expansion rates over the culture period, due to improved nutrient availability with decreased seeding densities.

Differences in culture processes, both within small-scale studies and large-scale clinical productions, make comparisons between studies difficult, with even small differences in activation timing potentially affecting the expansion rate of the T cell

product. The reduced expansion period, of 10 days, used within 10M and 100M G-REX® vessels mirrors the expansion period used within the production of Kymriah®, which states a 10 day expansion period, however the Kymriah® production method also includes the transfer of cells into a WAVE™ bioreactors for 4 – 6 days (Tyagarajan *et al.*, 2020). Despite the same length of time of expansion, the requirement to transfer T cells into a different culture vessel could significantly impact upon expansion rates, compared to T cells left undisturbed within a 100M GREX® vessel for the whole expansion period. The differences in manufacturing processes between different companies make the comparison of T cell therapy products difficult, as small changes within the culture process could impact upon product phenotype and overall fold expansion. These caveats must be considered within analysis of culture vessel comparisons.

Another aspect of the culture conditions that may have impacted upon the expansion rate of the T cells within the 10M and 100M G-REX® culture systems is that fact that CD4+ and CD8+ T cells were isolated from a leukopack that had been previously frozen, whereas small-scale T cell productions used CD4+ and CD8+ T cells isolated from fresh peripheral whole blood obtained a maximum of 24 hours prior to T cell isolation. Studies have demonstrated a significant drop in T cell viability within the first two days of culture within frozen PBMC samples compared to fresh PBMC samples (Panch *et al.*, 2019), suggesting that seeding densities used within 10M and 100M G-REX® studies may not be accurate due to a greater loss of cell numbers subsequent to activation. This could skew fold expansion results as it is not possible to accurately determine the number of T cells at the point of transduction.

If time and resourcing had permitted, it would have been of interest to perform a direct comparison between the culture vessels using the same donor T cells, sourced either fresh or frozen, to better control for some of these potentially confounding factors. If use of previously frozen CD4+ and CD8+ T cells were found to impact upon the final fold expansion of the T cell product, this could have a significant impact upon the clinical manufacturing process, in which it is most common for the leukapheresis product from patients to have been frozen prior to CD4+/CD8+ T cell isolation, transduction and expansion. However, within the study performed by Panch *et al.,* it was found that despite the reduced viability of cryopreserved PBMC starting material, there was no difference in transduction efficiency, fold expansion, CD4+ or CD8+ ratio,

in vivo persistence or clinical efficacy between the fresh and frozen starting material arms of the study (Panch *et al.*, 2019). This suggests that use of cryopreserved starting material may not pose an issue during manufacturing, even when performed using patient T cells compared to healthy donor T cells.

A comparison of fold expansion rates from small-scale productions (24- and 6-well G-REX®) to large-scale productions (CliniMACS Prodigy®) demonstrated a correlation in the expansion of T cells between the two production methods, even with small differences within the culture processes. Further comparison studies between the small-scale and large-scale processes would be required to determine whether the differentiation of T cell subsets and expression of exhaustion markers differs between the two processes. However, this initial data set provides confidence that further expansion optimisation experiments performed at small-scale may be translatable to large-scale production methods, particularly if small-scale processes were optimised to mimic the culture process of the CliniMACS Prodigy® as closely as possible. The translatability of small-scale production optimisation to large-scale culture would be particularly beneficial, as it enables a greater number of conditions to be investigated with reduced cost and time requirements. The ability to test a number of conditions at once during the optimisation of the expansion process would enable further investigation into whether decreased expansion rates *in vitro* could result in a higher quality final product, for example through the maintenance of a more clinically desirable T cell phenotype or reduction in exhaustion markers.

If time and resourcing had permitted, I would have liked to have investigated the expansion profile of patient T cells to enable comparison to the data sets gathered using healthy donors T cells within this chapter. A high level of donor-to-donor variability was observed within the healthy donors within these studies, and this level of variability would be expected to be even greater within a pool of patient T cells where both disease state and prior treatment regimens could impact upon the expansion of the T cell population. For this reason, any studies conducted utilising patient T cells would need to be performed on a high number of donor samples, which can pose difficulties to study design due to the difficulties in obtaining suitable patient T cell samples.

4.2.3.3. Impact of Cytokines

The final aspect of the T cell culture method that I wanted to investigate was the impact that the choice of cytokine used during the culture process had upon the expansion and quality of the final T cell product, including impact upon the final T cell phenotype. Research is ongoing to correlate the frequency of differentiated T cell populations and the success of clinical trials, however there is currently no clear answer on what the optimal T cell phenotype for a T cell product would be.

The use of IL-2 is believed to skew towards a differentiated effector phenotype (Crompton *et al.*, 2014), with several studies demonstrating a potent cytotoxic functionality *in vitro,* without translation of the same potency *in vivo* (Gattinoni *et al.*, 2011) . A study performed by Xu *et al.,* investigated the *in vivo* expansion of T cells cultured with IL-2, finding that the CD8+ Stem Cell Memory T cell population (CD45RA+ and CCR7+) expanded most strongly.

The use of IL-7 and IL-15 is widely used to push the final product towards a more memory phenotype, which is believed to improve the persistence of the therapy (McLellan & Ali Hosseini Rad, 2019). Additional pre-clinical models indicated that use of IL-7/IL-15 within the culture of the T cells further increased the frequency of this Stem Cell Memory T cell (T_{SCM}) population, resulting in increased anti-tumour activity (Xu *et al.*, 2014). Multiple clinical trials have demonstrated that the persistence of T cells *in vivo* correlates with the anti-tumour activity (Louis *et al.*, 2011), and it is thought that the T_{SCM} population demonstrates enhanced persistence when compared to the Central Memory T cell population (Gattinoni *et al.*, 2012). Recent follow-up analysis of patients enrolled within the NY-ESO-1 SPEAR trial demonstrated that T_{SCM} populations persisted within patients that achieved complete response, despite all subsets of T cells being present within the infused cell population (Stadtmauer *et al.*, 2019). This highlights that investigating methods that enable T_{SCM} populations to be preserved may be more beneficial than increasing the frequency of these populations within the infused cell product.

In order to provide further clarity on the impact that the choice of cytokine may be having upon T cell production, I compared the impact of IL-2 or combined IL-7 and IL-15 upon fold expansion, T cell transduction efficiency and phenotype from small-scale productions. There are significantly more cytokine combinations that could have been investigated, including use of IL-21 which is also believed to push T cells towards a memory phenotype (Li & Cong *et al.*, 2021), however in the interest of time, I limited my research to the two commonly used conditions described above.

Initially, I investigated the fold expansion observed in small-scale cultures when either IL-2 (100IU/mL) or a combination of IL-7 and IL-15 (10ng/mL) were used throughout the culture period to determine if any significant differences were apparent. The concentrations of cytokines were chosen based on clinical manufacturing processes within GSK for two different T cell assets, and units differ due to differences in the method of determining the specific activity of cytokines between the manufacturing companies. As shown in Figure 66, no significant differences were observed when either IL-2 or IL-7/IL-15 were used within with the 24-well or 6-well G-REX® plates. The average fold expansions were 60.2 for 24-well IL-2, 55.2 for 24-well IL-7/IL15, 68.6 for 6-well IL-2 and 68.8 for 6-well IL-7 & IL-15. This demonstrated that the choice of cytokine with the culture method used at small-scale did not have an impact upon the expansion of the T cells.

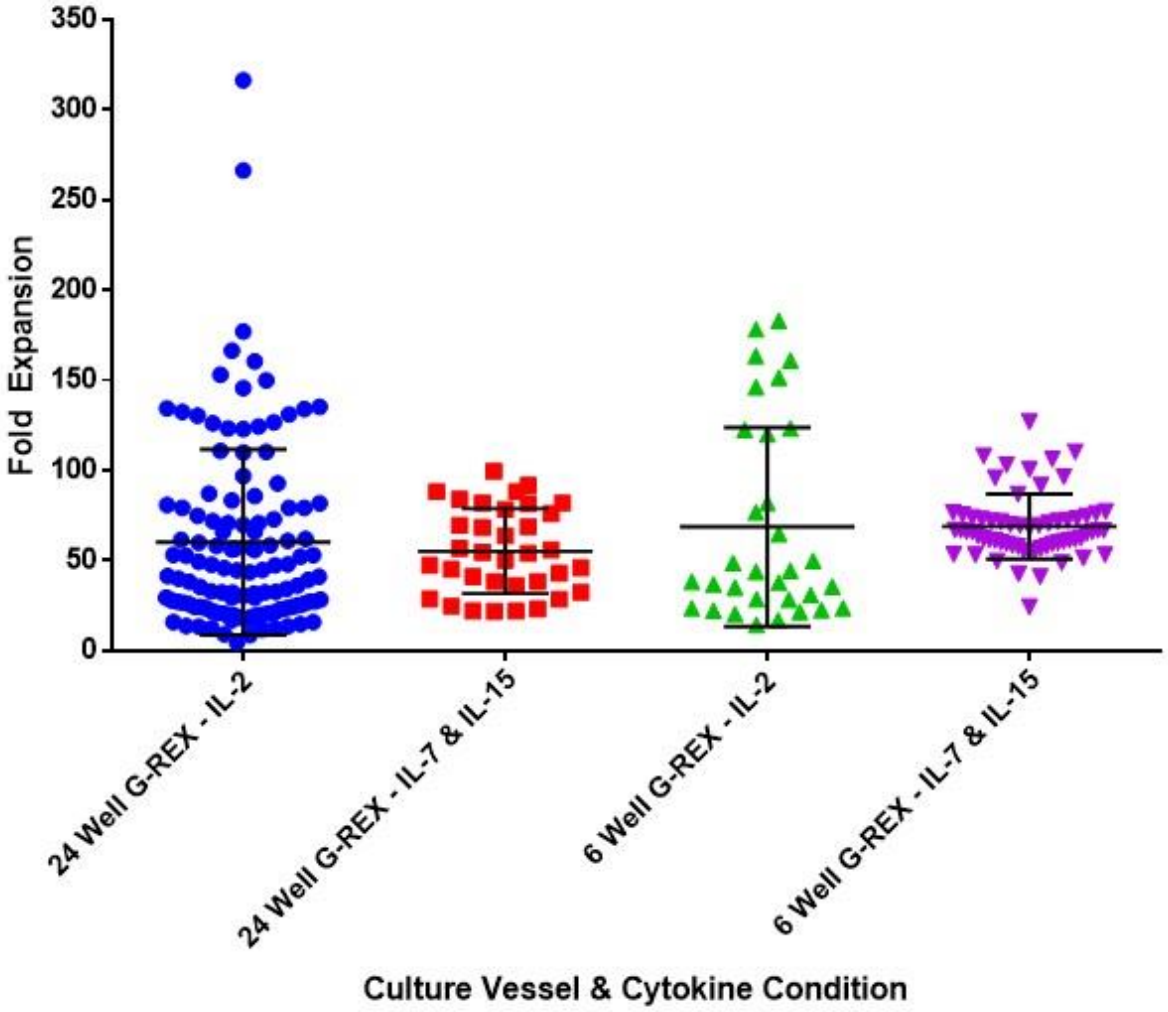

Figure 66: Impact of Cytokine on Expansion of T cell Product within Small-scale Culture

CD4+ and CD8+ T cells were seeded into 24-well or 6-well G-REX® plates and cultured with either 100IU/mL of IL-2 or a combination of 10ng/mL IL-7 and 10ng/mL IL-15. n=121 for 24-well G-REX® on IL-2 (21 donors), n=35 for 24-well G-REX® on IL-7/IL-15 (8 donors), n=32 for 6-well G-REX® on IL-2 (11 donors) and n=63 for 6-well G-REX® on IL-7/IL-15 (11 donors). A one-way ANOVA with Tukey's multiple comparison test was performed to determine the significance of the fold expansion differences between each pair of conditions. There were no significant differences between conditions. Error bars display mean with SD.

With cytokine choice having no significant impact upon the expansion of the T cell product at small-scale, it was then investigated whether the choice of cytokine could impact upon the transduction efficiency of the CD3+ T cell population. As shown in Figure 67, no significant difference in transduction efficiency was observed within the total CD3+ T cell population, CD4+ T cell population or CD8+ T cell population for two different CAR T products when T cells were cultured on either IL-2 or IL-7/IL-15.

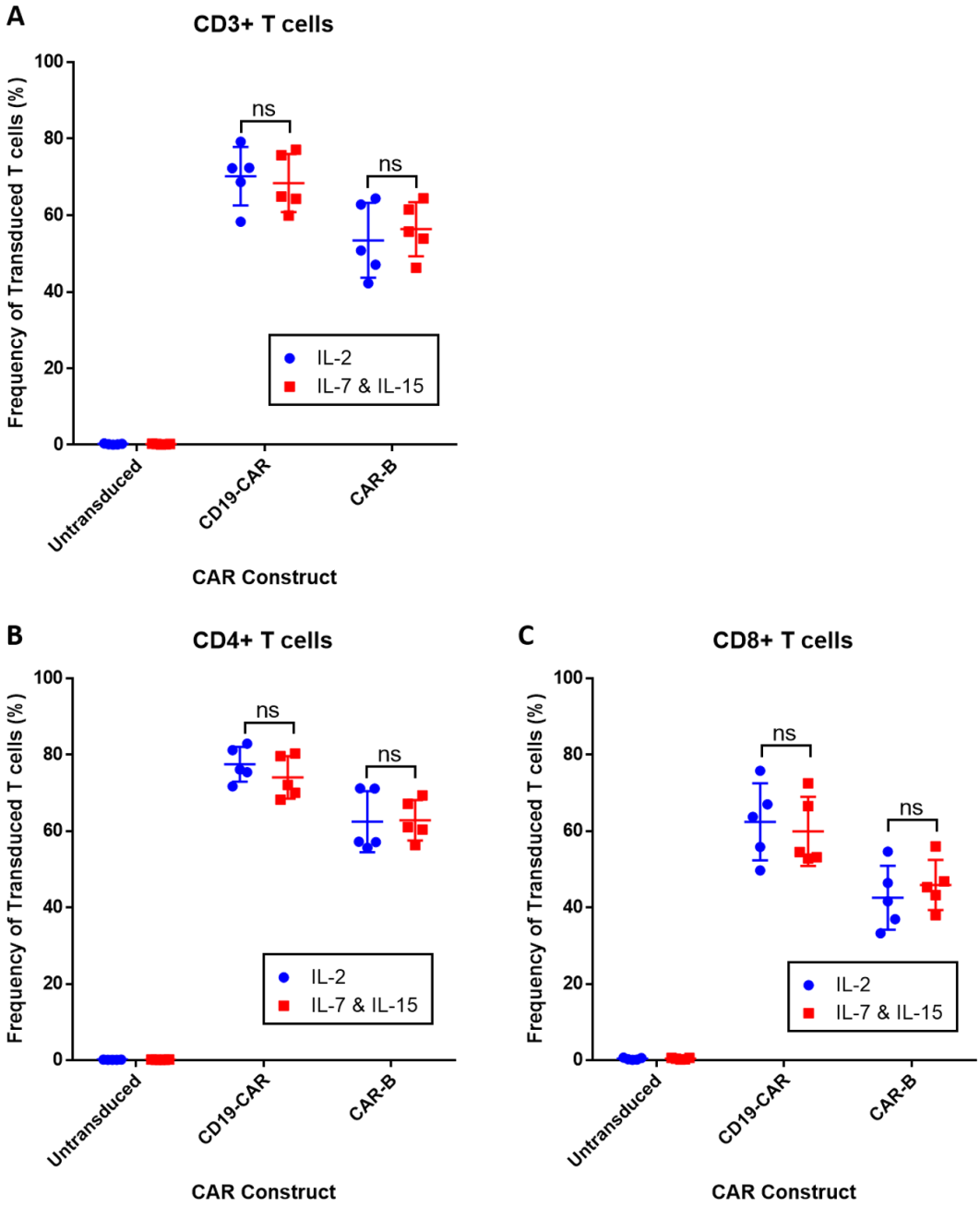

Figure 67: Impact of Cytokine Condition on T cell Transduction

A pooled population of CD4+ and CD8+ T cells were transduced with either a CD19-CAR or CAR-B encoding lentiviral vector after 24 hours of activation. T cell populations

were then cultured with either 100IU/mL of IL-2 or a combination of 10ng/mL IL-7 and 10ng/mL IL-15. Transduction efficiency of A) CD3+ T cells B) CD4+ T cells and C) CD8+ T cells was analysed by flow cytometry. (n=5). Error bars show mean with SD. Paired two-tailed T tests were performed to determine the significance of the differences in transduction efficiency observed between each T cell population. ns = not significant.

In addition to this, it was important to determine the impact that the cytokine condition may have upon the final phenotype of the T cell population. In order to do so, I firstly investigated the impact that use of IL-2 or IL-7/IL-15 had upon the frequency of CD4+ and CD8+ T cells within the CD3+ T cell population. As shown in Figure 69, there was a significant increase in the frequency of CD4+ T cells when IL-7/IL-15 was used with the average frequency increasing to 61.5% compared to 52.8% when IL-2 was used. Similarly, a reduction in the frequency of CD8+ T cells was observed when IL-7/IL-15 was used with the average frequency reducing to 38.3% from 47% when IL-2 was used.

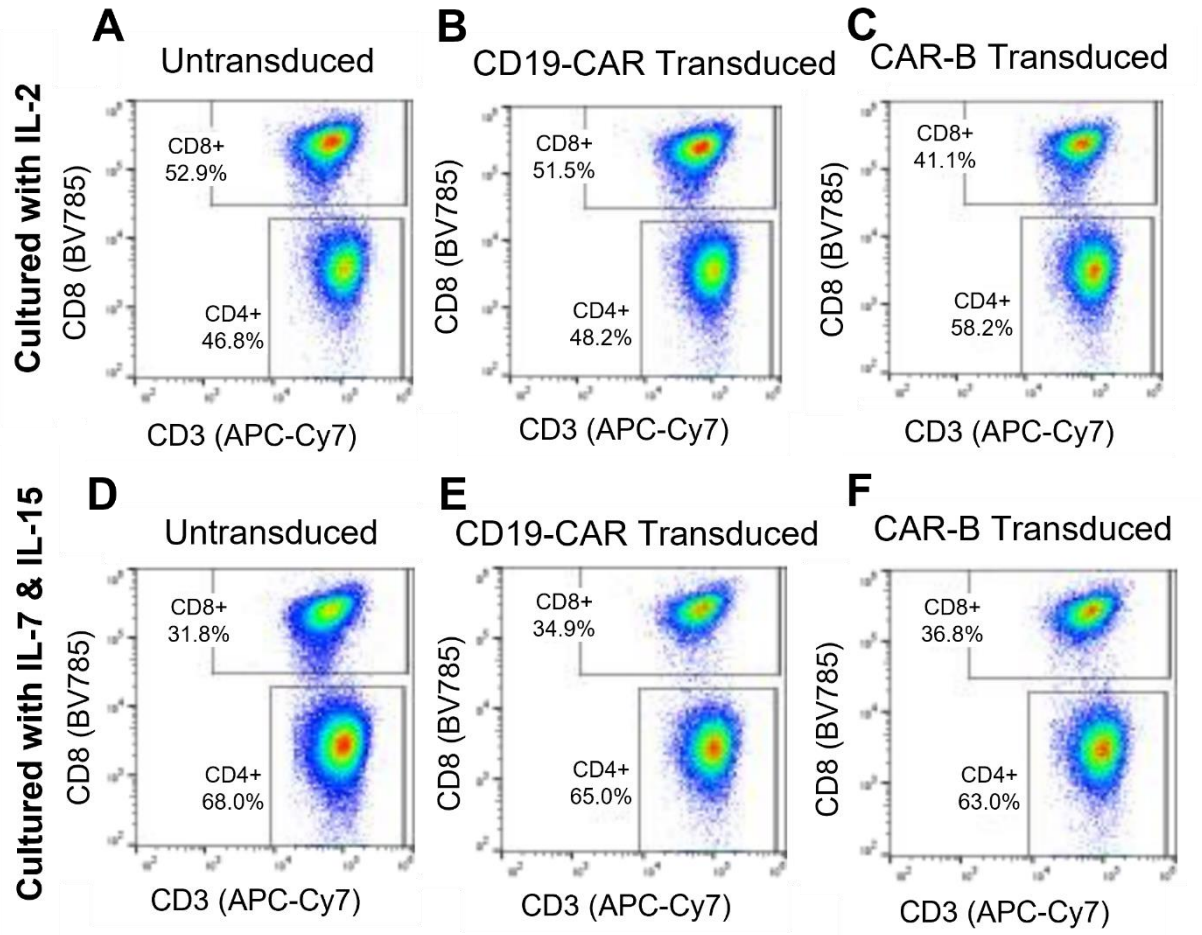

Figure 68: Flow Plots of CD4+ and CD8+ T cell Frequency within T cell Populations Cultured with Either IL-2 or IL-7 & IL-15

CD4/CD8 T cells isolated from healthy donor PR19T133635 were cultured with either 100IU/mL of IL-2 (top panel) or a combination of 10ng/mL IL-7 and 10ng/mL IL-15 (bottom panel). After 24 hours of activation, T cells were left untransduced (A and D) or transduced with either a CD19-CAR encoding LVV (B and E) or CAR-B encoding LVV (C and F). At day 12 of culture, samples were removed and stained with an APC-Cy7 anti-CD3 antibody and a BV786 anti-CD8 antibody to determine the frequency of CD4+ and CD8+ T cells within each population via flow cytometry analysis.

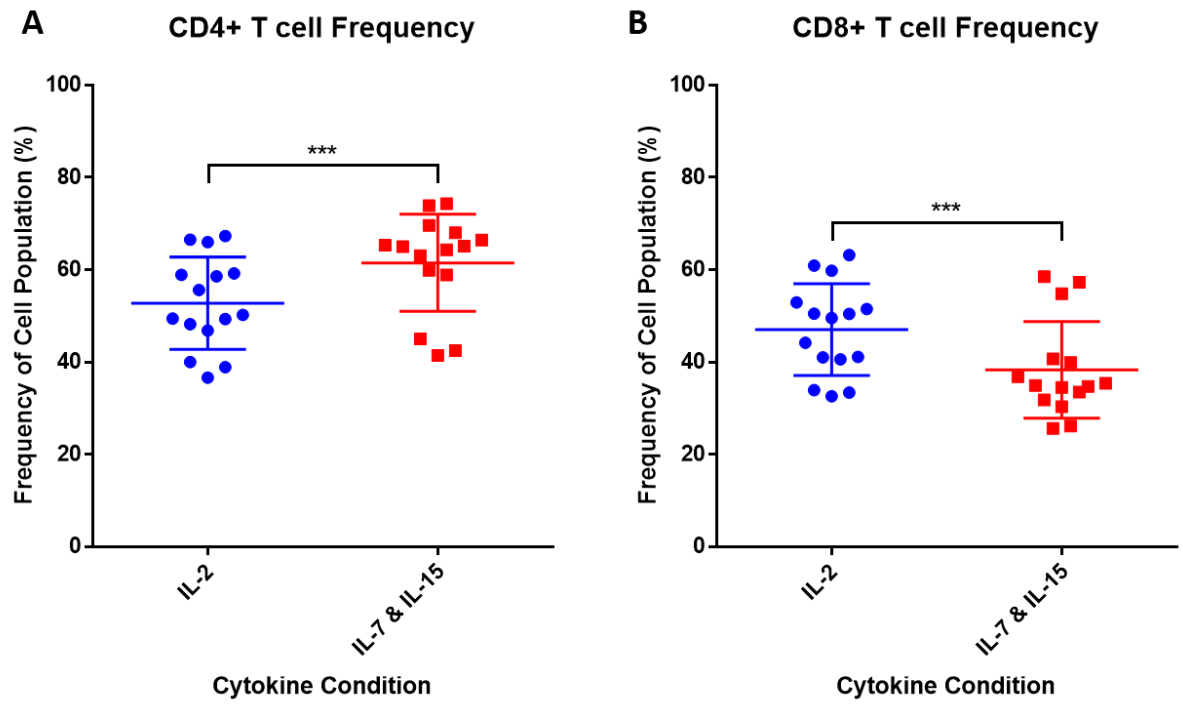

Figure 69: Impact of cytokines on CD4:CD8 ratio

*CD4/CD8 T cells isolated from 5 healthy donors were cultured with either 100IU/mL of IL-2 or a combination of 10ng/mL IL-7 and 10ng/mL IL-15. After 24 hours of activation, T cells were left untransduced or transduced with either a CD19-CAR encoding LVV or CAR-B encoding LVV. At day 12 of culture, samples were removed and stained with an APC-Cy7 anti-CD3 antibody and a BV786 anti-CD8 antibody to determine the frequency of CD4+ and CD8+ T cells within each population via flow cytometry analysis. (n=5). Error bars show mean with standard deviation. A fixed effect comparison was performed to determine the significance of the differences observed, with donor differences contributing to 91.5% random variation with 8.4% residual variation. The effect of the cytokine condition significantly contributed to the differences observed within both the CD4+ and CD8+ T cell populations. *** indicates that p = ≤0.001.*

Further to this, I investigated the impact that the cytokine choice had upon the differentiation of CD4+ and CD8+ T cells into subsets including naïve T cells (T_N), effector T cells (T_{EFF}), effector memory T cells (T_{EM}), central memory T cells (T_{CM}) and stem cell memory T cells (T_{SCM}). T cell populations cultured with either IL-2 or IL-7/IL-15 were analysed by flow cytometry and T cell subsets were defined based on the expression of phenotypic markers, as described in Table 23 .

Upon activation, naïve T cells upregulate CD95 expression differentiating into either effector or memory T cells. By day 12 of culture, there were no remaining naïve T cells within the T cell populations. Within the populations analysed, there were negligible effector T cells remaining, with all T cells differentiating into one of the three memory T cell subsets. Two donors (PR19T133651 & PR19C133904) demonstrated a frequency of stem cell memory T cells within both CD4+ and CD8+ T cell populations of between 2 – 5%, with negligible numbers of stem cell memory T cells observed within the other three donors. The predominant T cell subsets within all five donors were central memory and effector memory T cells, with the central memory subset dominating within both the CD4+ and CD8+ T cell populations for all donors.

Within the CD8+ T cell population, there were no significant differences between the frequency of central memory or effector memory T cells when the T cell populations were cultured with either IL-2 or IL-7/IL-15. However, the CD4+ population did demonstrate a significantly higher frequency of central memory T cells when cultured with IL-2 compared to IL-7/IL-15 and vice versa for the effector memory subset.

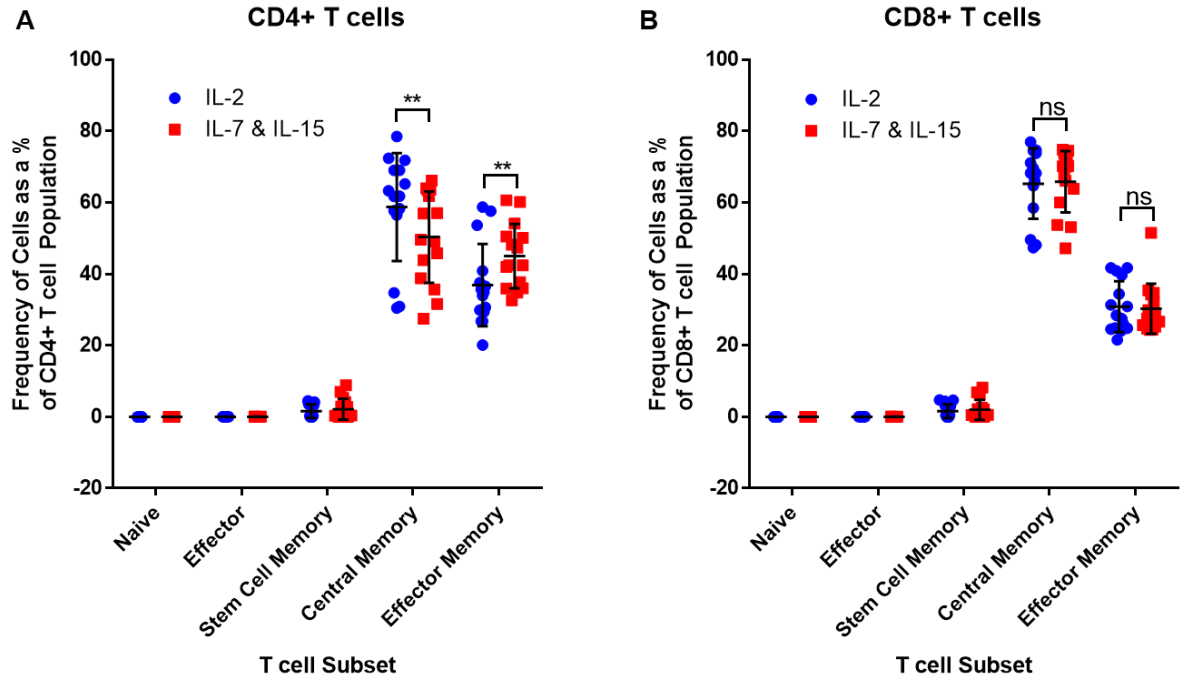

Figure 70: Impact of cytokines on T cell differentiation

*CD4/CD8 T cells isolated from 5 healthy donors were cultured with either 100IU/mL of IL-2 or a combination of 10ng/mL IL-7 and 10ng/mL IL-15. After 24 hours of activation, T cells were left untransduced or transduced with either a CD19-CAR encoding LVV or a CAR-B encoding LVV. At day 12 of culture, samples were removed, stained and analysed via flow cytometry to determine the frequency of T cell differentiation subsets within the A) CD4+ and B) CD8+ T cell populations. (n=5). Error bars show mean with standard deviation. A mixed model was fitted to determine the significance of the differences observed between the central memory and effector memory T cell populations within both the CD4 and CD8 T cell subsets, with fixed effect terms "Cytokine" + "CAR Construct" + "Cytokine*CAR Construct" and random effect term "Donor ID". The effect of the cytokine condition significantly contributed to the differences observed within the CD4+ effector memory and central memory T cell populations but did not significantly impact upon the frequency of CD8+ effector*

*memory or central memory T cell populations. ** indicates that p ≤0.01 and ns indicates not significant.*

With the frequency of CD4+ and CD8+ T cells, as well as the frequency of Central Memory and Effector Memory T cells within the CD4+ population, impacted by cytokine choice, I investigated the impact that these phenotypic changes may be having upon IFN-γ production by the T cell populations upon exposure to antigen. CD19-CAR transduced and CAR-B transduced T cell populations generated from three healthy donors were co-cultured with a CAR-B antigen expressing cell line for 48 hours, after which supernatant samples were removed for analysis of IFN-γ concentration by MSD®. As expected, CD19-CAR transduced T cell populations produced no IFN-γ after co-culture with a CAR-B antigen expressing cell line. The average IFN-γ concentration produced by the CAR-B T cell populations for the three donors was 313ng/mL for IL-2 and 530ng/mL for IL-7/IL-15 cultured populations, demonstrating a significant increase in IFN-γ production (P = 0.0327) when T cells were cultured with IL-7/IL-15 (Figure 71).

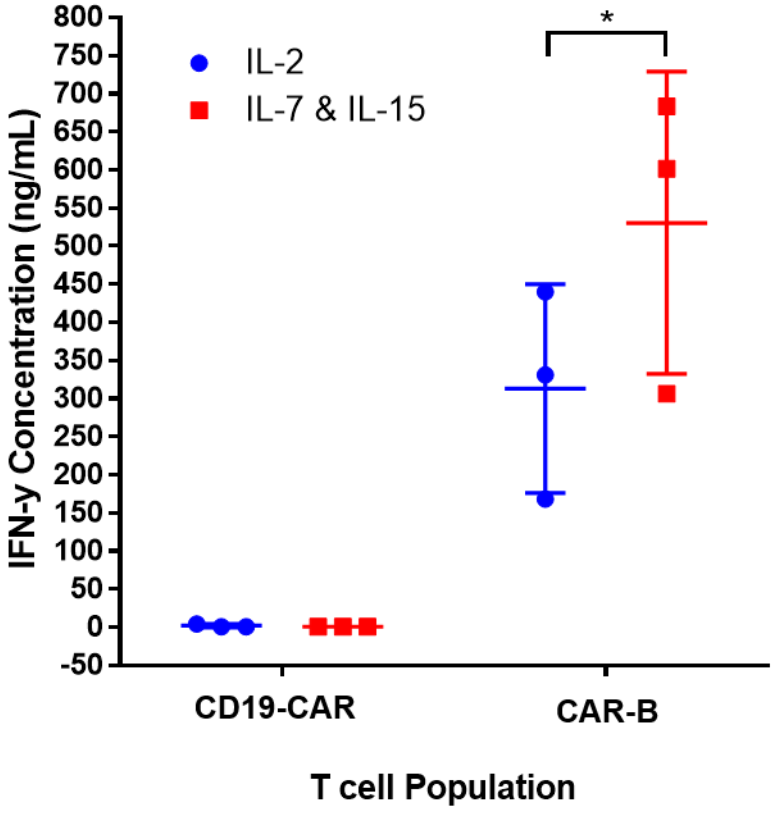

Figure 71: Impact of Cytokines on IFN-γ Production

*CD4/CD8 T cells isolated from 3 healthy donors were cultured with either 100IU/mL of IL-2 or a combination of 10ng/mL IL-7 and 10ng/mL IL-15. After 24 hours of activation, T cells were left untransduced or transduced with either a CD19-CAR encoding LVV or CAR-B encoding LVV. At day 12 of culture, T cell populations were co-cultured with a CAR-B antigen expressing cell line for 48 hours, at which point supernatant samples were removed for MSD® analysis. A paired two-tailed T test was performed to determine the significance of the difference in IFN-γ concentration between the IL-2 and IL-7/IL-15 CAR-B T cell populations. * indicates p = ≤0.05. Error bars display the mean with SD of the average IFN-γ concentrations taken from triplicate readings for three healthy donors.*

An effort to further optimise the culture of T cells within the 10M G-REX® vessels was performed by tracking the concentration of IL-7/IL-15 within the media of the G-REX® vessel to determine the impact that different cytokine feeding schedules had upon the fold expansion. Within this experiment, T cells were given 10ng/mL of IL-7/IL-15 at four time points (day 0, day 2, day 4 and day 7) or were frontloaded with 40ng/mL of IL-7/IL-15 at day 0 and day 2. Within both conditions, culture vessels were topped up to the full volume on day 2 with media supplemented with the appropriate concentration of IL-7/IL-15, either 10ng/mL or 40ng/mL.

As shown in Figure 72A, the fold expansion of continually fed or frontloaded T cell populations followed a very similar pattern, with the exception of a peak in total viable cell number at day 7 for one of the 40ng/mL IL-7 samples which caused a large standard deviation. This result is likely erroneous due to counting error.

When IL-7 (Figure 72B) and IL-15 (Figure 72C) were frontloaded, there was a sharp decline in the concentration of IL-7/IL-15 within the media from day 0 to day 4, during which there was a low rate of expansion within the T cell populations. This demonstrates that large concentrations of the cytokines were being consumed during this initial activation phase, despite low proliferation of T cells. At the point at which the fold expansion of the T cells rapidly increases, between day 4 and day 7, there was a plateau in the consumption of IL-7/IL-15 within the frontloaded populations. There was a slight peak in the IL-7 concentration measured at day 7, which is of interest as it is not expected that T cells can endogenously produce IL-7. As only one of the data points appears to have been impacted, it is likely that a technical error caused this increased in cytokine concentration. Finally, as the growth curve plateaus again from day 7 to day 10, there is another sharp decrease in the concentration of IL-7/IL-15 within the frontloaded samples. When 10ng/mL IL-7/IL-15 were added over the culture period, this sharp decrease in concentration was not observed from day 0 to day 4. Peaks in concentration occurred subsequent to cytokine addition, with a gradual drop in cytokine concentration after each addition between day 4 to day 10. The viability of all of the T cell populations remained above 90% throughout the T cell culture process (data not shown). This data has demonstrated that there is not a large difference in the expansion of T cells when cytokines are either frontloaded or added throughout the culture period.

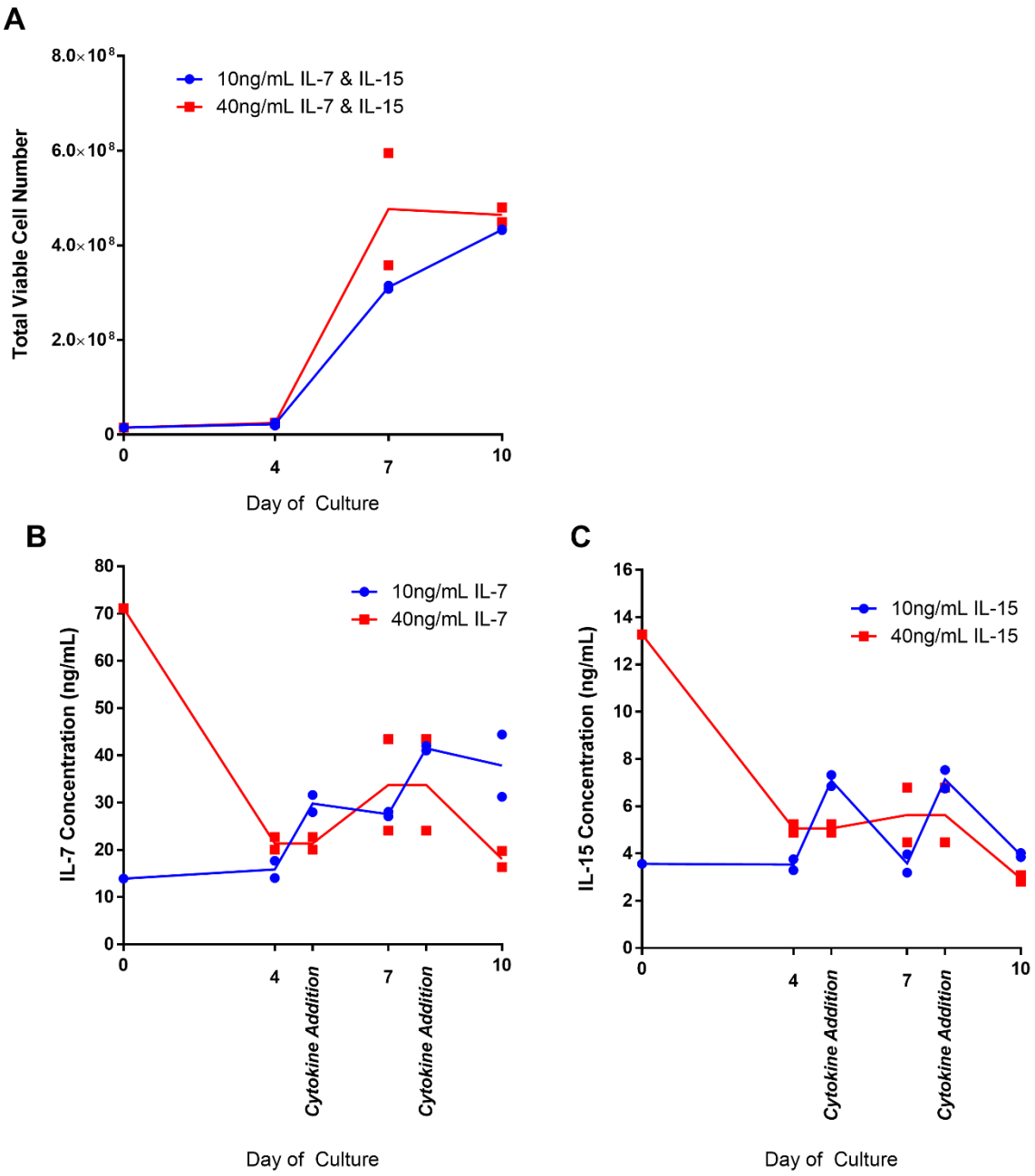

Figure 72: Impact of Cytokine Addition Protocol on Fold Expansion

CD4+/CD8+ T cells from two donors were seeded into 10M G-REX® culture vessels at 1.5x10^6 cells per cm^2 and were then either frontloaded with 40ng/mL of IL-7 and IL-15 at day 0 or provided with 10ng/mL of IL-7 and IL-15 at four time points (Day 0, Day 4 and Day 7). Samples were removed at days 0, 4, 7 and 10 for analysis of A) Total viable cell number, B) Concentration of IL-7 or C) Concentration of IL-15 to determine the impact that cytokine feeding schedule may have upon the expansion of the T cells. The connecting lines demonstrate the mean of the two data points for each condition.

4.2.3.3.1. Cytokine Impact Discussion

Within CAR T and engineered T cell therapies, the expansion and persistence of the infused T cell product *in vivo* has been correlated with the long-term survival of patients (Gattinoni *et al.*, 2005; Louis *et al.*, 2011; Kochenderfer *et al.*, 2012; Sommermeyer *et al.*, 2016; Turtle, Hanafi, Berger & Hudecek *et al.*, 2016).

Upon activation *ex vivo*, naïve T cells within the patient T cell population differentiate into either effector or memory phenotypes. The effector phenotype has been associated with the rapid cytotoxicity of tumour cells, whilst the memory phenotype is more involved in the renewal and persistence of the T cell population (Gattinoni *et al.*, 2012; McLellan & Ali Hosseini Rad, 2019). Upon stimulation, the central memory phenotype has the ability to form additional effector T cells, central memory T cells or effector memory T cells, enabling the continuation of a cytotoxic effect through the production of effector subsets, but with poor cytotoxic ability itself (McLellan & Ali Hosseini Rad, 2019). Effector T cells and effector memory T cells demonstrate the greatest capacity for cytokine production and cytotoxicity *in vitro,* however naïve, stem cell memory and central memory T cells have all demonstrated superior functionality *in vivo (Berger et al., 2008; Hinrichs et al., 2011; Gattinoni et al., 2012).* The stem cell memory subset has the greatest capacity for self-renewal, which is important for the long-term persistence of the therapy (McLellan & Ali Hosseini Rad, 2019).

It was reported by Xu *et al.* that the use of IL-7 and IL-15 within the T cell culture would push the T cell population towards a stem cell memory phenotype (Xu *et al.*, 2014), with many T cell protocols suggesting the use of IL-7 and IL-15 to enrich for a memory phenotype (McLellan & Ali Hosseini Rad, 2019), whereas, the use of IL-2 was suggested to enrich for a differentiated effector phenotype (Crompton *et al.*, 2014). However, the results generated within this study do not correlate with those suggested within scientific literature. Both IL-2 and IL-7/IL-15 generated T cell populations consisting of a majority of central memory and effector memory T cells with no difference between the two cytokine conditions within the CD8+ population. Within the CD4+ population, there was an increase in the frequency of effector memory T cells when IL-7/IL-15 was used within the culture, which contradicts the hypothesised results based on previous scientific literature which suggested that a skew towards an

effector phenotype would be observed for T cell populations cultured with IL-2. There was a minimal increase in the frequency of stem cell memory T cells when cultured with IL-7/IL-15; however, the frequency of this subset was very low (<5%) within both cytokine conditions. The lack of effector T cell populations within either population was not expected but may have occurred due to culture conditions causing the differentiation of T cell populations from effector to memory phenotypes, or due to the analytical method used. As was described within section 3.8, optimisations to the differentiation phenotyping methodology improved the separation of cell populations, particularly the CD45RA and CD45RO cell populations, enabling for more accurate gating. Due to portfolio prioritisation at GSK, I was unable to repeat this study using the optimised methodology, as described in section 3.8.2, to determine whether an increased number of effector phenotype T cells could have been identified. However, I would envisage that a repeat of this study using the optimised protocol would have enabled improved differentiation of the T cell subsets and enabled investigation into the impact that cytokines were having upon the T_{EFF} subset.

The use of either IL-2 or IL-7/IL-15 did not have a significant impact on either the fold expansion or transduction efficiency of T cell populations, nor did the feeding schedule of IL-7/IL-15 impact upon the expansion of the T cell populations. The main impact that choice of cytokine was discovered to be having upon the T cell populations was the ratio of CD4+ and CD8+ T cells, with a significant increase in the frequency of CD4+ T cells when IL-7/IL-15 was used, and a significant increase in the frequency of CD8+ T cells when IL-2 was used. This result is of interest, as it suggests the choice of cytokine could help to boost the frequency of one of the two T cell populations within patients. CD8+ T cells are known to have strong cytotoxic functionality and are required for the initial killing of tumour cells. However, studies performed both in animals (Berger *et al.*, 2008) and humans (Louis *et al.*, 2011) have demonstrated that the presence of CD4+ helper T cells is essential for continued persistence and cytotoxicity *in vivo.* In addition to this, studies performed whereby tumour infiltrating lymphocytes (TILs) have been infused into patients have demonstrated a greater persistence of CD4+ TILs compared to CD8+ TILS (Dudley *et al.*, 2002).

Interestingly, despite the decrease in the frequency of CD8+ population when cultured with IL-7/IL-15, the concentration of IFN-γ produced was significantly higher within the IL-7/IL-15 cultured T cell population. It would have been expected that the population with the highest frequency of CD8+ T cells would have had the highest concentration of IFN-γ produced, as CD8+ T cells produce higher levels of IFN-γ than CD4+ T cells. This increased IFN-γ production observed within the IL-7/IL-15 T cell population could be attributed to the higher frequency of effector memory T cells within the CD4+ population, which would produce increased concentration of IFN-γ compared to central memory T cells.

An additional study that I would have liked to have performed had time and resourcing permitted would have been to investigate the cytotoxic potential of the T cell populations *in vitro*. Although it has been suggested that cytotoxicity functionality of T cell populations does not necessarily translate *in vivo,* it would have been of interest to determine whether the changes in the frequency of CD4+ and CD8+ T cells impacted upon the cytotoxic potential of the T cell populations.

4.3. Chapter 3: Improving Transduction Efficiency

4.3.1. Introduction

There are multiple aspects of the production process that can impact upon the efficient transduction of T cells by lentiviral vectors, including the level of activation and expression of LDLr as was already observed within section 4.2.3.1, which in itself can be impacted by the quality of the starting material. The size of the packaging insert within lentiviral vectors can also impact upon transduction efficiency, with reduced rates of transduction efficiency as the encoded construct gets larger (Sweeney & Vink, 2021). The purity of the lentiviral vector preparation also has an impact, with decreased packaging of viral particles reducing the overall transduction efficiency of T cells. This results in high MOIs being required to ensure sufficient frequencies of transduced T cells within the final drug product, which increases both the cost and complexity of lentiviral vector manufacturing to supply for clinical trials (Höfig *et al.*, 2012). For this reason, the discovery of a compound that could improve the transduction efficiency of T cells would be hugely beneficial by allowing for reduced MOIs to be utilised for clinical trials thus reducing manufacturing costs. In addition to this, a transduction enhancing compound would help to improve the quality of final T cell products by ensuring sufficient frequency of transduced T cells within the final product. The use of reduced MOIs could also improve the safety of the final product by reducing vector copy numbers within T cells, thus reducing the risk of oncogenic insertions. Several transduction enhancing compounds have previously been identified, but these are frequently subject to proprietary license or not suitable for GMP manufacturing (Lo Presti *et al.*, 2021; Patel *et al.*, 2021). The experiments within this chapter were performed to evaluate whether small molecules with similar transduction-enhancing properties could be identified within GSK's compound library.

4.3.2. Hypothesis and Study Aims

The hypothesis of this study is that a compound could be discovered and utilised to increase the efficiency of lentiviral vector transduction of T cells, enabling the reduction of MOIs, improving the frequency of transduced T cells within the final drug product and therefore reducing the cost of product manufacture.

The aims of this study are to:

- Perform a screen of GSK's compound library to identify compounds that can improve transduction efficiency above the level observed with an untreated control.
- Determine the impact that transduction enhancing compounds have upon T cell fold expansion and viability.
- Determine the impact that transduction enhancing compounds have upon T cell phenotype.
- Determine the impact that transduction enhancing compounds have upon the cytotoxic functionality and cytokine production in response to antigen expressing cell lines.
- Investigate the risk that use of a transduction enhancing compound may lead to an increased number of oncogenic insertions.

4.3.3. Results

4.3.3.1. Investigation of Transduction Enhancing Compounds

In order to identify transduction-enhancing compounds within GSKs compound library, a high-throughput screen was designed by the Screening, Profiling and Mechanistic Biology (SPMB) department at GSK. Due to cost and throughput restrictions, it was not possible to screen the full 1.8million compounds available within GSKs compound library, therefore the SPMB group identified a subset of compounds enriched for biological activity – this included compounds that have been lead candidates within other GSK projects; compounds annotated with known activities within various biological assays; marketed drugs; and compounds with targets of interest (such as mTOR inhibitors, STING inhibitors and Wnt inhibitors). The screening process used to identify two lead compounds from the initial pool of 5167 compounds is shown within Figure 73.

Initially, the SPMB department performed a high-throughput screen of 5167 small molecules by transducing T cells with a green fluorescent protein (GFP)-encoding lentiviral vector and treating T cells with a single concentration (10µM) of each compound. This single shot screening method enabled the exclusion of compounds that reduced CD3+ T cell viability below 85%. 352 compounds, that demonstrated an increase in the frequency of GFP expression within the CD3+ T cell population that was over three times standard deviation compared to the vehicle control, were progressed into a hit confirmation screen. Within this confirmatory screen, duplicate wells of each compound were run at a single concentration (10µM) with the same pass criteria used as previously. 160 compounds showed increased transduction efficiency in the $CD3^+$ T cell population compared to an untreated control (data not shown), and these were further analysed in full-curve experiments where 11 different compound concentrations were used to generate a dose-response curve ranging from 100µM to 0.001µM. Transduction efficiency was measured in $CD3^+$, $CD4^+$ and $CD8^+$ T cell populations, and only those that produced a complete dose response curve with limited cytotoxicity at the highest concentration (100µM) were progressed to biology screening.

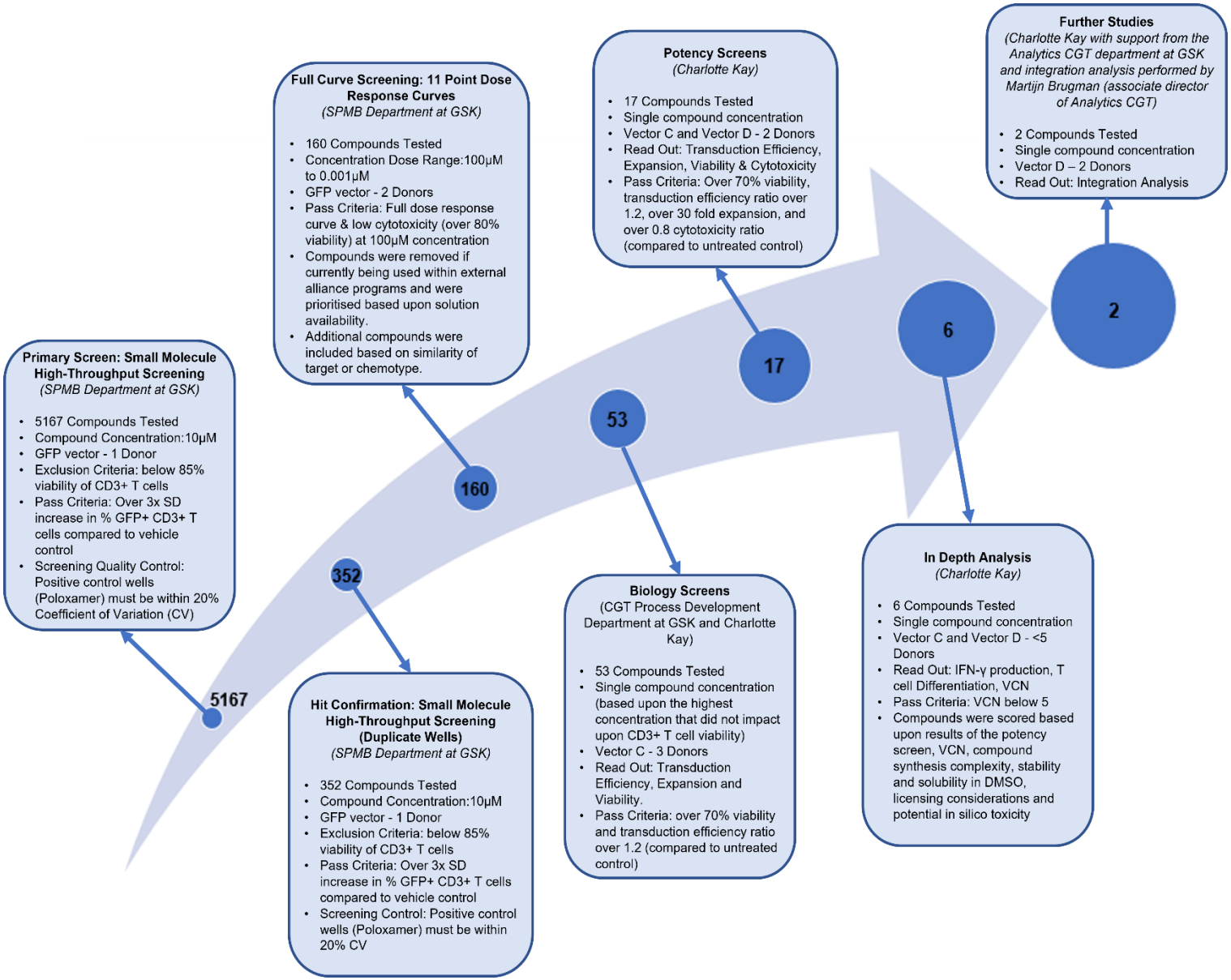

Figure 73: Screening Triage

5167 compounds were screened looking for "hits" that increased GFP expression. 160 were investigated in 11-point dose response curves. 53 were tested within biology screens and 17 were moved forward into potency screens. Finally, 2 lead candidates were progressed into further studies, including integration analysis

The impact of compounds upon the transduction efficiency of T cell populations varied, with some compounds found to increase the transduction efficiency in both CD4+ and CD8+ T cell populations whilst other compounds selectively increased the transduction efficiency within the CD8+ T cell population. Representative dose response curves demonstrating these two observations are shown in Figure 75.

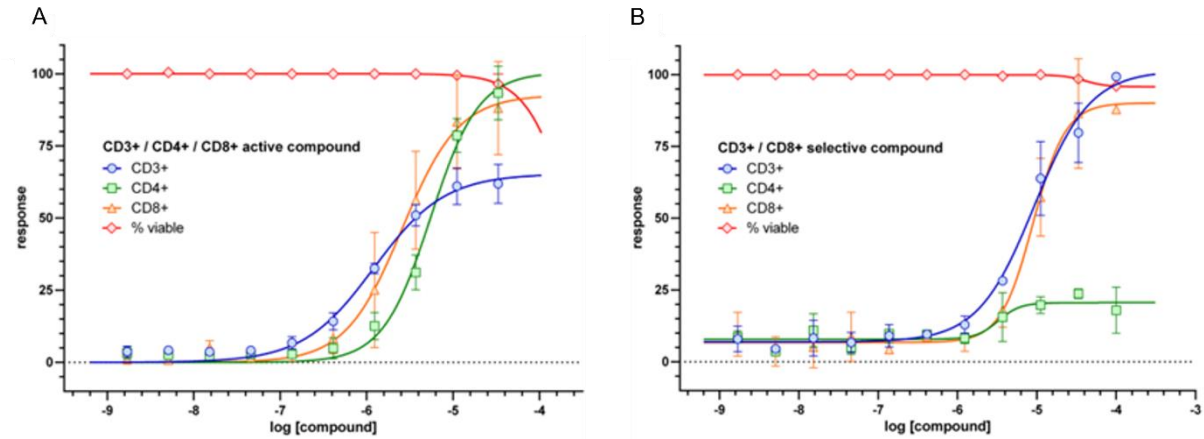

Figure 74: Representative Dose Response Curves

During the 11 point dose response curve screening, it was observed that some compounds were active within both the CD4+ and CD8+ T cell populations (A), whilst others were selective for the CD8+ T cell population (B). Blue lines represent the % of GFP+ CD3+ T cells, green lines represent the % of GFP+ CD4+ T cells, orange lines represent the % of GFP+ CD8+ T cells and red lines represent the % of viable T cells at each compound concentration.

In addition to the “hits” progressed into the biology screening, a number of compounds were included based upon their similarity of target or chemotype to the identified hit compounds. Of the compounds progressed, the largest cluster was of 13 compounds that were identified as STING1 macrocycles. Compounds were tested at a single concentration that ranged between 10µM and 100µM, which was determined based on the results of the 11 point dose response curve screening, with the optimum concentration for each compound being the highest concentration that did not impact upon the CD3+ T cell viability. The biology screening evaluated the impact of compounds upon the transduction efficiency of T cells, isolated from three healthy donors, with a therapeutic lentiviral vector (vector C). A transduction efficiency ratio of

1.2 compared to the relevant untreated control population was required for progression into the potency screening work package. Additional attributes investigated within the biology screens included T cell expansion and viability.

Following the screening of 53 compounds within basic biology assays, 17 compounds were chosen to be investigated further with testing performed on T cells isolated from five healthy donors and transduced with two lentiviral vectors (which will be referred to as vector C and vector D). Within all assays, a known transduction enhancer, Poloxamer Synperonics F108, an amphiphilic molecule able to form micelles and bind to lipid membranes decreasing membrane microviscosity and increasing lipid exchange (Höfig *et al.*, 2012) was used as a positive control compound. The transduction efficiency of T cell populations was analysed at the end of the culture process, and a transduction efficiency ratio was calculated by dividing the frequency of transduced CD3+ T cells from the compound treated population by the frequency of transduced CD3+ T cells from the relevant untreated transduced control population within each experiment. This enabled comparison of the relevant ratio of transduction efficiency across several experiments with the elimination of donor and lentiviral vector variability. Figure 75 shows the ratio of transduction efficiency calculated for 17 compounds, with a threshold ratio set at 1.2 to indicate an improvement in transduction efficiency above the level observed with the untreated transduced control population. A ratio of 1 would indicate no difference in transduction efficiency compared to the untreated transduced control population. All compound treated T cell populations achieved an average transduction efficiency ratio that surpassed the 1.2 threshold, with the exception of CMP425 which fell slightly below the threshold at 1.1.

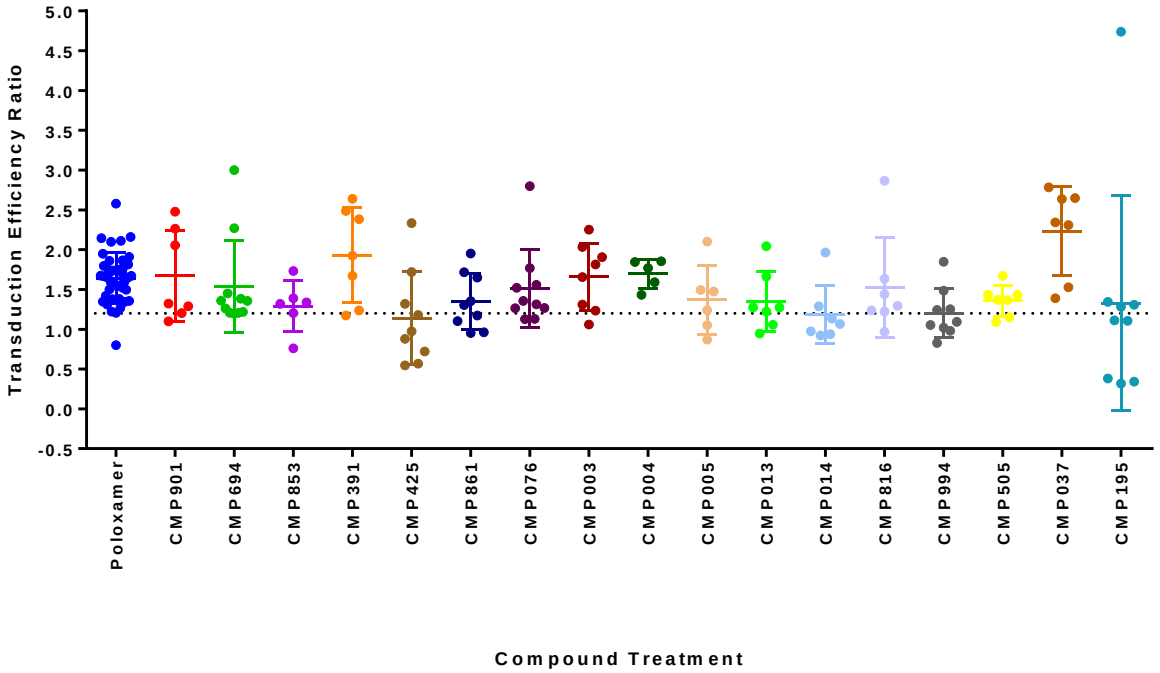

Figure 75: Ratio of Transduction Efficiency of Compound Treated T cell Populations

17 compound treated T cell populations and one positive control (Poloxamer) treated population were tested across five healthy donors using two lentiviral vectors to determine the ratio of transduction efficiency compared to an untreated transduced control population. A threshold ratio of 1.2 was set. Error bars display mean with SD.

With the confirmation that the 17 shortlisted compounds were able to increase transduction efficiency above the level observed with the untreated transduced control population, it was important to determine whether the use of compounds impacted upon the fold expansion of the T cell populations. Fold expansion data was gathered from up to four healthy donors treated with either vector C or vector D, with some compounds tested against both vectors (Figure 76). The number of conditions (donor number and vector) that could be tested was dependent upon the number of viable T cells recovered and therefore some compounds could not be tested within all conditions. A threshold was set at the expected level of 30-fold expansion (based on previous experience). Compounds that did not reach this threshold included: CMP391, CMP425, CMP013, CMP014, CMP816, CMP994 and CMP195. Within some of these compound treatment groups, it was clear that a single donor expanded poorly across all treatment conditions, as can be seen by the low outlier within T cell populations treated with Poloxamer, CMP694, CMP391, CMP013, CMP014, CMP816 & CMP994. With this outlier removed, the average fold expansion for many of these T cell populations increased above the 30-fold threshold. Compounds that appeared to be having a true impact on fold expansion with decreased fold expansion observed across all donors included CMP425 and CMP195, allowing these two compounds to be discarded based on this data. The viability of all T cell populations remained above 70%, with the exception of one donor treated with CMP425 in which the viability of the population fell to 65.8% within the vector C transduced population and 66.7% within the vector D transduced population (data not shown).

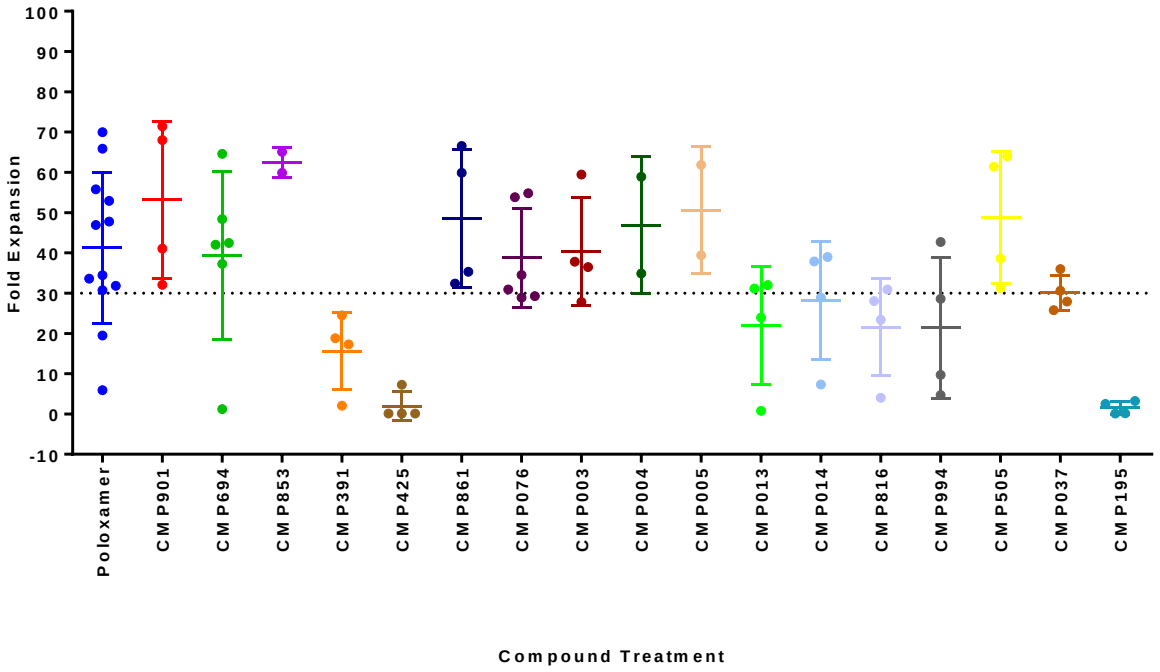

Figure 76: Fold Expansion of Compound Treated T cell Populations

The fold expansion of compound treated T cell populations was determined at the end of the culture process, with data gathered from up to four healthy donors using two lentiviral vectors. An average fold expansion of at least 30-fold was expected, with compounds suspected of impacting T cell growth not reaching this level of fold expansion. Error bars display mean with SD.

With impact upon transduction efficiency, fold expansion and viability assessed for the 17 compounds, the next aspect to be investigated further was whether compound treatment had any impact upon the cytotoxic function of the T cell populations. In order to assess this, co-culture assays were set up on the xCELLigence® platform using an antigen positive cell line and an antigen negative cell line to assess the time it took for each T cell population to kill 50% of the antigen positive cell line (KT_{50}), with minimal cytotoxicity of the antigen negative cell line. For each donor, T cell populations were normalised down to the transduction efficiency of the relevant untreated transduced control population – to enable equal numbers of transduced and untransduced T cells to be seeded for each condition and ensure comparison of cytotoxic functionality (T cell potency) rather than the impact that increased transduction efficiency had upon

cytotoxicity. Figure 77 shows the KT_{50} ratio, calculated by dividing the KT_{50} of the relevant untreated transduced control population by the KT_{50} of the compound treated population, allowing comparison of KT_{50} results from various experiments and donors. A threshold was set at a ratio of 0.8, with populations falling below a ratio of 0.8 defined as having cytotoxic functionality impacted by the compound treatment. All the compound treated populations apart from two, CMP853 and CMP195, achieved KT_{50} ratios above the threshold – with one low result pulling the average KT_{50} ratio of CMP853 just below 0.8. There was a large range in KT_{50} ratios achieved by some T cell populations, particularly CMP003 and CMP005, in which a single donor population achieved a particularly fast KT_{50} leading to a high KT_{50} ratio. If time had permitted, it would have been beneficial to repeat these compound treatments on an increased number of donors to gain a better understanding of the cytotoxic performance of these populations.

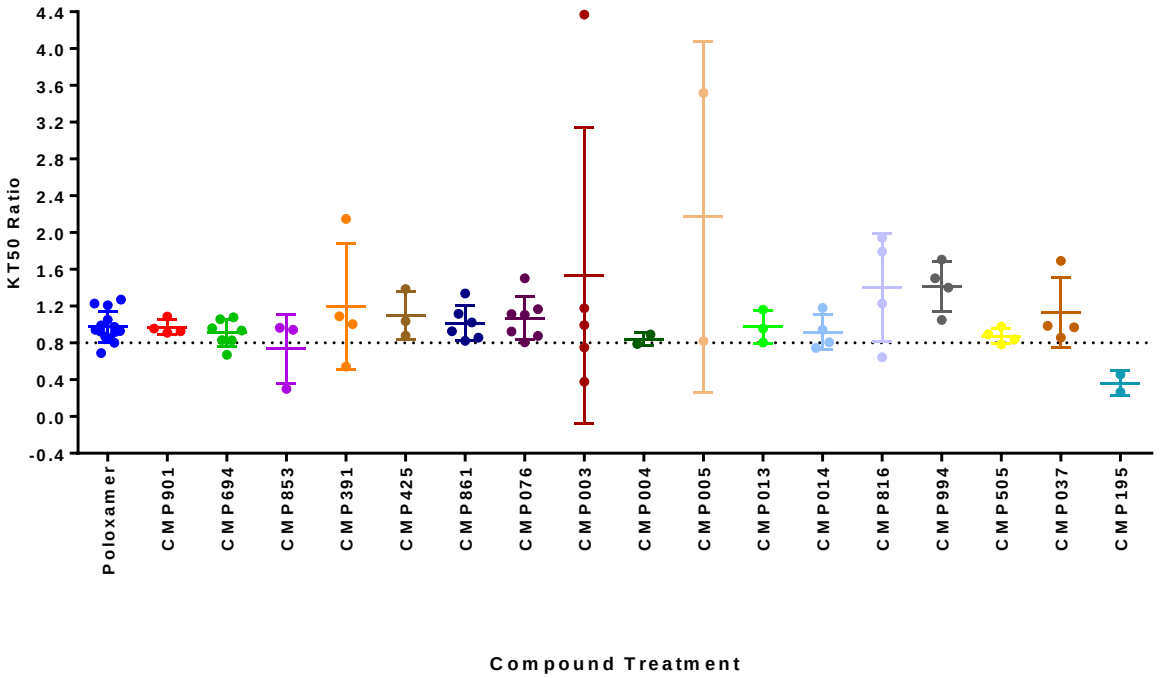

Figure 77: KT_{50} Ratio of Compound Treated T cell Populations

The cytotoxic functionality of compound treated T cell populations was analysed using an xCELLigence® co-culture assay to determine the time taken for 50% of antigen expressing target cell line to be killed by the T cell population (KT_{50}). The ratio of the KT_{50} of the untreated transduced control T cell population compared to the compound treated transduced T cell populations was calculated to determine the impact that compound treatment may be having upon the cytotoxic functionality of T cells. A threshold of 0.8 was applied, with ratios below 0.8 indicative of a decreased cytotoxic functionality. Data was gathered from up to four healthy donors using up to two lentiviral vectors. Error bars display mean with SD.

The compounds were then scored based upon the impact on T cell expansion, viability, transduction efficiency and cytotoxicity to narrow the selection down to a shortlist of six compounds. All six compounds surpassed the required threshold for both transduction efficiency ratio and KT_{50} ratio. Two of the six compounds, CMP391 and CMP816, fell below the 30-fold threshold for fold expansion but were progressed to further analysis to allow investigation of their impact on fold expansion in a larger number of donors, as it was not clear whether the impact upon fold expansion was due to compound or donor. These 6 compounds, as shown in Figure 78, were then

further investigated to determine the impact upon the production of IFN-γ subsequent to antigen encounter, the differentiation of T cell subsets and vector copy number (VCN). Data for VCN analysis is not shown, however all compound treated populations remained below the FDA recommended threshold of 5, thus impact upon VCN was not a concern.

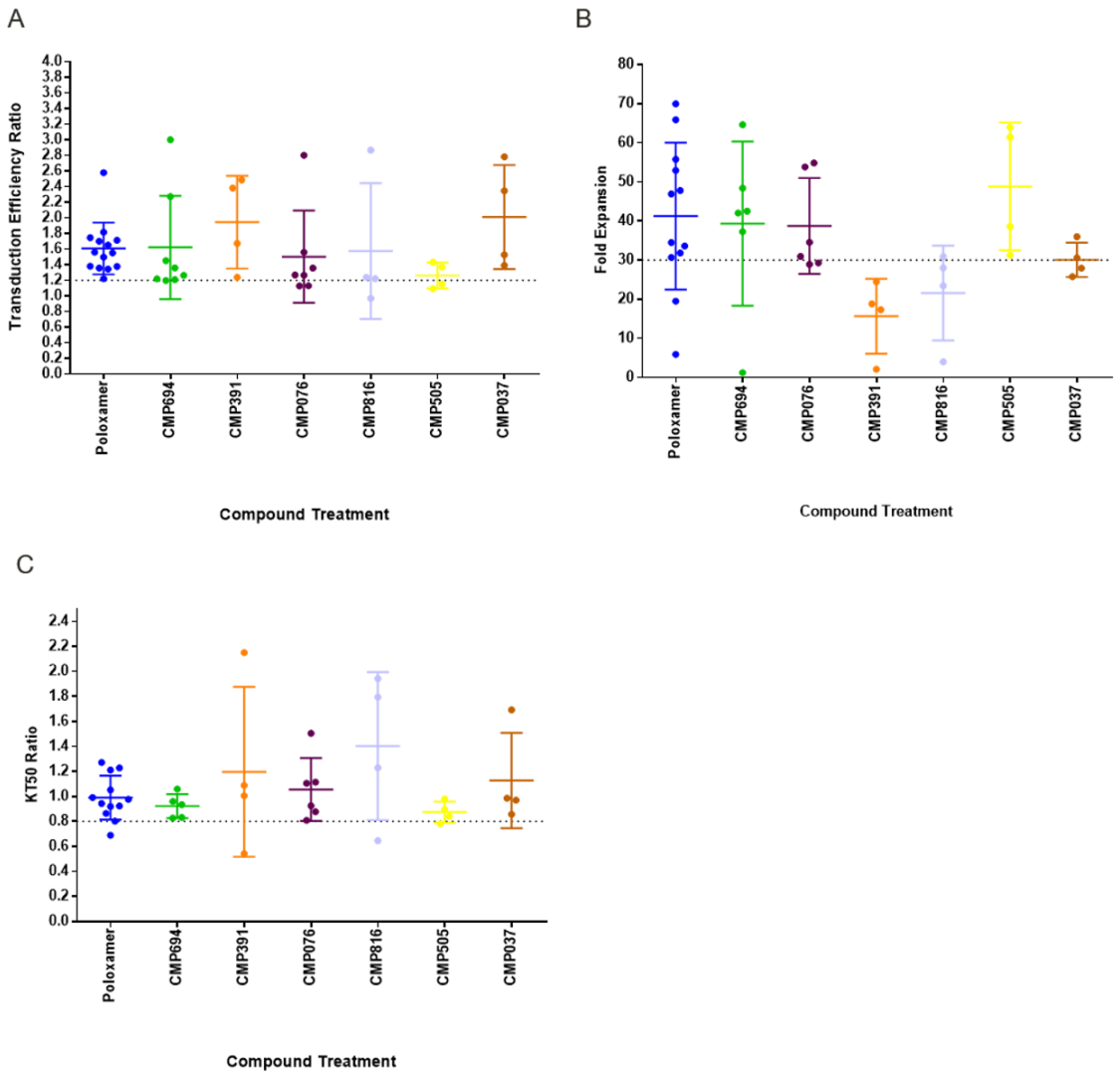

Figure 78: Summary of Results of Six Shortlisted Compounds

Of the original 53 compounds tested within biology screening assays, 17 compounds were analysed further as part of potency screening assays. From these results, 6 compounds were shortlisted for further analysis. A summary of the results of the 6 compounds gathered from potency screening assays in up to four healthy donors with vector C and/or vector D are shown. A) Transduction Efficiency Ratio; B) Fold Expansion; C) KT_{50} Ratio. Error bars display mean with SD.

In order to investigate the production of IFN-γ subsequent to antigen encounter, supernatant samples were removed from the xCELLigence® co-culture experiments after either 24 or 48 hours and analysed via MSD®. This method enables quantification of IFN-γ concentration within the supernatant, allowing comparisons to be made against the untreated transduced control population. Each compound was tested in up to 4 healthy donors with vector C and/or vector D, depending on sample availability (Figure 79). The majority of T cell populations demonstrated increased concentration of IFN-γ after 48 hours of co-culture compared to 24 hours, as a higher number of transduced T cells would have been activated and initiated cytotoxicity of target cells at this time point. Poloxamer treated T cell populations performed similarly to the untreated transduced control population. All 6 of the compound treated populations produced lower levels of IFN-γ compared to the untreated control population, with the exception of CMP694 and CMP076 after 48 hours of co-culture where IFN-γ concentration was similar to that of both the untreated and poloxamer treated T cell populations. CMP391 treated T cell populations produced the lowest concentration of IFN-γ. A one-way ANOVA using Dunnett's multiple comparison test was used to determine the significance of the differences of the compound treated populations compared to the untreated transduced control population. This demonstrated that only one of the compound treated populations, CMP391, at the 24 hour timepoint had a significantly lower concentration of IFN-γ produced compared to the untreated control population. The difference in concentration was not significant at the 48-hour timepoint.

Figure 79: IFN-γ Production of Compound Treated T cell Populations

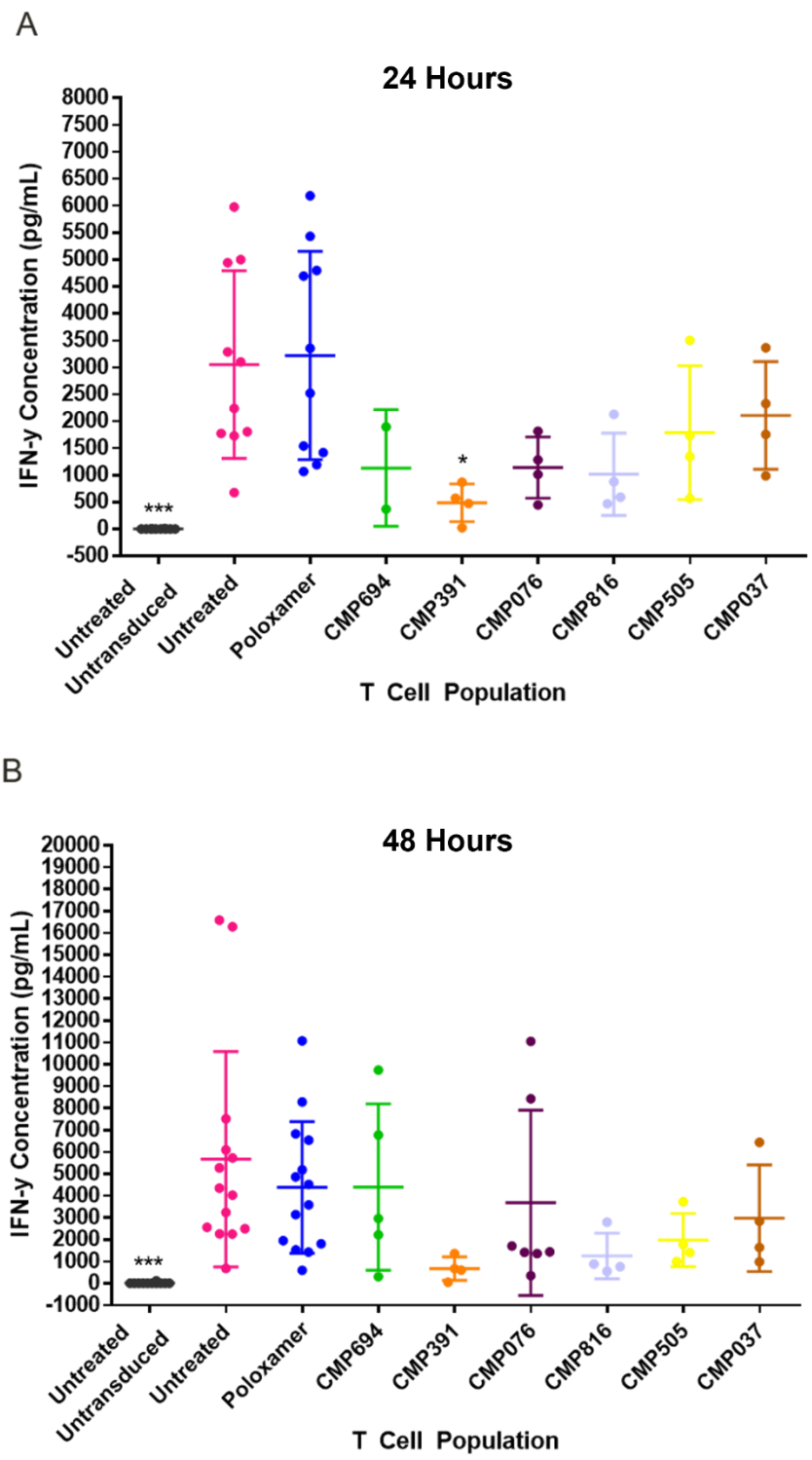

*MSD® analysis of the production of IFN-γ by compound treated T cell populations was performed after A) 24 hours or B) 48 hours of co-culture with target cell lines. A one-way ANOVA using Dunnett's multiple comparison test was used to investigate the significance of the differences between compound treated T cell populations and the untreated transduced control T cell population. Unless indicated by an asterisk, there was no significant difference. Where significant differences were found asterisk have been used to display the level of significance, with *** indicating P≤0.001 and * indicating P≤0.05.*

Finally, it was of interest to investigate the impact that the compounds had upon the differentiation phenotype of T cells, which could impact upon the *in vivo* functionality or persistence of the T cell populations. At the end of the culture period, T cell populations were analysed by flow cytometry to determine the frequency of T_{EM}, T_{CM}, T_{SCM}, T_{EFF} and T_N cell populations within both the CD4+ and CD8+ subsets. The phenotypic markers used to define each T cell subset are listed within Table 23. The data gathered across up to four healthy donors and two lentiviral vectors was combined within Figure 80 to give an overview of differentiation results and an indication of what impact each compound may be having upon T cell differentiation. The results demonstrated that there were minimal differences in the differentiation phenotypes of T cell populations between Poloxamer, CMP076 treated T cell populations and untreated T cell populations.

Both CMP391 and CMP816 treated T cell populations showed increased CD4+ T_{CM} populations, decreased CD4+ T_{EM} populations and increased CD4+ T_{EFF} populations compared to the untreated population. CMP391 treated populations also demonstrated an increased CD4+ T_{SCM} population but a decreased CD8+ T_{SCM} population. CMP816 treated populations had a decreased CD8+ T_{SCM} population, with no change in CD4+ T_{SCM} population. CMP694 and CMP505 treated populations showed similar differentiation profiles, both with slightly increased CD4+ T_{SCM} populations but otherwise having similar profiles to the untreated T cell population. CMP037 treated populations demonstrated a particularly interesting differentiation phenotype, with a large increase in the frequency of CD8+ T_{SCM} and a small increase in the frequency of CD8+ T_{EFF} populations compared to the untreated control. This was the only compound treated population that such a large change in the frequency of differentiated populations within the CD8+ subset was observed. The other differentiation subsets for CMP037 treated populations remained similar to that of the untreated control population, with just a small decrease in the frequency of CD4+ T_{EM} and CD4+ T_{CM} populations.

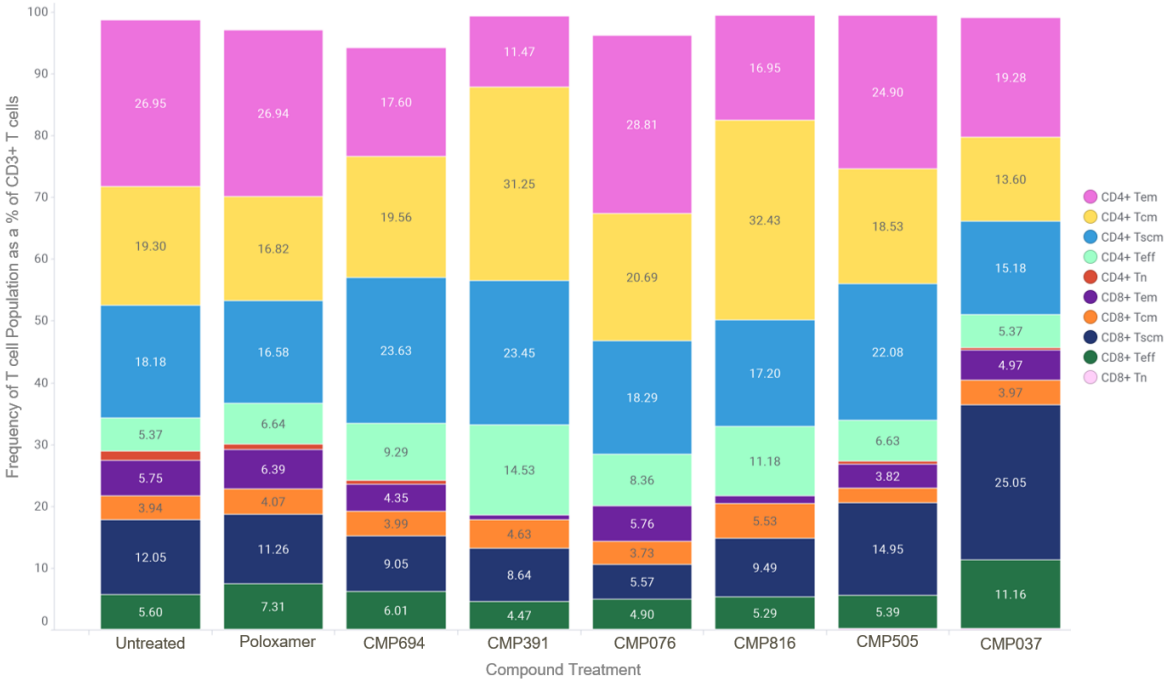

Figure 80: Average T cell Differentiation Subset Frequencies as a Percentage of the CD3+ T cell Population

Analysis of the frequencies of T cell differentiation subsets, including T_{EM}, T_{CM}, T_{SCM}, T_{EFF} and T_N, within the CD4+ and CD8+ T cell populations across up to four donors with two lentiviral vectors was performed at the end of the culture period to determine the impact that compounds had upon the differentiation of T cell populations. Broad analysis of the average results demonstrated general trends that could indicate compound effect on T cell differentiation.

Subsequent to this further analysis, the 6 compounds were scored again to differentiate between them and narrow down the choice to two lead candidates, which could be carried through into more expensive analyses, including integration site analysis, gene activation analysis and large-scale culture experiments. During this selection, additional consideration was given to the complexity of compound synthesis, stability and solubility within DMSO, licensing considerations and *in silico* toxicity (Figure 81).

Compound	Viability (Over 70%)	TE Ratio (Over 1.2)	Fold Expansion (Over 30 Fold)	KT50 Ratio (Over 0.8)	VCN (Below 5)	Compound Synthesis Complexity	DMSO Stability	*In Silico* toxicity	Licensing
CMP694									
CMP391									
CMP076									
CMP816									
CMP505									
CMP037									

Figure 81: Compound Scoring

Traffic light scoring was performed to differentiate between the final six compounds to enable two lead candidates to be progressed into further studies. Compounds were scored based upon performance within potency screens (over 70% viability of T cells, transduction efficiency ratio over 1.2 compared to untreated control, over 30 fold expansion, KT50 ratio over 0.8 compared to untreated control and VCN under 5). In addition to this, compounds were scored based upon the complexity of compound synthesis, DMSO stability, potential in silico toxicity and licensing considerations

.

CMP694, CMP076 and CMP037 were not chosen due to the complexity of compound synthesis, which adds significant cost to the production of T cells thus negating the savings achieved by reduction of lentiviral vector costs. In addition to this, CMP037 was discarded as further investigation demonstrated potential *in silico* toxicity and DMSO stability issues. The final three compounds (CMP505, CMP391 and CMP816) passed the majority of the criteria. Although, CMP391 and CMP816 demonstrated slightly lower fold expansion than expected, this required further investigation to confirm that this was not due to donor variability, rather than compound impact. CMP816 was the same chemotype as CMP505, therefore in order to diversify the compounds progressed, CMP505 and CMP391 were chosen as the final two candidates to be progressed into further analysis packages.

4.3.3.2. Insertion Site Analysis of Transduction Enhancer Treated T cells

One such analysis package that was performed on the two candidate compounds was the investigation of the impact that the compounds may be having upon the integration profile of lentiviral vectors within the T cell genome, in order to assess the risk of insertional mutagenesis, which was discussed in detail within section 1.4.1.4.3.

Within clinical trials, insertion site analysis has been an essential tool used to monitor the proliferation of infused cell products (Shah *et al.*, 2019), enabling the tracking of the T cell repertoire and identification of clones in which vector insertion may have conferred a proliferative advantage, potentially indicating oncogenesis. Insertion site analysis was used to identify that an LMO2 locus insertion was the cause of clonal dominance within two patients that developed leukaemia during the SCID-X1 trial (Hacein-Bey-Abina *et al.*, 2003) However, it must be noted that clonal dominance does not always indicate oncogenesis: within a trial conducted by Bruce Levine *et al.* the analysis of a patient that achieved complete response demonstrated that over 94% of the CD8+ CAR T cell population originated from a single clone, in which transgene integration had disrupted the *tet2* gene (Fraietta *et al.*, 2018). The *tet2* gene has been indicated within the initiation of leukaemia but is also known to be involved in the regulation of haematopoiesis. Within this trial, the dominance of a T cell clone with an integration that disrupted this gene had resulted in therapeutic benefit, rather than oncogenesis. Similarly, Shah *et al.* described the secondary expansion of a single T cell clone with an insertion within the *CBL* gene in response to ongoing low level tumour burden, which resulted in complete remission and amelioration of the expanded T cell clone upon tumour clearance (Shah *et al.*, 2019) . Within this case, the expansion of a single clone may have originated from a single memory CAR T cell, whose persistence enabled the re-activation of therapy when low level tumour burden persisted.

To further advance insertion site analysis of high-throughput datasets, the Retroviral Tagged Cancer Gene Database (RTCGD) was developed to identify genomic positions of retroviral insertions within mouse tumour samples and the proximity to nearby genes (Akagi *et al.*, 2004). The database has enabled the identification of sites within the genome in which insertions have a high chance of causing oncogenesis – these sites are referred to as Common Insertion Sites (CIS's).

Analysis of samples in which there has been uncontrolled proliferation due to an oncogenic insertion would demonstrate high abundance of a particular insertion site, as all daughter cells originating from the parent oncogenic cell would carry the same mutation due to insertion of the lentiviral vector DNA within the same location in the host DNA. Many integrations within CIS's are located upstream of known cancer genes (Wu & Burgess, 2004). Within large data sets, it can become more difficult to analyse insertion site data due to the background noise of non-oncogenic insertions and "piggy-backing" cases in which non-oncogenic insertions and oncogenic insertions occur within the same parent cells, leading to the false correlation of a non-oncogenic insertion with a particular tumour (Ridder *et al.*, 2006).

Analysing data in the context of CIS's helps to identify only insertion sites of significance, as CIS's will have been identified within multiple independent tumours – thus reducing the risk of false positives. The method used for the analysis of the integration site data within this project was the Kernel Convolution Framework, as described in a paper by Ridder *et al.* This method improves upon analysis methods used within the RTCGD (Akagi *et al.*, 2004) by correcting for the bias of integration for different viral vectors, evaluating significance at biologically relevant scales and controlling for family-wise error (Ridder *et al.*, 2006).

Initially during analysis of CIS's, the insertion sites identified for each sample are distributed across an artificial chromosome. Figure 82 shows the Kernel Convolution analysis for each of the seven samples analysed, with the X axis displaying the location of the insertion site along the artificial chromosome and the Y axis demonstrating the density of insertion sites at each location. The higher the peak, the more insertion sites that were identified at that location. Within this analysis, a scale parameter of 100kb was utilised, which describes the width of each kernel function placed at each insertion site – this results in insertion sites within 100kb of one another to be smoothed into a single insertion site reading. A larger scale parameter of 300kb would reduce the number of insertion sites identified, as each kernel function would be larger thus smoothing more of the data. A study undertaken by Rittelmeyer *et al.* demonstrated the suitability of a 100kb analysis window, with 22.6% of integrations occurring outside of a 250kb analysis window (Rittelmeyer *et al.*, 2013).

Table 42 displays the number of insertion sites and the number of peaks that were identified when using either 100kb or 300kb scale parameters. Within Figure 82, each red circle identifies the placement of a kernel function, identifying a distinct insertion site. The green line demonstrates the threshold of significance, with insertion sites below this threshold identified as insignificant or “noise” within the analysis. The insertion site peaks are within similar locations and are of similar density for each of the three samples within each donor tested, with Figure 82A to C T cell samples from donor PR21D395287 and Figure 82D to Figure 82F T cell samples from donor PR21C395292. These plots look distinct to that of the polyclonal HEK cell control (Figure 82G) which demonstrates a different pattern of insertion sites across the artificial chromosome. A study by Deichmann *et al.* demonstrated the influence that the gene expression profile can have upon the integration of RVV, with gene expression influencing the tethering of the preintegration complex of viral vectors (Deichmann *et al.*, 2007). This indicates that the difference in gene expression between activated T cells and HEK cells at the time of LVV transduction may have contributed to these differences in integration pattern observed within this study.

There were a higher number of total insertion sites identified within the CMP391 treated sample for donor PR21D395287 compared to the CMP505 and untreated samples; however, the number of peaks identified with both 100kb and 300kb kernels were within a similar range. For 100kb analysis within both donors, the highest number of peaks identified was within CMP391 treated samples, and the lowest number of peaks identified was within the untreated samples (Table 42).

Table 42: Number of Insertion Sites and Peaks Identified using 100kb or 300kb kernel scale parameters

Sample Number	Donor ID	Treatment	Total Number of Insertions	Number and percentage of peaks - 100kb	Number and percentage of peaks - 300kb
1	PR21D395287	CMP391	33891	615 (1.8%)	252 (0.7%)
2		CMP505	24467	574 (2.3%)	244 (0.9%)
3		Untreated	21847	543 (2.4%)	283 (1.2%)
4	PR21C395292	CMP391	24713	631 (2.5%)	265 (1.1%)
5		CMP505	24574	582 (2.4%)	255 (1.0%)
6		Untreated	24771	528 (2.1%)	224 (0.9%)
7	N/A	Polyclonal HEK Cell Control	18957	468 (2.4%)	212 (1.1%)

Table 42: The number of individual insertion sites and the number of peaks identified when using either 100kb or 300kb scale parameters, with the percentage of total insertion sites displayed within brackets.

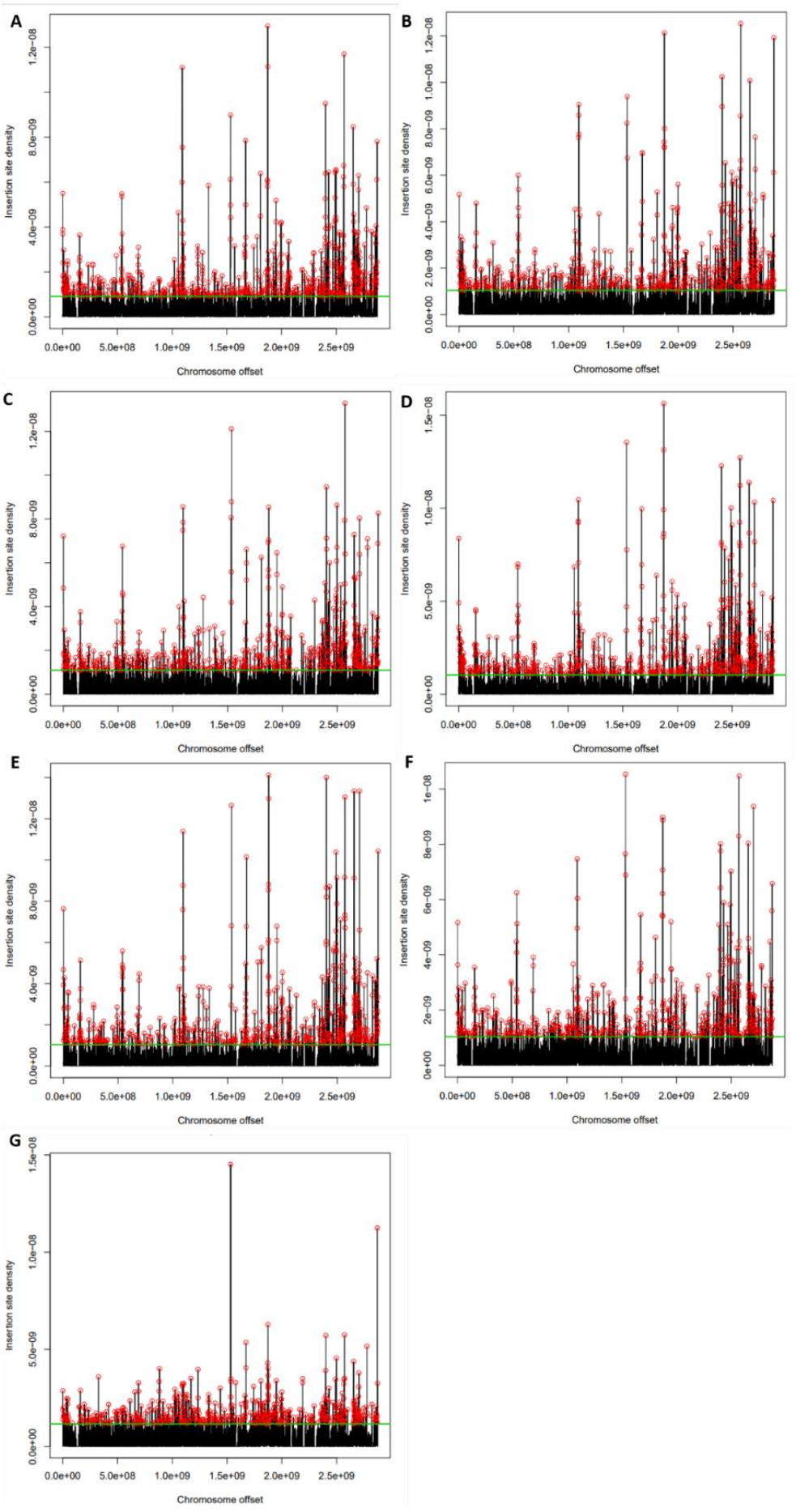
A
B
C
D
E
F
G
Insertion site density
Chromosome offset
0.0e+00
5.0e+08
1.0e+09
1.5e+09
2.0e+09
2.5e+09

Figure 82: Kernel Convolution Analysis of Integration Sites of Seven Samples

The density of insertion sites along an artificial chromosome are identified by the height of each peak, with red circles identifying kernel functions signifying unique insertion sites. The green line demonstrates the significance threshold. A) PR21D395287 – CMP391 Treated, B) PR21D395287 – CMP505 Treated C) PR21D395287 – Untreated, D) PR21C395292 – CMP391 Treated, E) PR21C395292 – CMP505 Treated, F) PR21C395292 – Untreated, G) Polyclonal HEK Cells

The number of peaks identified within the 100kb kernel analysis were analysed using a R script developed by Martijn Brugman (Associate Director, CGT Analytical Development) to identify CIS locations with gene annotations and enable the plotting of UpSet graphs to display the number of gene name overlaps between the samples (Figure 83). The top section of the UpSet graphs displays the number of overlapping genes within each comparison – with identification of the comparison performed described below each bar. The bar graph to the lower left of each plot demonstrates the size of each CIS set, with CMP391 treated samples having the largest CIS set size. A comparison of the overlapping gene names between untreated, CMP505 and CMP391 demonstrates 93 and 99 overlapping CIS locations for donors PR21D395287 and PR21C395292 respectively. Overall, CIS locations were more frequently shared between T cell samples than between T cell samples and the HEK polyclonal control sample.

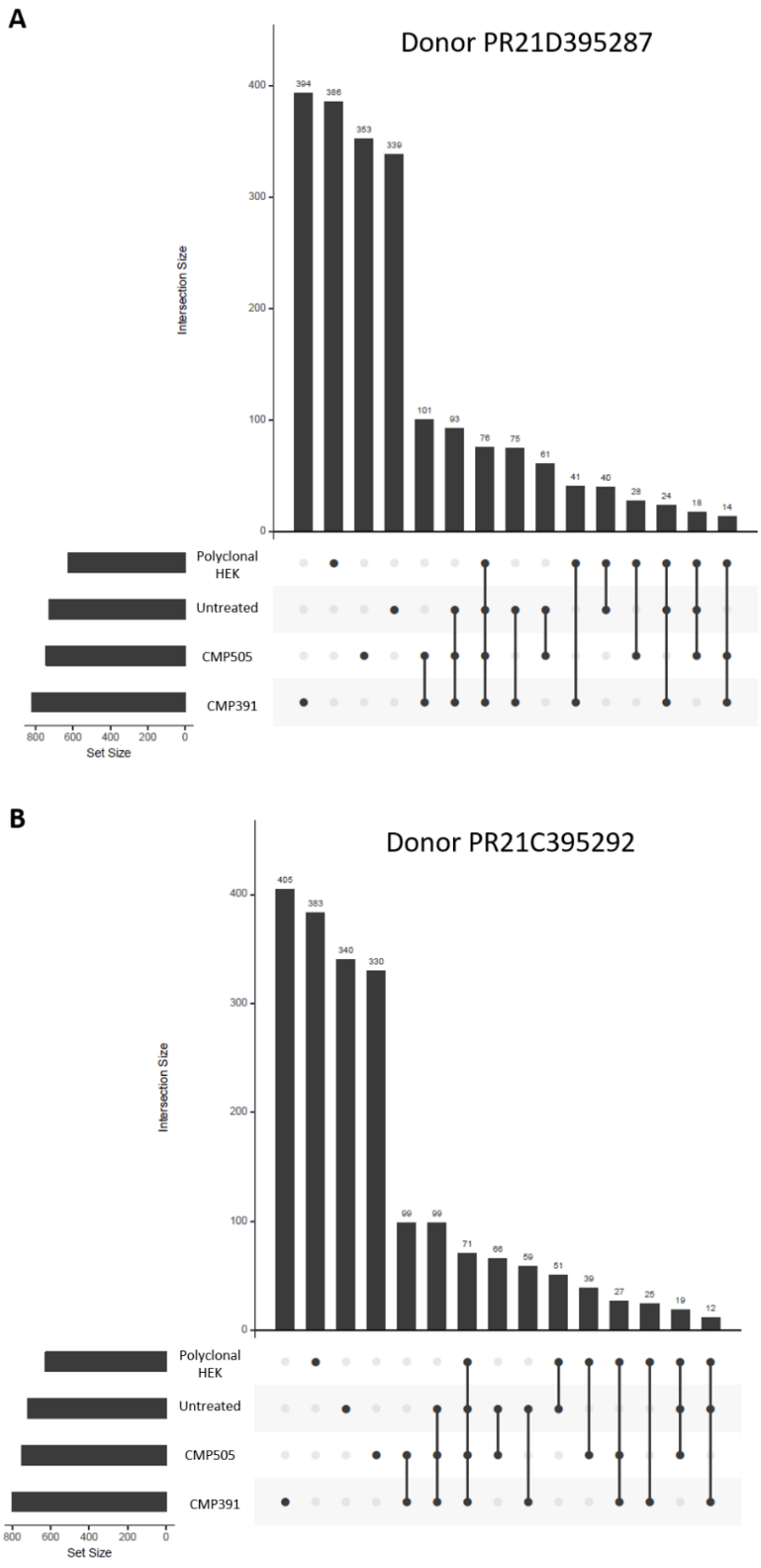

Figure 83: Intersection of CIS Locations Displayed as UpSet Graphs

UpSet Graphs displaying the overlap of CIS locations between A) Donor PR21D395287 samples and the HEK Polyclonal control and B) Donor PR21C395292 and the HEK Polyclonal control. The top section displays the number of overlapping genes within each comparison – with comparisons performed shown below. The bar graph to the lower left of each plot demonstrates the size of each CIS set.

In addition to this method of analysis, insertion site tables were also analysed within an R analysis package known as the RIPAT Bioconductor Package (RIPAT_1.0.0), which identifies the genes and transcription start sites closest to the identified insertion sites. The number of occurrences of annotated gene names within each sample enables the identification of common insertion sites. As the method of data processing within the RIPAT method is distinct to that of the CIS analysis method, some differences in the data output are expected. Figure 84 demonstrates the UpSet Graphs plotted for RIPAT analysis demonstrating the number of occurrences of shared gene annotations between the samples. For both donors, the highest number of shared gene annotations was between all T cell samples and the polyclonal HEK cell sample. Within donor PR21C395292 the most observed integrations were then those that were individual for each of the four conditions, followed by those shared between the three T cell samples. Within donor PR21D395287, integrations shared between the three T cell samples was the third most common subset, with only the CMP391 treated sample demonstrating a higher number of integrations distinct to that sample.

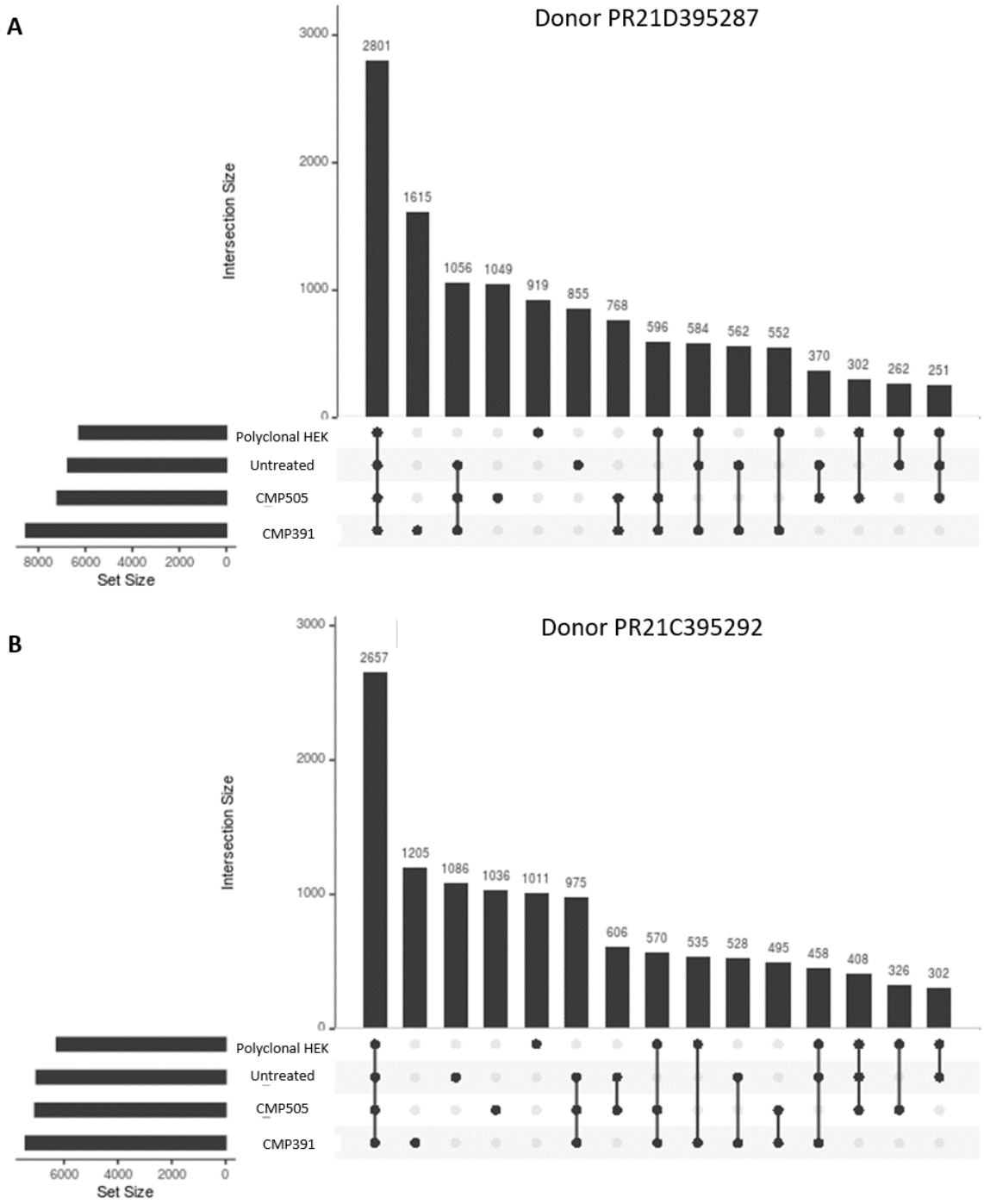

Figure 84: Intersection of Annotated Gene Occurrences Displayed as UpSet Graphs

UpSet Graphs displaying the overlap of annotated gene occurrences identified through the RIPAT analysis method between A) Donor PR21D395287 samples and the HEK Polyclonal control and B) Donor PR21C395292 and the HEK Polyclonal control. The top section displays the number of annotated gene occurrences within each comparison – with comparisons performed shown below.

The annotated genes for the 10 most frequently identified CISs for each cell populations are described within Table 43 and the 10 most frequent occurrences of genes identified closest to insertion sites through RIPAT analysis are described within Table 44. PACS1, NPLOC4, PPP6R2 were all genes identified as T cell CIS's within the literature (Biffi *et al.*, 2011) and were also identified within the top 10 CIS's within our samples. This indicates that treatment with either CMP391 or CMP505 does not alter vector integration on a global level. Differences in the top 10 genes identified via the two methods of analysis are expected as CIS analysis uses kernel density estimates to identify peaks based on insertion location, whereas RIPAT analysis annotates the gene closet to the insertion site.

Table 43: Top 10 Identified CIS's for Each Cell Population

PR21D395287			**PR21C395292**			**Polyclonal HEK**
CMP391	**CMP505**	**Untreated**	**CMP391**	**CMP505**	**Untreated**	
PACS1	*NPLOC4*	*NPLOC4*	KDM2A	*PACS1*	HSF1	RP11-953B20.2
NPLOC4	*PACS1*	BOP1	BOP1	JPT2	*NPLOC4*	TBC1D22A
KDM2A	SBF1	MAPK8IP3	SCX	POLR2E	NOSIP	CDC42BPG
BAG6	MAPK8IP3	ZNF34	*PACS1*	NOSIP	PRRG2	*NPLOC4*
MAPK8IP3	ABCA7	POLR2A	*NPLOC4*	PRRG2	*PACS1*	TSPAN10
BOP1	MROH1	MSH5	JPT2	*NPLOC4*	KDM2A	MAPK8IP3
SBNO2	LTA	MSH5-SAPCD1	SBNO2	KDM2A	TNRC6C	TRAF2
TRAF2	TRAF7	KDM2A	ALYREF	BOP1	ARHGAP45	ZGPAT
PPP6R2	VWA7	SBF1	PPP1R2P1	PRRC2A	MAPK8IP3	RP4-583P15.15
PSMB9	TNRC6C	RP11-953B20.2	SBF1	SBF1	IL32	TNFSF12

Table 43: Top 10 CIS's identified by CIS analysis

Table 44: Top Genes Identified through RIPAT Analysis for Each Cell Population

PR21D395287			PR21C395292			Polyclonal HEK
CMP391	**CMP505**	**Untreated**	**CMP391**	**CMP505**	**Untreated**	
PACS1	*PACS1*	*NPLOC4*	KDM2A	*PACS1*	*NPLOC4*	DST
KDM2A	*NPLOC4*	TNRC6C	*PACS1*	*NPLOC4*	*PACS1*	RBFOX1
NPLOC4	TNRC6C	KDM2A	*NPLOC4*	KDM2A	TNRC6C	MAD1L1
RPTOR	RPTOR	*PACS1*	RPTOR	RPTOR	KDM2A	*NPLOC4*
TNRC6C	KDM2A	RPTOR	TNRC6C	TNRC6C	NOSIP	EYS
ANKRD11	RBM6	EHMT1	FANCA	FANCA	*PPP6R2*	ANKRD11
PPP6R2	*PPP6R2*	MAD1L1	MECP2	IKZF3	PBRM1	EHD1
RNF157	MROH1	MROH1	MROH1	*PPP6R2*	RPTOR	RASA3
TNRC6B	NFATC3	ANKRD11	NFATC3	TNRC6B	HSF1	SESN1
FANCA	SMG1P5	CARD8	RBM6	NOSIP	NFATC3	SPIDR

Table 44: Top 10 occurrences of the closest genes identified by RIPAT analysis

Within Table 44, the identified top 10 closest genes as determined through RIPAT analysis appeared to demonstrate an increased number of shared integration sites between the six T cells samples, with distinct genes identified for the Polyclonal HEK sample. In order to determine the impact that host cell type may be having upon the integration of vectors, the RIPAT data was displayed within an UpSet graph focussing on only the top 50 genes most frequently identified for each sample (Figure 85).

Literature searches were performed in order to determine whether any of the genes identified multiple times within these analyses had an association with cancer (Table 45). The top 8 most commonly identified genes were found to have associations with cancer, with roles in tumourigenesis, cancer progression, poor prognosis and metastasis.

Table 45: Association between genes identified frequently within CIS and RIPAT analysis and cancer

Gene Name	Number of Times Identified Within CIS or RIPAT Analysis	Cancer Associated (Y/N)	Details of Cancer Association	Reference
NPLOC4	14	Y	Upregulated expression in clear cell renal cell carcinoma	(Yoshino *et al.*, 2020)
KDM2A	11	Y	Role in Tumourigenesis and Progression	(Liu, Liu & Lin, 2021)
PACS1	11	Possible	Potential role in oncogenesis	(Ohkawa *et al.*, 2022)
TNRC6C	8	Y	Functions as tumour suppressor - downregulated in thyroid cancer	(Cai *et al.*, 2021)
RPTOR	6	Y	Associated with Breast cancer	(Yin *et al.*, 2022)
MAPK8IP3	5	Y	Associated with tumour progression	(Cheng *et al.*, 2020)
PPP6R2	5	Possible	Potential role in metastasis	(Márquez *et al.*, 2013)
BOP1	4	Y	Associated with tumour progression	(Li & Song *et al.*, 2021)
MROH1	4	N	-	-

NOSIP	4	N	-	-
SBF1	4	N	-	-
ANKRD11	3	Y	Functions as a tumour suppressor – identified in breast cancer	(Lim *et al.*, 2012)
FANCA	3	Y	Associated with Fanconi Anaemia and pre-disposition to cancer	(Castella *et al.*, 2011)
NFATC3	3	Y	Downregulated in non-small cell lung cancer tissues	(Peng *et al.*, 2021)
HSF1	2	Y	Associated with cancer initiation, development and progression	(Chen *et al.*, 2021)
JPT2	2	N	-	-
MAD1L1	2	Y	Associated with lung cancer susceptibility	(Guo *et al.*, 2010)
PRRG2	2	N	-	
RBM6	2	Y	Often deleted or mutated in cancer	(Bechara *et al.*, 2013)
RP11-953B20.2	2	N	-	-
SBNO2	2	Y	Associated with gastric cancer	(Wu *et al.*, 2020)
TNRC6B	2	Y	Variation in methylation associated with cancer development time	(Joyce *et al.*, 2018)
TRAF2	2	Y	Low expression associated with unfavourable prognosis in Hepatocellular Cancer	(Schneider *et al.*, 2017)

Table 45: Literature searches were performed to determine whether the genes that were most frequently identified as genes of interest within CIS and RIPAT analysis have been reported to have a cancer association

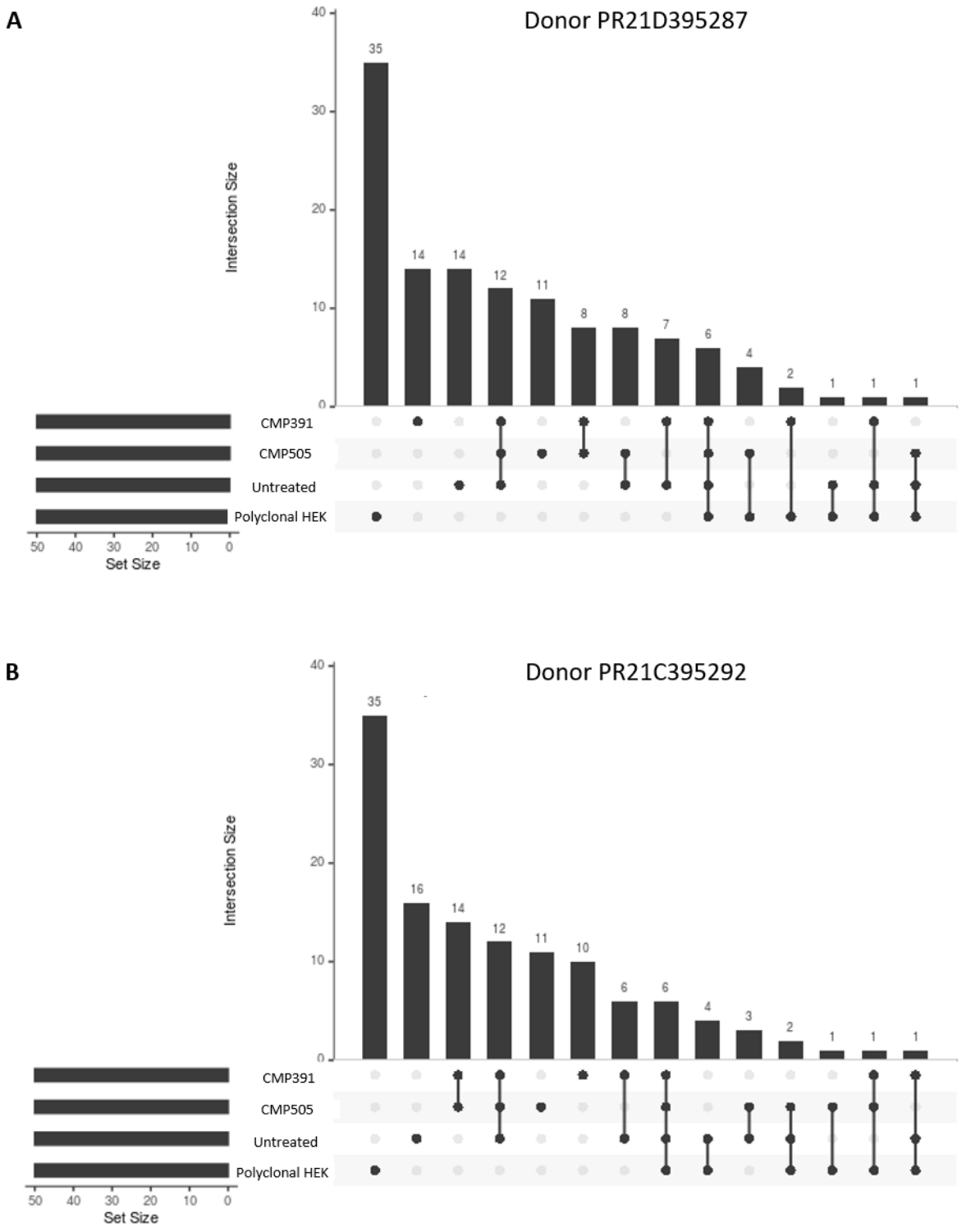

Figure 85: Intersection of the Top 50 Genes Displayed as UpSet Graph

Upset graphs displaying the intersection of the 50 most frequently retrieved genes to a vector integration site annotated using the RIPAT tool comparing A) donor PR21D395287 and B) Donor PR21C395292 T cell samples compared to a Polyclonal HEK control sample.

Visualisation of the intersection of only the top 50 most common gene names identified close to integration sites demonstrated that Polyclonal HEK cell samples had the highest number of unique insertion sites (35), with the most common shared genes being between the treatment conditions for each donor. This indicates that host cell type does impact upon vector integration.

4.3.4. Discussion

The experiments performed within this chapter have enabled the identification of compounds with the potential to enhance lentiviral transduction of T cells. The application of transduction enhancer compounds to the manufacturing process or T-cell based gene therapies would enable the reduction of the MOI used (and therefore the volume of lentiviral vector), resulting in reduced manufacturing costs. In addition, use of reduced vector volumes may also reduce the risk of potential insertional mutagenesis.

Transduction enhancing compounds are particularly beneficial for second- and third-generation cell therapy products, in which additional features, including safety switches and tumour microenvironment manipulators, are included within the construct design, resulting in a large vector packaging size which reduces the efficiency of transduction (Sweeney & Vink, 2021). Multiple studies have demonstrated the potential for transduction enhancing reagents, including polycations, bridging molecules and poloxamers, to be used to improve viral vector transduction of mammalian cells (Cornetta & Anderson, 1989; Hodgson & Solaiman, 1996; Höfig *et al.*, 2012; Amadeo *et al.*, 2022; Strack *et al.*, 2022), however there is limited information on their impact upon a T cell gene therapy product. Two commercially available transduction enhancing reagents, Vectofusin-1® and LentiBOOST®, have shown promising results within studies assessing their suitability for the clinical manufacture of CAR T cell products (Radek *et al.*, 2019; Kim-Hoehamer *et al.*, 2022), however proprietary license fees may limit their use within the GSK manufacturing process due to cost implications, making it beneficial for GSK to search within their compound library for transduction enhancing compounds.

In order to take advantage of the benefits provided by the use of a transduction enhancing compound, it was important to investigate the risks and potential adverse effects that compounds could have on the manufacture of T cell products.

As was discussed within chapter 2 (Section 4.2), robust T cell expansion during manufacturing is critical to ensure patients are able to receive a suitable dose and reduces costs through transduction of a lower starting number of cells, which requires less lentiviral vector. Therefore it was essential to determine the impact that compounds were having upon the fold expansion of T cell populations. Within section 4.2.3.2, experimental data demonstrated that average fold expansions would range between 30 – 60-fold, when G-REX® culture vessels were used. The lower end of this range was applied as the threshold within transduction enhancer fold expansion analysis to provide an indication as to whether compound treatment was impacting upon fold expansion rates. Only two of the six final shortlisted compounds fell below this fold expansion threshold, with CMP391 and CMP816 reaching an average fold expansion of 20.2 and 27.5 respectively when the single donor outlier is removed from the dataset. CMP391 was chosen as one of the two final candidate compounds despite this slight reduction of fold expansion, with analysis of the impact on fold expansion within a larger number of donors still pending. If a slight reduction in fold expansion was observed within a larger poor of donors, a cost analysis would be required to determine whether the improvements in transduction efficiency achieved were sufficient to overcome this slight reduction in fold expansion. It would also be important to investigate whether CMP391 resulted in even further reductions in the rate of fold expansion when patient T cells are used within the production.

The cytotoxic functionality (or potency) of the T cell populations was another aspect that needed to be assessed to ensure that compound treatment did not detrimentally impact upon the ability of the T cell populations to kill antigen expressing cells. xCELLigence® assays were used to compare the potency of T cell populations, with all T cell populations normalised to the same transduction efficiency as the relevant untreated transduced control population. It was important that assays were set up in this manner, as improved cytotoxicity would always be expected from T cell populations with an increased frequency of transduced T cells, however the potency of each T cell may be reduced compared to an untreated transduced control population. The majority of the compound treatments tested did not adversely impact

upon the cytotoxic functionality of the T cell populations, with similar KT_{50} rates for all of the populations.

Interestingly, despite the cytotoxicity of T cell populations remaining similar to that of the untreated control population, there were some observed differences in the production of IFN-γ, with a lower production in compound treated T cell populations compared to the untreated transduced control. Although the reduction in IFN-γ production was not statistically significant for the treatment groups (apart from CMP391 at 24 hours), this observed trend in reduced IFN-γ concentration could be biologically relevant. Autocrine production of IFN-γ by CD8+ T_{EFF} has been shown to be important *in vivo* to maintain CD8+ T_{EFF} function, motility and cytotoxicity (Bhat *et al.*, 2017). Therefore, a reduction in the ability of T cells to produce IFN-γ may impact upon the persistence and *in vivo* functionality of compound treated T cell populations. It will be of importance to keep these results in mind for future studies in which comparisons between untreated and transduction enhancer treated T cell populations will be investigated *in vivo.*

The impact that transduction enhancing compounds have upon the differentiation of T cell populations could be a factor contributing towards this reduction in IFN-γ production. Upon differentiation from naïve CD8+ T cells, CD8+ T cells differentiate into T_{EFF} subsets before differentiating into long term memory subsets. All CD8+ T cell subsets apart from naïve CD8+ T cells can produce IFN-γ, TNF and IL-2 (Kaech *et al.*, 2002), with CD8+ T_{EFF} producing the highest levels of IFN-γ and memory CD8+ T cells producing higher levels of IL-2, which aids in the differentiation of effector T cells into additional memory T cells (Westerhof *et al.*, 2019). This would correlate with the results observed within these experiments, with the highest frequency of CD8+ T cells, both effector and stem cell memory, observed within the CMP037 treated T cell population, which had the highest IFN-γ concentration after 24 hours of co-culture out of all of the compound treated T cell populations, potentially due to the fast cytotoxicity exhibited by the prevalent CD8+ T_{EFF} population. Despite having a higher frequency of CD8+ T cells overall, the CMP037 treated populations did not produce IFN-γ levels higher than the untreated and poloxamer treated T cell populations. Around 15% of both the untreated and poloxamer treated T cell populations consisted of effector memory and effector CD8+ T cells, both of which are known to produce the highest levels of IFN-γ compared to the other T cell subsets, which could have boosted IFN-γ

production above that seen within the CMP037 treated populations which demonstrated a particularly high frequency of CD8+ T_{SCM} population that are known to produce lower levels of IFN-γ compared to the other T cell subsets (Pilipow *et al.*, 2018). CMP391 treated T cell populations had the lowest frequency of CD8+ T cells, and were also found to produce the lowest levels of IFN-γ. Interestingly, CMP076 treated T cell populations, which had only a frequency of CD8+ T cells just above that observed within CMP391 treated T cell populations produced much higher levels of IFN-γ. It would appear that this response may correlate with the frequency of CD8+ effector memory T cells within the population, as the three compound treated populations with the lowest frequency of CD8+ T_{EM} cells (CMP391, CMP816 and CMP505) all displayed the lowest concentration of IFN-γ production after 48 hours of co-culture.

It would be of interest to investigate the response of these compound treated populations *in vivo* to further determine the impact that these changes in phenotype may be having. As it was previously discussed, T_{EFF} and T_{EM} CD8+ T cells have been shown to display high levels of cytotoxicity and cytokine production *in vitro,* but T_{CM} and T_{SCM} have been shown to have preferable response rates *in vivo (Berger et al., 2008; Hinrichs et al., 2011; Gattinoni et al., 2012).* In addition to this, T_{SCM} have been shown to be essential for the persistence of the therapy (McLellan & Ali Hosseini Rad, 2019), and are undergoing extensive research due to their ability for self-renewal and capability to differentiate into both long-lived T_{CM} and short-lived T_{EFF}. For this reason, CMP391 treated T cells, despite being one of the final candidates chosen for further research, may not be clinically viable due to the reduction of the CD8+ T_{SCM} population that was observed. This could result in a less durable product, particularly if both the lower fold expansion and decreased IFN-γ production that were observed within these studies were confirmed to be an issue within future studies. In terms of impact upon differentiation phenotype, CMP037 would have been the most interesting treatment group to have carried through into further analysis due to the observed increase in both the T_{SCM} and T_{EFF} populations, which may have translated into a highly efficacious and persistent therapy. However, due to issues with DMSO stability, *in silico* toxicity and synthesis complexity, CMP037 was not a viable option for large-scale manufacture. The other aspect that is not able to be investigated fully *in vitro* is the impact of the CD4+ T cell populations on the cytotoxic functionality of T cells. It is

known the helper CD4+ T cells are essential for the continued persistence and cytotoxicity *in vivo* (Berger *et al.*, 2008; Louis *et al.*, 2011), and the impact that CD4+ differentiation subsets may be having may not be immediately apparent within *in vitro* studies.

For the two final candidate compounds (CMP505 and CMP391), investigation of the impact upon lentiviral vector insertion site was performed to increase the understanding as to the effect that compound treatment may have upon the pattern of lentiviral vector integration. As the mode of action of transduction enhancement for the compounds is not yet understood, there is the possibility that compound treatment could cause differential expression of factors that aid pre-integration complex binding, resulting in distinct patterns of integration.

Two methods of analysis were utilised within this study to identify genes of interest, firstly CIS analysis was utilised to identify CIS's close to insertion sites and secondly a RIPAT analysis was performed to identify genes and transcription start sites nearest to insertion sites irrespective of whether they have previously been associated with cancer. Both methods have advantages and disadvantages, the CIS method enables analysis of potentially significant genes of interest, as only those that have been independently identified in multiple tumours should be highlighted, which helps to reduce the risk of false positives. However, with this method you may miss novel insertion sites that have not been previously identified and could be highlighted using RIPAT analysis, which highlights all genes and transcription start sites close to the insertion site.

The CIS analysis method identified that the highest number of 100kb peaks were observed within the CMP391 treated T cell populations. However, comparison of the three T cell populations within each donor demonstrated that the CIS's were frequently shared between the three populations, indicating that there was little difference between the untreated transduced and compound treated populations. The top 10 genes identified by both methods of analysis demonstrated a correlation with genes that have been previously identified as CIS's within T cells (Biffi *et al.*, 2011), indicating the compound treatment was having little impact on lentiviral vector integration at a global level. Visualisation of the intersection of the top 50 genes most frequently

identified as being close to the integration site demonstrated that the highest number of shared insertion sites was between the T cell samples (Figure 85), correlating with the findings of the Biffi *et al.* paper which indicates that host cell type does somewhat dictate the integration pattern of the vector.

A caveat to these methods of analysis is that the closest genes to the insertion sites may not be the only genes impacted by the insertion, as it has been noted that vector integrations may impact upon the functionality of genes located far away from the insertion site (Singhal *et al.*, 2011), and may even impact upon multiple genes. Within a study performed by Ha *et al.* multiple genes within the vicinity of a Bcl-xL RVV insertion site were able to influence haematopoiesis, with co-operative genes able to recover functionality if one was affected by an integration (Ha *et al.*, 2021). This adds a layer of complexity to the analysis, as integration site influence on distant genes could lead to oncogenesis that would not have been identified based on CIS analysis.

An additional aspect to consider is the fact that multiple oncogenic insertions may be identified within any cell therapy production; however only a limited number of these oncogenic insertions lead to the development of tumours. Table 45 highlights any cancer associations described within the literature for the identified genes, however this does not mean that the insertion would lead to the development of cancer. This was demonstrated within the Bruce Levine study, in which an insertion within the cancer associated *tet2* gene, resulted in clonal dominance with therapeutic benefit rather than oncogenesis (Fraietta *et al.*, 2018). As was described by Hanahan and Wienberg, the development of tumours is believed to be a multistep process in which cells must acquire a number of biological capabilities to progress into oncogenic cells (Hanahan & Weinberg, 2011). The eight hallmarks of cancer identified by Hanahan and Weinberg are highlighted within Figure 86, and demonstrate that a single insertion within a CIS may not result in the number of cell changes required to lead to oncogenesis. This element of chance that contributes to oncogenesis is also highlighted within clinical trials, for example within the X-SCID trials (Hacein-Bey-Abina *et al.*, 2003; Gaspar *et al.*, 2004), a total of 20 patients were enrolled but only 5 patients developed leukaemia.

If time had permitted, I would have fully characterised the genes that were most frequently impacted by vector integration, most notably NPLOC4, KDMA2 and PACS1.

It would have been of interest to determine the relative expression of each gene and the pathways impacted by changes in gene expression, to gain a wider understanding of how integrations close to these genes could potentially increase the risk of tumourigenesis. In light of recent studies demonstrating the influence of DNA methylation profiles upon CAR T treatment efficacy (Garcia-Prieto *et al.*, 2022), it would have been of interest to investigate how the compounds impacted upon the epigenetic status of the transduced T cells, and whether any changes may boost the therapeutic response in patients.

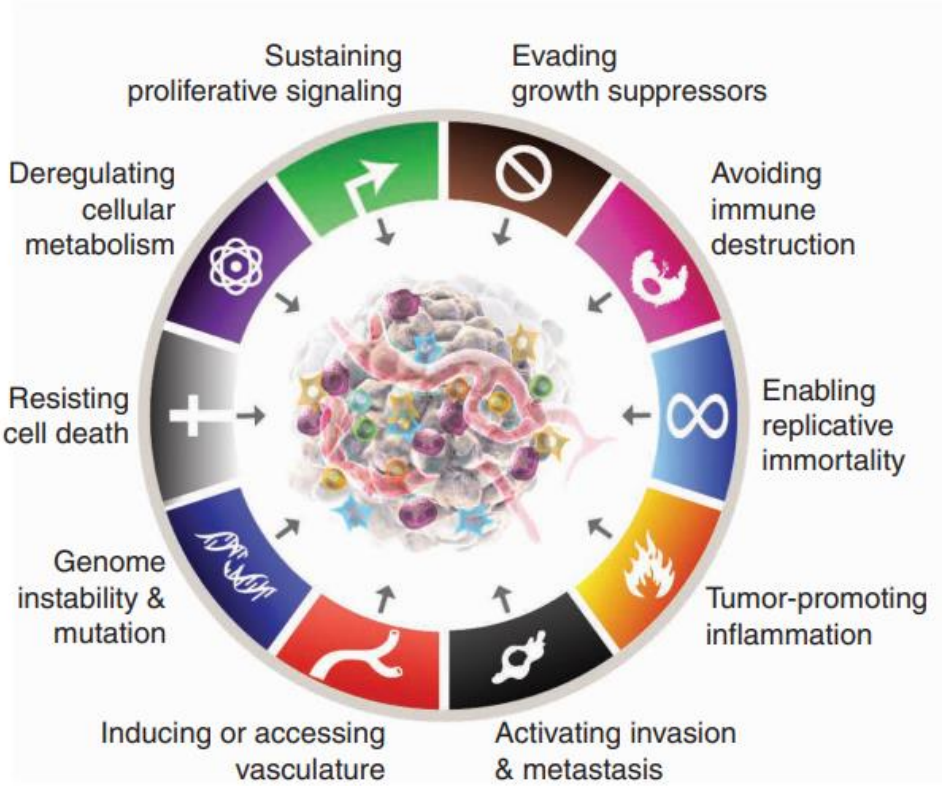

Figure 86: Hallmarks of Cancer (Hanahan, 2022)

Eight biological capabilities that were required for the formation of tumours were described by Hanahan and Weinberg.

As differentiation between the compound treated and untreated T cell populations was difficult based on CIS and RIPAT analysis, a further study was planned to investigate the impact that the compound treatment was having upon the activation of genes within T cells. Samples from T cell populations will be taken at early activation time points, including pre-activation; post-activation but pre-compound addition; 6 hours

post-transduction, 10 hours post-transduction and 24 hours post-transduction, to undergo RNA-Seq analysis. These results would enable determination as to whether compound treatment is leading to differential gene expression within the T cell populations. As lentiviral vectors are known to preferentially integrate within actively transcribed genes, a differential gene activation could lead to previously unactivated genes being activated within compound treated populations, resulting in a distinct integration site. These results may correlate with those of the Diechmann study, demonstrating the influence that gene expression profile may have upon LVV integration (Deichmann *et al.*, 2007). Comparisons will be made between the genes identified within the CIS analysis to the gene activation analysis, to determine whether the compound treatments could be impacting upon lentiviral vector integration.

Subsequent to the completion of this thesis, this study was completed and the results have been documented within a scientific paper that is currently under review. Full details of the results will be available upon publication of the paper “Identification of a novel small molecule for enhancing lentiviral transduction of T cells” (Malach, unpublished results), however in brief the results indicate that CMP391 may act as an inhibitor of MDN1, which is a member of the AAA ATPase family, and impact upon ribosome assembly. Within a paper by Chen *et al. (Chen et al., 2018),* compounds known as ribozinoindoles were also identified as MDN1 inhibitors and demonstrated to impact upon ribosome assembly (Chen *et al.*, 2018). It has been shown that inhibition of ribosome activity can impair type I IFN production, enabling the replication of human cytomegalovirus (Bianco & Mohr, 2019) and it is believed that it is this mechanism that may be resulting in the improved transduction efficiency observed when T cells are treated with CMP391.

5. Discussion

The aim of this thesis was to investigate methods by which improvements could be made throughout the early development phase to ensure that constructs progressed into later stages of development are of the highest quality. In order to do so, I chose a selection of attributes defined within the Critical Quality Attributes (CQA) criteria which I hypothesised could be improved within early-stage development. These attributes included the purity, quantity, and potency of the T cell product, which enabled me to focus my research on process improvements that could be made to increase T cell viability, the percentage of CD3+ T cells, the transduction efficiency of CD3+ T cells, the total number of T cells, the cytotoxic functionality of T cells and production of IFN-γ in response to antigen expressing cell lines. In addition to this, I also investigated technology that could be utilised to improve the specificity of constructs that were progressed into later stage development. The investigations performed within this thesis are hoped to enable translation of early-stage development improvements into later stage development processes helping to increase the quality of developed cell therapy product. It is hoped the improvements made will help to reduce the costs associated with early-stage development, and also clinical manufacture, ensuring that a higher number of cell therapy products are able to be made available to patients.

Within Results Chapter 1, I investigated the use of a technology platform known as Retrogenix™ as an early development screening tool, with the intention to determine whether it could be used to help reduce the number of constructs being carried through into later development stages. One of the issues during the early development of cell therapy products is the inability to easily assess the specificity of constructs, which can result in several candidates being progressed to a later stage before off-target binding is identified and flagged. This significantly contributes to the costs associated with early-stage development, as a large pool of candidates undergo functional testing, which contributes to a large investment of time and money to differentiate between constructs and determine which are candidates for progression. As was discussed within Chapter 1, a number of caveats were identified with the Retrogenix™ technology which made it unsuitable for inclusion within late-stage safety studies. This

included the inability to ensure presentation of the target protein in its native form with appropriate glycosylation on the surface of HEK cells, which increased the risk of false negative results in which off-target binding hits were missed. This risk was further exemplified within these studies as a known off-target binding interaction between CAR-A T cells and an off-target protein family member was not identified during the screen.

Despite the caveats in the technology, the investigation did demonstrate its suitability for use as an early development screening tool. The cost per construct is still high, at approximately £5000 per construct, so would need to be used at a stage in which the number of constructs had already been narrowed down to a reduced shortlist, rather than at very early stages of development where the number of constructs remains high. A disadvantage of the Retrogenix™ technology is that it is only suitable for use with CAR T cell products and is not able to be utilised for the screening of engineered TCR T cell products, which require peptide presentation in the context of MHC. Therefore, additional technologies would need to be investigated to enable full cost saving within a department involved in the development of both CAR T and engineered TCR T therapies.

CAR constructs could be initially screened for transduction efficiency, correct expression of the CAR on the surface of T cells, impact upon viability and expansion of the T cell population and cytokine production in response to antigen expressing target cell lines. This would enable constructs in which issues are observed to be discarded at an early stage before significant investment of time. At this point, the shortlist of candidates could be screened with Retrogenix™ to help to ensure that only constructs of the highest quality with no identified off-target binding hits would be progressed into more expensive *in vivo* and safety studies. This is also beneficial as it enables a reduced number of animals to be used within *in vivo* studies, improving study ethics. Any final candidates shortlisted based on the results of Retrogenix™ technology screening would need to be further investigated, as there would always be the potential for off-target binding hits to have been missed within the Retrogenix™ screen. The importance of ensuring the suitability of cell models for safety screens was highlighted within the study performed by Linette *et al.* in which Titin expression was only found upon actively beating cardiomyocytes and not standard cultured cardiomyocytes (Linette *et al.*, 2013), resulting in an off-target binding event being

missed for the MAGE-A3 TCR within safety studies. Therefore, it would be essential for target appropriate cell models to be investigated to further test the safety and specificity of final candidate constructs.

Within Results Chapter 2, I focussed upon manufacturing processes that I hypothesised could be adapted to improve critical quality attributes such as the purity and quantity of T cells within the final product.

The first process that I investigated was the impact that the starting material had upon critical quality attributes. Within a clinical setting, the starting material available for manufacturing of these autologous therapies will be extremely variable, with the cellular composition differing dramatically depending on patient age, ethnicity, tumour type and prior treatments, such as chemotherapy which can lead to low leukocyte counts and cause difficulties during apheresis (Ceppi *et al.*, 2018). This is exacerbated by the fact that enrolment for these clinical trials is limited to those patients who have exhausted all other treatment options. Many clinical trials have investigated the manufacturing success rates associated with different starting materials, including use of PBMC populations (Itzhaki *et al.*, 2020), isolation of bulk CD4+ and CD8+ populations (Brentjens *et al.*, 2013; Grupp *et al.*, 2013) or isolation of specific T cell lineages, such as central memory T cells (Vormittag *et al.*, 2018).

A significant contributor to manufacturing failures is the inability to produce sufficient T cell numbers to provide the required dose of cell therapy (Lam *et al.*, 2020), with Novartis reportedly facing issues with the number of inactive cells during the manufacture of Kymriah® leading to the product being given compassionately to patients despite being out-of-specification (Palmer, 2018). This attribute is reliant upon the expansion of the T cell product during *ex vivo* manufacture. Additional selection processes prior to transduction and expansion of the product could exacerbate the rate of failure due low recoveries leading to low starting cell numbers, with the inability to expand sufficiently to reach required dosages. Studies may try to overcome this issue through extension of the expansion period; however, this risks the exhaustion of T cells within the product preventing efficacy upon infusion, in addition to risking the health of terminal patients who may be requiring treatment as quickly as possible to ensure complete response and prevent further disease progression.

It had been noted that use of PBMC populations as a starting material could increase the rate of manufacturing failures due to the impact of monocytes upon T cell expansion (Stroncek *et al.*, 2016). However, the results of studies performed within this thesis demonstrated no significant difference between the fold expansion of PBMC populations and isolated CD4+/CD8+ T cell populations, with the only significant decrease in fold expansion observed within the CD4+ T cell population cultured in isolation. The use of either 100IU/mL of IL-2 or 10ng/mL IL-7 & IL-15 also did not appear to impact upon the fold expansion of the final T cell product. Improvements in the fold expansion of the T cell product were only observed within the optimisation of small-scale culture vessel use, in which use of G-REX® culture vessels significantly improved upon the fold expansion observed within standard flat bottom culture plates that were previously used at small-scale. There were not significant differences between the fold expansion of T cell products at small-scale (G-REX® plates) compared to large-scale (CliniMACs Prodigy®), demonstrating the potential to use small-scale productions to optimise culture conditions and provide translatable data for large scale productions. Together, these results suggest that in terms of fold expansion of the final drug product, use of a bulk starting population (either PBMCs or CD4+/CD8+ T cells) and either IL-2 or IL-7/IL-15 would not impact upon the final number of T cells. Impact upon fold expansion at small-scale was more dependent upon the culture vessel system used, however there were no significant increases in fold expansion compared to the large-scale CliniMACs Prodigy® process. Overall, this indicated that improvements to the expansion process investigated within this thesis would not lead to improved T cell numbers for the final product produced at large-scale; however, the understanding that process improvements within small-scale culture would be translatable to large-scale culture will help to simplify future investigations into additional factors that could help to improve cell expansion, including additional media supplementation and improvements in gas perfusion. The decreased fold expansion observed when CD4+ T cells were cultured in isolation could indicate that additional selection processes used prior to transduction could impact upon the expansion of the final product, however this would need to be investigated further within a larger pool of donors and using particular T cell subsets of interest such as CD8+ T_{SCM} cells.

With no improvement in the expansion of T cells observed, based on the investigation of the manufacturing processes assessed, I investigated the impact that the T cell product phenotype may be having upon the critical quality attributes of the final product. Studies have demonstrated that reduced doses of T cell products could be efficacious if the phenotype of the T cell population is optimal (Turtle, Hanafi, Berger & Hudecek *et al.*, 2016), however there is not clear evidence on the optimal phenotype of T cell products. This could be due to the large impact that disease burden, antigen expression and immune cell response has upon the outcome for patients – every case is unique, and potentially needs to be treated uniquely. Novartis has developed a CAR-T expansion protocol termed "T-Charge™", which maintains a stem-cell like phenotype within the CAR T product enabling infusion of a low cell dose with high *in vivo* proliferative potential, with reported improvements in patient outcome whilst significantly shortening manufacturing times (Novartis).

Donor to donor variation within the frequency of CD4+ and CD8+ T cells within the lymphocyte population is observed within healthy donors, and is known to be more variable within lymphoma patients (McLellan & Ali Hosseini Rad, 2019) with T cell dysfunction reported within patients suffering from several different types of cancer (Zhang & Liu *et al.*, 2020). During my investigation, I observed that there was a significant difference in the frequency of transduced T cells and the MFI of CAR expression when CD4+ and CD8+ T cells were transduced within a pooled CD4+/CD8+ T cell population. When further investigating the impact that cytokine use may have upon the CD4+ and CD8+ T cell populations, I found that use of IL-7/IL-15 significantly increased the frequency of CD4+ T cells and decreased the frequency of CD8+ T cells, but use of either IL-2 or IL-7/IL-15 did not impact upon the overall transduction efficiency of the populations.

This highlights an important aspect of the manufacturing process that needs to be investigated further – the determination of what is the optimal ratio of CD4+ to CD8+ T cells within the final drug product and how changes within the manufacturing process could be used to positively skew populations towards the optimal ratio. As was previously discussed, Turtle *et al.* demonstrated the feasibility of manufacturing CAR T products at a defined 1:1 ratio of transduced CD4+ to transduced CD8+ T cells with manufacturing success within 90% of the patients. However, it is still not clear whether a 1:1 ratio of CD4+ to CD8+ T cells would be optimal for the T cell product. Studies

have demonstrated the importance of the presence of CD4+ T cells within the infused population, with central memory T cells thought to be particularly beneficial for the long term persistence of therapies (Louis *et al.*, 2011), but it is still not known what frequency of CD4+ T cells are required to have this positive impact. CD8+ T cells are known to be essential for effective cytotoxicity of tumours (Raskov *et al.*, 2021), but it is not known what frequency of CD8+ T cells would be most desirable. There is the risk that infusion of a highly cytotoxic T cell population into a patient with a high disease burden could lead to rapid cytokine release and the detrimental effect of cytokine release syndrome. Within these patients, it could be more beneficial to infuse a product with a lower frequency of cytotoxic CD8+ T cells and a higher frequency of CD4+ T cells to aid with the creation of memory T cells to help with the slow but persistent cytotoxicity of tumours.

Adding to the complexity of optimal product phenotype and its impact upon therapy efficacy, is the additional implication that the differentiation subsets of CD4+ and CD8+ T cells may have. Naïve, stem cell memory and central memory T cell populations have all been demonstrated to have superior functionality *in vivo* compared to effector memory and effector T cell populations, which demonstrate superior cytotoxic functionality *in vitro*. It has been hypothesised that this could be due to the inability of effector T cell subsets to effectively create a niche upon infusion (McLellan & Ali Hosseini Rad, 2019). An additional issue with effector T cell subsets is their increased susceptibility to exhaustion and activation induced cell death, which rapidly reduces their persistence *in vivo*, which is why the presence of a memory T cell population that can continually re-populate the effector pool of T cells is beneficial for the efficacy of the treatment (McLellan & Ali Hosseini Rad, 2019). Within this thesis, I investigated the impact that cytokine use had upon the prevalence of differentiation subsets within the CD4+ and CD8+ T cell populations and discovered the predominance of central memory and effector memory phenotypes. Choice of cytokine appeared to only be having a significant impact upon the differentiation subsets within the CD4+ population, with IL-2 significantly increasing the frequency of CD4+ central memory T cells and decreasing the frequency of CD4+ effector memory T cells. This was seen to translate to the concentration of IFN-γ produced when T cell populations were co-cultured with antigen expressing cell lines, with decreased IFN-γ production from

populations cultured on IL-2 in which there was a decreased CD4+ effector memory T cell population.

Further research upon the impact that phenotype has upon the efficacy of the T cell product would be important and could help to define the optimal T cell product composition. However, it must be balanced with the increased difficulties that creating products of defined ratio would have upon the manufacturing process. Additional selection methods prior to transduction would add complexity to the manufacturing process, and would also not be possible within all patients in which disease state or prior treatments may lead to variable lymphocyte composition – for example, studies have demonstrated that B cell lymphoma patients can typically have increased frequency of CD8+ T cells, but low frequency of naïve T cells upon apheresis (Sommermeyer *et al.*, 2016). If T cell populations were required to be cultured in isolation, for example CD4+ and CD8+ T cells expanded separately, prior to being combined at defined ratios prior to infusion, this could lead to difficulties with the expansion of the product – with decreased fold expansion of CD4+ T cells cultured alone observed within the studies performed within this thesis, and also reports of increased expansion periods of up to 10 extra days required when central memory T cells are expanded in isolation compared to standard PBMC expansion (McLellan & Ali Hosseini Rad, 2019). Increased expansion periods could result in T cells within the final product being more prone to exhaustion and activation induced cell death upon infusion to patients, would increase treatment time for patients in potentially critical condition and increase manufacturing costs. Finally, advanced manufacturing techniques would require the additional training of doctors providing the therapy to patients to ensure that products are provided at the appropriate ratio and dosage, which risks an increased number of errors upon delivery of the therapy to patients. With such a focus on decreasing the vein-to-vein time for cell therapy products, the increased manipulation of a product may not be beneficial and requires significantly more research prior to implementation.

Within Results Chapter 3, I investigated the use of transduction enhancing compounds to improve T cell transduction efficiency to ensure T cell therapy products are able to meet the required critical quality attributes. With improving technologies allowing the

introduction of safety features within both CAR T and engineered TCR T cell construct designs, the size of packaging inserts within lentiviral vectors are increasing in size – which is known to reduce the efficiency of T cell transduction (Sweeney & Vink, 2021). This results in an increased MOI being required to achieve an acceptable level of transduction within patient samples, increasing the risk of the integration of multiple vector copies and also increasing manufacturing costs by increasing vector volume requirements. It would be important that transduction enhancing compounds were only utilised within instances in which lentiviral vector transduction efficiency is poor, preventing a suitable frequency of transduced T cells to be produced within the product. It is not understood how infusion of a highly transduced population could impact upon the efficacy and potential toxicity of a treatment, with T cell dosages potentially requiring adjustment to prevent cytokine release syndrome.

Transduction enhancing reagents, including polycationic reagents, bridging molecules and poloxamers, have been shown to enhance viral vector transduction of mammalian cells in multiple studies (Cornetta & Anderson, 1989; Hodgson & Solaiman, 1996; Höfig *et al.*, 2012; Amadeo *et al.*, 2022; Strack *et al.*, 2022), however data specifically related to T cell transduction enhancement, particularly within a GMP-compliant setting is limited. The most promising commercially available transduction enhancing reagents are Vectofusin-1®, a histidine-rich cationic peptide that promotes vector and cell membrane fusion through the production of alpha-helical nanofibrils which has been demonstrated to be suitable for use within the closed-system CliniMACS Prodigy® for the transduction of T cells (Radek *et al.*, 2019), and LentiBOOST® , a poloxamer that increases cell membrane permeability to increase viral particle uptake (Strack *et al.*, 2022), which has been used successfully in the manufacture of GMP-compliant CD19-CAR T cells (Kim-Hoehamer *et al.*, 2022). However, proprietary licenses result in increased cost to manufacture if commercially available products are used, for this reason, it was beneficial for GSK to search within their compound library for transduction enhancing compounds.

Within this study, two candidate compounds were able to be identified which were able to meet the desired criteria. However, the data gathered did raise additional questions that would need further investigation prior to the progression of transduction enhancer use.

Firstly, how do transduction enhancing compounds impact upon the phenotype of T cell populations? It was observed within this study that each of the six shortlisted compounds demonstrated different impacts upon the composition of the T cell subsets. As was previously discussed, it is not currently known what T cell phenotype would be the most desirable for the final drug product – however, it would be of importance to investigate this further, especially as additional data is gathered through clinical trials to help define the optimal T cell product. If use of a transduction enhancing compound was able to both improve T cell transduction efficiency and also push the T cell population towards a phenotype that was deemed most desirable, such as improving the frequency of CD8+ T_{SCM} populations, then the use may be more beneficial to the improvement of T cell therapies than other manufacturing changes such as use of defined T cell ratios. If no impact upon fold expansion was observed within the compound treated populations, then decreased vein to vein time could be preserved whilst maintaining optimal T cell phenotypes – whereas use of defined T cell populations could lead to increased expansion time requirements.

How safe are transduction enhancing compounds? Within this study, I investigated the impact that transduction enhancing compounds had upon the integration of lentiviral vectors and also designed a further study to enable comparison of CIS's to the activation of genes within T cells treated with candidate compounds. These studies address an important safety question, as to whether increased transduction efficiency is leading to increased vector integrations and integrations within locations that could result in oncogenesis. However, there are additional safety questions that need to be addressed, for example how much residual compound remains within the culture at the point of infusion? Would compound remain within the product in sufficient quantities to cause adverse effects in patients? In addition to this, how would the changing phenotype of the T cell population impacts upon the safety of the final T cell product? Further studies will need to be planned to investigate these questions.

How do compounds impact upon the manufacturing process of T cell therapies? Within this study, I investigated the impact upon expansion and viability within a small-scale culture process. However, this analysis would now need to be performed at large-

scale to determine the feasibility of introducing a compound into a closed manufacturing system, with potential issues including compound sticking to tubing. Studies will need to be performed to assess whether the results gathered at small-scale translate to large-scale productions. In addition to this, cost analysis will need to be performed to determine whether the introduction of compound manufacture at GMP scale and addition of an extra step within the manufacturing process provides a beneficial cost saving by significantly reducing vector volume requirements.

Finally, how do these compounds impact upon patient T cells? All of the studies described here were carried out using T cells isolated from healthy donors. As it has already been described, the composition and stability of T cells from patients is vastly different – therefore it would be essential to test the impact that these compounds have upon the viability and expansion of patient T cells. If there were significant impact on the expansion of patient T cells, then it would negate the benefit of being able to reduce the MOI used, as a higher starting cell number would be required thus increasing vector volume requirements. This could also cause issues as patients with advanced disease progression may not have sufficient T cell numbers to allow a higher starting number of T cells, resulting in increased expansion times and potentially the inability to meet the critical quality attribute of the number of transduced T cells required. It would also be of importance to investigate the impact that compounds have upon the exhaustion status of T cell products to ensure *in vivo* efficacy is maintained.

Overall, this thesis has provided a starting point to enable further investigation of aspects of the manufacturing process that can be improved to increase the quality of a final drug product and enable critical quality attributes to be met. I have been able to evaluate the Retrogenix™ technology platform to enable improved screening of T cell constructs increasing the quality of constructs progressing to early-stage development; investigate aspects of the manufacturing process that could be modified to help improve the expansion and purity of T cell products; and also investigated the use of transduction enhancing compounds for the improvement of transduction efficiency. The aspects investigated will help to improve construct quality during development, but also reduce the overall cost of goods by improving manufacturing costs. Further investigation is still required to determine the impact that these improvements would have upon patient T cell samples, and many aspects will require continual investigation as further research is gathered from ongoing clinical trials.

Table 46: Summary of Thesis Impact

Thesis Section	Short Term Impact	Long Term Impact
Section 4.1: Retrogenix™ Evaluation	Inclusion of Retrogenix™ platform into CGT strategy for the screening of constructs in early development	Closure of GSK's CGT department discontinued use of Retrogenix™. However, inclusion of Retrogenix™screening within early development of T cell engager bispecific antibodies was suggested and has been implemented
	Identification and validation of off-target binding hit led to the closure of a project	Project was closed
Section 4.2.3.1: Starting Material Impact	Data gathered provided confidence that use of either PBMCs or CD4/CD8 T cells could be utilised for T cell productions	Recommended standardisation of production methods through CD4/CD8 T cell isolation to mimic clinical manufacturing methods. CD4/CD8 T cell isolation was implemented for all T cell productions.
Section 4.2.3.2: Culture Vessel Impact	G-REX® vessel culture method was implemented as the standard T cell production method at small scale	Continued use of G-REX® vessels for both small and large scale T cell productions

	Data gathered provided confidence in the translatability between small scale and large scale productions. Further optimisations were performed at small scale to improve large scale production methods	Further studies at small scale were ongoing to optimise large scale production methods, however these were ceased with the closure of CGT at GSK
Section 4.2.3.3: Cytokine Impact	No change to production methods were implemented	-
Section 4.3: Transduction Enhancing Compounds	Further studies were performed to determine suitability of compounds for large scale CliniMACS™ Prodigy productions, with initial results showing successful T cell productions at large scale	Studies were ceased due to the closure of the CGT department. Scientific paper in process of being written to publicise the results of studies allowing implementation of transduction enhancing compound use in other companies.

Table 46: The studies performed within this thesis have enabled the implementation of a number of improvements to GSKs cell product production methods and helped to reduce development costs through the reduction in early development candidate construct numbers. Due to the closure of the CGT department at GSK, ongoing studies were ceased. Process improvements may transferred to partner companies as part of technology transfers.

6. References

Abou-El-Enein, M., Elsallab, M., Feldman, S.A., Fesnak, A.D., Heslop, H.E. & Marks, P. et al. (2021) Scalable Manufacturing of CAR T cells for Cancer Immunotherapy. *Blood Cancer Discovery*, 2(5), 408–422. Available from: https://doi.org/10.1158/2643-3230.BCD-21-0084.

Ahmed, N., Brawley, V.S., Hegde, M., Robertson, C., Ghazi, A. & Gerken, C. et al. (2015) Human Epidermal Growth Factor Receptor 2 (HER2) -Specific Chimeric Antigen Receptor-Modified T Cells for the Immunotherapy of HER2-Positive Sarcoma. *Journal of Clinical Oncology : Official Journal of the American Society of Clinical Oncology*, 33(15), 1688–1696. Available from: https://doi.org/10.1200/JCO.2014.58.0225.

Aiuti, A., Slavin, S., Aker, M., Ficara, F., Deola, S. & Mortellaro, A. et al. (2002) Correction of ADA-SCID by stem cell gene therapy combined with nonmyeloablative conditioning. *Science*, 296(5577), 2410–2413. Available from: https://doi.org/10.1126/science.1070104.

Akagi, K., Suzuki, T., Stephens, R.M., Jenkins, N.A. & Copeland, N.G. (2004) RTCGD: retroviral tagged cancer gene database. *Nucleic Acids Research*, 32(Database issue), D523-7. Available from: https://doi.org/10.1093/nar/gkh013.

Allen, E.S., Stroncek, D.F., Ren, J., Eder, A.F., West, K.A. & Fry, T.J. et al. (2017) Autologous lymphapheresis for the production of chimeric antigen receptor T cells. *Transfusion*, 57(5), 1133–1141. Available from: https://doi.org/10.1111/trf.14003.

Amadeo, F., Hanson, V., Murray, P. & Taylor, A. (2022) DEAE-Dextran Enhances the Lentiviral Transduction of Primary Human Mesenchymal Stromal Cells from All Major Tissue Sources Without Affecting Their Proliferation and Phenotype. *Molecular Biotechnology*. Available from: https://doi.org/10.1007/s12033-022-00549-2.

Amirache, F., Lévy, C., Costa, C., Mangeot, P.-E., Torbett, B.E. & Wang, C.X. et al. (2014) Mystery solved: VSV-G-LVs do not allow efficient gene transfer into unstimulated T cells, B cells, and HSCs because they lack the LDL receptor. *Blood*, 123(9), 1422.

Bajgain, P., Mucharla, R., Wilson, J., Welch, D., Anurathapan, U. & Liang, B. et al. (2014) Optimizing the production of suspension cells using the G-Rex "M" series. *Molecular Therapy - Methods & Clinical Development*, 1, 14015. Available from: https://doi.org/10.1038/mtm.2014.15.

Baum, C. (2007) What are the consequences of the fourth case? *Molecular Therapy*, 15(8), 1401–1402. Available from: https://doi.org/10.1038/sj.mt.6300263.

Baum, C., Dullmann, J., Li, Z., Fehse, B., Meyer, J. & Williams, D.A. et al. (2003) Side effects of retroviral gene transfer into hematopoietic stem cells. *Blood*, 101(6), 2099–2114. Available from: https://doi.org/10.1182/blood-2002-07-2314.

Beatty, G.L. & O'Hara, M. (2016) Chimeric antigen receptor-modified T cells for the treatment of solid tumors: Defining the challenges and next steps. *Pharmacol Ther*, 166, 30–39. Available from: https://doi.org/10.1016/j.pharmthera.2016.06.010.

Bechara, E.G., Sebestyén, E., Bernardis, I., Eyras, E. & Valcárcel, J. (2013) RBM5, 6, and 10 differentially regulate NUMB alternative splicing to control cancer cell

proliferation. *Molecular Cell*, 52(5), 720–733. Available from: https://doi.org/10.1016/j.molcel.2013.11.010.
Benedicenti, F.V., Calabria, A., Cesana, D., Albertini, A., Tenderini, E. & Spinozzi, G. et al. (2022) Sonication Linker Mediated-PCR (SLiMPCR), an Efficient Method for Quantitative Retrieval of Vector Integration Sites. *Molecular Therapy*, 29(4), 417 [Accessed January 2023].
Bentzen, A.K. & Hadrup, S.R. (2019) T-cell-receptor cross-recognition and strategies to select safe T-cell receptors for clinical translation. *Immuno-Oncology Technology*, 2, 1–10. Available from: https://doi.org/10.1016/j.iotech.2019.06.003.
Berger, C., Jensen, M.C., Lansdorp, P.M., Gough, M., Elliott, C. & Riddell, S.R. (2008) Adoptive transfer of effector CD8+ T cells derived from central memory cells establishes persistent T cell memory in primates. *Journal of Clinical Investigation*, 118(1), 294–305. Available from: https://doi.org/10.1172/JCI32103.
Berois, N., Pittini, A. & Osinaga, E. (2022) Targeting Tumor Glycans for Cancer Therapy: Successes, Limitations, and Perspectives. *Cancers*, 14(3). Available from: https://doi.org/10.3390/cancers14030645.
Bersenev, A. (2017) CAR-T cell manufacturing: time to put it in gear. *Transfusion*, 57(5), 1104–1106. Available from: https://doi.org/10.1111/trf.14110.
Bhat, P., Leggatt, G., Waterhouse, N. & Frazer, I.H. (2017) Interferon-γ derived from cytotoxic lymphocytes directly enhances their motility and cytotoxicity. *Cell Death & Disease*, 8(6), e2836. Available from: https://doi.org/10.1038/cddis.2017.67.
Bianco, C. & Mohr, I. (2019) Ribosome biogenesis restricts innate immune responses to virus infection and DNA. *ELife*, 8. Available from: https://doi.org/10.7554/eLife.49551.
Biffi, A., Bartolomae, C.C., Cesana, D., Cartier, N., Aubourg, P. & Ranzani, M. et al. (2011) Lentiviral vector common integration sites in preclinical models and a clinical trial reflect a benign integration bias and not oncogenic selection. *Blood*, 117(20), 5332–5339. Available from: https://doi.org/10.1182/blood-2010-09-306761.
BioPharm International (2021) *Lonza and Sheba Medical Center Demonstrate Successful Cell Therapy Results with Cocoon Automated Platform*. Available from: https://www.biopharminternational.com/view/lonza-and-sheba-medical-center-demonstrate-successful-cell-therapy-results-with-cocoon-automated-platform [Accessed 9th October 2021].
BioRad (2017) *Cell Frequency: Flow Cytometry*. Available from: https://www.bio-rad-antibodies.com/static/2017/flow/flow-cytometry-cell-frequency.pdf [Accessed 14th March 2019].
Blaese, R.M., Culver, K.W., Miller, A.D., Carter, C.S., Fleisher, T. & Clerici, M. et al. (1995) T Lymphocyte-Directed Gene Therapy for ADA- SCID: Initial Trial Results After 4 Years. *Science*, 270(5235), 475–480. Available from: https://doi.org/10.1126/science.270.5235.475.
BlueBird Bio (2022) *Cellular, Tissue, and Gene Therapies Advisory Committee Meeting: ELIVALDOGENE AUTOTEMCEL BRIEFING DOCUMENT*. Available from: https://www.fda.gov/media/159012/download.
BlueBird Bio *bluebird bio Provides Updated Findings from Reported Case of Acute Myeloid Leukemia (AML) in LentiGlobin for Sickle Cell Disease (SCD) Gene*

Therapy Program. Available from: https://investor.bluebirdbio.com/news-releases/news-release-details/bluebird-bio-provides-updated-findings-reported-case-acute [Accessed 27th September 2021].
Bokhoven, M., Stephen, S.L., Knight, S., Gevers, E.F., Robinson, I.C. & Takeuchi, Y. et al. (2009) Insertional gene activation by lentiviral and gammaretroviral vectors. *J Virol*, 83(1), 283–294. Available from: https://doi.org/10.1128/JVI.01865-08.
Boyiadzis, M.M., Dhodapkar, M.V., Brentjens, R.J., Kochenderfer, J.N., Neelapu, S.S. & Maus, M.V. et al. (2018) Chimeric antigen receptor (CAR) T therapies for the treatment of hematologic malignancies: Clinical perspective and significance. *Journal for Immunotherapy of Cancer*, 6(1), 137. Available from: https://doi.org/10.1186/s40425-018-0460-5.
Braun, C.J., Boztug, K., Paruzynski, A., Witzel, M., Schwarzer, A. & Rothe, M. et al. (2014) Gene therapy for Wiskott-Aldrich syndrome--long-term efficacy and genotoxicity. *Sci Transl Med*, 6(227), 227ra33. Available from: https://doi.org/10.1126/scitranslmed.3007280.
Brentjens, R., Davila, M.L., Riviere, I., Park, J., Wang, X. & Cowell, L.G. et al. (2013) CD19-targeted T cells rapidly induce molecular remissions in adults with chemotherapy-refractory acute lymphoblastic leukemia. *Science translational medicine*, 5(177), 177ra38-177ra38. Available from: https://doi.org/10.1126/scitranslmed.3005930.
Brudno, J.N. & Kochenderfer, J.N. (2016) Toxicities of chimeric antigen receptor T cells: recognition and management. *Blood*, 127(26), 3321–3330. Available from: https://doi.org/10.1182/blood-2016-04-703751.
Budi, H.S., Ahmad, F.N., Achmad, H., Ansari, M.J., Mikhailova, M.V. & Suksatan, W. et al. (2022) Human epidermal growth factor receptor 2 (HER2)-specific chimeric antigen receptor (CAR) for tumor immunotherapy; recent progress. *Stem Cell Research & Therapy*, 13(1), 40. Available from: https://doi.org/10.1186/s13287-022-02719-0.
Busek, P., Mateu, R., Zubal, M., Kotackova, L. & Sedo, A. (2018) Targeting fibroblast activation protein in cancer - Prospects and caveats. *Frontiers in Bioscience (Landmark Edition)*, 23(10), 1933–1968. Available from: https://doi.org/10.2741/4682.
Cai, Z., Zhai, T., Muhanhali, D. & Ling, Y. (2021) TNRC6C Functions as a Tumor Suppressor and Is Frequently Downregulated in Papillary Thyroid Cancer. *International Journal of Endocrinology*, 2021, 6686998. Available from: https://doi.org/10.1155/2021/6686998.
Cameron, B.J., Gerry, A.B., Dukes, J., Harper, J.V., Kannan, V. & Bianchi, F.C. et al. (2013) Identification of a Titin-derived HLA-A1-presented peptide as a cross-reactive target for engineered MAGE A3-directed T cells. *Science Translational Medicine*, 5(197), 197ra103. Available from: https://doi.org/10.1126/scitranslmed.3006034.
Castella, M., Pujol, R., Callén, E., Trujillo, J.P., Casado, J.A. & Gille, H. et al. (2011) Origin, functional role, and clinical impact of Fanconi anemia FANCA mutations. *Blood*, 117(14), 3759–3769. Available from: https://doi.org/10.1182/blood-2010-08-299917.

Casucci, M., Bondanza, A., Falcone, L., Provasi, E., Magnani, Z. & Bonini, C. (2012) Genetic engineering of T cells for the immunotherapy of haematological malignancies. *Tissue Antigens*, 79(1), 4–14. Available from: https://doi.org/10.1111/j.1399-0039.2011.01799.x.

Casucci, M., Hawkins, R.E., Dotti, G. & Bondanza, A. (2015) Overcoming the toxicity hurdles of genetically targeted T cells. *Cancer Immunology, Immunotherapy : CII*, 64(1), 123–130. Available from: https://doi.org/10.1007/s00262-014-1641-9.

Catapult (2022) *Cell and Gene Therapy Catapult ATMP clinical trials report 2021*. Available from: https://cgt.ams3.cdn.digitaloceanspaces.com/clinical-trials-commentary-final-2021.pdf [Accessed 15th December 2022].

Cavazzana-Calvo, M. (2000) Gene Therapy of Human Severe Combined Immunodeficiency (SCID)-X1 Disease. *Science*, 288(5466), 669–672. Available from: https://doi.org/10.1126/science.288.5466.669.

Cell BioLabs, Inc. (2009) *ViraSafe™ Lentiviral Packaging System, Pantropic: Product Manual*. Available from: https://www.cellbiolabs.com/sites/default/files/VPK-206-virasafe-lentiviral-packaging-system.pdf [Accessed 6 June 2023].

Ceppi, F., Rivers, J., Annesley, C., Pinto, N., Park, J.R. & Lindgren, C. et al. (2018) Lymphocyte apheresis for chimeric antigen receptor T-cell manufacturing in children and young adults with leukemia and neuroblastoma. *Transfusion*, 58(6), 1414–1420. Available from: https://doi.org/10.1111/trf.14569.

Chabannon, C. (2020) *Product Release Tests: Helping Ensure Patient Safety and Guaranteeing Drug Product Quality*. Available from: https://emj.emg-health.com/wp-content/uploads/sites/2/2020/05/CAR-T-From-Bed-to-Bench-and-Back-Again.pdf [Accessed 11th October 2021].

Chandler, R.J., LaFave, M.C., Varshney, G.K., Trivedi, N.S., Carrillo-Carrasco, N. & Senac, J.S. et al. (2015) Vector design influences hepatic genotoxicity after adeno-associated virus gene therapy. *J Clin Invest*, 125(2), 870–880. Available from: https://doi.org/10.1172/JCI79213.

Check, E. (2005) Gene therapy put on hold as third child develops cancer. *Nature*, 433(7026), 561. Available from: https://doi.org/10.1038/433561a.

Chen, F., Fan, Y., Cao, P., Liu, B., Hou, J. & Zhang, B. et al. (2021) Pan-Cancer Analysis of the Prognostic and Immunological Role of HSF1: A Potential Target for Survival and Immunotherapy. *Oxidative Medicine and Cellular Longevity*, 2021, 5551036. Available from: https://doi.org/10.1155/2021/5551036.

Chen, Y.H., Pallant, C., Sampson, C.J., Boiti, A., Johnson, S. & Brazauskas, P. et al. (2020) Rapid Lentiviral Vector Producer Cell Line Generation Using a Single DNA Construct. *Molecular Therapy - Methods & Clinical Development*, 19, 47–57. Available from: https://doi.org/10.1016/j.omtm.2020.08.011.

Chen, Z., Suzuki, H., Kobayashi, Y., Wang, A.C., DiMaio, F. & Kawashima, S.A. et al. (2018) Structural Insights into Mdn1, an Essential AAA Protein Required for Ribosome Biogenesis. *Cell*, 175(3), 822-834.e18. Available from: https://doi.org/10.1016/j.cell.2018.09.015.

Cheng, Y., Li, L., Qin, Z., Li, X. & Qi, F. (2020) Identification of castration-resistant prostate cancer-related hub genes using weighted gene co-expression network analysis. *Journal of Cellular and Molecular Medicine*, 24(14), 8006–8017. Available from: https://doi.org/10.1111/jcmm.15432.

Cohen, A.D., Parekh, S., Santomasso, B.D., Gállego Pérez-Larraya, J., van de Donk, N.W.C.J. & Arnulf, B. et al. (2022) Incidence and management of CAR-T neurotoxicity in patients with multiple myeloma treated with ciltacabtagene autoleucel in CARTITUDE studies. *Blood Cancer Journal*, 12(2), 32. Available from: https://doi.org/10.1038/s41408-022-00629-1.

Comisel, R.-M., Kara, B., Fiesser, F.H. & Farid, S.S. (2021) Lentiviral vector bioprocess economics for cell and gene therapy commercialization. *Biochemical Engineering Journal*, 167, 107868. Available from: https://doi.org/10.1016/j.bej.2020.107868.

Cornetta, K. & Anderson, W.F. (1989) Protamine sulfate as an effective alternative to polybrene in retroviral-mediated gene-transfer: implications for human gene therapy. *Journal of Virological Methods*, 23(2), 187–194. Available from: https://doi.org/10.1016/0166-0934(89)90132-8.

Crise, B., Li, Y., Yuan, C., Morcock, D.R., Whitby, D. & Munroe, D.J. et al. (2005) Simian immunodeficiency virus integration preference is similar to that of human immunodeficiency virus type 1. *Journal of Virology*, 79(19), 12199–12204. Available from: https://doi.org/10.1128/JVI.79.19.12199-12204.2005.

Crompton, J.G., Sukumar, M. & Restifo, N.P. (2014) Uncoupling T-cell expansion from effector differentiation in cell-based immunotherapy. *Immunological Reviews*, 257(1), 264–276. Available from: https://doi.org/10.1111/imr.12135.

Cui, J., Chen, N., Pu, C., Zhao, L., Li, N. & Wang, C. et al. (2022) A phase 1 dose-escalation study of GCC19 CART a novel coupled CAR therapy for subjects with metastatic colorectal cancer. *Journal of Clinical Oncology*, 40(16_suppl), 3582. Available from: https://doi.org/10.1200/JCO.2022.40.16_suppl.3582.

Deichmann, A., Hacein-Bey-Abina, S., Schmidt, M., Garrigue, A., Brugman, M.H. & Hu, J. et al. (2007) Vector integration is nonrandom and clustered and influences the fate of lymphopoiesis in SCID-X1 gene therapy. *Journal of Clinical Investigation*, 117(8), 2225–2232. Available from: https://doi.org/10.1172/JCI31659.

Delville, M., Soheili, T., Bellier, F., Durand, A., Denis, A. & Lagresle-Peyrou, C. et al. (2018) A Nontoxic Transduction Enhancer Enables Highly Efficient Lentiviral Transduction of Primary Murine T Cells and Hematopoietic Stem Cells. *Molecular Therapy - Methods & Clinical Development*, 10, 341–347. Available from: https://doi.org/10.1016/j.omtm.2018.08.002.

Donsante, A., Vogler, C., Muzyczka, N., Crawford, J.M., Barker, J. & Flotte, T. et al. (2001) Observed incidence of tumorigenesis in long-term rodent studies of rAAV vectors. *Gene Ther*, 8(17), 1343–1346. Available from: https://doi.org/10.1038/sj.gt.3301541.

Du, Y., Jenkins, N.A. & Copeland, N.G. (2005) Insertional mutagenesis identifies genes that promote the immortalization of primary bone marrow progenitor cells. *Blood*, 106(12), 3932–3939. Available from: https://doi.org/10.1182/blood-2005-03-1113.

Dudley, M.E., Wunderlich, J.R., Robbins, P.F., Yang, J.C., Hwu, P. & Schwartzentruber, D.J. et al. (2002) Cancer regression and autoimmunity in patients after clonal repopulation with antitumor lymphocytes. *Science*, 298(5594), 850–854. Available from: https://doi.org/10.1126/science.1076514.

Duncan, B.B., Dunbar, C.E. & Ishii, K. (2022) Applying a clinical lens to animal models of CAR-T cell therapies. *Molecular Therapy - Methods & Clinical Development*, 27, 17–31. Available from: https://doi.org/10.1016/j.omtm.2022.08.008.

Elleder, D., Pavlíček, A., Pačes, J. & Hejnar, J. (2002) Preferential integration of human immunodeficiency virus type 1 into genes, cytogenetic R bands and GC-rich DNA regions: Insight from the human genome sequence. *FEBS Letters*, 517(1-3), 285–286. Available from: https://doi.org/10.1016/S0014-5793(02)02612-1.

Engelman, A.N. & Singh, P.K. (2018) Cellular and molecular mechanisms of HIV-1 integration targeting. *Cellular and Molecular Life Sciences : CMLS*, 75(14), 2491–2507. Available from: https://doi.org/10.1007/s00018-018-2772-5.

European Medicines Agency (2017) *ICH guideline Q8 (R2) on pharmaceutical development: Step 5*. Available from: https://www.ema.europa.eu/en/documents/scientific-guideline/international-conference-harmonisation-technical-requirements-registration-pharmaceuticals-human-use_en-11.pdf [Accessed 9th October 2021].

FDA/CBER *Package Insert - KYMRIAH*.

Fernández, L., Fernández, A., Mirones, I., Escudero, A., Cardoso, L. & Vela, M. et al. (2019) GMP-Compliant Manufacturing of NKG2D CAR Memory T Cells Using CliniMACS Prodigy. *Frontiers in Immunology*, 10, 2361. Available from: https://doi.org/10.3389/fimmu.2019.02361.

Fesnak, A., Lin, C., Siegel, D.L. & Maus, M.V. (2016) CAR-T Cell Therapies From the Transfusion Medicine Perspective. *Transfusion Medicine Reviews*, 30(3), 139–145. Available from: https://doi.org/10.1016/j.tmrv.2016.03.001.

Fesnak, A.D., June, C.H. & Levine, B.L. (2016) Engineered T cells: The promise and challenges of cancer immunotherapy. *Nature Reviews. Cancer*, 16(9), 566–581. Available from: https://doi.org/10.1038/nrc.2016.97.

Filion, L.G., Izaguirre, C.A., Garber, G.E., Huebsh, L. & Aye, M.T. (1990) Detection of surface and cytoplasmic CD4 on blood monocytes from normal and HIV-1 infected individuals. *Journal of Immunological Methods*, 135(1-2), 59–69. Available from: https://doi.org/10.1016/0022-1759(90)90256-U.

Firouzi, S., López, Y., Suzuki, Y., Nakai, K., Sugano, S. & Yamochi, T. et al. (2014) Development and validation of a new high-throughput method to investigate the clonality of HTLV-1-infected cells based on provirus integration sites. *Genome Medicine*, 6(6), 46. Available from: https://doi.org/10.1186/gm568.

Fraietta, J.A., Nobles, C.L., Sammons, M.A., Lundh, S., Carty, S.A. & Reich, T.J. et al. (2018) Disruption of TET2 promotes the therapeutic efficacy of CD19-targeted T cells. *Nature*, 558(7709), 307–312. Available from: https://doi.org/10.1038/s41586-018-0178-z.

Freeth, J. (2019) *Screening CAR-T cells for Target Specificity using Human Cell Microarray Technology.* Retrogenix, Feb 2019 [Accessed 14th March 2019].

Friedmann, T. (1992) A brief history of gene therapy. *Nature Genetics*, 2(2), 93–98. Available from: https://doi.org/10.1038/ng1092-93.

Fujiwara, K., Masutani, M., Tachibana, M. & Okada, N. (2020) Impact of scFv structure in chimeric antigen receptor on receptor expression efficiency and

antigen recognition properties. *Biochemical and Biophysical Research Communications*, 527(2), 350–357. Available from: https://doi.org/10.1016/j.bbrc.2020.03.071.
Gagliardi, C., Khalil, M. & Foster, A.E. (2019) Streamlined production of genetically modified T cells with activation, transduction and expansion in closed-system G-Rex bioreactors. *Cytotherapy*, 21(12), 1246–1257. Available from: https://doi.org/10.1016/j.jcyt.2019.10.006.
Garcia-Prieto, C.A., Villanueva, L., Bueno-Costa, A., Davalos, V., González-Navarro, E.A. & Juan, M. et al. (2022) Epigenetic Profiling and Response to CD19 Chimeric Antigen Receptor T-Cell Therapy in B-Cell Malignancies. *JNCI: Journal of the National Cancer Institute*, 114(3), 436–445. Available from: https://doi.org/10.1093/jnci/djab194.
Gardner, R., Finney, O., Smithers, H., Leger, K.J., Annesley, C.E. & Summers, C. et al. (2016) CD19CAR T Cell Products of Defined CD4:CD8 Composition and Transgene Expression Show Prolonged Persistence and Durable MRD-Negative Remission in Pediatric and Young Adult B-Cell ALL. *Blood*, 128(22), 219. Available from: https://doi.org/10.1182/blood.V128.22.219.219.
Gaspar, H.B., Parsley, K.L., Howe, S., King, D., Gilmour, K.C. & Sinclair, J. et al. (2004) Gene therapy of X-linked severe combined immunodeficiency by use of a pseudotyped gammaretroviral vector. *Lancet*, 364(9452), 2181–2187. Available from: https://doi.org/10.1016/s0140-6736(04)17590-9.
Gattinoni, L., Klebanoff, C.A., Palmer, D.C., Wrzesinski, C., Kerstann, K. & Yu, Z. et al. (2005) Acquisition of full effector function in vitro paradoxically impairs the in vivo antitumor efficacy of adoptively transferred CD8+ T cells. *Journal of Clinical Investigation*, 115(6), 1616–1626. Available from: https://doi.org/10.1172/JCI24480.
Gattinoni, L., Klebanoff, C.A. & Restifo, N.P. (2012) Paths to stemness: building the ultimate antitumour T cell. *Nature Reviews. Cancer*, 12(10), 671–684. Available from: https://doi.org/10.1038/nrc3322.
Gattinoni, L., Lugli, E., Ji, Y., Pos, Z., Paulos, C.M. & Quigley, M.F. et al. (2011) A human memory T cell subset with stem cell-like properties. *Nature Medicine*, 17(10), 1290–1297. Available from: https://doi.org/10.1038/nm.2446.
Gee, M.H., Yang, X. & Garcia, K.C. (2018) *Facile method for screening clinical T cell receptors for off-target peptide-HLA reactivity*.
Geginat, J., Sallusto, F. & Lanzavecchia, A. (2001) Cytokine-driven proliferation and differentiation of human naive, central memory, and effector memory CD4(+) T cells. *The Journal of Experimental Medicine*, 194(12), 1711–1719. Available from: https://doi.org/10.1084/jem.194.12.1711.
Ginn, S.L., Amaya, A.K., Alexander, I.E., Edelstein, M. & Abedi, M.R. (2018) Gene therapy clinical trials worldwide to 2017: An update. *The Journal of Gene Medicine*, 20(5), e3015. Available from: https://doi.org/10.1002/jgm.3015.
Gorin, N.C. (1998) Autologous Stem Cell Transplantation in Acute Myelocytic Leukaemia. *The Journal of The American Society of Hematology*, 92(4), 1073–1090.
Grupp, S.A., Kalos, M., Barrett, D., Aplenc, R., Porter, D.L. & Rheingold, S.R. et al. (2013) Chimeric antigen receptor-modified T cells for acute lymphoid leukemia.

The New England Journal of Medicine, 368(16), 1509–1518. Available from: https://doi.org/10.1056/NEJMoa1215134.
GSK (2019) Points to Consider in the Nonclinical Assessment of the Safety and Disposition of Cell and Gene Therapies (C&GT).
Guedan, S., Posey, A.D., Shaw, C., Wing, A., Da, T. & Patel, P.R. et al. (2018) Enhancing CAR T cell persistence through ICOS and 4-1BB costimulation. *JCI Insight*, 3(1). Available from: https://doi.org/10.1172/jci.insight.96976.
Guo, B., Chen, M., Han, Q., Hui, F., Dai, H. & Zhang, W. et al. (2016) CD138-directed adoptive immunotherapy of chimeric antigen receptor (CAR)-modified T cells for multiple myeloma. *Journal of Cellular Immunotherapy*, 2(1), 28–35. Available from: https://doi.org/10.1016/j.jocit.2014.11.001.
Guo, Y., Zhang, X., Yang, M., Miao, X., Shi, Y. & Yao, J. et al. (2010) Functional evaluation of missense variations in the human MAD1L1 and MAD2L1 genes and their impact on susceptibility to lung cancer. *Journal of Medical Genetics*, 47(9), 616–622. Available from: https://doi.org/10.1136/jmg.2009.074252.
Gust, J., Hay, K.A., Hanafi, L.-A., Li, D., Myerson, D. & Gonzalez-Cuyar, L.F. et al. (2017) Endothelial Activation and Blood-Brain Barrier Disruption in Neurotoxicity after Adoptive Immunotherapy with CD19 CAR-T Cells. *Cancer Discovery*, 7(12), 1404–1419. Available from: https://doi.org/10.1158/2159-8290.CD-17-0698.
Ha, T.-C., Stahlhut, M., Rothe, M., Paul, G., Dziadek, V. & Morgan, M. et al. (2021) Multiple Genes Surrounding Bcl-xL, a Common Retroviral Insertion Site, Can Influence Hematopoiesis Individually or in Concert. *Human Gene Therapy*, 32(9-10), 458–472. Available from: https://doi.org/10.1089/hum.2019.344.
Hacein-Bey-Abina, S., Garrigue, A., Wang, G.P., Soulier, J., Lim, A. & Morillon, E. et al. (2008) Insertional oncogenesis in 4 patients after retrovirus-mediated gene therapy of SCID-X1. *Journal of Clinical Investigation*, 118(9), 3132–3142. Available from: https://doi.org/10.1172/JCI35700.
Hacein-Bey-Abina, S., Kalle, C. von, Schmidt, M., McCormack, M.P., Wulffraat, N. & Leboulch, P. et al. (2003) LMO2-associated clonal T cell proliferation in two patients after gene therapy for SCID-X1. *Science*, 302(5644), 415–419.
Hacein-Bey-Abina, S., Le Deist, F., Carlier, F., Bouneaud, C., Hue, C. & Villartay, J.P. de et al. (2002) Sustained correction of X-linked severe combined immunodeficiency by ex vivo gene therapy. *N Engl J Med*, 346(16), 1185–1193. Available from: https://doi.org/10.1056/NEJMoa012616.
Hacker, C.V., Vink, C.A., Wardell, T.W., Lee, S., Treasure, P. & Kingsman, S.M. et al. (2006) The integration profile of EIAV-based vectors. *Mol Ther*, 14(4), 536–545. Available from: https://doi.org/10.1016/j.ymthe.2006.06.006.
Hanahan, D. (2022) Hallmarks of Cancer: New Dimensions. *Cancer discovery*, 12(1), 31–46. Available from: https://doi.org/10.1158/2159-8290.CD-21-1059.
Hanahan, D. & Weinberg, R.A. (2011) Hallmarks of cancer: the next generation. *Cell*, 144(5), 646–674. Available from: https://doi.org/10.1016/j.cell.2011.02.013.
Hanenberg, H., Hashino, K., Konishi, H., Hock, R.A., Kato, I. & Williams, D.A. (1997) Optimization of fibronectin-assisted retroviral gene transfer into human CD34+ hematopoietic cells. *Human Gene Therapy*, 8(18), 2193–2206. Available from: https://doi.org/10.1089/hum.1997.8.18-2193.

Hay, A.E. & Cheung, M.C. (2019) CAR T-cells: costs, comparisons, and commentary. *Journal of Medical Economics*, 22(7), 613–615. Available from: https://doi.org/10.1080/13696998.2019.1582059.
He, Q., Jiang, X., Zhou, X. & Weng, J. (2019) Targeting cancers through TCR-peptide/MHC interactions. *Journal of hematology & oncology*, 12(1). Available from: https://doi.org/10.1186/s13045-019-0812-8.
Henig, I. & Zuckerman, T. (2014) Hematopoietic stem cell transplantation-50 years of evolution and future perspectives. *Rambam Maimonides Medical Journal*, 5(4), e0028. Available from: https://doi.org/10.5041/RMMJ.10162.
Hinrichs, C.S., Borman, Z.A., Gattinoni, L., Yu, Z., Burns, W.R. & Huang, J. et al. (2011) Human effector CD8+ T cells derived from naive rather than memory subsets possess superior traits for adoptive immunotherapy. *Blood*, 117(3), 808–814. Available from: https://doi.org/10.1182/blood-2010-05-286286.
Hodgson, C.P. & Solaiman, F. (1996) Virosomes: cationic liposomes enhance retroviral transduction. *Nat Biotechnol*, 14(3), 339–342. Available from: https://doi.org/10.1038/nbt0396-339.
Höfig, I., Atkinson, M.J., Mall, S., Krackhardt, A.M., Thirion, C. & Anastasov, N. (2012) Poloxamer synperonic F108 improves cellular transduction with lentiviral vectors. *The Journal of Gene Medicine*, 14(8), 549–560. Available from: https://doi.org/10.1002/jgm.2653.
Holmgaard, R.B., Zamarin, D., Munn, D.H., Wolchok, J.D. & Allison, J.P. (2013) Indoleamine 2,3-dioxygenase is a critical resistance mechanism in antitumor T cell immunotherapy targeting CTLA-4. *The Journal of Experimental Medicine*, 210(7), 1389–1402. Available from: https://doi.org/10.1084/jem.20130066.
Howe, S.J., Mansour, M.R., Schwarzwaelder, K., Bartholomae, C., Hubank, M. & Kempski, H. et al. (2008) Insertional mutagenesis combined with acquired somatic mutations causes leukemogenesis following gene therapy of SCID-X1 patients. *J Clin Invest*, 118(9), 3143–3150. Available from: https://doi.org/10.1172/JCI35798.
Ino, K., Ageitos, A.G., Singh, R.K. & Talmadge, J.E. (2001) Activation-induced T cell apoptosis by monocytes from stem cell products. *International Immunopharmacology*, 1(7), 1307–1319. Available from: https://doi.org/10.1016/S1567-5769(01)00062-5.
Invivogen *InvivoGen Insights: Lentiviral Vector Production and Cell Transduction*. Available from: https://www.invivogen.com/sites/default/files/invivogen/old/docs/Insight_201004.pdf [Accessed 14th March 2019].
Itzhaki, O., Jacoby, E., Nissani, A., Levi, M., Nagler, A. & Kubi, A. et al. (2020) Head-to-head comparison of in-house produced CD19 CAR-T cell in ALL and NHL patients. *Journal for Immunotherapy of Cancer*, 8(1). Available from: https://doi.org/10.1136/jitc-2019-000148.
Jayaraman, J., Mellody, M.P., Hou, A.J., Desai, R.P., Fung, A.W. & Pham, A.H.T. et al. (2020) CAR-T design: Elements and their synergistic function. *EBioMedicine*, 58, 102931. Available from: https://doi.org/10.1016/j.ebiom.2020.102931•.
Johnson, L.A. & June, C.H. (2017) Driving gene-engineered T cell immunotherapy of cancer. *Cell Res*, 27(1), 38–58. Available from: https://doi.org/10.1038/cr.2016.154.

Joyce, B.T., Zheng, Y., Zhang, Z., Liu, L., Kocherginsky, M. & Murphy, R. et al. (2018) miRNA-Processing Gene Methylation and Cancer Risk. *Cancer Epidemiology, Biomarkers & Prevention : a Publication of the American Association for Cancer Research, Cosponsored by the American Society of Preventive Oncology*, 27(5), 550–557. Available from: https://doi.org/10.1158/1055-9965.EPI-17-0849.

Kaech, S.M., Wherry, E.J. & Ahmed, R. (2002) Effector and memory T-cell differentiation: implications for vaccine development. *Nature Reviews. Immunology*, 2(4), 251–262. Available from: https://doi.org/10.1038/nri778.

Kawalekar, O.U., O'Connor, R.S., Fraietta, J.A., Guo, L., McGettigan, S.E. & Posey, A.D. et al. (2016) Distinct Signaling of Coreceptors Regulates Specific Metabolism Pathways and Impacts Memory Development in CAR T Cells. *Immunity*, 44(2), 380–390. Available from: https://doi.org/10.1016/j.immuni.2016.01.021.

Kim-Hoehamer, Y.-I., Riberdy, J.M., Zheng, F., Park, J.J., Shang, N. & Métais, J.-Y. et al. (2022) Development of a cGMP-compliant process to manufacture donor-derived, CD45RA-depleted memory CD19-CAR T cells. *Gene Ther*. Available from: https://doi.org/10.1038/s41434-021-00307-0.

KITE Pharma (2021) *How YESCARTA Works: YESCARTA IMMUNOTHERAPY: ENGINEERED TO IDENTIFY AND ATTACK TARGET CELLS*. Available from: https://www.yescartahcp.com/large-b-cell-lymphoma/how-yescarta-works [Accessed 11th October 2021].

Kochenderfer, J.N., Dudley, M.E., Feldman, S.A., Wilson, W.H., Spaner, D.E. & Maric, I. et al. (2012) B-cell depletion and remissions of malignancy along with cytokine-associated toxicity in a clinical trial of anti-CD19 chimeric-antigen-receptor-transduced T cells. *Blood*, 119(12), 2709–2720. Available from: https://doi.org/10.1182/blood-2011-10-384388.

Krishna, D., Rittié, L., Tran, H., Zheng, X., Chen-Rogers, C.-E. & McGillivray, A. et al. (2021) Short Time to Market and Forward Planning Will Enable Cell Therapies to Deliver R&D Pipeline Value. *Human Gene Therapy*, 32(9-10), 433–445. Available from: https://doi.org/10.1089/hum.2020.212.

Lam, C., van Velthoven, M.H. & Meinert, E. (2020) Developing a Blockchain-Based Supply Chain System for Advanced Therapies: Protocol for a Feasibility Study. *JMIR Research Protocols*, 9(12), e17005. Available from: https://doi.org/10.2196/17005.

Lee, D.W., Kochenderfer, J.N., Stetler-Stevenson, M., Cui, Y.K., Delbrook, C. & Feldman, S.A. et al. (2015) T cells expressing CD19 chimeric antigen receptors for acute lymphoblastic leukaemia in children and young adults: A phase 1 dose-escalation trial. *The Lancet*, 385(9967), 517–528. Available from: https://doi.org/10.1016/S0140-6736(14)61403-3.

Lenz, A., Zeng, J., Xiu, J., Algaze, S., Jayachandran, P. & Soni, S. et al. (2022) Claudin 18 (CLDN18) gene expression and related molecular profile in gastric cancer (GC). *Journal of Clinical Oncology*, 40(16_suppl), 4048. Available from: https://doi.org/10.1200/JCO.2022.40.16_suppl.4048.

Levine, B.L. (2015) Performance-enhancing drugs: design and production of redirected chimeric antigen receptor (CAR) T cells. *Cancer Gene Therapy*, 22(2), 79–84. Available from: https://doi.org/10.1038/cgt.2015.5.

Li, W., Song, P., Zhao, M., Gao, L., Xie, J. & You, C. (2021) BOP1 Used as a Novel Prognostic Marker and Correlated with Tumor Microenvironment in Pan-Cancer. *Journal of Oncology*, 2021, 3603030. Available from: https://doi.org/10.1155/2021/3603030.

Li, Y., Cong, Y., Jia, M., He, Q., Zhong, H. & Zhao, Y. et al. (2021) Targeting IL-21 to tumor-reactive T cells enhances memory T cell responses and anti-PD-1 antibody therapy. *Nature Communications*, 12(1), 951. Available from: https://doi.org/10.1038/s41467-021-21241-0.

Li, Y., Huo, Y., Yu, L. & Wang, J. (2019) Quality Control and Nonclinical Research on CAR-T Cell Products: General Principles and Key Issues. *Engineering*, 5(1), 122–131. Available from: https://doi.org/10.1016/j.eng.2018.12.003.

Lim, S.P., Wong, N.C., Suetani, R.J., Ho, K., Ng, J.L. & Neilsen, P.M. et al. (2012) Specific-site methylation of tumour suppressor ANKRD11 in breast cancer. *European Journal of Cancer (Oxford, England : 1990)*, 48(17), 3300–3309. Available from: https://doi.org/10.1016/j.ejca.2012.03.023.

Linette, G.P., Stadtmauer, E.A., Maus, M.V., Rapoport, A.P., Levine, B.L. & Emery, L. et al. (2013) Cardiovascular toxicity and titin cross-reactivity of affinity-enhanced T cells in myeloma and melanoma. *Blood*, 122(6), 863–871. Available from: https://doi.org/10.1182/blood-2013-03-490565.

Lipsitz, Y.Y., Milligan, W.D., Fitzpatrick, I., Stalmeijer, E., Farid, S.S. & Tan, K.Y. et al. (2017) A roadmap for cost-of-goods planning to guide economic production of cell therapy products. *Cytotherapy*, 19(12), 1383–1391. Available from: https://doi.org/10.1016/j.jcyt.2017.06.009.

Liu, G., Rui, W., Zhao, X. & Lin, X. (2021) Enhancing CAR-T cell efficacy in solid tumors by targeting the tumor microenvironment. *Cellular & Molecular Immunology*, 18(5), 1085–1095. Available from: https://doi.org/10.1038/s41423-021-00655-2.

Liu, L., Liu, J. & Lin, Q. (2021) Histone demethylase KDM2A: Biological functions and clinical values (Review). *Experimental and Therapeutic Medicine*, 22(1), 723. Available from: https://doi.org/10.3892/etm.2021.10155.

Liu, X., Jiang, S., Fang, C., Yang, S., Olalere, D. & Pequignot, E.C. et al. (2015) Affinity-Tuned ErbB2 or EGFR Chimeric Antigen Receptor T Cells Exhibit an Increased Therapeutic Index against Tumors in Mice. *Cancer Research*, 75(17), 3596–3607. Available from: https://doi.org/10.1158/0008-5472.CAN-15-0159.

Lo Presti, V., Cornel, A.M., Plantinga, M., Dünnebach, E., Kuball, J. & Boelens, J.J. et al. (2021) Efficient lentiviral transduction method to gene modify cord blood CD8+ T cells for cancer therapy applications. *Molecular Therapy - Methods & Clinical Development*, 21, 357–368. Available from: https://doi.org/10.1016/j.omtm.2021.03.015.

Lock, D., Mockel-Tenbrinck, N., Drechsel, K., Barth, C., Mauer, D. & Schaser, T. et al. (2017) Automated Manufacturing of Potent CD20-Directed Chimeric Antigen Receptor T Cells for Clinical Use. *Human Gene Therapy*, 28(10), 914–925. Available from: https://doi.org/10.1089/hum.2017.111.

Locke, F.L., Neelapu, S.S., Bartlett, N.L., Siddiqi, T., Chavez, J.C. & Hosing, C.M. et al. (2015) Phase 1 Clinical Results of the ZUMA-1 (KTE-C19-101) Study: A Phase 1-2 Multi-Center Study Evaluating the Safety and Efficacy of Anti-CD19 CAR T

Cells (KTE-C19) in Subjects with Refractory Aggressive Non-Hodgkin Lymphoma (NHL). *Blood*, 126(23), 3991. Available from: https://doi.org/10.1182/blood.V126.23.3991.3991.
Lonez, C., Verma, B., Hendlisz, A., Aftimos, P., Awada, A. & van den Neste, E. et al. (2017) Study protocol for THINK: A multinational open-label phase I study to assess the safety and clinical activity of multiple administrations of NKR-2 in patients with different metastatic tumour types. *BMJ Open*, 7(11), e017075. Available from: https://doi.org/10.1136/bmjopen-2017-017075.
Lopes, A.G., Noel, R. & Sinclair, A. (2020) Cost analysis of vein-to-vein CAR T-cell therapy: automated manufacturing and supply chain. *Cell and Gene Therapy Insights*, 6(3), 487–510. Available from: https://doi.org/10.18609/cgti.2020.058.
Louis, C.U., Savoldo, B., Dotti, G., Pule, M., Yvon, E. & Myers, G.D. et al. (2011) Antitumor activity and long-term fate of chimeric antigen receptor-positive T cells in patients with neuroblastoma. *Blood*, 118(23), 6050–6056. Available from: https://doi.org/10.1182/blood-2011-05-354449.
Ludwig, J. *Wilson Wolf - G-REX Specifications*.
Mackensen, A., Koenecke, C., Haanen, J., Alsdorf, W., Desuki, A. & Wagner-Drouet, E. et al. (2021) 958 BNT211: a phase I/II trial to evaluate safety and efficacy of CLDN6 CAR-T cells and vaccine-mediated in vivo expansion in patients with CLDN6-positive advanced solid tumors. *Journal for immunotherapy of cancer*, 9(Suppl 2), A1008. Available from: https://doi.org/10.1136/jitc-2021-SITC2021.958.
Mahnke, Y.D., Brodie, T.M., Sallusto, F., Roederer, M. & Lugli, E. (2013) The who's who of T-cell differentiation: human memory T-cell subsets. *European Journal of Immunology*, 43(11), 2797–2809. Available from: https://doi.org/10.1002/eji.201343751.
Malach, unpublished results.
Marín Morales, J.M., Münch, N., Peter, K., Freund, D., Oelschlägel, U. & Hölig, K. et al. (2019) Automated Clinical Grade Expansion of Regulatory T Cells in a Fully Closed System. *Frontiers in Immunology*, 10, 38. Available from: https://doi.org/10.3389/fimmu.2019.00038.
Márquez, J., Kohli, M., Arteta, B., Chang, S., Li, W.-B. & Goldblatt, M. et al. (2013) Identification of hepatic microvascular adhesion-related genes of human colon cancer cells using random homozygous gene perturbation. *International Journal of Cancer*, 133(9), 2113–2122. Available from: https://doi.org/10.1002/ijc.28232.
Maude, S.L., Barrett, D., Teachey, D.T. & Grupp, S.A. (2014) Managing cytokine release syndrome associated with novel T cell-engaging therapies. *Cancer Journal (Sudbury, Mass.)*, 20(2), 119–122. Available from: https://doi.org/10.1097/PPO.0000000000000035.
Maude, S.L., Frey, N., Shaw, P.A., Aplenc, R., Barrett, D.M. & Bunin, N.J. et al. (2014) Chimeric antigen receptor T cells for sustained remissions in leukemia. *N Engl J Med*, 371(16), 1507–1517. Available from: https://doi.org/10.1056/NEJMoa1407222.
McLellan, A.D. & Ali Hosseini Rad, S.M. (2019) Chimeric antigen receptor T cell persistence and memory cell formation. *Immunology and Cell Biology*, 97(7), 664–674. Available from: https://doi.org/10.1111/imcb.12254.

Miklík, D., Šenigl, F. & Hejnar, J. (2018) Proviruses with Long-Term Stable Expression Accumulate in Transcriptionally Active Chromatin Close to the Gene Regulatory Elements: Comparison of ASLV-, HIV- and MLV-Derived Vectors. *Viruses*, 10(3). Available from: https://doi.org/10.3390/v10030116.

Miltenyi Biotec *Magnetic Separation*. Available from: https://www.miltenyibiotec.com/GB-en/resources/macs-handbook/macs-technologies/cell-separation/magnetic-cell-separation.html#gref [Accessed 31st January 2023].

Mitchell, R.S., Beitzel, B.F., Schroder, A.R., Shinn, P., Chen, H. & Berry, C.C. et al. (2004) Retroviral DNA integration: ASLV, HIV, and MLV show distinct target site preferences. *PLoS Biol*, 2(8), E234. Available from: https://doi.org/10.1371/journal.pbio.0020234.

Miyahira, A. (2012) *Types of immune cells present in human PBMC*. Available from: https://technical.sanguinebio.com/types-of-immune-cells-present-in-human-pbmc/ [Accessed 14th March 2019].

Miyoshi, H., Blömer, U., Takahashi, M., Gage, F.H. & Verma, I.M. (1998) Development of a Self-Inactivating Lentivirus Vector. *Journal of Virology*, 72(10), 8150–8157.

Mock, U., Nickolay, L., Philip, B., Cheung, G.W.-K., Zhan, H. & Johnston, I.C.D. et al. (2016) Automated manufacturing of chimeric antigen receptor T cells for adoptive immunotherapy using CliniMACS prodigy. *Cytotherapy*, 18(8), 1002–1011. Available from: https://doi.org/10.1016/j.jcyt.2016.05.009.

Modlich, U., Bohne, J., Schmidt, M., Kalle, C. von, Knoss, S. & Schambach, A. et al. (2006) Cell-culture assays reveal the importance of retroviral vector design for insertional genotoxicity. *Blood*, 108(8), 2545–2553. Available from: https://doi.org/10.1182/blood-2005-08-024976.

Modlich, U., Navarro, S., Zychlinski, D., Maetzig, T., Knoess, S. & Brugman, M.H. et al. (2009) Insertional transformation of hematopoietic cells by self-inactivating lentiviral and gammaretroviral vectors. *Molecular Therapy : the Journal of the American Society of Gene Therapy*, 17(11), 1919–1928. Available from: https://doi.org/10.1038/mt.2009.179.

Montini, E., Cesana, D., Schmidt, M., Sanvito, F., Bartholomae, C.C. & Ranzani, M. et al. (2009) The genotoxic potential of retroviral vectors is strongly modulated by vector design and integration site selection in a mouse model of HSC gene therapy. *J Clin Invest*, 119(4), 964–975. Available from: https://doi.org/10.1172/JCI37630.

Montini, E., Cesana, D., Schmidt, M., Sanvito, F., Ponzoni, M. & Bartholomae, C. et al. (2006) Hematopoietic stem cell gene transfer in a tumor-prone mouse model uncovers low genotoxicity of lentiviral vector integration. *Nat Biotechnol*, 24(6), 687–696. Available from: https://doi.org/10.1038/nbt1216.

Morgan, R.A., Chinnasamy, N., Abate-Daga, D., Gros, A., Robbins, P.F. & Zheng, Z. et al. (2013) Cancer regression and neurological toxicity following anti-MAGE-A3 TCR gene therapy. *Journal of Immunotherapy (Hagerstown, Md. : 1997)*, 36(2), 133–151. Available from: https://doi.org/10.1097/CJI.0b013e3182829903.

Morgan, R.A., Yang, J.C., Kitano, M., Dudley, M.E., Laurencot, C.M. & Rosenberg, S.A. (2010) Case report of a serious adverse event following the administration of

T cells transduced with a chimeric antigen receptor recognizing ERBB2. *Mol Ther*, 18(4), 843–851. Available from: https://doi.org/10.1038/mt.2010.24.
Nault, J.C., Datta, S., Imbeaud, S., Franconi, A., Mallet, M. & Couchy, G. et al. (2015) Recurrent AAV2-related insertional mutagenesis in human hepatocellular carcinomas. *Nat Genet*, 47(10), 1187–1193. Available from: https://doi.org/10.1038/ng.3389.
Newrzela, S., Cornils, K., Li, Z., Baum, C., Brugman, M.H. & Hartmann, M. et al. (2008) Resistance of mature T cells to oncogene transformation. *Blood*, 112(6), 2278–2286. Available from: https://doi.org/10.1182/blood-2007-12-128751.
NHS England (2018) *Axicabtagene Ciloleucel Chimeric Antigen Therapy: Schedule 2*. Available from: https://www.england.nhs.uk/wp-content/uploads/2018/12/Axicabtagene-Ciloleucel-Chimeric-Antigen-Receptor-T-Cell-CAR-T-Therapy-for-the-treatment-of-adult-patients-wit.pdf [Accessed 11th October 2021].
Novartis *Charging towards the next-generation of CAR-T*. Available from: https://www.novartis.com/research-development/technology-platforms/cell-therapy/charging-towards-next-generation-car-t [Accessed 26th January 2021].
Novartis *Kymriah, INN-tisagenlecleucel: Summary of Product Characteristics* [Accessed 2 September 2020].
Nowrouzi, A., Cheung, W.T., Li, T., Zhang, X., Arens, A. & Paruzynski, A. et al. (2013) The fetal mouse is a sensitive genotoxicity model that exposes lentiviral-associated mutagenesis resulting in liver oncogenesis. *Mol Ther*, 21(2), 324–337. Available from: https://doi.org/10.1038/mt.2012.224.
Ohkawa, T., Nishimura, A., Kosaki, K., Aoki-Nogami, Y., Tomizawa, D. & Kashimada, K. et al. (2022) PAX3/7-FOXO1 fusion-negative alveolar rhabdomyosarcoma in Schuurs-Hoeijmakers syndrome. *Journal of Human Genetics*, 67(1), 51–54. Available from: https://doi.org/10.1038/s10038-021-00965-3.
Orchard Therapeutics *Orchard Statement on Strimvelis®, a Gammaretroviral Vector-Based Gene Therapy for ADA-SCID*. Available from: https://ir.orchard-tx.com/index.php/news-releases/news-release-details/orchard-statement-strimvelisr-gammaretroviral-vector-based-gene [Accessed 27th September 2021].
Pagliarulo, N. (2019) *Novartis still hasn't solved its CAR-T manufacturing issues*. Available from: https://www.biopharmadive.com/news/novartis-kymriah-car-t-manufacturing-difficulties-cell-viability/568830/ [Accessed 1st October 2021].
Palmer, E. (2018) *Novartis, Still Struggling with Kymriah Manufacturing, is Providing Some Out-Of-Spec Doses to Patients That Ask*. Available from: https://www.fiercepharma.com/manufacturing/novartis-still-struggling-kymriah-manufacturing-providing-some-out-spec-doses-to [Accessed 26th January 2023].
Panch, S.R., Srivastava, S.K., Elavia, N., McManus, A., Liu, S. & Jin, P. et al. (2019) Effect of Cryopreservation on Autologous Chimeric Antigen Receptor T Cell Characteristics. *Molecular Therapy : the Journal of the American Society of Gene Therapy*, 27(7), 1275–1285. Available from: https://doi.org/10.1016/j.ymthe.2019.05.015.
Parham, P. (2009) *The Immune System*. Garland Science.

Patel, R., Devashish, K., Singh, S., Nath, P., Gohel, D. & Prasad, R. et al. (2021) *Vectofusin-1–based T-cell transduction approach compared with RetroNectin-based transduction for generating murine chimeric antigen receptor T-cells*.
Peng, L., Tao, Y., Wu, R., Su, J., Sun, M. & Cheng, Y. et al. (2021) NFAT as a Biomarker and Therapeutic Target in Non-Small Cell Lung Cancer-Related Brain Metastasis. *Frontiers in Oncology*, 11, 781150. Available from: https://doi.org/10.3389/fonc.2021.781150.
PeproTech *Haematopoietic Stem Cell Differentiation*. Available from: https:// www.peprotech.com/download/2023 [Accessed 14th March 2019].
Perera, M.P.J., Thomas, P.B., Risbridger, G.P., Taylor, R., Azad, A. & Hofman, M.S. et al. (2022) Chimeric Antigen Receptor T-Cell Therapy in Metastatic Castrate-Resistant Prostate Cancer. *Cancers*, 14(3). Available from: https://doi.org/10.3390/cancers14030503.
Pilipow, K., Scamardella, E., Puccio, S., Gautam, S., Paoli, F. de & Mazza, E.M. et al. (2018) Antioxidant metabolism regulates CD8+ T memory stem cell formation and antitumor immunity. *JCI Insight*, 3(18). Available from: https://doi.org/10.1172/jci.insight.122299.
Poletti, V. & Mavilio, F. (2018) Interactions between Retroviruses and the Host Cell Genome. *Molecular Therapy - Methods & Clinical Development*, 8, 31–41. Available from: https://doi.org/10.1016/j.omtm.2017.10.001.
Porter, D.L., Levine, B.L., Kalos, M., Bagg, A. & June, C.H. (2011) Chimeric antigen receptor-modified T cells in chronic lymphoid leukemia. *The New England Journal of Medicine*, 365(8), 725–733. Available from: https://doi.org/10.1056/NEJMoa1103849.
Qi, C., Gong, J., Li, J., Liu, D., Qin, Y. & Ge, S. et al. (2022) Claudin18.2-specific CAR T cells in gastrointestinal cancers: phase 1 trial interim results. *Nature medicine*, 28(6), 1189–1198. Available from: https://doi.org/10.1038/s41591-022-01800-8.
Radek, C., Bernadin, O., Drechsel, K., Cordes, N., Pfeifer, R. & Sträßer, P. et al. (2019) Vectofusin-1 Improves Transduction of Primary Human Cells with Diverse Retroviral and Lentiviral Pseudotypes, Enabling Robust, Automated Closed-System Manufacturing. *Human Gene Therapy*, 30(12), 1477–1493. Available from: https://doi.org/10.1089/hum.2019.157.
Rajabzadeh, A., Hamidieh, A.A. & Rahbarizadeh, F. (2021) Spinoculation and retronectin highly enhance the gene transduction efficiency of Mucin-1-specific chimeric antigen receptor (CAR) in human primary T cells. *BMC Molecular and Cell Biology*, 22(1), 57. Available from: https://doi.org/10.1186/s12860-021-00397-z.
Raman, M.C.C., Rizkallah, P.J., Simmons, R., Donnellan, Z., Dukes, J. & Bossi, G. et al. (2016) Direct molecular mimicry enables off-target cardiovascular toxicity by an enhanced affinity TCR designed for cancer immunotherapy. *Scientific Reports*, 6(1), 18851. Available from: https://doi.org/10.1038/srep18851.
Ramezani, A., Hawley, T.S. & Hawley, R.G. (2000) Lentiviral vectors for enhanced gene expression in human hematopoietic cells. *Mol Ther*, 2(5), 458–469. Available from: https://doi.org/10.1006/mthe.2000.0190.

Raskov, H., Orhan, A., Christensen, J.P. & Gögenur, I. (2021) Cytotoxic CD8+ T cells in cancer and cancer immunotherapy. *British Journal of Cancer*, 124(2), 359–367. Available from: https://doi.org/10.1038/s41416-020-01048-4.

Ravin, S.S. de, Su, L., Theobald, N., Choi, U., Macpherson, J.L. & Poidinger, M. et al. (2014) Enhancers are major targets for murine leukemia virus vector integration. *Journal of Virology*, 88(8), 4504–4513. Available from: https://doi.org/10.1128/JVI.00011-14.

Ridder, J. de, Uren, A., Kool, J., Reinders, M. & Wessels, L. (2006) Detecting statistically significant common insertion sites in retroviral insertional mutagenesis screens. *PLoS Computational Biology*, 2(12), e166. Available from: https://doi.org/10.1371/journal.pcbi.0020166.

Rittelmeyer, I., Rothe, M., Brugman, M.H., Iken, M., Schambach, A. & Manns, M.P. et al. (2013) Hepatic lentiviral gene transfer is associated with clonal selection, but not with tumor formation in serially transplanted rodents. *Hepatology*, 58(1), 397–408. Available from: https://doi.org/10.1002/hep.26204.

Roddie, C. (2020) *From Patient to Commercial Production: Apheresis to Sample Shipping*. Available from: https://emj.emg-health.com/wp-content/uploads/sites/2/2020/05/CAR-T-From-Bed-to-Bench-and-Back-Again.pdf [Accessed 11th October 2021].

Ruella, M., Xu, J., Barrett, D.M., Fraietta, J.A., Reich, T.J. & Ambrose, D.E. et al. (2018) Induction of resistance to chimeric antigen receptor T cell therapy by transduction of a single leukemic B cell. *Nature Medicine*, 24(10), 1499–1503. Available from: https://doi.org/10.1038/s41591-018-0201-9.

Sallusto, F., Lenig, D., Förster, R., Lipp, M. & Lanzavecchia, A. (1999) Two subsets of memory T lymphocytes with distinct homing potentials and effector functions. *Nature*, 401(6754), 708–712. Available from: https://doi.org/10.1038/44385.

Schneider, A.T., Gautheron, J., Feoktistova, M., Roderburg, C., Loosen, S.H. & Roy, S. et al. (2017) RIPK1 Suppresses a TRAF2-Dependent Pathway to Liver Cancer. *Cancer Cell*, 31(1), 94–109. Available from: https://doi.org/10.1016/j.ccell.2016.11.009.

Schröder, A.R.W., Shinn, P., Chen, H., Berry, C., Ecker, J.R. & Bushman, F. (2002) HIV-1 Integration in the Human Genome Favors Active Genes and Local Hotspots. *Cell*, 110(4), 521–529. Available from: https://doi.org/10.1016/S0092-8674(02)00864-4.

Šenigl, F., Miklík, D., Auxt, M. & Hejnar, J. (2017) Accumulation of long-term transcriptionally active integrated retroviral vectors in active promoters and enhancers. *Nucleic Acids Research*, 45(22), 12752–12765. Available from: https://doi.org/10.1093/nar/gkx889.

Shah, K., Al-Haidari, A., Sun, J. & Kazi, J.U. (2021) T cell receptor (TCR) signaling in health and disease. *Signal Transduction and Targeted Therapy*, 6(1), 412. Available from: https://doi.org/10.1038/s41392-021-00823-w.

Shah, N.N., Qin, H., Yates, B., Su, L., Shalabi, H. & Raffeld, M. et al. (2019) Clonal expansion of CAR T cells harboring lentivector integration in the CBL gene following anti-CD22 CAR T-cell therapy. *Blood Advances*, 3(15), 2317–2322. Available from: https://doi.org/10.1182/bloodadvances.2019000219.

Shalabi, H., Wolters, P.L., Martin, S., Toledo-Tamula, M.A., Roderick, M.C. & Struemph, K. et al. (2018) Systematic Evaluation of Neurotoxicity in Children and Young Adults Undergoing CD22 Chimeric Antigen Receptor T-Cell Therapy. *Journal of Immunotherapy (Hagerstown, Md. : 1997)*, 41(7), 350–358. Available from: https://doi.org/10.1097/CJI.0000000000000241.

Shen, C. & van de Wiel, L. (2020) *From Sample Receipt to CAR T-cell Product*. Available from: https://emj.emg-health.com/wp-content/uploads/sites/2/2020/05/CAR-T-From-Bed-to-Bench-and-Back-Again.pdf [Accessed 11th October 2021].

Singh, H., Figliola, M.J., Dawson, M.J., Olivares, S., Zhang, L. & Yang, G. et al. (2013) Manufacture of clinical-grade CD19-specific T cells stably expressing chimeric antigen receptor using Sleeping Beauty system and artificial antigen presenting cells. *PLoS One*, 8(5), e64138. Available from: https://doi.org/10.1371/journal.pone.0064138.

Singhal, R., Deng, X., Chenchik, A.A. & Kandel, E.S. (2011) Long-distance effects of insertional mutagenesis. *PLoS One*, 6(1), e15832. Available from: https://doi.org/10.1371/journal.pone.0015832.

Somerville, R.P.T., Devillier, L., Parkhurst, M.R., Rosenberg, S.A. & Dudley, M.E. (2012) Clinical scale rapid expansion of lymphocytes for adoptive cell transfer therapy in the WAVE® bioreactor. *Journal of Translational Medicine*, 10, 69. Available from: https://doi.org/10.1186/1479-5876-10-69.

Sommermeyer, D., Hudecek, M., Kosasih, P.L., Gogishvili, T., Maloney, D.G. & Turtle, C.J. et al. (2016) Chimeric antigen receptor-modified T cells derived from defined CD8+ and CD4+ subsets confer superior antitumor reactivity in vivo. *Leukemia*, 30(2), 492–500. Available from: https://doi.org/10.1038/leu.2015.247.

Stadtmauer, E.A., Faitg, T.H., Lowther, D.E., Badros, A.Z., Chagin, K. & Dengel, K. et al. (2019) Long-term safety and activity of NY-ESO-1 SPEAR T cells after autologous stem cell transplant for myeloma. *Blood Advances*, 3(13), 2022–2034. Available from: https://doi.org/10.1182/bloodadvances.2019000194.

Stanton, D. (2023) *Novartis at JPM: '7-day CAR-T process an alternative to allogeneic*. Available from: https://bioprocessintl.com/bioprocess-insider/therapeutic-class/novartis-at-jpm-7-day-car-t-process-an-alternative-to-allogeneic/ [Accessed August 2023].

Strack, A., Deinzer, A., Thirion, C., Schrödel, S., Dörrie, J. & Sauerer, T. et al. (2022) Breaking Entry-and Species Barriers: LentiBOOST® Plus Polybrene Enhances Transduction Efficacy of Dendritic Cells and Monocytes by Adenovirus 5. *Viruses*, 14(1). Available from: https://doi.org/10.3390/v14010092.

Strati, P., Ahmed, S., Kebriaei, P., Nastoupil, L.J., Claussen, C.M. & Watson, G. et al. (2020) Clinical efficacy of anakinra to mitigate CAR T-cell therapy-associated toxicity in large B-cell lymphoma. *Blood Advances*, 4(13), 3123–3127. Available from: https://doi.org/10.1182/bloodadvances.2020002328.

Stroncek, D.F., Lee, D.W., Ren, J., Sabatino, M., Highfill, S. & Khuu, H. et al. (2017) Elutriated lymphocytes for manufacturing chimeric antigen receptor T cells. *Journal of Translational Medicine*, 15(1), 59. Available from: https://doi.org/10.1186/s12967-017-1160-5.

Stroncek, D.F., Ren, J., Lee, D.W., Tran, M., Frodigh, S.E. & Sabatino, M. et al. (2016) Myeloid cells in peripheral blood mononuclear cell concentrates inhibit the

expansion of chimeric antigen receptor T cells. *Cytotherapy*, 18(7), 893–901. Available from: https://doi.org/10.1016/j.jcyt.2016.04.003.

Sweeney, N.P. & Vink, C.A. (2021) The impact of lentiviral vector genome size and producer cell genomic to gag-pol mRNA ratios on packaging efficiency and titre. *Molecular Therapy - Methods & Clinical Development*, 21, 574–584. Available from: https://doi.org/10.1016/j.omtm.2021.04.007.

Tarnowski, J., Krishna, D., Jespers, L., Ketkar, A., Haddock, R. & Imrie, J. et al. (2017) Delivering advanced therapies: the big pharma approach. *Gene Ther*, 24(9), 593–598. Available from: https://doi.org/10.1038/gt.2017.65.

Taylor, N.P. (2021) *Bluebird stops gene therapy trials after 2 sickle cell patients develop cancer*. Available from: https://www.fiercebiotech.com/biotech/bluebird-stops-gene-therapy-trials-after-2-sickle-cell-patients-develop-cancer?mkt_tok=eyJpIjoiTXpFNU5HWmxPVEF4TURoaSIsInQiOiJcL3p2azRqZTVoemxUZ0l1WURxZFR5NGVPa2Y1RkNlb3lBMEhDOFdhVG1vRG4zc2ZoYWdEa2U5b2JJemx0STNoOEVYaGE5UVYrR0ZRbjZFSVZ6QU1nOVhCU3NiUzI1MVczeE8yVXJpTWNKYXN2VTFSSmZXc2xpTHpCK0VVZ1ZwWWgifQ%3D%3D&mrkid=5361387 [Accessed 19th February 2021].

Themis, M., Waddington, S.N., Schmidt, M., Kalle, C. von, Wang, Y. & Al-Allaf, F. et al. (2005) Oncogenesis following delivery of a nonprimate lentiviral gene therapy vector to fetal and neonatal mice. *Mol Ther*, 12(4), 763–771. Available from: https://doi.org/10.1016/j.ymthe.2005.07.358.

Till, B.G., Jensen, M.C., Wang, J., Chen, E.Y., Wood, B.L. & Greisman, H.A. et al. (2008) Adoptive immunotherapy for indolent non-Hodgkin lymphoma and mantle cell lymphoma using genetically modified autologous CD20-specific T cells. *Blood*, 112(6), 2261–2271. Available from: https://doi.org/10.1182/blood-2007-12-128843.

Tsokas, K., McFarland, R., Burke, C., Lynch, J.L., Bollenbach, T. & Callaway, D.A. et al. (2019) Reducing Risks and Delays in the Translation of Cell and Gene Therapy Innovations into Regulated Products. *NAM Perspectives*, 2019. Available from: https://doi.org/10.31478/201909d.

Turtle, C.J., Hanafi, L.-A., Berger, C., Gooley, T.A., Cherian, S. & Hudecek, M. et al. (2016) CD19 CAR-T cells of defined CD4+:CD8+ composition in adult B cell ALL patients. *The Journal of Clinical Investigation*, 126(6), 2123–2138. Available from: https://doi.org/10.1172/JCI85309.

Turtle, C.J., Hanafi, L.A., Berger, C., Hudecek, M., Pender, B. & Robinson, E. et al. (2016) Immunotherapy of non-Hodgkin's lymphoma with a defined ratio of CD8+ and CD4+ CD19-specific chimeric antigen receptor-modified T cells. *Sci Transl Med*, 8(355), 355ra116. Available from: https://doi.org/10.1126/scitranslmed.aaf8621.

Tyagarajan, S., Spencer, T. & Smith, J. (2020) Optimizing CAR-T Cell Manufacturing Processes during Pivotal Clinical Trials. *Molecular Therapy. Methods & Clinical Development*, 16, 136–144. Available from: https://doi.org/10.1016/j.omtm.2019.11.018.

Vormittag, P., Gunn, R., Ghorashian, S. & Veraitch, F.S. (2018) A guide to manufacturing CAR T cell therapies. *Current Opinion in Biotechnology*, 53, 164–181. Available from: https://doi.org/10.1016/j.copbio.2018.01.025.

Waddington, S.N., Mitrophanous, K.A., Ellard, F.M., Buckley, S.M.K., Nivsarkar, M. & Lawrence, L. et al. (2003) Long-term transgene expression by administration of a lentivirus-based vector to the fetal circulation of immuno-competent mice. *Gene Ther*, 10(15), 1234–1240. Available from: https://doi.org/10.1038/sj.gt.3301991.
Wang, G.P., Levine, B.L., Binder, G.K., Berry, C.C., Malani, N. & McGarrity, G. et al. (2009) Analysis of Lentiviral Vector Integration in HIV+ Study Subjects Receiving Autologous Infusions of Gene Modified CD4+ T Cells. *Molecular Therapy*, 17(5), 844–850. Available from: https://doi.org/10.1038/mt.2009.16.
Wei, J., Han, X., Bo, J. & Han, W. (2019) Target selection for CAR-T therapy. *Journal of Hematology & Oncology*, 12(1), 62. Available from: https://doi.org/10.1186/s13045-019-0758-x.
Westerhof, L.M., McGuire, K., MacLellan, L., Flynn, A., Gray, J.I. & Thomas, M. et al. (2019) Multifunctional cytokine production reveals functional superiority of memory CD4 T cells. *European Journal of Immunology*, 49(11), 2019–2029. Available from: https://doi.org/10.1002/eji.201848026.
Woods, N.B., Bottero, V., Schmidt, M., Kalle, C. von & Verma, I.M. (2006) Gene therapy: therapeutic gene causing lymphoma. *Nature*, 440(7088), 1123. Available from: https://doi.org/10.1038/4401123a.
Wu, H., Chaudhary, A.K. & Mahato, R.I. (2019) Gene Therapy. In: Crommelin, D.J.A., Sindelar, R.D. & Meibohm, B. (Eds.) *Pharmaceutical Biotechnology: Fundamentals and Applications.* Springer International Publishing: Cham, pp. 323–355.
Wu, R., Sun, J.-Y., Zhao, L.-L., Fan, Z.-N. & Yang, C. (2020) Systematic Identification of Key Functional Modules and Genes in Gastric Cancer. *BioMed Research International*, 2020, 8853348. Available from: https://doi.org/10.1155/2020/8853348.
Wu, X. & Burgess, S.M. (2004) Integration target site selection for retroviruses and transposable elements. *Cellular and Molecular Life Sciences : CMLS*, 61(19-20), 2588–2596. Available from: https://doi.org/10.1007/s00018-004-4206-9.
Wu, X., Li, Y., Crise, B. & Burgess, S.M. (2003) Transcription start regions in the human genome are favored targets for MLV integration. *Science*, 300(5626), 1749–1751. Available from: https://doi.org/10.1126/science.1083413.
Wurm, M., Schambach, A., Lindemann, D., Hanenberg, H., Ständker, L. & Forssmann, W.-G. et al. (2010) The influence of semen-derived enhancer of virus infection on the efficiency of retroviral gene transfer. *The Journal of Gene Medicine*, 12(2), 137–146. Available from: https://doi.org/10.1002/jgm.1429.
Xu, L., Zhang, Y., Luo, G. & Li, Y. (2015) The roles of stem cell memory T cells in hematological malignancies. *Journal of hematology & oncology*, 8(1), 113. Available from: https://doi.org/10.1186/s13045-015-0214-5.
Xu, Y., Zhang, M., Ramos, C.A., Durett, A., Liu, E. & Dakhova, O. et al. (2014) Closely related T-memory stem cells correlate with in vivo expansion of CAR.CD19-T cells and are preserved by IL-7 and IL-15. *Blood*, 123(24), 3750–3759. Available from: https://doi.org/10.1182/blood-2014-01-552174.
Yin, Y., Lei, S., Li, L., Yang, X., Yin, Q. & Xu, T. et al. (2022) RPTOR methylation in the peripheral blood and breast cancer in the Chinese population. *Genes &*

Genomics, 44(4), 435–443. Available from: https://doi.org/10.1007/s13258-021-01182-0.

Ylä-Herttuala, S. (2016) ADA-SCID Gene Therapy Endorsed By European Medicines Agency For Marketing Authorization. *Molecular Therapy : the Journal of the American Society of Gene Therapy*, 24(6), 1013–1014. Available from: https://doi.org/10.1038/mt.2016.98.

Yoshino, H., Yamada, Y., Enokida, H., Osako, Y., Tsuruda, M. & Kuroshima, K. et al. (2020) Targeting NPL4 via drug repositioning using disulfiram for the treatment of clear cell renal cell carcinoma. *PLoS One*, 15(7), e0236119. Available from: https://doi.org/10.1371/journal.pone.0236119.

Zhang, H., Zhao, P. & Huang, H. (2020) Engineering better chimeric antigen receptor T cells. *Experimental Hematology & Oncology*, 9(1), 34. Available from: https://doi.org/10.1186/s40164-020-00190-2.

Zhang, Z., Liu, S., Zhang, B., Qiao, L. & Zhang, Y. (2020) T Cell Dysfunction and Exhaustion in Cancer. *Frontiers in Cell and Developmental Biology*, 8, 17. Available from: https://doi.org/10.3389/fcell.2020.00017.

Zhao, R., Cui, Y., Li, S., Le Qin & Li, P. (2019) Current status and hurdles for CAR-T cell immune therapy. *Blood Science*, 1(2). Available from: https://journals.lww.com/bls/Fulltext/2019/10000/Current_status_and_hurdles_for_CAR_T_cell_immune.6.aspx.

Zhou, S., Fatima, S., Ma, Z., Wang, Y.D., Lu, T. & Janke, L.J. et al. (2016) Evaluating the Safety of Retroviral Vectors Based on Insertional Oncogene Activation and Blocked Differentiation in Cultured Thymocytes. *Mol Ther*, 24(6), 1090–1099. Available from: https://doi.org/10.1038/mt.2016.55.

Zhou, S., Ma, Z., Lu, T., Janke, L., Gray, J.T. & Sorrentino, B.P. (2013) Mouse transplant models for evaluating the oncogenic risk of a self-inactivating XSCID lentiviral vector. *PLoS One*, 8(4), e62333. Available from: https://doi.org/10.1371/journal.pone.0062333.

Zhou, S., Mody, D., DeRavin, S.S., Hauer, J., Lu, T. & Ma, Z. et al. (2010) A self-inactivating lentiviral vector for SCID-X1 gene therapy that does not activate LMO2 expression in human T cells. *Blood*, 116(6), 900–908. Available from: https://doi.org/10.1182/blood-2009-10-250209.

Zufferey, R., Donello, J.E., Trono, D. & Hope, T.J. (1999) Woodchuck hepatitis virus posttranscriptional regulatory element enhances expression of transgenes delivered by retroviral vectors. *J Virol*, 73(4), 2886–2892.

Zufferey, R., Dull, T., Mandel, R.J., Bukovsky, A., Quiroz, D. & Naldini, L. et al. (1998) Self-Inactivating Lentivirus Vector for Safe and Efficient In Vivo Gene Delivery. *Journal of Virology*, 72(12), 9873–9880.

Zychlinski, D., Schambach, A., Modlich, U., Maetzig, T., Meyer, J. & Grassman, E. et al. (2008) Physiological promoters reduce the genotoxic risk of integrating gene vectors. *Mol Ther*, 16(4), 718–725. Available from: https://doi.org/10.1038/mt.2008.5.

7. Appendices

7.1. Abbreviations

Abbreviation	Definition
%	Percentage
+	Positive
<	Less Than
>	Greater Than
°C	Degrees Celsius
µg	Microgram
µg/mL	Microgram per mL
µL	Microlitre
AAV	adeno-associated virus
Ab	Antibody
ADA	Adenosine Deaminase
ADA-SCID	Adenosine Deaminase Deficiency Severe Combined Immunodeficiency
AML	Acute Myeloid Leukaemia
ANOVA	Analysis of Variance
AO	Acridine Orange
APC	Allophycocyanin
APC-Vio770	Allophycocyanin Violet 770
B-ALL	B cell Acute Lymphoblastic Leukaemia
BCMA	B cell Maturation Antigen
BM	Bone Marrow
BV421	Brilliant Violet 421
CAR	Chimeric Antigen Receptor
CD	Cluster of Differentiation
CDR	Complementarity Determining Region
cDNA	Complementary DNA
CGD	Chronic Granulomatous Disease
CGT	Cell and Gene Therapy
CIS	Common Insertion Site
CMC	Chemistry, Manufacturing and Control
CO2	Carbon Dioxide
CQA	Critical Quality Attributes
CRS	Cytokine Release Syndrome
CTLS	Clinical Trials Laboratory Service
CV	Coefficient of Variation
DAPI	4',6-diamidino-2-phenylindole
DCC	Netrin 1 Receptor
DMEM	Dulbecco's Modified Eagle Medium
DMSO	Dimethyl Sulfoxide

DNA	deoxyribonucleic acid
EBV	Epstein Barr Virus
EDTA	Ethylenediaminetetraacetic Acid
EF1a	Elongation Factor 1a
EIAV	Equine Infectious Anaemia Virus
EMA	European Medicines Agency
ErbB2	Erythroblastic Oncogene B
FACS	Fluorescence Activated Cell Sorting
FACT	Foundation of the Accreditation of Cellular Therapy
FAP	Fibroblast Activation Protein
FBS	Fœtal Bovine Serum
FC	Fragment Crystallisable Region
FDA	Food and Drug Administration
FMO	Fluorescence Minus One
FTIH	First Time in Human
GCC	Guanylate Cyclase-C
GD2	Glycoprotein D2
GFP	Green Fluorescent Protein
GMP	Good Manufacturing Practise
GSK	GlaxoSmithKline
GvHD	Graft vs Host Disease
HBS	Human Biological Sample
HCC	Hepatocellular Carcinoma
HEK	Human Embryonic Kidney
HER	Human Epidermal Growth Factor Receptor
hFIX	Human Factor 9
hIgG	Human Immunoglobulin G
HIV	Human Immunodeficiency Virus
HLA	Human Leukocyte Antigen
hPGK	Human Phosphoglycerate Kinase
HSC	Haematopoietic Stem Cell
ICANS	Immune Effector Cell-Associated Neurotoxicity Syndrome
IDO	Indoleamine 2,3 dioxygenase
IFN-γ	Interferon Gamma
IL	Interleukin
IL2R	IL-2 Receptor
IL2RG	gamma-chain of the IL-2 receptor
IM	Insertional Mutagenesis
iPSC	Inducible Pluripotent Stem Cell
IRES	Internal Ribosome entry Site
ITAM	Immunoreceptor Tyrosine-Based Activation Motif
IU	International Units
KT_{50}	Time taken to kill 50% of target cell line
LDLr	Low Density Lipoprotein Receptor
LNGFR	low affinity nerve growth factor receptor

LTR	Long Terminal Repeat
LTRs	Long Terminal Repeat
LVV	Lentiviral Vector
mAb	Monoclonal Antibody
MAGE	Melanoma Associated Antigen
MAGE A12	Melanoma Associated Antigen A12
MAGE A3	Melanoma Associated Antigen A3
MAS	Macrophage Activation Syndrome
MEM NEAA	Minimum Essential Medium Non-Essential Amino Acids
MFI	Median Fluorescence Intensity
MHC	Major Histocompatibility Complex
mL	Millilitre
MOI	Multiplicity of Infection
MSD®	Meso Scale Discovery®
NC3R	National Centre for the 3Rs
ng/mL	Nanogram per Millilitre
NK	Natural Killer
NS	Not Significant
NY-ESO-1	New York Esophageal Squamous Cell Carcinoma 1
PBMC	Peripheral Blood Mononuclear Cells
PBS	Phosphate Buffered Saline
PD-1	Programmed Cell Death Protein 1
PD-L1	Programmed Death Ligand 1
PE	Phycoerythrin
PE-Cy7	Phycoerythrin Cyanin 7
Pen/Strep	Penicillin/Streptomycin
pg	Picogram
pg/mL	Picogram per Millilitre
pH	Potential Hydrogen
PMN	Polymorphonuclear Leukocytes
PP	Physical Particles
PP/TU	Physical Particles per Transduction Unit
PSMA	Prostate Specific Membrane Antigen
QBD	Quality By Design
QP	Qualified Person
QTPP	Quality Target Product Profile
RBC	Red Blood Cells
RNA	Ribonucleic Acid
RT	Room Temperature
RTCGD	Retroviral Tagged Cancer Gene Database
RVV	Retroviral Vector
ScFv	Single Chain Variable Fragment
SCID	Severe Combined Immunodeficiency
SEM	Standard Error of the Mean
SIN	Self-inactivating

SPMB	Screening, Profiling and Mechanistic Biology
STING	Stimulator of Interferon Genes
T_{CM}	Central Memory T cells
TCR	T cell Receptor
T_{EFF}	Effector T cells
T_{EM}	Effector Memory T cells
TGF-beta	Transforming Growth Factor Beta
TIL	Tumour Infiltrating Lymphocyte
TIGET	Telethon Institute for Gene Therapy
T_N	Naïve T cells
Treg	Regulatory T cell
T_{SCM}	Stem cell Memory T cells
TSSM	Tromethamine, sodium chloride, sucrose and D mannitol
TU/mL	Transduction Units per Millilitre
U/mL	Units per Millilitre
UT	Untransduced
VCN	Vector Copy Number
vH	Variable Heavy
VioBlue	Violet Blue
vL	Variable Light
VSV-G	Vesicular Stomatitis Virus G Protein
WAS	Wiskott-Aldrich Syndrome
WBC	White Blood Cells
WPRE	Woodchuck Hepatitis Virus Post-Transcriptional Regulatory Element
WT	Wild Type
xg or g	Times Gravity
X-SCID	X-linked Severe Combined Immunodeficiency
y	Gamma Chain
z	Zeta

7.2. Table of Figures

7.3. Data Integrity Tracking of Figures

Figure Number / Table Number	eLNB Reference / PIER ID	Notes
Figure 18	N68596-14	-
Figure 22	N67636-8	-
Figure 23	N72737-4	-
Figure 24	N69525-6	-
Figure 25	N67082-21	-
Figure 26	N67082-18	-
Figure 27	N72737-4	-
Figure 28	N78815-8	-
Figure 29	N67636-8	-
Figure 30	N67636-8	-
Figure 31	N67636-8	-
Figure 32	N67636-8	-
Figure 34	N67082-18 and N67082-21	-
Figure 35	Summary of Data and Graph Documentation within N78815-8	Original data taken from eLNBs: N78815-1, N78815-3, N78815-5, N71151-33
Figure 36	Summary of Data and Graph Documentation within N78815-8	Original data taken from eLNBs: N78815-1, N78815-3, N78815-5, N71151-33
Table 27, Table 28, Table 29, Table 30	N64357-14	-
Table 33	N68499-4	Included within summary eLNB N67636-10
Figure 38	N68499-4	Included within summary eLNB N67636-10

Figure 39	PIER 6912517	Included within summary eLNB N67636-10
	N69525-6 & N69525-7	Included within summary eLNB N67636-10
Table 34	N69525-6 & N69525-7	Included within summary eLNB N67636-10
Figure 41	PIER 6912517	Included within summary eLNB N67636-10
Figure 42	PIER 6912517	Included within summary eLNB N67636-10
Figure 43	N73760-2	Included within summary eLNB N67636-10
Figure 44	N72737-6	Included within summary eLNB N67636-10
Table 35	N72737-6	Included within summary eLNB N67636-10
Figure 45	N72737-4	-
Figure 46	Figure 6A eLNB Reference: N72737-4 Figure 6B eLNB Reference: N73760-2 Figure 6C eLNB Reference: N64357-16	Included within summary eLNB N67636-10
Figure 47	N72737-2 (Pre-Freeze Data) N72737-4 (Post-Thaw Data)	-
Table 36	N72737-2 (Pre-Freeze Data) N72737-4 (Post-Thaw Data)	Included within summary eLNB N67636-10

Figure 48	N72737-2 (Pre-Freeze Data) N72737-4 (Post-Thaw Data)	Included within summary eLNB N67636-10
Figure 49	N72737-4	Included within summary eLNB N67636-10. Statistical analysis performed within eLNB N72737-8.
Table 37	N72737-8	Included within summary eLNB N67636-10.
Figure 50	N67636-8	Donor PR20F384542. Day -1 Phenotyping Data. Summary of data and DI check documentation provided in N67636-11.
Figure 51	N67636-8	Day -1 Phenotyping Data. Average of Two Donors (PR20F384542 and PR20H384548) Summary of data and DI check documentation provided in N67636-11.
Figure 52	N67636-8	Day -1 Phenotyping Data Summary of data and DI check documentation provided in N67636-11.
Table 38	N67636-8	Day -1 Phenotyping Data Summary of data and DI check documentation provided in N67636-11.

Figure 53	N67636-8	Day 0 Activation Data Summary of data and DI check documentation provided in N67636-11.
Figure 54	N67636-8	Day 0 Activation Data Summary of data and DI check documentation provided in N67636-11.
Figure 55	N67636-8	Day 0 Activation Data Summary of data and DI check documentation provided in N67636-11.
Figure 56	N67636-8	Day 9 Transduction Efficiency Analysis Summary of data and DI check documentation provided in N67636-11.
Figure 57	N67636-8	Day 9 Transduction Efficiency Analysis Summary of data and DI check documentation provided in N67636-11.
Table 39	N67636-8	Day 9 Transduction Efficiency Analysis Summary of data and DI check documentation provided in N67636-11.
Figure 58	N67082-18 and N67082-21	Summary of data and DI check documentation provided in N67636-11.
Table 40	N67082-18 and N67082-21	Summary of data and DI check documentation provided in N67636-11.

Figure 59	N67636-8	Summary of data and DI check documentation provided in N67636-11.
Table 41	N67636-8	Summary of data and DI check documentation provided in N67636-11.
Figure 61	N67636-3	Summary of data and DI check documentation provided in N67636-11.
Figure 62	N67636-4 N67636-3	24-well G-REX® (N67636-4) 24 flat bottom plate (N67636-3) Summary of data and DI check documentation provided in N67636-11.
Figure 63	24-well G-REX®: N72737-2, N67082-15, N67082-18, N67082-21, N67263-10, N67636-8, N62758-36, N74334-2 6-well G-REX®: N72736-5, N62758-36, N74334-2, N74546-3	Summary of data and DI check documentation provided in N67636-11.
Figure 64	N76293-7 and N76293-8	Fold expansion values only used for conditions were 40ng/mL of IL-7 and IL-15 were used. Summary of data and DI check documentation provided in N67636-11.

Figure 65	24-well G-REX®: N72737-2, N67082-15, N67082-18, N67082-21, N67263-10, N67636-8, N62758-36, N74334-2 6-well G-REX®: N72736-5, N62758-36, N74334-2, N74546-3 Prodigy®: N67050-7, N67050-9, N67050-11, N67050-13, N70338-3, N70338-2, N70338-5, N67050-15	Summary of data and DI check documentation provided in N67636-11.
Figure 66	24-well IL-2: N72737-2, N67082-15, N67082-18, N67082-21, N67263-10, N67636-8, N62758-36, N74334-2 6-well IL-2: N72736-5, N62758-36, N74334-2, N74546-3 24-well IL-7/IL-15: N67082-15, N67082-18, N67082-21 6-well IL-7/IL-15: N67082-17, N67082-20, N67082-24, N67082-30	Summary of data and DI check documentation provided in N67636-11.
Figure 67	N67082-18 and N67082-21	Day 12 Phenotyping Data. 5 donors. Summary of data and DI check documentation provided in N67636-11.

Figure 68	N67082-18 and N67082-21	Summary of data and DI check documentation provided in N67636-11.
Figure 69	N67082-18 and N67082-21	Statistical analysis performed within eLNB N67636-12. Summary of data and DI check documentation provided in N67636-11.
Figure 70	N67082-18 and N67082-21	Statistical analysis performed within eLNB N67636-12. Summary of data and DI check documentation provided in N67636-11.
Figure 71	N67082-25	-
Figure 72	N76293-7 N78941-1	All data taken from cells cultured within 10M G-REX® vessels (A1, A2, B1 and B2) with either 40ng/mL of cytokine frontloaded or 10ng/mL of cytokine added at regular intervals. Summary of data and DI check documentation provided in N67636-11.
Figure 75	Summary of Data and Graph Documentation within N78815-8	Original data taken from eLNBs: N78815-1, N78815-3, N78815-5, N71151-33

Figure 76	Summary of Data and Graph Documentation within N78815-8	Original data taken from eLNBs: N78815-1, N78815-3, N78815-5, N71151-33
Figure 77	Summary of Data and Graph Documentation within N78815-8	Original data taken from eLNBs: N78815-2, N78815-4, N78815-6, N78815-7, N79931-1, N79931-2, N79931-3
Figure 78	Summary of Data and Graph Documentation within N78815-8	Original data taken from eLNBs: N78815-1, N78815-3, N78815-5, N71151-33, N78815-2, N78815-4, N78815-6, N78815-7, N79931-1, N79931-2, N79931-3
Figure 79	Summary of Data and Graph Documentation within N78815-8	Original data taken from eLNBs: N78815-10, N78815-12, N78815-13
Figure 80	Summary of Data and Graph Documentation within N78815-8	Original data taken from eLNBs: N78815-1, N78815-3, N78815-5, N71151-33
Table 42	N78815-11	-
Figure 82	N78815-11	-
Figure 83	N78815-11	-
Figure 84	N78815-11	-
Table 43	N78815-11	-
Table 44	N78815-11	-
Figure 85	N78815-11	-